

Dissertation zur Erlangung des Doktorgrades der Fakultät für Chemie und Pharmazie
der Ludwig-Maximilians-Universität München

Structural insights into yeast translation elongation
and the integrated stress response
using cryo-EM



Agnieszka Anna Pochopień-Pobel (geb. Pochopień)

aus Kattowitz, Polen

2021

Erklärung:

Diese Dissertation wurde im Sinne von §7 der Promotionsordnung vom 28. November 2011 von Prof. Dr. Roland Beckmann betreut.

Eidesstaatliche Erklärung:

Diese Dissertation wurde eigenständig und ohne unerlaubte Hilfe erarbeitet.

München, den 06.05.2021

.....

Agnieszka Anna Pochopień-Pobel

Dissertation eingereicht am: 31.05.2021

1. Gutachter: Herr Prof. Dr. Roland Beckmann

2. Gutachter: Herr Prof. Dr. Daniel N. Wilson

Mündliche Prüfung am: 14.07.2021

Table of Contents

Acknowledgements.....	1
List of original publications	3
Contributions report.....	4
List of abbreviations.....	6
Summary.....	9
1 Introduction	11
1.1 The eukaryotic ribosome.....	11
1.2 The eukaryotic translation cycle.....	13
1.2.1 Initiation.....	13
1.2.2 Elongation	15
1.2.3 Termination	18
1.2.4 Recycling.....	19
1.3 The yeast ABC protein family and the ABCF ATPases.....	20
1.3.1 The eukaryotic elongation factor 3 (eEF3).....	24
1.3.2 The [NU+] prion formation protein 1 (New1).....	26
1.4 Ribosome stalling and the ribosome-associated quality control (RQC).....	26
1.5 The integrated stress response (ISR) in yeast.....	30
1.5.1 The protein kinase Gcn2	34
1.5.2 Activation and regulation of Gcn2.....	37
2 Objective of these studies.....	45
3 Cumulative Thesis: Summary of Publications.....	47
3.1 Publication 1 - A role for the <i>Saccharomyces cerevisiae</i> ABCF protein New1 in translation termination/recycling.....	47
3.2 Publication 2 – Yeast translation elongation factor eEF3 promotes late stages of tRNA translocation.....	47
3.3 Publication 3 - Structure of Gcn1 bound to stalled and colliding 80S ribosomes.....	49
4 Discussion and Outlook.....	51
4.1 The <i>S. cerevisiae</i> eEF3-80S complex.....	51
4.2 The <i>S. cerevisiae</i> New1-80S complex	56
4.3 The <i>S. cerevisiae</i> Gcn1-Disome complex	57
5 References.....	62
6 Publications.....	92

Acknowledgements

First of all, I want to thank Prof. Daniel N. Wilson for giving me the opportunity to join his lab for my PhD, although I initially did not have much experience with the dark and powerful side of structural biology. I am deeply grateful for your great (Gcn!) project selection, the inspirational discussions and your brilliant and opened minded way of thinking about science (and life). Thank you for your willingness to keep me in Munich, while the rest of the Wilson lab moved to Hamburg and giving me the opportunity to regularly visit for personal supervision and project discussions. The transition from the Wilson (one side of the floor) to the Beckmann lab (the other side of the floor) on the legendary 3rd floor was not very hard, since the Wilson and the Beckmann group were always one big family, providing me with all the equipment, brain power and many amazing people, who made the PhD journey an unforgettable one.

I also want to thank Prof. Roland Beckmann for hosting me in his lab during that time and including me in all activities and group meetings as well as his feedback and support on the projects. I want to thank the cryo-EM power team Dr. Otto Berninghausen together with his cryo-queens, Susi Rieder and Charlotte Ungewickell for handling samples, the infinite data collections for the eEF3 and Gcn1 samples and fixing all the microscope problems.

Thanks to all past and present Wilson and Beckmann group members (and their supervisors), who provided a fantastic working and living atmosphere over the last few years. Thank you for all the shared conference experiences, Gene Center and hiking retreats as well as the Oktoberfest, Nockherberg, defense, pool, Gin and various 'just because it's a day of the week' parties and of course the Christmas celebrations including the legendary 'the year in review' presentation (powered by Dr. Thomas Becker) for the audience, who virtually died of laughter (yes, there was a time before March 2020 and we did it all live!).

Further I want to thank: Dr. Maximiliane Wieland and Dr. Claudia Müller for all the technical and mental support during the entire thesis time and for going through the journey together; Dr. Bertrand Beckert for all his advice, an open ear for all my questions and his great support on the eEF3 and Gcn1 projects; Dr. Michael Graf for the general support on modelling and his help on the New1 model; Dr. Paul Huter for the support on eEF3 processing, general processing advice and a great time before leaving and after returning to Munich. Dr. Fabian Nguyen for the many inspirational and extensive conversations about yeast and fungi (and psychology) in the hidden catacombs of the back computer room; Dr. Thomas Becker, who was always patient and supportive for all kind of questions and Joanna Musial, Andrea Gilmozzi and Heidemarie Sieber for their never-ending support in the lab as well as Dr. Christian Schmidt for the first protocol for the 'magic' native pullout. Hanna Kratzat: thank you for your general support, an artistic eye on figures, your good mood, joy and laughter and the various delicious cakes, for which I also want to thank the macaron king Timur Mackens-Kiani. Katharina Best and Dr. Lukas Kater: thank you for your infinite IT knowledge and your excellent Gin/Whisky and coffee taste. I want to thank Dr.

Andre Heuer for organizing so many events for all of us. Special thanks to Daniela Hess-Otto for always being helpful with organizational and bureaucratic obstacles and who always found a way to support me. Finally, many thanks to my (now) husband Dr. Roman Pobel for all your loving support during my PhD time, to my mum and brother as well as my best friends Paulina, Anki and Ruth.

List of original publications

Publication 1

Villu Kasari*, **Agnieszka A. Pochopien***, Tõnu Margus, Victoriia Murina, Kathryn Turnbull, Yang Zhou, Tracy Nissan, Michael Graf, Jiří Nováček, Gemma C. Atkinson, Marcus J. O. Johansson, Daniel N. Wilson, Vasili Hauryliuk (2019). A role for the *Saccharomyces cerevisiae* ABCF protein New1 in translation termination/recycling. *Nucleic Acids Research*. 47, 8807-8820.

Publication 2

Namit Ranjan*, **Agnieszka A. Pochopien***, Colin Chih-Chien Wu*, Bertrand Beckert, Sandra Blanchet, Rachel Green, Marina V. Rodnina, Daniel N. Wilson (2021). eEF3 promotes late stages of tRNA translocation on the ribosome. *EMBO J*. 10.15252/embj.2020106449.

Publication 3

Agnieszka A Pochopien*, Bertrand Beckert*, Sergo Kasvandik, Otto Berninghausen, Roland Beckmann, Tanel Tenson, Daniel N. Wilson (2021). Structure of Gcn1 bound to stalled and colliding 80S ribosomes. *PNAS*. 10.1073/pnas.2022756118.

*These authors contributed equally to this work.

Contributions report

This dissertation contains my PhD research, which was supervised by Prof. Daniel N. Wilson between March 2016 and December 2020 at the Gene Center of the Ludwig-Maximilians University in Munich. Multiple collaborations supported this work. The project on the eukaryotic elongation factor 3 (eEF3) (publication 1) was conducted in collaboration with the laboratories of Prof. Roland Beckmann (Gene Center, University of Munich, Germany), Prof. Marina V. Rodnina (Max Planck Institute for Biophysical Chemistry, Göttingen, Germany) and Prof. Rachel Green (Johns Hopkins University School of Medicine, Baltimore, MD, USA). The work on New1 (publication 2) was performed in collaboration with Prof. Vasili Hauryliuk (Umeå University, Sweden and University of Tartu, Estonia) and Dr. Jiří Nováček (Central European Institute of Technology (CEITEC), Masaryk University, Brno, Czech Republic). The study on the Gcn1-disome structure (publication 3) was done in collaboration with Prof. Roland Beckmann and Dr. Otto Berninghausen (Gene Center, University of Munich, Germany), and Prof. Tanel Tenson (University of Tartu, Estonia).

Publication 1 | Kasari and Pochopien et al. (2019)

This study comprises the *in vitro* reconstituted structure of the yeast eEF3 homologue New1 bound to the 80S ribosome. I performed protein purification, *in vitro* sample reconstitution and processing of the cryo-EM data. I interpreted the structure (identification of the truncated CD of New1 in comparison to eEF3), built the majority of the molecular New1-80S model, prepared figures 3, 4, S2, S3, S6, S7, S8 and contributed to manuscript preparation.

Publication 2 | Ranjan, Pochopien and Chih-Chien et al. (2021)

This publication reports a cryo-EM structure of a native yeast eEF3-80S complex at 3.3 Å resolution as well as presents seven additional cryo-EM structures of the complex in different rotation, swiveling and tRNA occupation states, ranging from 3.3 - 4.2 Å. It shows how the chromo domain (CD) of eEF3 is directly interacting with the ribosomal L1-stalk and contributes to the release of the E-site tRNA during elongation. I performed the preparation of the native eEF3 pull-out sample, processing of the cryo-EM data as well as the analysis and interpretation of the structural data. I was responsible for building the majority of the molecular eEF3-80S model and refinement. I prepared the synopsis picture, figures 4, 5, 7, S2, S3, S4, S5, S6 and contributed to manuscript preparation.

Publication 3 | Pochopien and Beckert et al. (2021)

The publication presents the first structural insights into the integrated stress response (ISR) protein Gcn1 bridging two collided ribosomes as well as the binding of Rbg2-Gir2 and Mbf1 to the leading stalled and colliding ribosome, respectively. I performed the native Gcn20 pull-out and was responsible for the calculation of the cryo-EM data set. Furthermore, I contributed to the analysis and interpretation of the Gcn1-disome structure. I built the molecular model for Gcn1 and the leading stalled ribosome, prepared figures 1, 3 (panels G and H), 4, S1, S2, S3, S4, S5, S6, S7, S10 and contributed to writing of the manuscript.

List of abbreviations

2D	two-dimensional
3D	three-dimensional
4HB	four helix bundle
aa	amino acid
aa-tRNA	aminoacyl-tRNA
ABC	ATP-binding cassette
AMPMP	adenylyl-imidodiphosphate
ATP	adenosine-5'-triphosphate
ATPase	adenosine-5'-triphosphatase
CD	chromo domain
CR	colliding ribosome
CTD	C-terminal domain
cryo-EM	cryogenic electron microscopy
DC	decoding center
DNA	deoxyribonucleic acid
Drg2	developmentally regulated GTP-binding protein 2
eEF3	eukaryotic elongation factor 3
eIF2 α -P	eIF2 α phosphorylation
E-tRNA	exit transfer ribonucleic acid
EM	electron microscopy
FRET	fluorescence resonance energy transfer
GAAC	general amino acid control
GAC	GTPase-activating center
Gcn1/2/20	general control non-derepressible 1/2/20
G-domain	GTPase domain
GDP	guanosine-5'-diphosphate

Dfrp2	DRG family-regulatory protein 2
GGQ-motif	glycine-glycine-glutamine motif
Gir2	genetically interacts with ribosomal genes protein 2
GTP	guanosine-5'-triphosphate
GTPase	guanosine-5'-triphosphatase
HEAT	Huntingtin, elongation factor 3 (EF3), protein phosphatase 2A (PP2A), and the yeast kinase TOR1
HisRS	histidyl-tRNA synthetase
HTH	helix-turn-helix
IC	initiation complex
IF	initiation factor
IRS	integrated stress response
kDa	kilodalton
LSR	leading stalled ribosome
LSU	large ribosomal subunit
mRNA	messenger RNA
NMR	nuclear magnetic resonance
NTD	N-terminal domain
ORF	open reading frame
P _i	inorganic phosphate
PIC	pre-initiation complex
PK	protein kinase
POST	post-translocation
PoTC	post-termination complex
PRE	pre-translocation
PreTC	pre-termination complex
P-tRNA	peptidyl-tRNA
PTC	peptidyl transferase center

Rbg 1/2	ribosome-interacting GTPase 2
RF	release factor
RNA	ribonucleic acid
RRF	ribosome release factor
rRNA	ribosomal RNA
RNC	ribosome nascent chain complex
RQC	ribosome-associated quality-control
RWD	RING-finger proteins, WD repeat-containing proteins and the yeast DEAD-like helicases
S5D2L	S5 domain 2-like
SD	Shine-Dalgarno
SRL	sarcin-ricin loop
SSU	small ribosomal subunit
TGS	ThrRS (threonyl-tRNA synthetase), GTPase, and SpoT (guanosine-3',5'-bis(diphosphate) 3'-pyrophosphohydrolase)
TC	ternary complex
Tma46	translation machinery-associated protein 46
tRNA	transfer RNA
UTR	untranslated region
wt	wild type

Summary

Protein biosynthesis represents one of the central processes within the cells of all living organisms. Proteins are synthesized by ribosomes, passing through the stages of translation initiation, elongation and termination. When cells possess enough nutrients, translation elongation occurs in a fast and efficient way. In mammals, two translational GTPases eEF1A and eEF2 are required for this process, whereas yeast needs a third essential factor, the eukaryotic elongation factor 3 (eEF3), which is responsible for the release of the E-site tRNA. Using cryo-electron microscopy, we investigated a native structure of the eEF3-80S complex at 3.3 Å and determined its detailed molecular interactions with the ribosome. We showed that the chromo domain (CD) of eEF3 is involved in repositioning of the L1-stalk from an 'in' into an 'out' conformation by directly interacting with it and thus is substantial for E-site tRNA release. Furthermore, we provided seven additional eEF3-bound 80S complexes, ranging from 3.3 Å - 4.2 Å in different ribosomal rotation, swiveling and tRNA occupation states - structures, completing the yeast elongation cycle and thus contributing to a wider understanding of this process.

Moreover, we determined an *in vivo* reconstituted structure of a close eEF3 homologue, the non-essential *S. cerevisiae* protein New1, bound to the 80S ribosome. This study revealed a similar binding site of New1 on the ribosome. New1 possesses a truncated CD, which in our study did not interact with the ribosomal L1-stalk, explaining why New1 is not able to efficiently fulfill the function of eEF3 in E-tRNA release and suggesting another role of New1 in fungi translation.

During diverse stress conditions, e.g. nutrient deprivation, the activation of the integrated stress response (ISR) pathway leads to adaptation and ensures cell survival. The yeast system comprises the kinase Gcn2, which is suggested to be activated via binding of deacetylated tRNAs (tRNA^{deacyl}) within the ribosomal A-site. The subsequent phosphorylation of eIF2 α leads to a reprogramming of the general gene expression profile, counteracting amino acid deficiency. The protein Gcn1 (and Gcn20) is essential for Gcn2 activation. Since the ISR leads to severe metabolic changes, it requires a tight regulation carried by various modulators, including the Rbg2-Gir2 complex. We obtained the first structure of the Gcn2 effector protein Gcn1 and the Gcn2 modulator complex Rbg2-Gir2, binding to two colliding ribosomes (disome). The disome consists of a leading stalled ribosome (LSR) and a colliding ribosome (CR). The LSR is non-rotated with A- and P-tRNA as well as eIF5A in the E-site, whereas the CR is rotated, bearing hybrid A/P-, P/E-tRNA and Mbf1 located between the 40S body and head. We observe, that Gcn1 spans both ribosomes and its termini form extensive interactions with both P-stalks and 40S ribosomal heads. The Rbg2-Gir2 complex binds the A-site on the LSR, in which Rbg2 is directly interacting with the A-site tRNA, while the RWD domain of Gir2 reaches toward the C-terminal Gcn1. The latter observation illustrates how Gir2-RWD is competing with Gcn2-RWD for the essential Gcn1 binding and thus suppresses Gcn2 activation under certain conditions. Simultaneously, our study serves as a structural basis for the Gcn1-mediated Gcn2 activation during the induction of the ISR. Since Gcn1 is binding a disome in simultaneous absence of tRNA^{deacyl}, we propose ribosome collisions as the signal for the activation

of the ISR - a structure, which does not only have implication for the ISR, but also for the ribotoxic stress response and the ribosome-associated protein quality control (RQC).

1 Introduction

In the 'Central Dogma of Molecular Biology' (Crick, 1970), Francis Crick postulated a concept of the flow of genetic information. The genetic information stored in the DNA propagates through RNA molecules followed by the translation into polypeptide chains, which fold into proteins. Within cells, DNA molecules are stored in a compact and protected form as chromosomes. After 'unpacking' of the genome, the genetic information can be used for three basic processes. In the first one, the DNA is propagated by the process of replication to pass it on the next cell generation. In the second step, specific DNA sequences called genes are transcribed into RNA, a process catalyzed by an RNA polymerase. RNA molecules fulfil different functions, for example as ribosomal RNA (rRNA), transfer RNA (tRNA), small non-coding RNA (snRNA) or can act as a template in the form of messenger RNA (mRNA) for the third function, namely that of translation. In the latter, the mRNA is translated into a polypeptide chain by the ribosome. After folding into its 3D native structure, active proteins participate in nearly all activities in the cell acting as enzymes, hormones, antibodies, transport and contractile proteins or giving the cell its overall shape. In the course of evolution, each step of the cellular transcription and translation machinery became fast and efficient, but also tightly regulated and adaptable to different environmental conditions to ensure cell survival.

1.1 The eukaryotic ribosome

The overall process of protein biosynthesis is orchestrated by a large macromolecular complex – the ribosome (Crick, 1958). Its function and basic architecture is highly conserved in all three domains of life - prokaryotes, eukaryotes and archaea - with some species-specific differences. The eukaryotic 80S ribosome (70S in prokaryotes) is composed of a large 60S (LSU, 50S in prokaryotes) and a small 40S subunit (SSU, 30S in prokaryotes), which consists of a head and body/platform domains (**Figure 1A**). Both subunits are composed of ribosomal proteins (r-proteins) and rRNA. The yeast 60S contains 25S, 5.8S and 5S rRNA moieties and 46 r-proteins, whereas the 40S consists of the 18S rRNA and 33 r-proteins. The eukaryotic ribosome is substantially larger (3.5-4.0 MDa) than its prokaryotic counterpart (2.5 MDa) due to some additional protein-RNA and RNA-RNA layers, which are surrounding the highly conserved ribosomal core (Anger et al., 2013; Melnikov et al., 2012). Whereas yeast ribosomes feature some of these additional protein-RNA layer in contrast to the basic architecture in bacteria, ribosomes in *Drosophila* and humans exhibit in addition some RNA layers forming outwards extended expansion segments (Anger et al., 2013; Natchiar et al., 2017; Wilson and Doudna Cate, 2012). It is thought that the more complex the organism and thus the translation (regulation) machinery, the more layers the ribosome features.

During translation, the ribosome binds an aminoacyl-tRNA and transfers the attached amino acid to the end of a growing polypeptide chain. The interaction between the tRNA and the mRNA is mediated through the decoding center (DC) on the SSU (**Figure 1B**) (Carter et al., 2000; Ogle et al.,

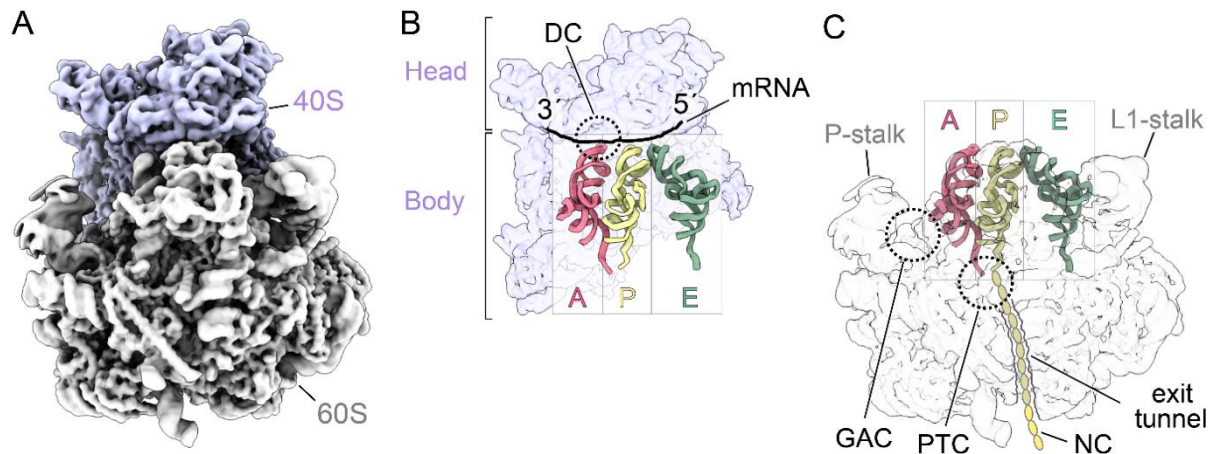


Figure 1. The *S. cerevisiae* 80S ribosome. (A) Cryo-EM reconstruction of the yeast 80S at 2.6 Å resolution low-pass filtered to 4 Å (EMD ID: 10377) (Tesina et al., 2020). 60S is shown in gray and 40S in pastel purple. (B) Schematic of the 40S subunit bound by A- (red), P- (yellow) and E-tRNA (green). The mRNA is shown as black line and the decoding center (DC) is highlighted as dashed circle. 40S head and body are denoted in purple. (C) 60S subunit occupied with tRNAs as in (B). The peptidyl transferase center (PTC), the GTPase-activating center (GAC) and the nascent chain (NC) with the peptide exit tunnel as well as the L1- and P-stalk of the 60S are denoted.

2001). Within the DC, the mRNA codons - consisting of triplets of nucleotides coding for a single amino acid - are decoded by accommodation of the anti-codon of an aminoacyl-tRNA (Berg and Offengand, 1958; Crick et al., 1961; Ogle et al., 2001). Peptide bond formation is catalysed via the peptidyl transferase center (PTC) and enables sequential growth of the polypeptide chain through the peptide exit tunnel within the LSU (Figure 1C) (Frank et al., 1995; Leung et al., 2011). Additionally, the LSU has a GTPase-activating center (GAC) - a region which is bound by translational GTPases (trGTPases) during proteins synthesis - comprising the sarcin-ricin loop (SRL) of 28S rRNA (23S in prokaryotes) and the P-stalk (Maracci and Rodnina, 2016; Shimizu et al., 2002; Uchiumi et al., 2002). The latter one consists of the P0 and P1/P2 (L10 and L7/L12 in prokaryotes) proteins, whereas the C-termini of the P1/P2 heterodimers are highly mobile and present in multiple copies within the cell (Diaconu et al., 2005; Maracci and Rodnina, 2016). The P-stalk not only stimulates the GTP hydrolysis of the ribosome-bound factors by stabilizing its GTPase conformation, but is also facilitates their recruitment. The inter-subunit space formed by the two ribosomal subunits harbours three binding sites for tRNAs termed as A (aminoacyl), P (peptidyl) and E (exit) sites (Figure 1B-C) (Agrawal et al., 1996; Rheinberger et al., 1981). During active protein synthesis, aminoacyl-tRNA is first binding to the A-site, followed by peptide bond formation between the amino acid and the growing polypeptide chain on the P-site tRNA. The A-site tRNA moves to the P-site and after another round of peptide bond formation finally enters the E-site, from which the deacetylated tRNA ($tRNA^{deacyl}$) can be released and leaves the ribosome. To enable the movement of the tRNAs and the mRNA, the ribosomal subunits move with respect to each other. This motion, termed as 'rotation', happens in both, the prokaryotic and the eukaryotic

ribosome (Frank and Agrawal, 2000; Valle et al., 2003). The ribosomal head is also able to swivel, a motion with respect to the body, which is important for the translocation of the tRNA-mRNA module during elongation (Adio et al., 2015; Behrmann et al., 2015; Ermolenko and Noller, 2011; Ramrath et al., 2013; Wasserman et al., 2016). The empty ribosomal A-site 'opens up' to facilitate its loading. This motion termed as 'SSU rolling' is a eukaryotic specific rotation of the 40S around its long axis and dependent on A- or E-site occupancy with a tRNA (Budkevich et al., 2014). During the translational process, the ribosome transiently associates with numerous components that are coordinating specific processes happening at the correct time of the cycle. These translational factors are not only ensuring the high speed and fidelity of the translation reaction, but are also involved in regulation of protein synthesis under certain conditions.

Since the ribosome plays such an important role in a central process of the cell, it was extensively studied through various structural techniques. The first atomic models of the bacterial and archaeal ribosome and ribosomal subunits were revealed by X-ray crystallography (Ban et al., 2000; Rabl et al., 2011; Schluenzen et al., 2000; Selmer et al., 2006; Wimberly et al., 2000). At that time, eukaryotic ribosomes were challenging to crystallize and thus exclusively studied by cryo-EM (Frank and Agrawal, 2000; Verschoor et al., 1998). By docking the crystallographic molecular models into low resolution cryo-EM maps, both methods went hand-in-hand and uncovered the basis of ribosome composition. Finally, 10 years ago, the first structure of the eukaryotic (yeast) ribosome was solved and enabled visualization of detailed atomic interactions (Ben-Shem et al., 2011; Ben-Shem et al., 2010). In cryo-EM, the implementation of direct electron detectors and other (still ongoing) technical improvements resulted in the so called 'resolution revolution' enabling near atomic resolution for large complexes and meanwhile atomic resolution from smaller molecules (1.2 Å for mouse apoferritin) (Cheng, 2015; Nakane et al., 2020; Nogales and Scheres, 2015; Van Drie and Tong, 2020). With these technical improvements cryo-EM contributes to new detailed insights of the ribosome, its intermediate and factor-bound states, increasing and completing the understanding of the translational process as well as its regulation.

1.2 The eukaryotic translation cycle

The basic principles of protein synthesis in pro- and eukaryotes are the same, but the eukaryotic one is more intricate and features more protein components. The translation cycle is divided into four basic steps: initiation, elongation, termination and recycling - processes, which will be discussed in more detail in the following section.

1.2.1 Initiation

During initiation, the SSU assembles around an mRNA template while placing the AUG codon that signals the start of an open reading frame (ORF) within the ribosomal P-site. Initiation is the process, which differs the most between pro- and eukaryotes (Myasnikov et al., 2009; Sonenberg

and Hinnebusch, 2009). Prokaryotic initiation requires only three initiation factors (IFs) - IF1, IF2 and IF3 - and the Shine-Dalgarno (SD) sequence of the mRNA (Shine and Dalgarno, 1974). The latter one is a purine-rich sequence located upstream of the AUG initiation codon, which base pairs with a pyrimidine-rich sequence (anti-SD) of the 16S rRNA of the 30S (Kaminishi et al., 2007; Korostelev et al., 2007). Through this base-pairing, the start codon is positioned correctly within the ribosomal P-site of the 30S and can interact with the formylated initiator (tRNA_i^{Met}). All these processes are mediated by IF1, IF2 and IF3. In the final step, the 50S ribosomal subunit joins forming the final elongation-competent complex.

By contrast, in eukaryotes, the correct placement of the AUG start codon within the ribosomal P-site does not involve the SD sequence, but takes place by a scanning mechanism, which involves at least 12 initiation factors (Aitken and Lorsch, 2012; Aylett and Ban, 2017; Hinnebusch and Lorsch, 2012; Jackson et al., 2010). Initially, the GTP-bound eIF2 consisting of an α , β and γ subunit is binding the initiator methionine tRNA (tRNA_i^{Met}) thus forming a ternary complex (TC) (Figure 2). The TC is binding the 40S ribosomal subunit, a process, which is promoted by eIF3, eIF5, eIF1 and eIF1A, and results in formation of the 43S pre-initiation complex (PIC). In the next step the

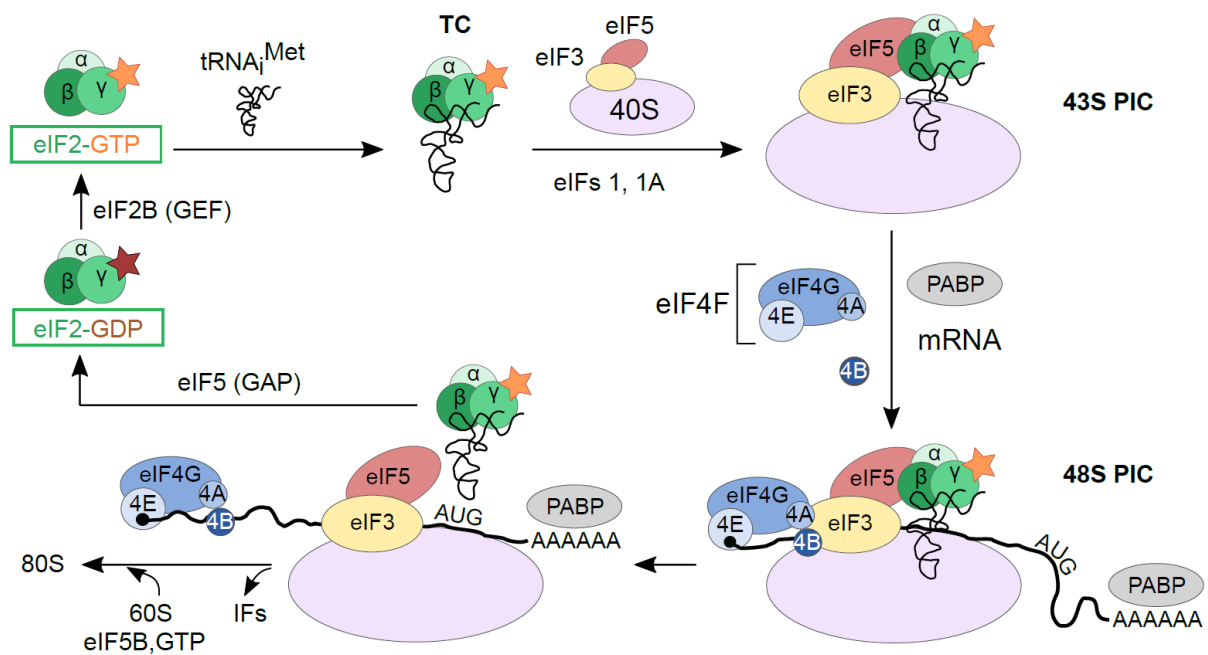


Figure 2. The eukaryotic translation initiation. The tRNA_i^{Met} is bound by eIF2-GTP forming the TC, which in turn binds the 40S subunit with the help of eIF3 and eIF5 and forming the 43S PIC. The subsequent 48S PIC forms through binding to mRNA, which is promoted by eIF4F (eIF4G, eIF4E, eIF4A), eIF4B and PABP, and scans the mRNA for the AUG initiation codon. After reaching it, the tRNA_i^{Met} base-pairs with the AUG within the ribosomal P-site. The 60S subunits joins with help of the GTP-bound GTPase eIF5B forming the complete 80S ribosome (scheme based on (Hinnebusch, 2005) and (Jackson et al., 2010)).

48S PIC forms through joining of the mRNA facilitated by the eIF4F complex (consisting of eIF4G, eIF4E, eIF4A), eIF4B and poly(A) binding protein (PABP) (Figure 2). Whereas eIF4E recognizes the mRNA 5' cap, eIF4G binds PABP, which in turn binds the 3' poly(A) tail leading to circularizing of the mRNA (Merrick, 2015). The 48S PIC scans the mRNA in the 5' to 3' direction for the AUG starting codon. After AUG recognition, the GTPase-activating protein (GAP) eIF5 binds and stimulates GTP hydrolysis of eIF2-GTP into eIF2-GDP, whereas the anticodon of the tRNA_i^{Met} base-pairs with the initiation codon of the mRNA. In the final step, all IFs dissociate, whereas the 60S ribosomal subunit joins the complex - a process stimulated by eIF5B-GTP. This results in an accommodated initiator tRNA within the P-site forming the elongation-competent 80S ribosome ready to bind an aminoacyl-tRNA within its A-site. For re-entering another round of the initiation cycle, eIF2-GDP becomes recycled in its GTP-bound form by its guanine nucleotide exchange factor (GEF) eIF2B (Figure 2). This step is a prominent target for regulatory mechanisms during cellular stress, which will be discussed in later parts of this thesis. The translation initiation process is rate-limiting and thus the most important step for translational regulation, which will be discussed in the later parts of this thesis.

1.2.2 Elongation

During elongation, the ribosome moves along the mRNA, while amino acids are sequentially attached to the growing polypeptide chain. The sequence of each amino acid within a polypeptide chain is determined by the three nucleotide triplets within the codon of the mRNA, which forms the genetic code. This process is physically mediated by the base pairing between the mRNA codon and the aminoacyl-tRNA anticodon. Elongation is characterized by three main steps: decoding, peptide bond formation and translocation.

Entering elongation, the ribosome features an initiator tRNA_i^{Met} occupied P-site and an empty A-site ready to accommodate a cognate aa-tRNA. The latter one is delivered to the ribosomal A-site as TC associated with the GTPase eEF1A (EF-Tu in prokaryotes) bound with GTP. Within the TC, the tRNA binds to the DC of the 40S in a distorted A/T hybrid state conformation. This bent conformation represents an energetic barrier, which is overcome when precise base-pairing between mRNA codon and a cognate tRNA anticodon takes place. A small mini helix is formed by establishing Watson-Crick geometry for the first two base pairs of the codon-anticodon interactions, whereas the third position allows 'more flexible' wobble base-pairing. Based on that, one tRNA is able to match multiple codons, which makes the genetic code degenerate (Crick, 1966). Within the 18S rRNA (16S in prokaryotes), the universally conserved nucleotides G530, A1492, A1493 undergo dramatic conformational rearrangements and establish interactions with the minor groove of the small codon-anticodon helix, which in turn become propagated in remote parts of the ribosome (Demeshkina et al., 2012). To distinguish between a cognate or near/non-cognate tRNA, the codon-anticodon interactions are monitored by the ribosomal DC before and after EF-Tu/eEF1A hydrolysis (Loveland et al., 2020). When a cognate tRNA is bound, GTP hydrolysis

allows the EF-Tu GTPase domain to extend away, leading to release from the tRNA, while the SSU locks the cognate tRNA in the DC and allows its stable accommodation into the PTC (Loveland et al., 2020). In presence of a near- or non-cognate tRNA, the DC is unable to lock the tRNA and thus allows a dissociation before or after GTP hydrolysis during the steps of initial selection and proofreading, respectively (Loveland et al., 2020). The kinked structure of the phosphodiester backbone of the mRNA was shown to be important for decoding on the ribosome (Keedy et al., 2018). While the G-domains of the GTP-bound eukaryotic eEF1A and the bacterial EF-Tu are mostly similar, the crystal structure of the GDP bound mammalian factor revealed that eEF1A stays longer bound after GTP hydrolysis and interacts with tRNA due to its different conformation in contrast to EF-Tu (Crepin et al., 2014).

The second step of peptide bond formation occurs by transferring the polypeptide chain from the P-tRNA to the amino acid attached to the A-tRNA – a process catalysed by the PTC of the 60S (Figure 3A-B). The deacetylation of the P-site ‘unlocks’ the ribosome resulting in a highly dynamic equilibrium between the classical non-rotated pre-translocational (PRE) state with A/A- and P/P-tRNA and a rotated state with hybrid A/P- and P/E-tRNA (Figure 3A-B) (Agirrezabala et al., 2008; Blanchard et al., 2004; Budkevich et al., 2011; Cornish et al., 2008; Julian et al., 2008; Moazed and Noller, 1989). During this thermally driven back and forth rotation, the 40S rotates with respect to the 60S. In the hybrid state, the ribosomal A and P sites of the 40S are occupied by the anticodon stem loops of the tRNAs, whereas the P and E sites of the 60S are harbouring the acceptor ends of the tRNAs. Although both hybrid tRNAs cover the most distance relative to the 60S to translocate to P/P- and E/E-sites, the third and final translocation step requires the action of the GTPase eEF2 (EF-G in prokaryotes). eEF2-GTP binds the rotated ribosome, causes a partial back-rotation, back-rolling and a simultaneous 40S head swivel and allows the tRNA-mRNA module to shift further in the direction of translocation and to adopt a chimeric ap/P and pe/E state (Figure 3B-C) (Budkevich et al., 2014; Flis et al., 2018). In this state the anticodon loops of both tRNAs are bound between the 40S body and the swiveled head domain, while the acceptor ends fully moved into the P and E sites of the 60S. eEF2 dissociation via GTP hydrolysis causes the ribosome to fully back-rotate, back-roll and back-swivel, which allows the ap/P- and pe/E-tRNAs to move into their canonical P/P and E/E binding sites and the ribosome into non-rotated post-translocation (POST) state (Figure 3C-D). In eukaryotes and prokaryotes GTP hydrolysis was shown to be required for eEF2 dissociation from the ribosome rather than for the full translocation of the mRNA-tRNA module (Flis et al., 2018). A recent study revealed that the bacterial ribosome is able to spontaneously move from the classical PRE state to the chimeric ap/P and pe/E state with head swiveled, but without the presence of EF-G (Zhou et al., 2019). Notably, in this state the codon- anticodon interactions between the mRNA and tRNA are disrupted, from which the authors followed that EF-G is essential to maintain the coupled movement of the tRNA₂-mRNA module to maintain the reading frame, rather than being required for translocation *per se*. After a successful translocation from the PRE to a POST state, the deacetylated tRNA is released from the

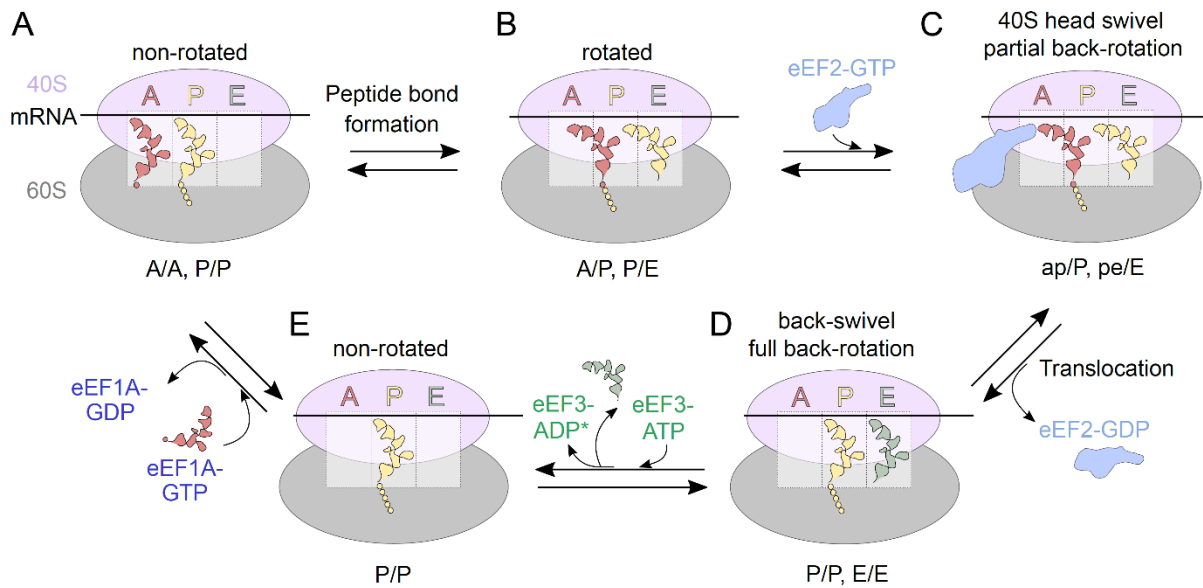


Figure 3. The eukaryotic translation elongation cycle. The ribosome is in a non-rotated, PRE state bearing A/A- (red) and P/P-tRNA (yellow). After peptide bond formation the ribosome is in an equilibrium between a classical PRE state and a hybrid state bearing A/P- and P/E- site tRNAs. eEF2-GTP (blue) binds the rotated state and causes a 40S head swivel, whereas the tRNAs are entering the ap/P and pe/E state. After GTP hydrolysis and eEF2 dissociation, the ribosome swivels and rotates back occupying the POST, non-rotated state with P/P- and E/E-site (dark green) tRNAs. In this state the empty A-site 'opens up' (40S rolling). In yeast and fungi (not in higher eukaryotes), eEF3-ATP (green) enters the elongation cycle releasing the tRNA^{deacyl} from the E-site, whereas the TC can be delivered to the empty ribosomal A-site. After E-tRNA release, eEF3-ADP* might leave the ribosome or stay bound (scheme based on (Andersen et al., 2006), (Behrmann et al., 2015) and (Dever and Green, 2012)).

ribosomal E-site, a process directed by the L1-stalk of the E-site of the ribosomal 60S (Bock et al., 2013; Cornish et al., 2009; Fei et al., 2008; Trabuco et al., 2010). The L1-stalk is a highly dynamic structure, which is able to rotate gradually up to 30° (60 Å) during the elongation process (Mohan and Noller, 2017). In the PRE state, the L1 stalk is in a fully opened state, whereas in the rotated hybrid state it adopts a fully closed conformation and interacts directly with the elbow of the deacetylated tRNA supporting the release of the E-tRNA after translocation. In yeast and fungi, E-tRNA release requires a third essential factor, the ATPase eEF3, which will be discussed in detail in later parts of this thesis (chapter 1.3.1) (Figure 3D-E) (Andersen et al., 2006; Triana-Alonso et al., 1995). eEF3 was reported to bind the ribosome and indirectly stabilize the ribosomal L1-stalk in an 'out' conformation thus facilitating E-site tRNA release. With an empty A-site, a new TC can bind and repeat the elongation cycle until translation is terminated by a stop codon. For yeast specifically, the allosteric three site model was suggested, which postulates that A- and E-sites are reciprocally linked and feature negative cooperativity, i.e. the occupation of the E-site reduced the affinity for the A-site and *vice versa* and that this mechanism contributes to the accuracy of protein

synthesis (Di Giacco et al., 2008; Nierhaus, 1990; Wilson and Nierhaus, 2006). Based on various studies and the work of Ranjan, Pochopien and Chih-Chien et al. (2021), the yeast allosteric three site model needs to be reconsidered, which will be discussed in detail in the discussion section 4.1.

1.2.3 Termination

The end of elongation and thus the completion of a polypeptide chain is signaled by one of the three stop codons (in most organisms UAA, UAG and UGA) within a protein-coding mRNA region, which reaches the ribosomal A-site forming the pre-termination complex (PreTC) (Dever and Green, 2012; Jackson et al., 2012) (**Figure 4A**). In prokaryotes, two class I termination factors recognize different stop codons. RF1 senses UAA and UAG, whereas RF2 is able to recognize UAA and UGA (Weixlbaumer et al., 2008; Zhou et al., 2012). In eukaryotes, one single release factor and a peptidyl-tRNA hydrolase eRF1 recognizes all three stop codons (Brown et al., 2015; Matheisl et al., 2015; Preis et al., 2014). Class I release factors are binding within the A-site and their overall shape and dimension resemble a functional tRNA, whereas their certain domains correspond to the tRNA anticodon loop and a CCA acceptor end (Song et al., 2000; Zhou et al., 2012). Although eukaryotic and prokaryotic factors are evolutionary distinct, they both rely on the universally conserved GGQ motif, which is crucial for the release of the NC. The motif positions a water molecule in the PTC, which allows a nucleophilic attack on the ester bond of the peptidyl-tRNA located in the P-site and a subsequent release of the polypeptide (Jackson et al., 2012; Kisselev et al., 2003; Korostelev, 2011; Song et al., 2000). The recognition of a stop codon is a highly accurate process based on the mechanism of class I RFs to distinguish between stop and sense codons, which in turn depends on structural rearrangements in the 60S and 40S (including the universally conserved nt G530 and A1492 in the DC) of the ribosome when a stop codon is recognized (Hoernes et al., 2018; Kryuchkova et al., 2013; Youngman et al., 2007). Whereas class I RFs recognize the stop codons and trigger the peptidyl-tRNA hydrolysis, class II RFs accelerate these processes in a GTP-dependent manner. In prokaryotes, RF3 functions after peptide release to promote RF1/RF2 dissociation from the ribosome. By contrast, the eukaryotic GTPase eRF3 delivers eRF1 to the ribosome (Alkalaeva et al., 2006; Preis et al., 2014; Shao et al., 2016; Zavialov et al., 2002) (**Figure 4A-B**). After GTP hydrolysis, eRF3 dissociates allowing the GGQ containing central domain of eRF1 to properly position itself within the PTC, followed by the release of the polypeptide and formation of the post-termination complex (PoTC) (**Figure 4B-C**). eRF1 releases the polypeptide by the action of its GGQ motif, forming the PoTC before or after dissociation of eRF3-GDP from complex (**Figure 4C-D**). More recently it was shown that termination efficiency is not only influenced by the presence of the stop codon within the A-site, but also by some downstream mRNA nucleotides (+4 to +9) within the ribosomal entry channel (Cridge et al., 2018).

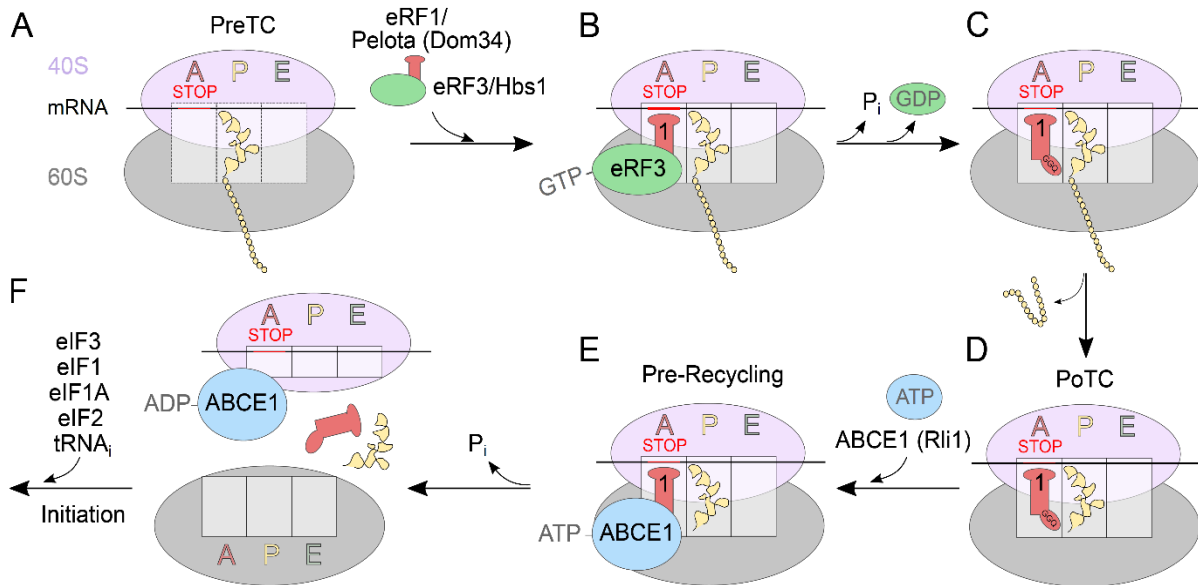


Figure 4. Eukaryotic translation termination and recycling. (A) The preTC bearing the peptidyl-tRNA within the P-site and a stop codon in the A-site (B) is bound by the eRF1-eRF3-GTP complex, whereas eRF1 is recognizing the stop codon. (C) GTP hydrolysis of eRF3 causes eRF3 dissociation and allows eRF1 to fully accommodate into the PTC thus (D) promoting polypeptide release by its conserved GGQ motif. (E) ABCE1 is binding the PoTC and (F) ATP hydrolysis of ABCE1 leads to splitting of the ribosomal subunits, the mRNA, the deacetylated P-tRNA and the factors. The 40S remains associated with the mRNA and ABCE1 or with mRNA and P- or P/E-tRNA (latter not shown). The release of the mRNA and the tRNA^{deacyl} from the 40S is fulfilled by subsequent action of eIF1, eIF1A and eIF3. The joining of further initiation factors and the TC induces a new round of translation initiation (scheme based on (Hellen, 2018), (Preis et al., 2014) and (Heuer et al., 2017)).

1.2.4 Recycling

Recycling is the last step of the translational process, in which the mRNA and tRNAs are released and the ribosome splits into its subunits, enabling a new translation cycle to be entered. Since RF3 and eRF3 have different functions in pro- and eukaryotes, the PoTC differs in both species.

In bacteria, the PoTC (consisting of the 70S ribosome bound to mRNA and a deacyl-tRNA within the P-site) is split by the GTPase EF-G together with the ribosomal recycling factor (RRF) (Agrawal et al., 2004; Hirashima and Kaji, 1973; Karimi et al., 1999; Peske et al., 2005). RRF binds directly to the ribosomal P-site, whereas the binding of EF-G and the subsequent GTP hydrolysis splits the ribosomal complex (Zavialov et al., 2005). Furthermore, IF3 binds the 30S subunit, promoting dissociation of the mRNA and deacyl-tRNA and simultaneously preventing the reassociation of the 40S and 60S subunits. Splitting of the eukaryotic PoTC (consisting of the 80S ribosome bound to mRNA, deacyl tRNA within the P- or P/E-site and eRF1(-eRF3)) in eukaryotes is initiated by the

highly conserved AAA+ ATPase ABCE1 (Rli1 in yeast). After eRF3 dissociation, eRF1 remain bound and ABCE1 binds near the eRF3 binding site (**Figure 4D**). Alternatively, ABCE1 can also bind to eRF1 before peptide release and stimulate the NC release (Shoemaker Green 2011, Pisarev 2010, Shoemaker 2010). ATP hydrolysis of ABCE1 leads to a power stroke that splits the PoTC into the ribosomal subunits (**Figure 4E-F**). The 40S remains associated with the mRNA and ABCE1 (Heuer 2017) (**Figure 4F**) or mRNA and a tRNA^{deacyl} within the P- or P/E-site (Heuer 2017, Pisarev 2010, Preis 2014). The tRNA^{deacyl} and mRNA can be released from the 40S by the subsequent action of eIF1, eIF1A and eIF3, which simultaneously lead – with the help of other initiation factors and the eIF2-GTP-tRNA_i TC – to a new round of initiation (Pisarev et al., 2010) (**Figure 4F**). Also, the presence of ABCE1 on the 40S after splitting was suggested to prime the next round of initiation by promoting the recruitment of initiation factors (Andersen and Leever, 2007; Dong et al., 2004; Heuer et al., 2017; Skabkin et al., 2013). ABCE1 not only splits ribosomes after canonical termination by eRF1, but also recycles vacant ribosomal complexes and stalled ribosomes after their recognition by the eRF1 homologous rescue factor Pelota (Dom34 in yeast) (Barthelme et al., 2011; Pisarev et al., 2010; Pisareva et al., 2011; Shoemaker and Green, 2011; van den Elzen et al., 2014).

Recycling does not need to be necessarily performed after termination. If recycling is incomplete (40S-mRNA) or completely blocked (80S PoTC) then the process of re-initiation takes place, for which the 40S ribosomal subunit is still associated with the mRNA and able to reinitiate at nearby up- or downstream AUGs (Gunisova et al., 2018; Jackson et al., 2012; Skabkin et al., 2013).

1.3 The yeast ABC protein family and the ABCF ATPases

All living cells and their subcellular compartments are separated from the external environment by the lipid bilayer. This plasma membrane allows the import of nutrients and export of cellular waste, which is crucial for cell survival. The transport is carried out by a variety of transporters embedded within the membrane. Importers are responsible for the uptake of amino acids, sugars, essential metals, ions as well as other small molecules up to macromolecules, whereas exporters translocate toxins, drugs, lipids and fatty acids out of the cell (Locher, 2016; Rees et al., 2009; ter Beek et al., 2014; Thomas and Tampe, 2018; Wilson et al., 2020). Exporters are present in eukaryotes and prokaryotes, whereas importers are only present in prokaryotes. 550 types of different transporters have been identified so far, many of which belong to the ATP-binding cassette (ABC) protein family representing one of the largest gene families across all kingdoms of life (Higgins, 1992; Locher, 2016; Wilkens, 2015). The human permeability glycoprotein (P-glycoprotein, ABCB1, MDR1) for example is responsible for the redistribution of cholesterol in the membrane and the efflux of amphiphilic compounds out of the cell including chemotherapeutic agents, which leads to multidrug resistance (MDR) in cancer cells (Garrigues et al., 2002; McCormick et al., 2015; Thomas and Tampe, 2020). The detailed investigation of the P-glycoprotein including its structure, led to the identification of promising inhibitors counteracting MDR (Nanayakkara et al., 2018).

A powerful tool for the studies of ABC proteins in higher eukaryotes represents the model organism *S. cerevisiae* since the yeast genome significantly matches the human genome up to 25% (Bassett et al., 1996; Decottignies and Goffeau, 1997). For the yeast genome, 29 ABC proteins (49 in human) were discovered and subdivided into 6 different clusters (8 subfamilies in human) and/or named alphabetically (ABC-A to ABC-H) based on their sequence similarity and topology (Dean et al., 2001; Decottignies and Goffeau, 1997; Murina et al., 2018; Vasiliou et al., 2009). (Figure 5A).

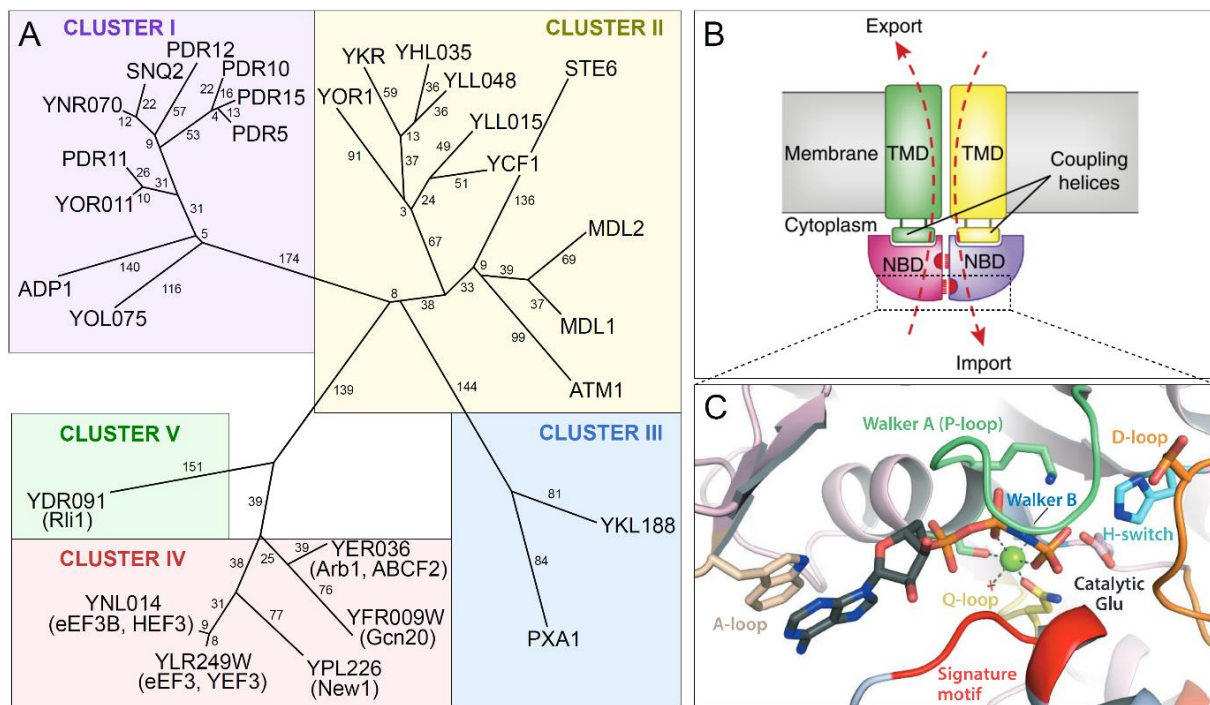


Figure 5. The yeast ABC proteins. (A) Phylogenetic unrooted tree of the yeast ABC protein family including 29 members (the only member of Cluster IV, the protein YFL028, is not shown). (B-C) Schematic of (B) the basic domain arrangement of ABC transporters including 2 TMDs and 2 NBDs as well as (C) a single NBD with an ATP molecule bound. Conserved and functionally crucial motifs are depicted and labeled (figures adapted from (Decottignies and Goffeau, 1997), (Locher, 2016) and (Thomas and Tampe, 2020)).

Despite the differences in their architecture, ABC transporters have 4 domains in common: the 2 transmembrane domains (TMDs) and 2 ABC domains (or nucleotide binding domains (NBDs)) (Figure 5B) (Locher, 2016; Rees et al., 2009; ter Beek et al., 2014). The TMDs are variable and embedded in the membrane, where they create a pathway for the translocating substrate. Based on their TMD sequence homology and folds assessed by numerous crystal structures, ABC transporters were classified into 7 different types (Type I - VII), which will not be discussed in further details here (Thomas and Tampe, 2020). In contrast, the two cytoplasmic and highly conserved ABCs are separated by an α -helical interdomain linker and are responsible for the ATP-coupled translocation of the substrate across the lipid bilayer (Murina et al., 2018; Ousalem et al.,

2019). Based on their sequence identity, the 2 ABCs can be homodimeric or heterodimeric, but in both cases they are structurally similar. Although ABC proteins possess 2 ABCs forming two ATP-binding sites, it is still not clear if they bind and hydrolyze 2 ATP molecules for a complete transport cycle. Based on the fact that some ABC proteins contain degenerated ABCs, in which one of the two ABCs is non-functional due to some mutations, it was shown that for some ABC proteins one active nucleotide binding site is sufficient for the transport of the target substrate and therefore multiple transport stoichiometries were suggested (Jones and George, 2013; Nikaido and Ames, 1999; ter Beek et al., 2014).

The ATP binding and hydrolysis reaction itself requires Mg^{2+} ions and an activated lytic water molecule surrounded by the conserved motifs of the 2 ABCs. The ABCs catalytic core is highly conserved and includes the Walker A and Walker B motifs as well as the A- and Q-loop and the H-motif, whereas the α -helical domain is more variable and encompasses the signature motif (Figure 5C) (Locher, 2016; Oswald et al., 2006; Rees et al., 2009; ter Beek et al., 2014; Thomas and Tampe, 2020). In the first step, the two ABCs are coming in close proximity (closed conformation) forming an interface, where each of them contributes its conserved residues to form two active ATP-binding sites enabling the binding of Mg^{2+} -ATP - an interaction based on attracting forces (Szollosi et al., 2020). Within the catalytic core, the A-loop contains an aromatic residue (often a Tyrosine), which stacks with the purine ring of the adenine of the ATP molecule and contributes to its correct positioning. Interactions to the ATP α - and β -phosphates are established by the Walker A motif (GXXGXGK(S/T), whereas X represents any amino acid) - also known as the phosphate binding loop (P-loop). The Walker B motif ($\phi\phi\phi\phi$ DE, whereas ϕ represents a hydrophobic residue) has two highly conserved Aspartate and Glutamate residues. Whereas Aspartate is responsible for coordinating the Mg^{2+} ion, the catalytic Glutamate serves as a general base polarizing the attacking water molecule. The H-loop (or the switch region) has the important role to stabilize the position between the general base, the Mg^{2+} ion and the attacking water (transition state) by a direct interaction with the general base and the ATP γ -phosphate via its conserved Histidine residue. In the closed state with bound Mg^{2+} -ATP, the D-loop (SALD motif) and the Q-loop (~8 residues with a conserved glutamine at the N-terminus) form a specialized geometry, which is disrupted after ATP is hydrolyzed. The crucial signature motif (or C-loop, LSGGQ) is located on the N-terminus of a helix, which directs the positive charge of the helical dipole towards the ATP γ -phosphate. Hybrid quantum mechanical/molecular mechanical (QM/MM) molecular dynamics (MD) simulations of the *E. coli* ABC protein BtuCD-F showed that the ATP hydrolysis reaction is a three step process (Priess et al., 2018). First, the ATP γ -phosphate is nucleophilically attacked by the polarized water molecule whereas the catalytic base near the γ -phosphate transiently accepts a proton (intermediate product 1: ADP + HPO_4^{2-}). In the second step, the proton is transferred back from the Glutamate to the ATP γ -phosphate (intermediate product 2: ADP + H_2PO_4) followed by third, a rearrangement of the hydrogen bond and coordination of the Mg^{2+} ion. After ATP hydrolysis, the Mg^{2+} is forming stabilizing interactions with ADP + P_i and the product remains

strongly bound to the ABCs, but by the interaction of a water molecule with Mg^{2+} -ATP + P_i the ABC dimers become separated and adopt an open state (Szollosi et al., 2020).

This conformational change of the two ABCs is transmitted to the TMDs via ‘coupling helices’ and this in turn enables the transport of the substrate (**Figure 5B**). The lack of TMDs is a characteristic feature of two exceptional clusters of the ABC protein family – the ABCE and ABCF proteins (Murina et al., 2018). Since they are missing their TMDs, they are not involved in transport, but function as cytoplasmic factors, some of which are involved in the translation process (Davidson et al., 2008; Fostier et al., 2020; Gerovac and Tampe, 2019). In bacteria, the ABCF protein family is particularly known for its antibiotic resistance (ARE) activity (Davidson et al., 2008; Murina et al., 2018). Since many antibiotics are targeting the bacterial ribosome and particularly the PTC or the polypeptide exit tunnel thus inhibiting translation, ARE ABCFs are able to protect these locations on the ribosome leading to ARE (Ero et al., 2019; Matzov et al., 2017; Schwarz et al., 2016; Sharkey and O'Neill, 2018; Wilson, 2014; Wilson et al., 2020; Wilson et al., 2008). ARE ABCs are widely distributed in Gram-positive and some Gram-negative bacteria. Some of them are able to bind directly to the antibiotic thus removing it (type I protection type) or indirectly after binding to the ribosome, which causes a conformational change leading to drug drop-off (type II protection type) (Wilson et al., 2020). The type III protection type binds the ribosome and restore its functionality despite the bound drug. The bacterial *Staphylococcus haemolyticus* VgaA, *Enterococcus faecalis* LsaA, *Bacillus subtilis* VmlR and *Listeria monocytogenes* VgaL proteins are examples for the type II protection type. Their cryo-EM structures revealed that the ABCF proteins are binding within the ribosomal E-site in an ATP-conformation and extend their individual antibiotic resistance domain (ARD) into the ribosomal PTC leading to a conformation change of the 23S rRNA, which in turn causes an antibiotic drop-off (Crowe-McAuliffe et al., 2018; Crowe-McAuliffe et al., 2021). Some of the bacterial ABCFs are not mediating ARE ability, but have other functions, like the *E. coli* energy-dependent translational throttle A (EttA). Although it binds in the same position at the ribosomal E-site, it regulates protein synthesis due to the energy status based on the ATP/ADP ratio (Boel et al., 2014; Chen et al., 2014). In contrast to bacteria, the yeast genome contains 5 ABCF proteins: the eukaryotic elongation factor 3 and 3B (eEF3/eEF3B, YEF3/HEF3, YLR249E/YNL014), the [NU+] prion formation protein 1 (New1, YPL226), the general control non-derepressible protein 20 (Gcn20, YFR009W) and the ABC transporter ATP-binding protein (Arb1, ABCF2, YER036) (**Figure 6A**) (Decottignies and Goffeau, 1997). eEF3 is the most prominent member of the yeast ABCF protein family and was shown to be essential in yeast and fungi during elongation (Andersen et al., 2006; Triana-Alonso et al., 1995). eEF3 has two close homologues, one of them named eEF3B (HEF3) (Murina et al., 2018). eEF3B shares 84% sequence identity with eEF3 and was suggested to arise from a whole genome duplication in the *Saccharomyces* lineage (Kellis et al., 2004; Maurice et al., 1998; Murina et al., 2018). New1 is the second closest homologue and exhibits 37% sequence identity, and was suggested to play a role in the eukaryotic ribosome biogenesis (Decottignies and Goffeau, 1997; Li et al., 2009). The same role was proposed for Arb1 (ABCF2),

but more recent studies revealed that Arb1 is occupying the ribosomal E-site, where it stimulates the Vms1-dependent cleavage of the tRNA during the ribosome-associated quality control (RQC) pathway – mechanism which will be discussed in more detail in section 1.4 (Dong et al., 2005; Li et al., 2009; Su et al., 2019). Gcn20 (ABCF3) - a part of the general amino acid control (GAAC) pathway - senses stresses, including amino acid starvation (Castilho et al., 2014; Hinnebusch, 2005; Masson, 2019). The previous examples of the human P-glycoprotein and bacterial ARE strains illustrate how important further investigations of ABC(F) proteins are, especially since their mutations lead to many human diseases like cystic fibrosis, retinal degeneration, adrenoleukodystrophy, cardiomyopathies or diabetes (Dean et al., 2001; Decottignies and Goffeau, 1997; Koehn et al., 2008).

1.3.1 The eukaryotic elongation factor 3 (eEF3)

Besides the two highly conserved GTPases eEF1A and eEF2, fungi translation elongation requires a third essential factor - the ATPase eEF3 (Kamath and Chakraburty, 1989; Skogerson and Wakatama, 1976; Uritani and Miyazaki, 1988a). For decades, this factor was suggested to be fungi specific, but some recent bioinformatic data revealed its presence in a wide range of unicellular eukaryotes such as oomycete *Phytophthora infestans* (Mateyak et al., 2018). Whereas eEF1A and eEF2 are strictly GTP dependent, eEF3 is more variable and accepts in addition to ATP, also GTP and ITP (Kamath and Chakraburty, 1989; Miyazaki et al., 1988; Moldave, 1985). Whereas yeast eEF1A and eEF2 were shown to be able to substitute for their counterparts in an *in vitro* translation system in mammals and *vice versa*, dependence on eEF3 was only shown for yeast translation so far (Skogerson and Engelhardt, 1977). The intrinsic ATPase activity of eEF3 is low, but strongly stimulated by the ribosome (Uritani and Miyazaki, 1988a). eEF3 was shown to predominantly bind to polysomes and suggested to promote the release of the tRNA^{deacyl} from the E-site during elongation (Andersen et al., 2006; Hutchison et al., 1984; Triana-Alonso et al., 1995). This activity is strictly dependent on the presence of ATP, but not ADPNP (Triana-Alonso et al., 1995). Simultaneously, eEF3 was proposed to influence the rate of the TC binding to the A-site (decoding) increasing translation fidelity, which was supported by the fact that eEF3 is directly interacting with eEF1A (Anand et al., 2006; Anand et al., 2003; Uritani and Miyazaki, 1988b). eEF3-eEF1A complex formation was enhanced in the presence of ADP, so in the post-ATP hydrolysis state of eEF3. eEF3's influence on TC binding also supports the allosteric three side model, which postulates that the ribosomal A- and E-sites are linked to each other in the manner that the tRNA occupation of the E-site reduces the affinity for tRNA of the A-site and *vice versa* (Triana-Alonso et al., 1995). Although *in vitro* studies proposed an additional function of eEF3 in ribosome recycling, where it was shown to split the PoTC in presence of ATP, ribosome profiling data of the yeast eEF3 depletion strain supported EF3's function in translation elongation rather than recycling (Kasari et al., 2019; Kurata et al., 2010; Kurata et al., 2013). Furthermore, eEF3 was suggested to be implicated in translational control, since it has many interaction partners involved in translational

efficiency including eEF2, She2 and Stm1 (Du et al., 2008; Szklarczyk et al., 2019; Van Dyke et al., 2009). Increased levels of Stm1 for example negatively alter the association of eEF3 with the ribosome thus modulating translation elongation (Balagopal and Parker, 2011; Van Dyke et al., 2009). Interestingly, eEF3 expression is altered during starvation for nutrients and its overexpression disturbs Gcn1's interaction with the ribosome, thus modulating the kinase activity of Gcn2 (Grousl et al., 2013; Visweswaraiah et al., 2012).

eEF3 is an 1044 amino acid large protein comprising a N-terminal HEAT (Huntingtin, elongation factor 3 (EF3) 1, protein phosphatase 2A (PP2A) 2, and the yeast PI3-kinase TOR1) repeat domain, a four-helix bundle (4HB) domain, the two ABC1 and ABC2 domains as well as an unique chromo domain (CD) insertion within ABC2 (Figure 6A) (Kambampati et al., 2000). In general, the solenoid structure of HEAT repeats was reported to function as scaffold and anchoring, whereas CD insertions in (mostly chromatin remodeling) proteins were shown to interact with RNA and DNA, especially with methylated lysines (me-K) in histone tails (Andrade and Bork, 1995; Brehm et al., 2004; Kobe et al., 1999; Nielsen et al., 2002; Yap and Zhou, 2011). The 9.9 Å cryo-EM structure of the *in vitro* reconstituted eEF3-80S complex revealed that the eEF3-HEATs contact the 40S head and the eEF3-ABC2 the CP of the 60S, whereas the CD was shown to point towards the ribosomal L-stalk and was therefore suggested to influence its conformation (Figure 6B) (Andersen et al., 2006). *In vitro* studies showed that mutations within the CD compromise ATPase activity, but not ribosome binding (Sasikumar and Kinzy, 2014). Based on the fact that the complex was reconstituted *in vitro* with RNCs lacking the E-site tRNA, it remained elusive, which ribosomal species eEF3 binds to *in vivo* and exactly how the eEF3-CD is able to influence the position of the L1-stalk.

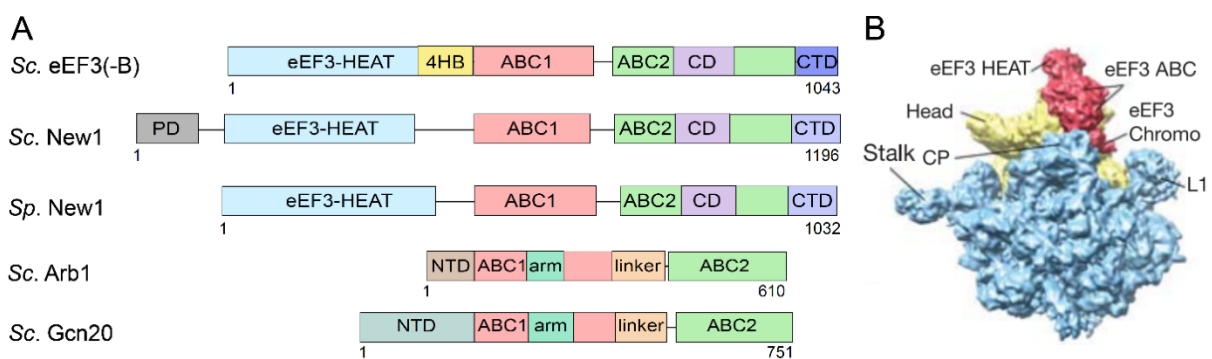


Figure 6. The yeast ABCF proteins. (A) Schematic of the domain organization of the five yeast ABCF proteins eEF3, eEF3-B, New1, Arb1 and Gcn20. PD, prion domain; 4HB, four-helix-bundle; CD, chromo domain; CTD, C-terminal domain; NTD, N-terminal domain; Sc, *Saccharomyces cerevisiae*; Sp, *Saccharomyces pombe*. (B) Cryo-EM structure of the *in vitro* reconstituted eEF3-80S complex at 9.9 Å resolution. (Scheme based on (Murina et al., 2018) and cryo-EM structure adapted from (Andersen et al., 2006)).

1.3.2 The [NU⁺] prion formation protein 1 (New1)

As mentioned previously, the fungi-specific New1 protein is the second closest homologue of eEF3. New1 knock-out revealed that it is non-essential and leads to cold sensitivity, but its exact function is unknown (Li et al., 2009). New1 and eEF3, both share the same domain architecture (HEAT, 4HB, ABC1/2, CD) with exception of an additional N-terminal prion domain present in New1 (**Figure 6A**) (Michelitsch and Weissman, 2000; Murina et al., 2018; Santoso et al., 2000). Prions are self-propagating β -sheet-rich amyloid protein aggregates and known to be infectious in mammals and involved in many neurodegenerative diseases including Huntington's and Alzheimer's Disease (Brundin et al., 2010; Gomez-Gutierrez and Morales, 2020). In contrast to its pathogenic quality in mammals, prions in yeast form predominantly in a sequence-specific manner and are responsible for the epigenetic control of protein activity leading to adaptation during changed environmental conditions (Liebman and Chernoff, 2012; True and Lindquist, 2000). Although the YNGQ repetitive prion region in New1 was shown to be responsible for formation of the [NU⁺] prion, it is not conserved among fungi, e.g. it is present in *S. cerevisiae* but missing in *S. pombe* (**Figure 6A**) (Murina et al., 2018; Osherovich and Weissman, 2001). Since New1 was shown to colocalize with actively translating polysomes, it makes an interesting potential target in the translational process (Li et al., 2009).

1.4 Ribosome stalling and the ribosome-associated quality control (RQC)

Correctly translated proteins are involved in all areas of cellular physiology and therefore the transcription and translation machineries developed numerous mechanisms to ensure accurate protein synthesis. Kinetic proofreading during codon-anticodon recognition or the editing mechanism of the aminoacyl-tRNA synthetases, which link the correct amino acid with the correct tRNA are only two of numerous examples leading to a remarkable translational accuracy, but however one of ten synthesized proteins show at least one miscoded amino acid (Drummond and Wilke, 2008; Hopfield, 1974; Perona and Gruic-Sovulj, 2014; Wolff et al., 2014; Yadavalli and Ibbá, 2012; Zaher and Green, 2009). Gene mutations, faulty gene expression or chemical damage lead to the synthesis of aberrant protein products, which compromise the cellular fitness and integrity of organelles such as mitochondria or the ER (Simms et al., 2014; Wurtmann and Wolin, 2009). Especially mRNA molecules are prone to constant changes and modifications. Hence, monitoring of the mRNA and protein quality during translation is highly important and performed by a variety of specialized machineries, which subject them to rapid degradation.

The cell senses potential aberrant protein products not directly by monitoring the faulty mRNA sequences or the composition of the nascent polypeptide, but by 'observing' the state of the ribosome. Ribosomes, which stall on mRNAs represent the key signal for the quality control machineries (Brandman and Hegde, 2016; Joazeiro, 2017; Matsuo et al., 2017). Stalled ribosomes indicate that whether the mRNA, the protein or even the ribosome itself might be corrupted, giving

the opportunity to target and remove a potentially toxic product(s) at a very early stage. Ribosome stalling can have many different causes, such as aberrant or damaged mRNA or tRNA, immature 60S subunits or nonstop mRNA generated by endonuclease cleavage or premature mRNA polyadenylation (Buskirk and Green, 2017; Joazeiro, 2017, 2019; Sarkar et al., 2017). The exact molecular mechanisms that inhibit elongation and drive ribosome stalling are widely unknown, but some structural and biochemical studies of ribosomes stalled on a poly(A) mRNA revealed that the mRNA is able to form a stable single-stranded helix within the DC of the ribosome leading to its deformation and a potential clash with an incoming A-tRNA, thus preventing elongation (Chandrasekaran et al., 2019; Tesina et al., 2020). Recent live-cell imaging and *in vitro* studies showed that ribosomes stalled on poly(A) mRNAs result in long queues of collided ribosomes and that the length of the queue as well as the collision frequency is connected to the efficiency of signal recognition (Goldman et al., 2021; Yan and Zaher, 2021). Ribosome stalling leads to numerous and specific cellular responses including the inhibition of translation initiation, activation of the nonstop- and no-go-mediated decay (NSD, NGD) of mRNA, dissociation of ribosomal subunits (ribosomal rescue) and the ribosome-associated quality control (RQC) pathway, whereas the focus in this thesis is put on the two latter ones (Brandman and Hegde, 2016; Buskirk and Green, 2017; Joazeiro, 2017).

As already discussed in section 1.2.4, after a successful translation of an mRNA ORF the ribosome reaches the stop codon and subsequently can be recognized by the canonical factors eRF1 and eRF3, and Rli1 splits the 80S ribosome into its individual subunits, followed by subunit recycling. The same mechanism takes place when ribosome stalling occurs before reaching the stop codon. This ribosomal stalling occurs on internal mRNAs or on the 3' end of truncated mRNA sequences, and both stalling substrates require a different set of rescue factors (**Figure 7**). The recognition of ribosomes stalled on internal mRNA sequences is initially sensed by the E3 ubiquitin-ligase Hel2 (also Rqt1, ZNF598 in mammals) together with Asc1 (RACK1 in mammals) as well as the RQC-trigger (RQT) complex composed of the RNA helicase family protein Slh1 (also Rqt2), the ubiquitin-binding protein Cue3 (Rqt3) and Ykr023w (Rqt4) (Garzia et al., 2017; Ikeuchi et al., 2019; Juszkiwicz and Hegde, 2017; Matsuo et al., 2017; Sitron et al., 2017; Sundaramoorthy et al., 2017). Hel2 together with the E2 enzyme Ubc4 catalyzes the mono-ubiquitylation of the 40S protein uS10 at a specific lysine residue and this tagging is responsible for the subsequent recruitment of ribosomal splitting factors (Matsuo et al., 2017). UV-crosslinking and mass spectrometry revealed that Hel2 is recruited to or stabilized on the 40S subunit in an Asc1-dependent manner (Winz et al., 2019). The C-terminus of Hel2 seems to directly interact with the 18S rRNA and mRNA – an interaction required for both the RQC pathway and the NGD. Deletion of the ubiquitin ligase Hel2 or the 40S ribosomal protein Asc1 leads to enhanced protein synthesis downstream of the stalling site (Brandman et al., 2012; Letzring et al., 2013). Stalling ribosomes form so-called disomes, consisting of a leading stalled and a second ribosome, which collided into it. A disome forms a unique structural unit between the leading stalled and the collided ribosome and was proposed by

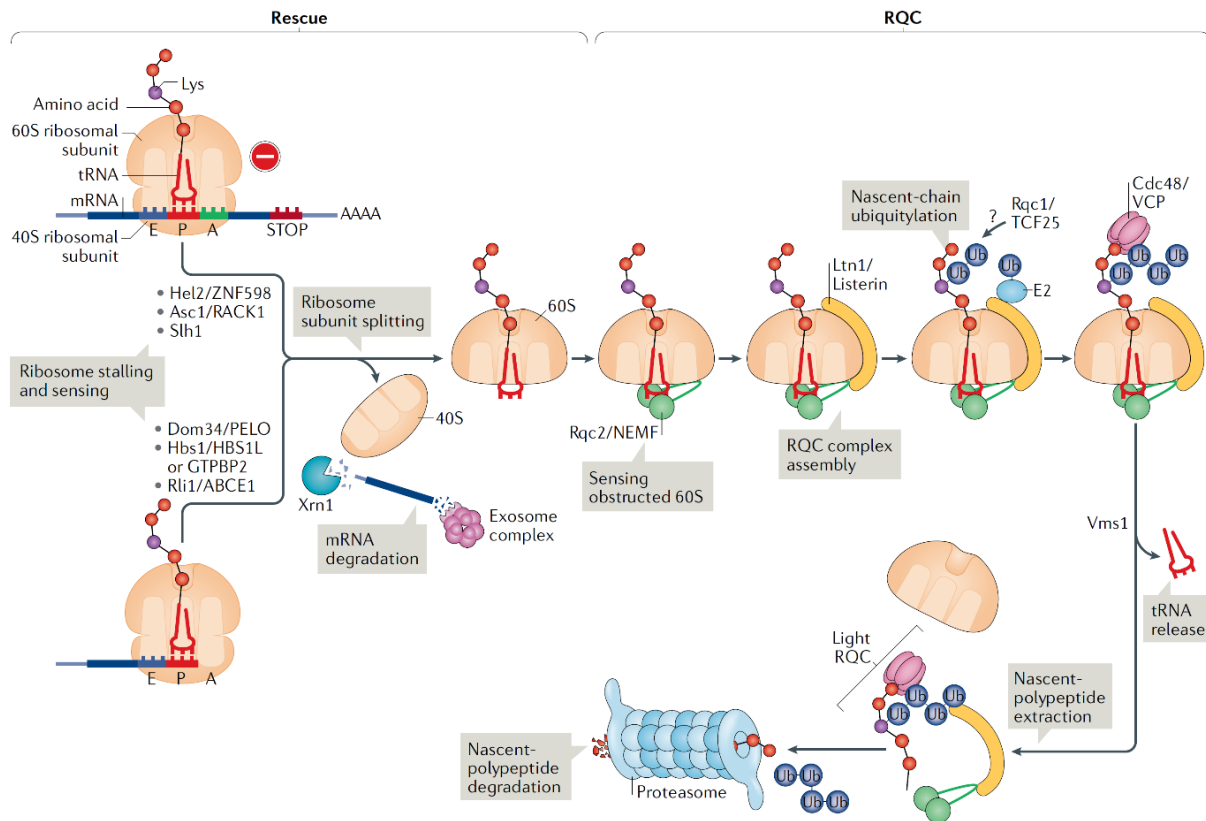


Figure 7. The eukaryotic ribosome rescue and the RQC pathway. Basic overview of the ribosome rescue and RQC system and their involved factors. In the first step Hel2/ZNF598, Asc1/RACK1 and Slh1 or Dom34/Pelota, Hbs1/HBS1L or GTPBP2 and Rli1/ABCE1 mediate and induce 80S ribosomal splitting, when the ribosome stall on internal mRNA and on the 3' end of an mRNA, respectively. The split 40S can be recycled and the mRNA degraded by Xrn1 and the exosome. In the second step, the 60S subunit bound to a P-site tRNA with a polypeptide nascent chain subsequently enters the RQC pathway. Initially, the 60S-tRNA-NC is recognized by Rqc2/NEMF subunit of the RQC complex, which binds the exposed 60S-tRNA and recruits the E3 ligase Ltn1/Listerin. Whereas Ltn1/Listerin attached polyubiquitin chains on the NC, the Rqc1/TCF25 subunit of the RQC complex binds the ribosome (in an until unknown way). The ubiquitin signal recruits the AAA+ ATPase Cdc48/VCP and its cofactors, which extracts the NC after the tRNA-NC conjugate become released from the 60S by Vms1/ANKZF1, and the NC can be finally degraded by the proteasome (scheme adapted from (Joazeiro, 2019)).

Simms et al. 2017 for the first time to be responsible for signal recognition by Hel2 (Simms et al., 2017). A recent selective ribosome profiling study reveals that Hel2 is recognizing collisions on mRNAs encoding secretory protein prior to ER engagement that preferentially lack the recognition site for the signal recognition particle (SRP) (Matsuo and Inada, 2021).

In contrast, Hbs1, Dom34 and Rli1 (HBS1L and GTPBP2, Pelota and ABCE1 in mammals) are key players when ribosomes stall at the 3' end of a truncated mRNA. In this scenario, the ribosomal A-site is not occupied by an mRNA and thus prevents the interaction with the tRNA-eEF1A complex,

which would continue elongation, or with the eRF1-eRF3 complex, which would induce termination. Hbs1 and Dom34 are the mammalian homologues to the canonical release factors eRF1 and eRF3 responsible for the recruitment of Rli1 and ribosomal splitting. Like eEF1A and eRF3, Hbs1 is a trGTPase, which all bind at the GTPase center near the ribosomal A-site (Becker et al., 2011). In the first step, the GTP-Hbs1-Dom34 complex binds the stalled ribosome. Hbs1 interacts via its C-terminus near the mRNA entry channel, whereas Dom34 binds within the empty ribosomal A-site inserting its β -loop into the mRNA channel (Hilal et al., 2016). After a subsequent hydrolysis of Hbs1-GTP, Hbs1-GDP dissociates, allowing full accommodation of Dom34 into the ribosomal A-site, which recruits the ATPase Rli1 responsible for the final splitting step of the stalled ribosome (Pisareva et al., 2011; Shoemaker et al., 2010; Shoemaker and Green, 2011). *In vitro* studies in yeast and mammals showed that Hbs1-Dom34 are also able to resolve stalled ribosomes in the case where the mRNA occupies the A-site, e.g. in the case of stalling on poly(A) and non-stop mRNAs, mRNAs including stable stem-loops or when aa-tRNAs are unavailable (Becker et al., 2011; Ikeuchi et al., 2016; Shao et al., 2013; Shoemaker et al., 2010; Shoemaker and Green, 2011).

In both cases the mRNA-80S complex is split into mRNA, 40S and 60S ribosomal subunits, whereas the 60S remains associated with the P-site tRNA attached to the NC (**Figure 7**) (Brandman and Hegde, 2016; Joazeiro, 2019). In the next step the nascent polypeptide and the mRNA need to be degraded since they are potentially aberrant. The mRNA becomes degraded by the 5'-3' exoribonuclease Xrn1 and 3'-5' by the Ski2-Ski3-Ski8 helicase together with the exosome. A recent cryo-EM structure of the 80S ribosome-Xrn1 nuclease complex revealed that the conserved core of Xrn1 is directly interacting with the ribosomal mRNA exit site in the manner that the mRNA is channeled directly into the nuclease center of Xrn1 and highlights its efficiency in rapid degradation (Tesina et al., 2019). Within the Ski2-Ski3-Ski8 complex, the Ski2 helicase is placed near the ribosomal mRNA entry tunnel, where the 3' mRNA overhang is directly channeled from the 40S subunit to the helicase core of Ski2 primed for degradation by the exosome (Schmidt et al., 2016). Concomitantly, the NC attached to the tRNA of the 60S subunit is targeted by the RQC complex (**Figure 7**). In the first step, Rqc2 (Tea2, NEMF in mammals) binds the 60S and the exposed P-tRNA, where it prevents 40S rejoining and recruits and stabilizes the RING domain E3 ubiquitin-protein ligase Ltn1 (originally Rkr1, Listerin in mammals) (Defenouillere et al., 2013; Shao et al., 2015). Ltn1 binds stably to the 60S and catalyzes the attachment of polyubiquitin chains on a lysine residue within the NC sequence (**Figure 7**) (Bengtson and Joazeiro, 2010; Shao et al., 2015; Shao et al., 2013). The now proteolytic tagged NC together with the Rqc1 subunit of the RQC complex, both serve as a signal for the recruitment of the AAA+ family ATPase Cdc48 (VPC or p97 in mammals) and its cofactors Npl4 and Ufd1. While the eRF1 paralogue Vms1 (ANKZF1 in mammals) - a peptidyl-tRNA hydrolase - releases the NC, Cdc48 extracts and transfers the NC to the 26S proteasome for its subsequent degradation (Su et al., 2019; Verma et al., 2018; Zurita Rendon et al., 2018). A recent cryo-EM structure showed, that Vms1 directly binds to the 60S, whereas its Vms1-like release factor 1 (VLR1) domain overlaps with that of the Rqc2 binding site

in the A-site, where it reaches via its GSQ motif towards the tRNA CCA-end for nucleolytic cleavage - a process promoted by the already mentioned ABCF ATPase Arb1 located within the ribosomal E-site (Su et al., 2019).

In case the NC cannot be ubiquitinated, because the portion of the NC is not long enough to be exposed to the outside of the exit tunnel or a short NC part does not contain an ubiquitination-competent lysine, Rqc2 recruits aa-tRNAs, which extend the NC with C-terminal alanine and threonine (CAT) tails (Shen et al., 2015). The CAT-tails attached via this non-canonical elongation reaction push the nascent polypeptide out of the ribosomal exit tunnel until a lysine becomes exposed, which can be in turn ubiquitinated and the NC mediated to degradation (Kostova et al., 2017; Shen et al., 2015; Sitron and Brandman, 2019). Newer studies revealed that CAT-tails also enable Ltn1 to access other NC residues than lysine for ubiquitinylation (Sitron and Brandman, 2019). Even when this mechanism fails, the CAT-tails serve as degrons and enable the proteasomal degradation of the NCs in a Ltn1-independent manner by the E3 ubiquitin ligase Hul5 (Sitron and Brandman, 2019; Sitron et al., 2020). Degradation of these potentially harmful polypeptides is essential, since 'free' CATylated NCs form myloid-like aggregates, which disrupt protein homeostasis and cause proteotoxic stress (Choe et al., 2016; Defenouillere et al., 2016; Yonashiro et al., 2016).

More recently, a similar RQC mechanism was found in some bacteria, involving the factor RqcH, which is the homologue of the eukaryotic Rqc2/NEMF and was suggested to act on some non-stop ribosomal complexes (Joazeiro, 2019; Muller et al., 2021; Yan and Zaher, 2019). But in contrast to eukaryotes, the major ribosome rescue pathway of trans-translation in bacteria use an entirely different quality control system for targeting defective mRNA and label the NC for degradation (Buskirk and Green, 2017; Muller et al., 2021). For example, in case of ribosomal stalling at the end of a truncated mRNA lacking a stop codon, the bacterial system developed a mechanism, which involves the action of tmRNA - an RNA with tRNA- and mRNA-like properties (Himeno et al., 2014; Janssen and Hayes, 2012; Moore and Sauer, 2007; Muller et al., 2021). The tRNA-like region is coding for alanine and binds within the ribosomal A-site where it restarts translation, whereas the mRNA-like part is translating a short degradation tag (ssrA peptide) attached to the C-terminus of the nascent polypeptide chain leading to termination, NC release and its degradation.

The importance and the need for further investigations of the RQC pathway is highlighted by the fact, that mutations in RQC components lead to neurodegeneration in mice as well as other human inherited diseases (Chu et al., 2009; Ishimura et al., 2014; Scheper et al., 2007).

1.5 The integrated stress response (ISR) in yeast

Cells must be able to adapt to environmental stresses in a fast and efficient way to maintain their health. In mammals, the integrated stress response (ISR) is able to sense environmental and pathological conditions via four specialized serine/threonine kinases: double-stranded RNA-

activated protein (protein kinase R, PKR), PKR-endoplasmic reticulum (ER)-related kinase (PERK), heme-regulated inhibitor (HRI) and the general control non-derepressible 2 (GCN2) (Figure 8) (Costa-Mattioli and Walter, 2020; Donnelly et al., 2013; Pakos-Zebrucka et al., 2016; Taniuchi et al., 2016). Each of the kinases is responsible for sensing a specific stressor. PKR counteracts viral infections by inhibiting translation of the viral mRNA and promoting apoptosis, whereas PERK is activated when misfolded proteins accumulate at the ER (ER stress) (Donnelly et al., 2013). HRI links heme availability with translation of globin mRNA, which together form hemoglobin and thus HRI is protecting erythroid cells from the accumulation of harmful globin aggregates (Chen, 2014; Han et al., 2001). Finally, the kinase Gcn2 is known to function as a sensor for amino acid availability and is activated during nutrient deprivation (Chaveroux et al., 2010; Hinnebusch, 2005).

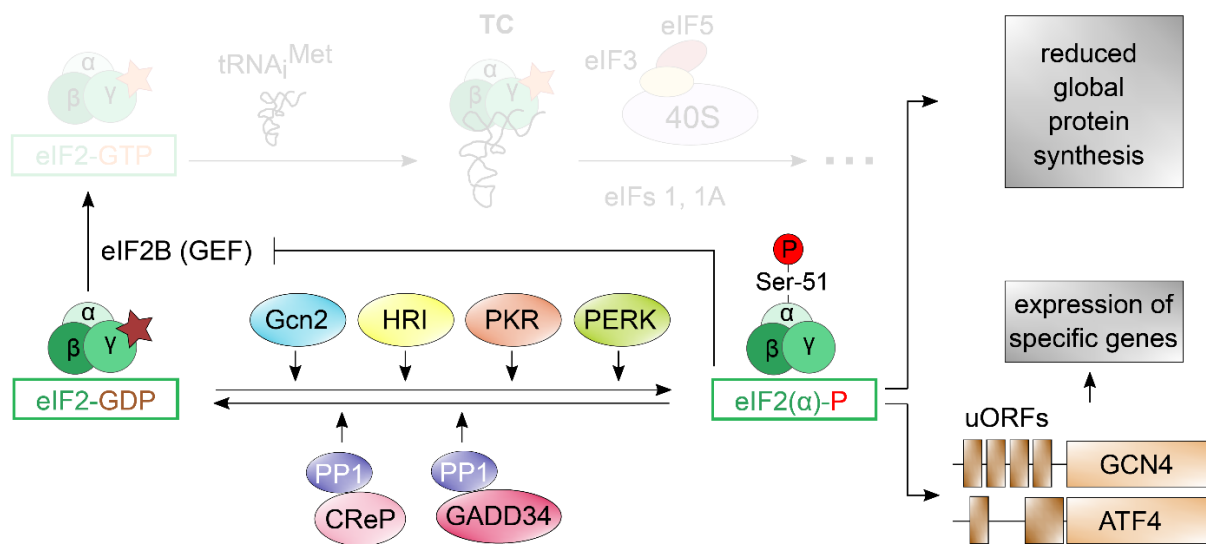


Figure 8. The ISR pathway in mammals. During different stress conditions, the four protein kinases Gcn2, HRI, PKR and PERK are able to phosphorylate Ser-51 of the eIF2 α . The phosphorylation of eIF2 α prevents the recycling of eIF2-GDP into eIF2-GTP by eIF2B and thus the involvement of eIF2-GTP into the formation of the TC. On the one hand this leads to a reduced global protein synthesis and on the other hand to a simultaneous translation of specific mRNAs containing uORFs coding for transcription activators such as GCN4 in yeast and ATF4 in mammals, which control the expression of a numerous genes involved in cellular adaptation. The PP1/CREP and PP1/GADD34 complexes dephosphorylate eIF2 α and terminate the ISR after the stress passed by to maintain cellular homeostasis. The ISR in yeast involves only the Gcn2 kinase as well as the phosphatase GLC7. Scheme based on (Castilho et al., 2014) and (Pakos-Zebrucka et al., 2016).

Importantly, all four kinases are stimulated via oxidative stress and additionally show an overlapping activation in response to different stimuli, e.g. PERK is able to sense glucose

deprivation and together with Gcn2 it is able to regulate host response to viral infection (Berlanga et al., 2006; Cheng et al., 2005; de la Cadena et al., 2014; Harding et al., 2003; Suragani et al., 2012). HRI can be induced in a heme-independent manner by cytoplasmic stress or 26 proteasome inhibition, but also relays mitochondrial stress to the cytosol together with Oma1 and Dele1 (Guo et al., 2020; Han et al., 2001; Lu et al., 2001; Yerlikaya et al., 2008). Interestingly, the kinases show the ability to compensate for each other, for example the knockdown of PERK in 'stressed' HeLa cells leads to upregulation and activation of Gcn2 and *vice versa* (Roobol et al., 2015). PKR, PERK, HRI and Gcn2 possess distinct regulatory domains, which gives each kinase the opportunity to fulfill specific functions (Pakos-Zebrucka et al., 2016). In contrast, all kinases have a homologous protein kinase (PK) domain, which need to dimerize and autophosphorylate for its activation and allow to converge on phosphorylation of a single serine (Ser-51) at the α subunit of the eukaryotic initiation factor eIF2 (eIF2 α -P) (**Figure 8**) (Baird and Wek, 2012; Chaveroux et al., 2010; Hinnebusch, 2005). In this form, eIF2-GDP is blocked and cannot be recycled to eIF2-GTP by its GEF eIF2B, thus disabling eIF2 to enter another round of translation initiation leading to a reduced formation of the TC (**Figure 8**) (Baird and Wek, 2012). A further mechanism contributing to the inhibition of translation initiation was shown recently for Gcn2 (Dokladal et al., 2021). Besides eIF2 α , Gcn2 was shown to also be able to directly phosphorylate eIF2 β and thus promote its association with eIF5, which prevents its spontaneous nucleotide exchange from eIF2-GDP to eIF2-GTP. This phosphorylation of eIF2 leads to a general decrease in global translation conserving nutrients and energy, and simultaneously to an increased translation of specific mRNAs containing unique upstream open reading frames (uORF) in their 5'-untranslated regions (**Figure 8**) (Harding et al., 2000; Hinnebusch, 2005). Under non-deprived conditions, ribosomes scan along these mRNAs and arrive at those inhibitory uORFs leading to ribosome dissociation before the ribosome has reached the ORF. In the case of stress and reduced TC availability, the scanning of the ribosome is 'leaky' and may bypass the inhibitory uORFs resulting in a de-repression of translation of specific mRNAs. The ORFs are coding for transcription factors that up-regulate the synthesis of a large array of proteins, which drive a new transcriptional program and thereby maintain or re-establish the physiological homeostasis during stress. For example, the transcriptional activator GCN4 in yeast (ATF4 in mammals) induces expression of genes encoding key amino acid biosynthetic enzymes that counteract amino acid deficiency (**Figure 8**) (Castilho et al., 2014; Hinnebusch, 2005). Although in the yeast system, the ISR pathway is induced by only one of the four mentioned kinases - the kinase Gcn2 - the ISR pathways are very similar in yeast and mammals (Pakos-Zebrucka et al., 2016). Since the yeast ISR was initially identified as a response to starvation for amino acids, which results in an up-regulation of genes required for amino acid synthesis, the pathway is also known as the GAAC pathway (Castilho et al., 2014; Hinnebusch, 2005). Activation of Gcn2 has been a subject of investigation for over three decades and the proposed key signal for kinase activation are tRNA^{deacyl} (Hinnebusch, 2005). The model postulates that starvation for one or several amino acids leads to accumulation of tRNA^{deacyl}, which bind and activate Gcn2 together with its regulators Gcn1 and Gcn20 (**Figure 9**) (Castilho et al., 2014; Hinnebusch, 2005).

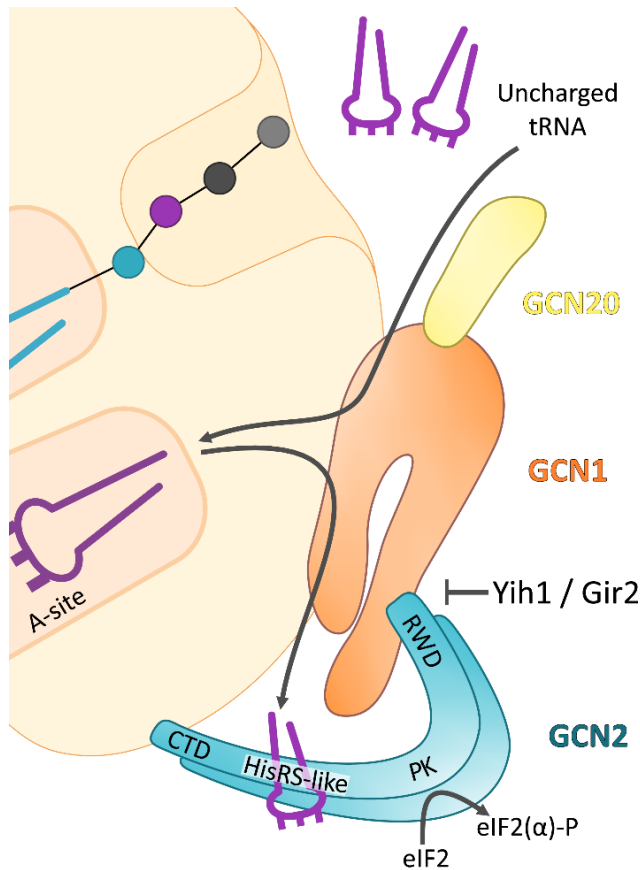


Figure 9. The ISR pathway in mammals. The scheme represents the current postulated model of Gcn2 activation. During starvation, $\text{tRNA}^{\text{deacyl}}$ bind within the ribosomal A-site, acting as a signal for the Gcn complex. In the first step Gcn1 contacts the ribosome and recruits or directly delivers Gcn2, and together Gcn1-Gcn2 bind to the ribosome. Gcn1 was also proposed to directly transfer the $\text{tRNA}^{\text{deacyl}}$ to the HisRS-like region of Gcn2, leading to its subsequent activation and phosphorylation of eIF2 α . Gcn20 itself does not establish any contacts, neither with the ribosome nor with Gcn2, but only with Gcn1 and was suggested to stabilize Gcn1 on the ribosome enhancing Gcn2 activation (adapted and adjusted from the Master's Thesis of Alexandra Spoetter and (Castilho et al., 2014)).

In addition to nutrient deprivation, other stress conditions were correlated with the activation of the kinase, including glucose starvation, high-salt conditions, starvation for purines, treatment with alkylating agents as well as oxidative and UV stress, which will be discussed in further detail in following parts of the thesis (Anda et al., 2017; Deloche et al., 2004; Goossens et al., 2001; Masson, 2019; Natarajan et al., 2001; Rolfes and Hinnebusch, 1993; Yang et al., 2000).

Whereas yeast cells express over 100 different protein kinases, phosphatases play a crucial role for maintaining cellular homeostasis after the stress has passed (Barford, 1995; Breikreutz et al., 2010). To do so and to terminate the ISR in mammals, eIF2 α -P becomes dephosphorylated by the serine/threonine protein phosphatase (PP1) complex. The complex consists of the PP1 catalytic subunit (PP1c) and one of the two regulatory subunits, one of which is the constitutive repressor of eIF2 α phosphorylation (CReP, also PPP1R15B) (Figure 8). CReP is constantly expressed during non-stress conditions and PP1c/CReP is responsible for keeping the eIF2 α -P levels low and thus ensuring translational homeostasis (Jousse et al., 2003). In contrast, the growth arrest and DNA damage-inducible protein (GADD34, also PPP1R15A) is expressed during stress and ISR induction (Figure 8) (Kojima et al., 2003). The GADD34/PP1c complex acts as an important negative regulator to restore translation after cellular stress, but was also implicated in the induction of apoptosis when cell homeostasis cannot be re-established (Novoa et al., 2003). In contrast, yeast lack the targeting subunit homologues CReP and GADD34, but possess only the functional

homologue of PP1c, the phosphatase GLC7, which alone is responsible for the dephosphorylation of eIF2 α -P (Feng et al., 1991; Wek et al., 1992). *In vitro* and *in vivo* studies showed that eIF2 γ by itself possesses a PP1-binding motif (KKVAF), which is able to recruit GLC7 leading to a subsequent dephosphorylation of eIF2 α (Rojas et al., 2014).

The ISR response in yeast and mammals is extremely complex and the GCN4 / ATF4 pathways have the potential to influence more than 400 genes which are inducing conflicting processes of cell survival and cell death (Pakos-Zebrucka et al., 2016). In higher eukaryotes, Gcn2 was implicated in many diseases, such as cancer and Alzheimer's disease, impaired viral defense, the immune system, the pathogenesis of COVID-19, and plays a role in important processes, such as long-term memory formation, neuronal cell development, aging, obesity and many more (Castilho et al., 2014; Kim et al., 2020; Lehman et al., 2015; Ma et al., 2013; Philips and Khan, 2021; Ye et al., 2010). New reports are constantly emerging on new biological roles for Gcn2 highlighting its importance as a pharmacological target.

1.5.1 The protein kinase Gcn2

The yeast Gcn2 kinase is a 1659 amino acid long (~190 kDa) protein that co-sediments with ribosomes, particularly with active polysomes, and was shown to have a higher affinity to 60S than to 40S subunits (Castilho et al., 2014; Ramirez et al., 1991). With 279 molecules/cell it has a relatively low abundance (Ghaemmaghami et al., 2003). Gcn2 contains five conserved folded domains, including an N-terminal RWD (termed from its presence in RING-finger proteins, WD repeat-containing proteins and the yeast DEAD-like helicases) domain, a pseudo protein kinase (ψ PK) domain (with no enzymatic function), a catalytically active eIF2 α protein kinase (PK) domain, a histidyl-tRNA synthetase-like (HisRS-like, enzymatically inactive) domain and a C-terminal domain (CTD) (**Figure 10**) (Castilho et al., 2014; Hinnebusch, 2005). In addition, a 'charged linker' connects the RWD to the ψ PK domain.

In vivo, Gcn2 forms a constitutive dimer mediated by its CTD, but also the HisRS-like and the PK have been shown to be involved in dimer formation (He et al., 2014; Qiu et al., 1998). The CTD is also responsible for the association with the 80S ribosome as well as (together with the HisRS-like domain) for binding of deacylated tRNAs (Castilho et al., 2014; Hinnebusch, 2005). Three lysine residues (K1552, K1553 and K1556) within the CTD are crucial for ribosome and tRNA binding (Wek et al., 1995). Notably, dimerization of Gcn2 was shown to be unnecessary for ribosome association. Crystal structures of yeast and mammalian CTDs revealed a common conserved core, but their interdigitated dimeric structures differed, suggesting some regulatory differences. Nevertheless, in both cases, dimerization via the CTD is critical for efficient translational control by Gcn2 (He et al., 2014). Interestingly, mouse Gcn2 does not appear to associate with ribosomes, whereas yeast Gcn2 does (He et al., 2014). In contrast to the yeast Gcn2-80S association via Gcn2-CTD, the human Gcn2 ribosomal interaction was shown to involve the CTD, ψ PK, PK as well as the HisRS-like domain (Inglis et al., 2019). The HisRS-like domain is similar to the histidyl-tRNA

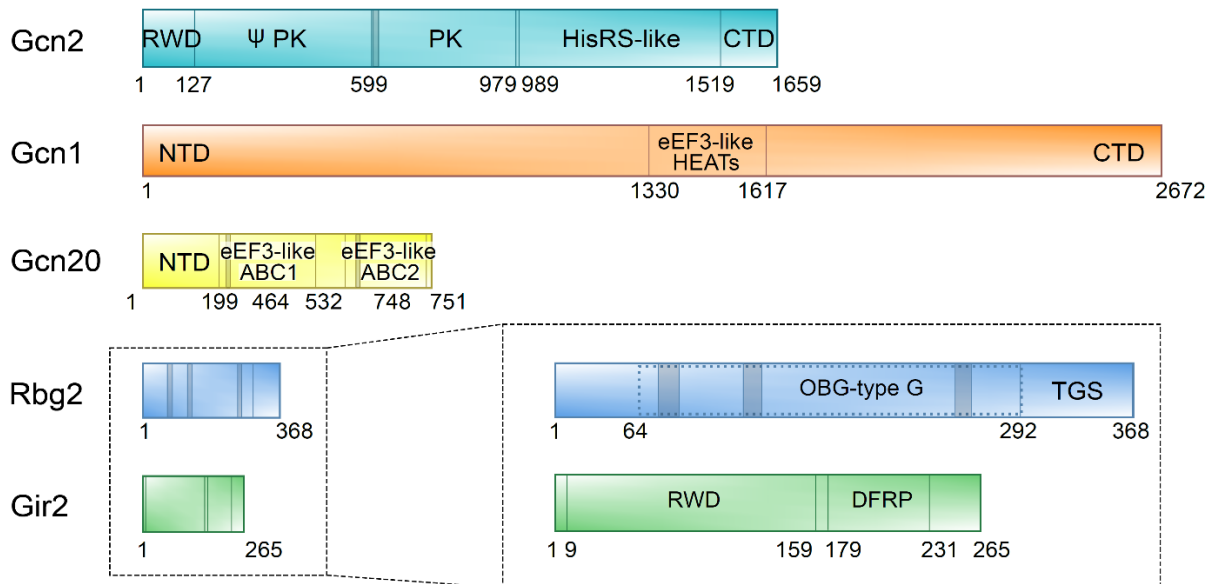


Figure 10. Simplified domain organization of Gcn1, Gcn2, Gcn20, Rbg2 and Gir2. Scheme of the mentioned proteins shown due to their domain organization as labeled. The shaded regions are representing the individual nucleotide binding domains (ATP binding for Gcn2 and Gcn20 and GTP for Rbg2). RWD, RING-finger proteins, WD repeat-containing proteins and the yeast DEAD-like helicases; ψ PK, pseudo protein kinase domain; PK, protein kinase domain; HisRS-like, histidyl-tRNA synthetase-like domain; CTD, C-terminal domain; NTD, N-terminal domain; eEF3-like, eEF3-like HEAT repeat region; OBG-type G, OBG-type GTPase domain; TGS, ThrRS, GTPase, and SpoT; DFRP, DRG family regulatory protein domain (adapted from (Castilho et al., 2014), (Ishikawa et al., 2013) and the database UniProt).

synthetase, which belongs to the class II synthetases (Castilho et al., 2014; Ruff et al., 1991). This class of synthetases contain a motif 2 (m2) involved in binding of the tRNA acceptor stem (Ruff et al., 1991). It was shown that mutations of Gcn2 m2 (Y1119, R1120) result in a severe decrease of phosphorylation of eIF2 α *in vivo* and *in vitro* (Wek et al., 1995; Zhu et al., 1996). Studies revealed that the HisRS region of Gcn2 needs to dimerize to efficiently bind tRNA (Qiu et al., 2001).

The PK domain is responsible for phosphorylation of the α subunit of eIF2 on Ser-51 (Hinnebusch, 2005). The catalytic site of the PK is located in a cleft between the N- and C-terminal lobes, which are interconnected by a hinge region (Castilho et al., 2014; Dong et al., 2000; Lageix et al., 2015). Based on the crystal structures of the PK domain of the mouse Gcn2, it could be shown that the wild-type structure bound to ATP/ADPNP exhibited a secluded position resulting from the rigid hinge region between the N- and C-terminal lobes (Padyana et al., 2005). In this closed state important residues for e.g. binding of the ATP triphosphate moiety are not accessible, preventing ATP and eIF2 α binding and catalysis. The binding of tRNA^{deacyl} to the HisRS-like region allows the release of the CTDs and the interaction between the PK and ψ PK domain (Masson, 2019; Padyana et al., 2005). In the consecutively activated state (R794G mutant activates Gcn2 independently of tRNA binding), a rearrangement within the hinge region residues was observed leading to a

breakdown of the hydrogen bonding surrounding the hinge region, which impairs flexibility and leads to separation of the lobes as well as widening of the catalytic cleft (Masson, 2019; Padyana et al., 2005). In the subsequent step, two threonine residues (T882 and T887 in yeast, T898 and T903 in mouse) within the activation loop of the PK are phosphorylated, leading to enhanced activity and stabilization, which was shown to be dependent on intermolecular salt bridge between the kinase domains (Dey et al., 2007; Lageix et al., 2015). The widened catalytic cleft exposes all the important residues to allow efficient binding of ATP and phosphorylation of eIF2 α on Ser-51. Based on the structure of PKR bound to eIF2 α , it was proposed that eIF2 α itself is unfolded and exposes the region carrying Ser-51 upon binding to the Gcn2 PK domain via an induced fit mechanism, thereby ensuring specificity for recognition and phosphorylation by Gcn2 (Dar et al., 2005; Dey et al., 2011). A very recent crystal structure of the human Gcn2 PK domain revealed a parallel dimer organization similar to PKR highlighting the difference to the yeast dimer, which is organized in an antiparallel manner (Maia de Oliveira et al., 2020).

In absence of an activation signal, Gcn2 exhibits an intrinsic mechanism holding itself in an inactive state by forming autoinhibitory interactions between the CTD, the HisRS-like region and the N-terminal lobes of the PK (Dong et al., 2000; Lageix et al., 2015). During amino acid starvation, the autoinhibitory interactions become resolved through binding of deacylated tRNAs and allowing the protein to rearrange, which results in an activation and autophosphorylation of the Gcn2 kinase domain (Lageix et al., 2014; Romano et al., 1998).

The ψ PK domain shows sequence similarity to eukaryotic serine/threonine protein kinases, but lacks the residues necessary for enzyme function (Castilho et al., 2014; Zhu et al., 1996). Nevertheless, this domain was shown to be required for Gcn2 kinase activity *in vitro* and *in vivo* (Wek et al., 1990; Zhu et al., 1996). A regulatory function was also proposed by directly binding to the Gcn2 PK domain during the auto-inhibitory state of Gcn2 (Boudeau et al., 2006; Qiu et al., 1998).

The RWD domain of Gcn2 is related to the ubiquitin-conjugating enzyme (UBC) domain, but also here the catalytic cysteine residues necessary for ubiquitin-conjugating activity are lacking (Castilho et al., 2014; Hunter et al., 2012). The structure of the mouse Gcn2 RWD domain solved by NMR spectroscopy revealed a characteristic YPXXXP motif forming a triple β -turn, which is unique for RWD, the UBC and the Ubiquitin E2 variants (Castilho et al., 2014; Nameki et al., 2004). A recent crystal structure of the human RWD dimer uncovered the formation of a novel crystal packing mode (Hei et al., 2021). The Gcn2 RWD domain is directly interacting with its effector protein Gcn1 and the minimal region for establishing these interactions encompasses residues 1-125 (Kubota et al., 2000). The interaction with Gcn1 is absolutely required for Gcn2 to sense amino acid starvation *in vivo* (Anda et al., 2017; Sattlegger and Hinnebusch, 2000).

1.5.2 Activation and regulation of Gcn2

Based on the energetic costs of a global gene expression reprogramming, the Gcn2 kinase needs to be efficiently activated, but also tightly regulated.

1.5.2.1 Gcn1/Gcn20

For an efficient sensing of the starvation signal, Gcn2 associates with the Gcn1/Gcn20 complex, in which Gcn1 and Gcn2 directly contact the ribosome (**Figure 9**) (Castilho et al., 2014; Hinnebusch, 2005). Both, Gcn1 and Gcn20 exhibit homology to eEF3, an already discussed essential and fungi-specific protein, which removes the tRNA^{deacyl} from the E-site during translation elongation (Andersen et al., 2006; Marton et al., 1997). The role of eEF3 led to a similar model for Gcn1-Gcn20, in which the complex removes the tRNA^{deacyl}, but from the A-site instead of the E-site and delivers it to the HisRS-like region of Gcn2 leading to its activation (Marton et al., 1997; Sattlegger and Hinnebusch, 2005).

With the length of 2672 amino acids (~297 kDa) Gcn1 belongs to a small group of the largest proteins present in yeast with 7,330 copies per cell. Gcn1 co-sediments with mono- and polysomes (Ghaemmaghami et al., 2003; Sattlegger and Hinnebusch, 2005). The protein itself was predicted to consist of at least 45 HEAT repeats through its entire length. No homology to any other protein was determined, but only its middle portion (residue 1330-1641) is homologous to the N-terminal eEF3 HEAT repeat region and was therefore suggested to compete with eEF3 for the same binding site on the 80S ribosome (**Figure 10**) (Visweswaraiyah et al., 2012). Overexpression of eEF3 lead to inhibition of Gcn2 activation, supporting this prediction (Visweswaraiyah et al., 2012). By contrast, overexpression of Gcn1 leads to an increased association with 80S and growth defects as well as sensitivity to paromomycin suggesting its spatial proximity to the ribosomal A-site (**Figure 9**) (Sattlegger and Hinnebusch, 2000). Importantly, Gcn1 is not required for Gcn2 kinase activity *per se*, but for its activation in response to amino acid starvation (Marton et al., 1993). It also seems to be required for all other stress rearrangements that activate Gcn2 (Castilho et al., 2014).

Gcn1 directly interacts with Gcn2-RWD via its highly conserved CTD (residues 2052-2428) (Sattlegger and Hinnebusch, 2000). Overexpression of the Gcn2-RWD domain sequesters Gcn1 away from its interaction with the full-length Gcn2 and impairs phosphorylation of eIF2 α *in vivo* (Masson, 2019; Sattlegger and Hinnebusch, 2000). Mutation of R2259, or neighboring regions impair Gcn1-Gcn2 interaction, but not influence the binding to the ribosome or Gcn20 (Sattlegger and Hinnebusch, 2000). Mutation of F2291 also leads to a reduced eIF2 α phosphorylation (Kubota et al., 2001). Gcn1 lacking one of its termini has reduced Gcn2 affinity *in vivo* and the lack of Gcn1-NTD results in impaired Gcn1-80S interaction (Sattlegger and Hinnebusch, 2000).

The Gcn1 interaction with the ribosome is mediated by residues 1-2052 (Sattlegger and Hinnebusch, 2000). The identified M7 and M1 mutations (residues 754-796 and 1458-1465 in yeast,

793-834 and 1508-1515 in human) result in reduced Gcn1-80S association and impaired Gcn2 activation, but do not influence Gcn1-Gcn20 interaction (Sattlegger and Hinnebusch, 2005). It could be shown that Gcn1 contacts the ribosomal protein uS10, which is required for full induction of the kinase Gcn2 (Lee et al., 2015).

The EF3-like HEAT repeat region was identified to interact with the N-terminus of Gcn20 (residues 1-189) (Marton et al., 1997; Vazquez de Aldana et al., 1995). In contrast to Gcn1, Gcn20 enhances, but is not required to induce the Gcn1-dependent Gcn2 activation (Marton et al., 1997; Vazquez de Aldana et al., 1995). Gcn20 belongs to the ABCF protein family and its two ABCs (residues 199-239 and 565-572) are homologous to those present in eEF3 (Vazquez de Aldana et al., 1995). With 14,600 molecules/cell, Gcn20 is twice as abundant as Gcn1, and post-translationally acetylated (Ghaemmaghami et al., 2003; Van Damme et al., 2012). The Gcn20-CTD contributes to the high affinity of the Gcn1-Gcn20 complex to the ribosome in an ATP-dependent manner, thus suggesting Gcn20's role in fine-modulation of the Gcn1-mediated Gcn2 activation (Castilho et al., 2014; Marton et al., 1997). Interestingly, a very recent study revealed that Gcn2 is able to phosphorylate Gcn20 and thus directly modulate its activity in a negative autoregulatory feedback loop, since phosphorylated Gcn20 is impaired to form the Gcn2-stimulating Gcn1-Gcn20 complex (Dokladal et al., 2021). Although Gcn20 seems not to interact directly with the ribosome, it possesses an intrinsic ribosome binding activity and co-sediments weakly with polysomes (Marton et al., 1997). In contrast to Gcn1 and Gcn2, no clear mammalian homologue of Gcn20 was reported so far. Although the mammalian ABC50 features some sequence similarity with Gcn20, it was reported to function during translation initiation, where it interacts with eIF2 and thus influences the accuracy of codon selection (Paytubi et al., 2009; Stewart et al., 2015). Furthermore, the mammalian ABC50 is not able to complement the function of a yeast Gcn20 deficient strain (unpublished observations from J. K. Tyzack, G. Pavitt, and C. G. Proud, cited in (Tyzack et al., 2000)).

As already mentioned, HEAT repeats, as structural motifs, are known to function as interaction sites for other proteins and nucleic acids and therefore the HEAT repeat protein Gcn1 was suggested to act as a scaffold (Andrade et al., 2001). Interestingly, global landscape analysis of protein complexes in yeast did not reveal any Gcn1 binding partners, not even the so far clearly identified ones like Gcn2, Gcn20, Yih1 etc. (Castilho et al., 2014; Ho et al., 2002; Krogan et al., 2006). Based on this observation and the fact that emerging studies reveal the involvement of Gcn1 in other various processes besides the ISR, e.g. Gcn1's involvement in cell cycle, cell proliferation and embryonic development in mice, it seems that Gcn1 might have many other interaction partners and that identification of these interactions is challenging due to their potentially weak nature (Yamazaki et al., 2020).

1.5.2.2 The Gir2/Rbg2 complex

Gcn2 has many further regulators modulating its activity, including the yeast Gir2 (Genetically Interacts with Ribosomal genes 2, DFRP2 in mammals) protein (Castilho et al., 2014). Like Gcn2,

Gir2 possesses an N-terminal RWD domain, which was shown to compete with Gcn2 for Gcn1-CTD binding (Figure 10) (Wout et al., 2009). This suggestion was based on the observation that Gir2 overexpression results in a decreased cellular eIF2 α phosphorylation levels under starvation conditions, which are restored by a simultaneous co-overexpression of Gcn2 (Wout et al., 2009). The deletion of Gir2 does not lead to a general increase of Gcn2 activity, suggesting that Gir2 is not a permanent inhibitor of Gcn2, but likely only under certain conditions (Castilho et al., 2014; Ishikawa et al., 2013). The protein itself is intrinsically unstructured, especially an acidic amino acid part of the RWD domain (residue 85-101) and the CTD (Alves and Castilho, 2005). Furthermore, the RWD domain contains a PEST sequence, which is targeted by proteases, so the protein is highly prone to proteolysis (Alves and Castilho, 2005; Castilho et al., 2014). However, binding of the C-terminus to its interaction partner, the small GTPase Rbg2 (Ribosome-interacting GTTPase 2), stabilizes the protein (Alves and Castilho, 2005). Gir2 is also capable of forming interactions with Rbg1, but Rbg2 was identified as its distinct interaction partner, whereas Rbg1 forms a complex with Tma46 (Daugeron et al., 2011; Francis et al., 2012). Although the Rbg2-Gir2 complex is predominantly formed, Gir2-Rbg1 was shown to bind polysomes together with Gcn1, whereas the association of Gir2 with polysomes is partially dependent on binding to Gcn1 (Wout et al., 2009). Notably, double deletion of Rbg1, Rbg2 and the helicase Slh1 leads to impaired translation and cell growth indicating a potential connection to the RQC pathway (Daugeron et al., 2011).

Rbg2 and Gir2 alone colocalize with non-polysomal fractions, Rbg1 with polysomes, and as already mentioned Gcn1 is observed in both the non-polysome and polysome fractions (Castilho et al., 2014; Ishikawa et al., 2013). Rbg2 and Gir2 were shown to be non-essential for the cell, but responsible for maintaining efficient cell growth under amino acid starvation conditions in the presence of GTP bound to Rbg2 (Ishikawa et al., 2013). Under these conditions, the formation and stability of the complex is greatly increased as well as its association to Gcn1 (Ishikawa et al., 2013). A point mutation in Rbg2 inactivating nucleotide binding decreases the level of Rbg2/Gir2 complex formation and disrupts the stress-induced cell growth (Ishikawa et al., 2013). Based on the fact that the Rbg2/Gir2 complex stabilization is strictly dependent on GTP binding to Rbg2 and, to a lesser extent, on GDP, it was suggested that the complex fine-tunes the threshold levels for Gcn2 activation to the availability of GTP within the cell and thus to its energetic state, e.g. high GTP levels and its binding to Rbg2 signal availability of sufficient energy for protein synthesis, following Rbg2/Gir2 complex formation and Gir2 interaction with Gcn1, which in turn blocks the crucial Gcn1-Gcn2 interaction suppressing Gcn2 activation (Castilho et al., 2014; Ishikawa et al., 2013).

Mammals contain a Gir2 orthologue Dfrp2 (DRG family-regulatory protein 2) and its binding partner Drg2 (developmentally regulated GTTP-binding protein) – a mammalian orthologue of Rbg2. Drg proteins are known to be crucial for embryonic development, proliferation, differentiation and cell cycle and are characterized by their high conservation through eukaryotes

and archaea, but their exact function remains unclear (Ishikawa et al., 2005; Ko et al., 2004; Schellhaus et al., 2017; Song et al., 2004; Wei et al., 2004).

1.5.2.3 Deacetylated tRNAs and ribosome pausing events

During amino acid starvation the aminoacyl-tRNA synthetase fails to link a tRNA^{deacyl} to an appropriate amino acid, leading to a significant increase in concentration of tRNA^{deacyl} under these conditions. In bacteria, tRNA^{deacyl} are binding the ribosomal A-site leading to RelA recruitment and the RelA-mediated synthesis of (p)ppGpp, which serves as a signal for amino acid availability (Arenz et al., 2016; Haurlyiuk et al., 2015). Based on this bacterial stringent response, a similar mechanism was proposed for yeast including Gcn2 as the key player and tRNA^{deacyl} as the activation signal, which are directly binding the HisRS-like region and the Gcn2-CTD leading to its activation (Dong et al., 2000; Qiu et al., 2001; Wek et al., 1995). Mutations in aaRS lead to human neurological disorders and it was recently shown that depletion of the yeast glutamine aaRS gene (GLN4) inhibited cellular growth and induce GCN4 response based on tRNA^{deacyl} accumulation and Gcn2 activation (McFarland et al., 2020). Binding of tRNA to Gcn2 was shown to be crucial for Gcn2 dimerization and eIF2 α phosphorylation (Zaborske et al., 2009). The yeast Gcn2 exhibits a 9-fold higher affinity to tRNA^{deacyl} than to acetylated tRNAs (Dong et al., 2000). Mutation of motif 2, a region within the HisRS-like region, led to a severe decrease of phosphorylation of eIF2 α *in vivo* and *in vitro* (Wek et al., 1995; Zhu et al., 1996). The mechanism of the tRNA^{deacyl}-mediated Gcn2 activation was shown to be conserved in yeast and mammals, but in contrast to yeast, mammals are not able to synthesize 10 of the essential amino acids (Hao et al., 2005; Li et al., 2013; Zhang et al., 2002). Interestingly, a new study revealed that under non-starvation conditions, aaRS are capable to bind and sequester tRNA^{deacyl}, and thus preventing an unwanted Gcn2 activation (McFarland et al., 2020).

As mentioned in section 1.5, the ISR pathway in yeast was initially discovered during starvation for amino acids, which is inevitably connected to the presence of tRNA^{deacyl}. More recent studies report numerous other stress conditions, which activate Gcn2, including starvation for glucose, acidic, high salinity, oxidative stress, UV irradiation, viral mRNAs, proteasome inhibition as well as protein misfolding (Anda et al., 2017; Castilho et al., 2014; Pakos-Zebrucka et al., 2016). Interestingly, Gcn1 was suggested to be required for all stress rearrangements that activate Gcn2 (Anda et al., 2017; Castilho et al., 2014). Since Gcn2 can be activated by a wide array of stressors, the central question is if all these stressors are connected to an increased pool of tRNA^{deacyl}. Some of the mentioned conditions were suggested to lead to an increased concentration of tRNA^{deacyl}, e.g. acidic stress was correlated with accumulation of uncharged tRNA^{Leu}, whereas high salinity was shown to cause a transient increase in the overall tRNA^{deacyl} amount (Hueso et al., 2012; Zaborske et al., 2009). Proteasome inhibition was shown to reduce the free amino acid pool leading to Gcn2 activation (Suraweera et al., 2012). For UV irradiation, several suggestions were delivered and one of them proposes a rapid consumption of Arg for the enzyme nitric oxide synthetase to produce

nitric oxide, whereas other reports delivered different theories but no evidence for an increased tRNA^{deacyl} pool (Lu et al., 2009). On the other hand, there was some clear evidence that not all of the mentioned stress conditions lead to accumulation of tRNA^{deacyl}, but to the previously discussed ribosome pausing events. Recent profiling data of mouse neurons lacking a potential ribosome recycling factor GTPBP2 and a certain neuronal tRNA (tRNA^{Arg}_{UCCU}) showed no evidence for tRNA^{deacyl} accumulation and a simultaneous presence of an increased amount of stalled translation elongation complexes accompanied by an increased Gcn2 activation and eIF2 α phosphorylation (Ishimura et al., 2016). In nutrient deprived cell lines with the most severe ribosome stalling, Gcn2 showed the highest Gcn2 activation, and it seems that Gcn2 is able to directly sense ribosome pausing and stalled ribosomes (Darnell et al., 2018; Ishimura et al., 2016). In contrast, a recent study shows contradictory results including decreased polysome and increased monosome formation in GLN4 depleted cells, which lead to a high abundance of tRNA^{deacyl} and a subsequent Gcn2 activation (McFarland et al., 2020).

Although these results are inconclusive, so far it can be stated that there is a clear evidence for Gcn2 activation events, which are clearly independent of tRNA^{deacyl}, so the long-established model and the sole involvement of tRNA^{deacyl} in Gcn2 activation needs to be questioned.

1.5.2.4 Ribosomes and the ribosomal P-stalk

Recent *in vitro* studies showed that human 80S ribosomes have a 20-fold greater potency and 3-fold higher maximal stimulation on the Gcn2-mediated eIF2 α -P (in absence of Gcn1) than tRNA^{deacyl} (Inglis et al., 2019). This activation is dependent on the HisRS-like region of Gcn2, the domain, which was reported to bind tRNA^{deacyl}. Furthermore, the work showed, that the ribosomal P-stalk alone is able to activate Gcn2 more potently than tRNA^{deacyl} (Inglis et al., 2019; Jimenez-Diaz et al., 2013). The importance of the P-stalk for Gcn2 activation was supported by another previous *in vivo* study showing an inefficient eIF2 α -P in cells lacking the P1/P2 genes, but notably only during stress conditions (osmotic stress or glucose starvation) (Jimenez-Diaz et al., 2013). In contrast, addition of purified P1/P2 proteins to a cell-free translation extract from cells lacking P1/P2 efficiently stimulate eIF2 α -P (Jimenez-Diaz et al., 2013). This P1/P2 mediated activation was furthermore shown to be specific to Gcn2 and did not activate other eIF2-kinases like HRI and PKR (Jimenez-Diaz et al., 2013). Moreover, a recent mammalian CHO cell-based CRISPR-Cas9 mutagenesis screen revealed, that the P-stalk is essential in activating Gcn2 in response to amino acid deprivation (Harding et al., 2019). The P-stalk is part of the GTPase-associated center and plays a key role in translational fidelity recruitment and stimulation of GTPases (e.g. eEF1A and eEF2) during translation elongation and interaction with ribosome inactivating elements (e.g. trichosanthin, ricin A-chain) (Bargis-Surgey et al., 1999; Choi et al., 2015; Ito et al., 2014; Wawiorka et al., 2017). The P-stalk consists of the uL10 protein and two P1-P2 heterodimers forming a heteropentameric complex (Lee et al., 2010; Lee et al., 2012). The P1 and P2 proteins possess a dynamic nature and exist in an equilibrium state between its ribosome-bound and a free form within the

cytoplasm, whereas uL10 remains ribosome-bound (Lee et al., 2010; Lee et al., 2012). All three P-stalk proteins possess short, acidic and highly conserved C-terminal tails (CTTs), which serve as recognition elements for the recruitment of GTPases and stimulation of their activity (Choi et al., 2015; Tchorzewski, 2002). It was shown that these CCTs of the P-stalk subunits and uL10 domain II are essential for a complete induction of the Gcn2 kinase (Inglis et al., 2019).

Hydrogen deuterium exchange mass spectrometry (HDX-MS) identified some direct interactions between the *in vitro* reconstituted complex of the purified human Gcn2 and the P-stalk proteins (Inglis et al., 2019). A reduced rate of exchange was observed in regions of the ψ PK domain, HisRS-like domain and the CTD, all implicated in ribosome binding, as well as in the activation loop of the PK domain (Inglis et al., 2019). Interestingly, a rearrangement of the ψ PK, PK and the HisRS-like domain of the Gcn2 protein was observed after exposure to P-stalk proteins. The P-stalk regions interacting with Gcn2 were determined to be domain II of uL10 as well as domain I, which establish contacts with the 28S rRNA within the ribosome (Inglis et al., 2019).

1.5.2.5 Others

Gcn2 has many other activators and inhibitors contributing to its tight regulation and the most prominent in the yeast Impact homologue 1 (Yih1) (IMPACT (imprinted and ancient protein) in mammals) (Pereira et al., 2005). The 258 amino acid long Yih1 is a two-domain protein consisting of an N-terminal RWD domain (low sequence identity between Yih1-RWD and mouse Gcn2-RWD of 24% for 76 amino acids) and a C-terminal YigZ or Ancient Domain (based on its presence in many proteins from all domains of life). Like Gir2-RWD, Yih1-RWD competes with Gcn2 for Gcn1 interaction, thus acting as a negative regulator of Gcn2 (Sattlegger et al., 2011). Using Nuclear Magnetic Resonance (NMR) and small angle X-ray scattering (SAXS), recent structural studies of Yih1 suggested that the protein adopts a latent closed state and undergoes a large conformational rearrangement into a primed opened state upon Gcn1 interaction (Harjes et al., 2021). The Gcn1-Yih1 interaction is mediated through Asp-102 and Glu-106 within the RWD of Yih1 and residues 2051-2428 (especially Arg-2259) of Gcn1 (Sattlegger et al., 2011; Sattlegger et al., 2004). Since Yih1 was proposed not to be a constitutive regulator of Gcn2, Yih1 is normally binding monomeric G-actin through residues 68-258 (including part of the RWD) and was proposed to be released during certain conditions or in specific cellular compartments to modulate Gcn2 activation (Sattlegger et al., 2004). Yih1 was shown to be preferentially expressed in neurons and suggested to efficiently inhibit Gcn2 to allow a maximal translation rate (Bittencourt et al., 2008; Pereira et al., 2005). The binding site of Yih1 to Gcn1 and actin are overlapping and the fact that Yih1 bound to Gcn1 fails to bind actin *in vivo*, led to the suggestion that Yih1 is generally implicated in the cross-talk between translation and the cytoskeleton (Sattlegger et al., 2011; Sattlegger et al., 2004). Indeed, Yih1/IMPACT were shown to interact with the cyclin dependent kinase Cdc28/CDK1, respectively, enhancing cell cycle progression and highlighting the conservation of these interactions in yeast and mammals (Silva et al., 2015). Yih1 directly binds to the ribosome (co-sediments with

polyribosomes) in an Gcn1-independent manner, contacting the ribosomal protein eL39 (Waller et al., 2012). Deletion of Yih1 in yeast was shown to have no detectable effect on Gcn2 activity and cellular phenotype, but in neuronal mouse cells it leads to an increased basal Gcn2 activation (Pereira et al., 2019; Sattlegger et al., 2004). These recent mouse studies revealed that lack of IMPACT leads to defective thermoregulation and weight loss in mammals and thus contributes to diet-induced obesity (Pereira et al., 2019).

Besides the function in delivery of aa-tRNA to the ribosomal A-site during elongation, the elongation factor eEF1A was shown to play a further role in inhibiting Gcn2 activation during nutrient-rich conditions. Under non-starving conditions, eEF1A was shown to directly bind to the C-terminus of Gcn2 keeping it in its latent state, whereas under starvation conditions in presence of tRNA^{deacyl} the interaction is diminished (Visweswaraiah et al., 2011). Recent *in vitro* studies identified eEF1A domain I and II encompassing residues 1-221 and 222-315 as crucial for Gcn2 kinase inhibition (Ramesh and Sattlegger, 2020).

Also Heat shock proteins were implicated in Gcn2 inhibition. *In vitro* and *in vivo*, the yeast molecular chaperone Hsp90 (expressed as two Hsp82 and Hsc82 isoforms) forms a complex with Gcn2 (residues 507-1092) required for the maintenance of its inactive state (Donze and Picard, 1999). Hsp90 is constitutively expressed within cells, also under non-stress conditions and was previously shown to also interact with the kinase HRI in rabbit reticulocyte lysate (Uma et al., 1997).

Since Gcn2 was also implicated in prevention of viral infections (a function, which is performed by the specialized kinase PKR), viral RNAs were shown to be able to directly bind the HisRS domain of Gcn2 thus leading to its activation (Berlanga et al., 2006). *In vivo* mutations of Gcn2 lead to an increased susceptibility to DNA virus infections of cytomegalovirus in mice and adenovirus in humans as well as to the mammalian RNA Sindbis virus (Berlanga et al., 2006; Won et al., 2012). Interestingly, HIV-1 viruses are able to activate Gcn2 leading to inhibited translation of viral RNAs, but simultaneously HIV-1 protease is able to proteolytically cleave Gcn2 to prevent its antiviral effect (del Pino et al., 2012).

Besides the yeast ISR - with Gcn2 as its key regulator - there is an additional pathway, which is activated during cell stress, and namely the (mammalian or mechanistic) target of rapamycin ((m)TOR) signaling (Laplante and Sabatini, 2012). Rapamycin, the inhibitor of mTOR and a potential anticancer therapeutic, led to the discovery of the kinase and its mTOR blocking action is based on its simultaneous binding to the prolyl isomerase FKBP and mTOR (to its FKBP-rapamycin binding domain FRB) leading to a formation of an FKBP:Rapamycin:FRB ternary complex, which directly blocks substrate recruitment to the kinase domain of mTOR (Banaszynski et al., 2005; Heitman et al., 1991; Yang et al., 2013). Deregulation of the TOR pathway in humans is widely implicated in various health conditions reaching from the progression of cancer to

metabolic diseases such as diabetes as well as the aging process (Saxton and Sabatini, 2017). Since both, the ISR and TOR, determine the balance between cell survival and cell death during environmental fluctuations, they established tight communication pathways between each other to control their activity.

TOR kinases belong to the family of phosphatidylinositol 3-kinase related family of kinases (Imseng et al., 2018). To fulfill its function, the mTOR effector kinase needs to be incorporated in one of the two multiprotein complexes, the mTOR complex 1 (mTORC1) and mTOR complex 2 (mTORC2), respectively, and both have different functions despite the kinase mTOR being the same (Imseng et al., 2018). Among other functions, the mTOR/TORC1 complex is also involved – like the Gcn complex - in sensing amino acid starvation (Kim, 2009; Proud, 2014; Sengupta et al., 2010). The mTOR kinase is highly active during nutrient-rich conditions leading to high translational rate through phosphorylation of two important translation regulators: the Sch9 kinase (S6 kinase (S6K) in mammals) leading to its activation and eIF4E-binding protein 1 (4E-BP1) (only in mammals) resulting in its inhibition (Fingar et al., 2002; Proud, 2014; Sengupta et al., 2010). Concomitantly, Gcn2 is inactivated by a mechanism leading to phosphorylation of Ser-577, a modification, which down-regulates Gcn2 activity by decreasing the affinity for tRNA^{deacyl} (Cherkasova and Hinnebusch, 2003; Kubota et al., 2003). In contrast, during nutrient deprivation or the drug Rapamycin, TOR is inactivated, whereas Gcn2 was shown to be activated by dephosphorylation of Gcn2 Ser-557 with the help of the Type 2A phosphatase-associated protein 42 (Tap42) (Cherkasova and Hinnebusch, 2003). Furthermore, it was shown that after its activation by nutrient deprivation, Gcn2 is able to maintain mTORC1 inhibition by inducing expression of Sestrin2 via ATF4 induction, which blocks the lysosomal localization of mTORC1 (Nikonorova et al., 2018; Ye et al., 2015). On the other hand, Gcn2 seems to have a mechanism to block mTOR1 upstream of ATF4 transcription during leucine starvation (Averous et al., 2016). Confusingly, other studies showed a simultaneous and full activation of both Gcn2 and TORC1, after UV irradiation and oxidative stress, and suggested a more complex cross-talk between the pathways dependent on different stress conditions (Rodland et al., 2014). The tight communication between Gcn2 and mTOR is highlighted by the fact that mTORC1 by itself is able to control ATF4, which in turn is required for expression of metabolic enzymes and amino acid transporters – a mechanism, which is independent of Gcn2 and eIF2 α phosphorylation (Park et al., 2017).

2 Objective of these studies

If cells possess enough nutrients, the general protein synthesis can occur in a fast and efficient way. During the translational cycle in eukaryotes, two translational GTPases (eEF2 and eEF1A) are essential to ensure the elongation of the growing polypeptide chain. Yeast requires a third essential factor, the ATPase eEF3, which directly binds the ribosome and plays a role in the release of the E-site tRNA during translation elongation (Andersen et al., 2006; Triana-Alonso et al., 1995). Why yeast cells specifically need this translation factor still remains unclear, but more recent studies have already identified the factor in some non-fungal species of unicellular eukaryotes (Mateyak et al., 2018). eEF3 belongs to the ABCF proteins, a protein family that has many implications in human diseases like diabetes or cystic fibrosis (Dean et al., 2001). The yeast protein eEF3 possesses a close homologue, namely New1. Compared to eEF3, New1 exhibits 37% sequence homology and a similar domain organization with an additional N-terminal prion domain, which was shown not to be conserved (Murina et al., 2018). Since New1 co-sediments with actively translating ribosome, it was suggested to be involved in the translation process, but because the protein was only identified recently, its function is not investigated so far. The aim of this project was to gain the first structural insights into the *in vitro* reconstituted New1-80S complex using cryo-EM analysis (**Publication 1**). To gain additional knowledge about New1's function, the study was accompanied by collaborative yeast genetics and ribosome profiling data.

An *in vitro* reconstitution of the eEF3-80S complex from purified components revealed the first structural insight into eEF3 bound to the ribosome (Andersen et al., 2006), but since the structure was at low (9.9Å) resolution it did not allow any detailed observations and thus no mechanistic conclusions. Furthermore, the complex was reconstituted using a RNC which was lacking the E-tRNA, therefore it is unclear which ribosomal state is recognized by eEF3 *in vivo*. To address these open questions, we performed a native pull-out on a C-terminally TAP-tagged eEF3 from yeast cells and visualized the complex(es) via Cryo-EM (**Publication 2**). To gain a better understanding of eEF3's exact mechanistic function during elongation, the study was also complemented by collaborative *in vitro* translational and *in vivo* ribosome profiling assays.

In the event of changed environmental conditions and/or stress, such as amino acid deprivation, cells need to adapt in a very fast and efficient way to ensure cell survival. The ISR in yeast comprises the phosphorylation of eIF2 α on Ser-51 by the kinase Gcn2, leading to reprogramming of the general gene expression profile, which enables adaptation to restriction conditions (Castilho et al., 2014; Hinnebusch, 2005). The protein kinase Gcn2 requires its effector proteins Gcn1 and Gcn20, whereas Gcn1 and Gcn2 directly bind to the ribosome. Since the action of Gcn2 causes severe metabolic changes within the cell, the pathway needs tight monitoring, which was suggested to be governed by the Rbg2-Gir2 complex. These proteins were shown to be able to bind directly to the ribosome, suppress Gcn2 activation and enable an efficient division of cells under certain

conditions (Ishikawa et al., 2013; Wout et al., 2009). The ISR pathway is highly conserved from yeast to humans and connected to various human conditions like aging, cancer, obesity, or COVID-19 (Kim et al., 2020; Philips and Khan, 2021; Ye et al., 2010). Some first structural insights of the Gcn-80S complex would open the possibility for mechanistic conclusions, however for decades the structure of Gcn proteins on the ribosome have remained elusive. Hence, the goal of the study was to visualize using cryo-EM the first structure of Gcn protein(s) binding to the ribosome by performing a native pull-out on a C-terminally TAP-tagged Gcn20 and a subsequent Cryo-EM analysis of the native sample (**Publication 3**).

3 Cumulative Thesis: Summary of Publications

3.1 Publication 1 - A role for the *Saccharomyces cerevisiae* ABCF protein New1 in translation termination/recycling

Villu Kasari*, [Agnieszka A. Pochopien*](#), Tõnu Margus, Victoriia Murina, Kathryn Turnbull, Yang Zhou, Tracy Nissan, Michael Graf, Jiří Nováček, Gemma C. Atkinson, Marcus J. O. Johansson, Daniel N. Wilson, Vasili Hauryliuk.

Nucleic Acids Research. 47, 8807–8820 (2019).

New1 is a close homologue of eEF3, an essential factor in yeast, which promotes the release of the E-site tRNA during translation elongation. The molecular function of the non-essential New1 is entirely unknown, but it seems to be involved in translation, since it co-sediments with actively translating polysomes (Li et al., 2009). By using a combination of single particle cryo-EM, yeast genetics and ribo-seq analysis, we gained insights into the New1 ribosomal binding site as well as its basic function during the translation process. For the structural part, we *in vitro* reconstituted a yeast New1-80S complex with purified (vacant) ribosomes, ATPase-deficient (EQ₂) New1 protein lacking the prion domain (PD) and ATP, and resolved this structure at 3.28 Å resolution using cryo-EM. Our results show that New1 binds a non-rotated vacant ribosome at a similar site than eEF3, including the interactions of HEAT, ABC2 and CD with the ribosomal 40S head and the 60S CP. Its truncated CD, missing the loop between β4 and β5, is pointing towards the ribosomal L1-stalk, but does not interact with it. Our results indicate, that due to the 'shorter' CD, the eEF3 homologue cannot efficiently perform the same function as eEF3 by interacting with the ribosomal L1-stalk. This agrees with our yeast genetic studies, showing that although overexpression of New1 is able to rescue a strain lacking eEF3, it is not able to perform this task efficiently. Both studies were complemented by ribo-sequencing analysis, which uncovered that loss of New1 leads to ribosomes queuing upstream of lysine and arginine codons immediately preceding a stop codon, and thus suggested New1's function in termination and/or recycling. The study provided the first structural insights into the unknown protein New1 and its binding to the yeast ribosome and could associate its function with translation termination and/or recycling.

3.2 Publication 2 – Yeast translation elongation factor eEF3 promotes late stages of tRNA translocation

Namit Ranjan*, [Agnieszka A. Pochopien*](#), Colin Chih-Chien Wu*, Bertrand Beckert, Sandra Blanchet, Rachel Green, Marina V. Rodnina, Daniel N. Wilson.

The EMBO Journal. 10.15252/embj.2020106449 (2021).

The eukaryotic translation cycle requires eEF2 and eEF1A, two highly conserved translational GTPases, for successful peptide elongation. In contrast, yeast needs a third essential factor, namely the eukaryotic elongation factor 3 (eEF3). *In vitro* translational studies revealed that eEF3 is required for the release of the tRNA from the E-site and suggested an allosteric three-site model of the ribosome, suggesting a reciprocal link between the ribosomal A- and the E-site (Gnirke et al., 1989; Triana-Alonso et al., 1995). Previous cryo-EM studies uncovered the first structure of eEF3 bound to the yeast ribosome at 9.9 Å, comprising the 60S CP and the 40S head, however high-resolution structural information of the interactions between eEF3 and the ribosome is unavailable (Andersen et al., 2006). Furthermore, the eEF3-80S complex was reconstituted *in vitro* using RNCs lacking the E-site tRNA and thus precluding a conclusion about the ribosomal state eEF3 is binding *in vivo*. By using a combination of cryo-EM, *in vitro* translation experiments and ribosome profiling, we gained insights into all these mentioned questions as well as reconsideration of the postulated allosteric three-site model. By performing co-immunoprecipitation (co-IP) of a C-terminally TAP-tagged eEF3 strain and a subsequent cryo-EM analysis, we were able to visualize seven eEF3-80S complexes ranging from 3.3 Å - 4.2 Å with different rotation, swiveling and tRNA occupation states. Surprisingly, eEF3 is binding nearly all ribosomal states during elongation, but is only able to stably interact with the non-rotated ribosome. Detailed molecular interactions of eEF3 with the ribosome showed that only in a non-rotated state eEF3's HEAT repeats can establish extensive contacts with ES39S and eS19 of the 40S head and that this binding is diminished as soon as the 40S is rotated or the head swiveled. Furthermore, the structures also uncovered eEF3's direct interaction with the ribosomal L1-stalk via its CD. The comparison of the different non-rotated ribosomal states enabled us to trace various L1-stalk positions (e.g. 'int' L1-stalk with P- and E-tRNAs and 'open' L1-stalk with P-tRNA after E-tRNA release and a shift of the L1 by 44 Å) and to conclude that the CD of eEF3 is actively involved in the repositioning of the L1-stalk from a 'closed' into an 'opened' conformation and thus is substantially involved in the release of the E-site tRNA. The cryo-EM study was complemented by *in vitro* translational analysis and ribosome profiling data, which confirmed EF3's function in E-tRNA release, but also determined that eEF3 promotes late steps in tRNA-mRNA translocation. Since A-site occupation (by the TC) is not required for the release of the E-site tRNA and in opposite case, the empty ribosomal A-site is able to be loaded despite the E-tRNA presence (after eEF3 depletion), resulting in a trapped ribosomal species occupied by all three tRNAs, the study challenges the long postulated allosteric three-site model of the yeast ribosome.

3.3 Publication 3 - Structure of Gcn1 bound to stalled and colliding 80S ribosomes

Agnieszka A Pochopien*, Bertrand Beckert*, Sergo Kasvandik, Otto Berninghausen, Roland Beckmann, Tanel Tenson, Daniel N. Wilson (2021). Structure of Gcn1 bound to stalled and colliding 80S ribosomes.

PNAS. 10.1073/pnas.2022756118 (2021).

The integrated stress response (ISR) is a highly conserved pathway and enables cells to adapt to numerous environmental conditions in a fast and efficient way to ensure survival. In yeast, this pathway, also known as the general amino acid control (GAAC), is activated during stress, e.g., nutrient deprivation, in the presence of increased amounts of deacetylated tRNAs (tRNA^{deacyl}), binding the ribosomal A-site (Castilho et al., 2014; Hinnebusch, 2005). The prevailing model postulates, that under these conditions, the effector protein Gcn1, together with Gcn2, contacts the ribosome and transfers the tRNA^{deacyl} to the histidyl-tRNA synthetase (HisRS) like region of Gcn2, leading to its activation and a subsequent eIF2 α -P. Since Gcn2 induction results in severe metabolic changes and the reprogramming of the general gene expression profile, the pathway is tightly monitored by numerous modulators, including the Rbg2-Gir2 complex. The complex was shown to enable an efficient cell growth under starvation conditions in simultaneous presence of GTP (Ishikawa et al., 2013), whereas recent studies report Rbg2's binding to ribosomes, containing problematic polybasic peptide motifs (Zeng et al., 2021). Although the function of the complex is not entirely clear, Gir2 is able to efficiently repress Gcn2 activation under certain conditions (Ishikawa et al., 2013). Although several crystal structures of single domains of Gcn2 presented valuable insights into the domain architecture, the structure of the functional Gcn1/2/20 proteins binding to the ribosome as well as the one of Gcn2 modulators like Rbg2-Gir2 remained elusive. By performing a co-IP on a yeast C-terminally TAP-tagged Gcn20 strain and a subsequent 3D reconstruction of the native complex via cryo-EM, we were able to visualize the first structure of a Gcn1/20 bound ribosomal species at 3.9 Å resolution. Interestingly, we observed, that the elongated structure of Gcn1 is spanning two ribosomes consisting of a leading stalled ribosome (LSR) and a colliding ribosome (CR), rather than a monosome. Both termini of Gcn1 are tightly interacting with both P-stalks and 40S heads of the LSR and CR, trapping the disome in a translation impotent state. The N-terminus of Gcn20 is binding the middle portion of Gcn1, including its eEF3-like HEAT region, in a manner, which induces a 'kink', compacting Gcn1 and leading to its previously suggested stabilization on the ribosome (Vazquez de Aldana et al., 1995). The LSR is in a non-rotated state occupied by A/A- and P/P-site tRNAs, and eIF5A within the E-site, whereas the CR is in a rotated state bearing hybrid A/P- and P/P-tRNAs and Mbf1 bound adjacent to the mRNA entry channel on the 40S. The Rbg2-Gir2 complex is located near the ribosomal A-site on the LSR, where Rbg2 directly contacts the A-tRNA and Gir2 binds the C-terminal region of Gcn1 via its RWD

domain, illustrating how Gir2 is able to compete with Gcn2 for the essential Gcn1 binding, as suggested before (Wout et al., 2009). Not only do our findings reveal the first insights into Gcn1-Gcn20 and Rbg2-Gir2 bound ribosomal species, but they also uncover the disome as the substrate for Gcn1 binding *in vivo* and thus serve as a structural basis for Gcn2 activation. Moreover, our work is consistent with the hypothesis that Gcn2 is activated by collisions and independently of the presence of tRNA^{deacyl}, as proposed previously (Inglis et al., 2019; Ishimura et al., 2016; Masson, 2019), questioning the long-postulated Gcn2 activation model. Since ribosome collisions induce not only the ISR but are key signals for the ribosome-associated quality control (RQC) and the ribotoxic stress response (Vind et al., 2020), our study has an important implication also for these pathways.

4 Discussion and Outlook

4.1 The *S. cerevisiae* eEF3-80S complex

Besides the strict GTP-dependent eukaryotic elongation factors eEF1A and eEF2, yeast and fungi require an additional factor for elongation - the ATPase eEF3. Despite the availability of an *in vitro* reconstituted eEF3-80S complex at 9.9 Å resolution (Triana-Alonso et al., 1995), it remains unclear which ribosomal state eEF3 is binding to *in vivo* (1) and at which stage the factor dissociates from the ribosome (2). Also questions on how E-tRNA release is mediated by the factor (3) and the role of ATP-hydrolysis in this process (4) remain open.

Answering the first and second question, our cryo-EM structures provide snapshots of seven eEF3-bound ribosomal species, four in the pre-translocational (PRE) (Fig. 5 A-D in Ranjan, Pochopien and Chih-Chien et al., 2021) and three in the post-translocational (POST) (Fig. 6 A-D) state. eEF3 is present on the ribosome throughout the entire elongation cycle, but can only stably bind the non-rotated ribosome (PRE-1, PRE-2, POST-2, POST-3). In all these states, eEF3 does not show any significant conformational change and the HEAT repeat region is able to establish extensive contacts with the 40S head proteins eS19 and uS13, and rRNA ES39S. These interactions are diminished as soon as the 40S rotates or swivels, and eEF3 is anchoring itself by the few remaining contacts of ABC2 with the 60S CP and thus showing a disordered and flexible nature or even dissociating (PRE-3, PRE-4, POST-1).

When stably bound to a non-rotated ribosome, eEF3 is in a closed state with both ABCs occupied by nucleotides, however the resolution is not sufficient to discriminate between ATP, ADP or ADPNP and thus to clarify how ATP hydrolysis is coupled to E-tRNA release. Several ABC proteins (e.g. the OpuA-transporter) possess degenerated ABCs and require only one functional ABC for a successful transport of the substrate (Jones and George, 2013; Nikaido and Ames, 1999; ter Beek et al., 2014). However, for eEF3 it was shown that both ABCs are functional and indispensable for the ribosome-activated ATP-hydrolysis and full eEF3 function (Yang et al., 1996). In order to stabilize eEF3 on the ribosome, ADPNP was added to the sample in the very last purification step, which might have two important implications. On the one hand, the usage of ADPNP does not allow any conclusions about ATP hydrolysis in eEF3 function, since the non-hydrolyzable analog might potentially replace one or two hydrolyzed ADP molecules with ADPNP trapping eEF3 in a closed state and preventing the visualization of eEF3's potential semi-open state. One needs to consider that even if ADPNP influenced the states in the mentioned manner, its presence would not result in artificial eEF3-80S complexes, but indeed be comparable to functional complexes present in the cell, since ADP might also be replaced by ATP, which is omnipresent *in vivo*. On the other hand, the application of ADPNP presumably enabled us to trap the crucial POST-2 state (eEF3-80S complex with P/P- and E/E-tRNA), because the occupation of the non-hydrolysable analog in at

least one of the two ABCs blocked the release of the E-site tRNA as reported previously (Triana-Alonso et al., 1995). The observation of the POST-2 state is crucial, since it uncovered the tight association of the eEF3 CD with the protein uL1 of the ribosomal L1-stalk. Interestingly, CDs in general were shown to be present in HP1/Chromobox and CDH subfamilies as well as chromatin remodelers binding methylated lysines (me-K) in histone tails (Kim et al., 2006; Nielsen et al., 2002; Yap and Zhou, 2011). Although a methylation was identified on K46 of the uL1 protein (Webb et al., 2011), our structure revealed that the CD-uL1 interaction is far away from the me-K46 on uL1. This finding suggested, that (at least in this case) the CD does not share the same mechanism in recognition of me-K in comparison to chromatin remodelers, but the interactions rather rely on a charge complementary to the lysine dense region within the uL1 protein interacting with the eEF3 CD. The presence of different tRNA-occupied eEF3-80S complexes enabled us to trace the position of the L1-stalk, which showed a dramatic shift of 44 Å between the state before (POST-2 with P/P- and E/E-tRNA) and after (POST-3 with P/P-tRNA) the release of the tRNA^{deacyl} from the E-site. From this dramatic repositioning of the L1-stalk and the continuous interaction of the CD with uL1 in all eEF3-80S complexes, we suggest that eEF3 is involved in the release of the E-site tRNA by directly influencing the L1-stalk position in an ATP-dependent manner, since presence of ATP is strictly required for E-tRNA release during elongation (Triana-Alonso et al., 1995).

The *in vitro* cell-free translation studies in presence and absence of eEF3 and *in vivo* ribosome profiling experiments under eEF3 depletion conditions uncovered that the A-site is able to be loaded before E-tRNA release and that E-tRNA release is possible without a preceding A-site loading, and moreover, that during eEF3 deletion the yeast ribosome is trapped with all three tRNAs. These observations challenged the long-postulated allosteric three side model, which states that the ribosomal A-site is linked to the E-site and *vice versa* in the manner that occupation of one binding site negatively influences the affinity of the other (Gnirke et al., 1989; Nierhaus, 1990). The allosteric model is plausible, since the A- or E-site occupation of the ribosome influences the structural state of the L1-stalk (Fei et al., 2008), which in turn potentially correlates with the global conformational change of the entire ribosome (Fei et al., 2009; Ning et al., 2014), and thus influences factor binding and dissociation during the entire translation process. However, the model is highly controversial in literature (Nierhaus, 1990; Nierhaus et al., 1995; Semenov et al., 1996). Single-molecule studies brought new insights into the topic by examining the transition of tRNAs through the *E. coli* ribosome during decoding, peptide bond formation and translocation (Chen et al., 2011; Choi and Puglisi, 2017; Uemura et al., 2010). As soon as translocation by eEF2/EF-G occurs, the E-site tRNA release is rapid (Uemura et al., 2010), which is consistent with our observation that eEF3 plays a role during late stages of mRNA-tRNA translocation. Importantly, E-site tRNA release is clearly not correlated with the arrival of the next A-site tRNA and the E-tRNA alone is able to dissociate spontaneously in later stages of elongation (at approximately cycle 3) (Chen et al., 2011; Uemura et al., 2010), which is in agreement with our *in vitro* biochemical results in Ranjan, Pochopien and Chih-Chien et al. as well with the previous

postulated model of the kinetically labile and 'transient' E-site occupation (Lill and Wintermeyer, 1987; Semenov et al., 1996). However, the E-tRNA needs to dissociate first before the ribosome can be translocated to the next codon by eEF2/EF-G (Choi and Puglisi, 2017). Uemura et al. showed that the rate of ribosomes occupied by A-, P- and E-site tRNA is very rare (1.7%) and forms under special conditions, when E-site tRNA dissociation is slow, e.g. due to frameshifting (Sanders and Curran, 2007), the dependency of the tRNA species or Mg^{2+} concentration (Choi and Puglisi, 2017; Fei et al., 2009)) with a simultaneously occurring rapid A-site occupation due to high micromolar concentrations of the TC (Uemura et al., 2010).

Since eEF3 ensures a rapid and efficient E-tRNA release, the percentage of the 80S complexes occupied by three tRNAs from our native pull-out sample should be hardly existent, which explains why we could not observe such a ribosomal species during processing of our cryo-EM data. Since E-tRNA release correlates with the fast rates required for efficient elongation (Uemura et al., 2010) and the ribosome being occupied by all three tRNAs slows translation elongation (Choi and Puglisi, 2017), the existence of such a factor like eEF3 might represent an evolutionary advantage for yeast in the processivity of translation, despite its high energetic costs. This is supported by the fact that no structure so far is available for the yeast ribosome occupied by A-, P- and E-tRNA, in contrast to the human variant (Behrmann et al., 2015). To summarize, the previous single-molecule (Chen et al., 2011; Choi and Puglisi, 2017; Uemura et al., 2010), structural (Behrmann et al., 2015) as well as our *in vitro* translation studies (Ranjan et al., 2021) show that the allosteric three site model is not valid during later stages of elongation, since the A- and E-site are not allosterically linked. However, a ribosome occupied by all three tRNAs seems to be a very rare state (Behrmann et al., 2015; Uemura et al., 2010) and represents a kinetic hurdle due to blocked translocation and a decrease in translation speed (Choi and Puglisi, 2017) - a process prevented by the ATPase eEF3.

Why yeast and fungi require a third soluble factor for E-tRNA release during elongation while higher eukaryotes do not, remains an enigma until today, especially since the elongation process is the most conserved process between all three kingdoms of life (Riis et al 1990). The elongation factors eEF1A and eEF2 for example feature 82% and 66% sequence identity between yeast and human species and are able to replace their counterpart in presence of rat liver or wheat germ ribosomes (Skogerson and Engelhardt, 1977). One prominent explanation for the absence of eEF3 in higher eukaryotes was the direct incorporation of the ATPase into the mammalian ribosome (Chakraborty and Triana-Alonso, 1998). The presence of an ATPase as a ribosomal protein responsible to the E-tRNA release during mammalian elongation was a long-debated and conflictive topic (Kovalchuk and Chakraborty, 1994; Rodnina et al., 1994), however structures of mammalian ribosomes (Anger et al., 2013; Flis et al., 2018; Muhs et al., 2015; Svidritskiy et al., 2014) clearly proved the absence of ATP domains within the mammalian ribosome.

The mammalian ribosome seems to have properties, which enable the ribosome to release the E-tRNA without an external soluble factor like eEF3, since the exchange of the yeast 40S subunit with the wheat germ one enables the translation to be eEF3-independent (Chakraborty and Kamath, 1988). Notably, the percentage of human ribosomes occupied by all three tRNAs derived from an *ex-vivo* pull-out is significantly higher (3-8%) (Behrmann et al., 2015) than for the already mentioned *E. coli* one (Uemura et al., 2010). Since mammals do not possess an eEF3 analogue, it is tempting to speculate that the energetic barrier for the E-tRNA dissociation during mammalian elongation is lower than in yeast, however which structural or functional property within the mammalian ribosome is responsible for this phenomenon remains unclear.

Intriguingly and controversially, under a limited concentration of eEF1A, the yeast eEF3 shows a small but consistent stimulatory effect on polyphenylalanine synthesis in presence of pig liver ribosomes (Kovalchuk and Chakraborty, 1994). Furthermore, rabbit liver ribosomes were shown to stimulate the ATPase activity of yeast eEF3 (Rodnina et al., 1994). Comparing the eEF3 binding site on the yeast ribosome with the similar location on the human one reveals that the residue composition (ES39S, eS19, uS13 of the 40S head and uL5 and uL18 and 5SrRNA of the 60S CP) of the human ribosome is similar to the yeast one (**Figure 11 A and B**). This suggests a potential binding ability of yeast eEF3 to the mammalian ribosome, which might explain the effect mentioned above, since eEF3's ATP-binding and -hydrolysis is strongly stimulated by the previous binding to its substrate, the ribosome ('ribosome model') (Andersen et al., 2006) - a model, which is in agreement with the 'switch model' postulated for ABC transporters (Higgins and Linton, 2004). Notably, our latest structural study revealed a similar binding site of the yeast Gcn1 to that of eEF3 on the ribosome based on its eEF3-like HEAT region. Since Gcn1 is highly conserved in yeast and human and the binding of the human Gcn1 to the ribosome is probably similar to the yeast one, it is tempting to speculate that yeast eEF3 indeed is potentially able to bind the human ribosome. In contrast, the *D. melanogaster* ribosome features an elongated ES9S, which forms a 'horn' and would preclude an eEF3 binding (**Figure 11 C**) (Anger et al., 2013).

Further investigations are needed to determine the mechanism of ATP hydrolysis on eEF3 function. It can be clearly stated that until now no structural and functional analog was detected in higher eukaryotes (Belfield and Tuite, 1993), however eEF3 was reported more recently to be present in some non-fungal species of unicellular eukaryotes (Mateyak et al., 2018). The essentiality of eEF3 in fungi and its absence in humans, makes eEF3 to an obvious target for antifungal drugs (Sturtevant, 2002). One billion people suffer from severe fungal diseases responsible for over 1.6 million deaths over the past few years and are the main cause of patient death after organ transplantation (Almeida et al., 2019; Brown et al., 2012; Sturtevant, 2002). Furthermore, fungal infestations are causing massive damage to plant-based food production worldwide (Almeida et al., 2019; Savary and Willocquet, 2020). The four clinically available drug classes are polyenes, azoles, 5'-fluorocytosine and echinocandins, all of which are targeting compounds within the fungal cell

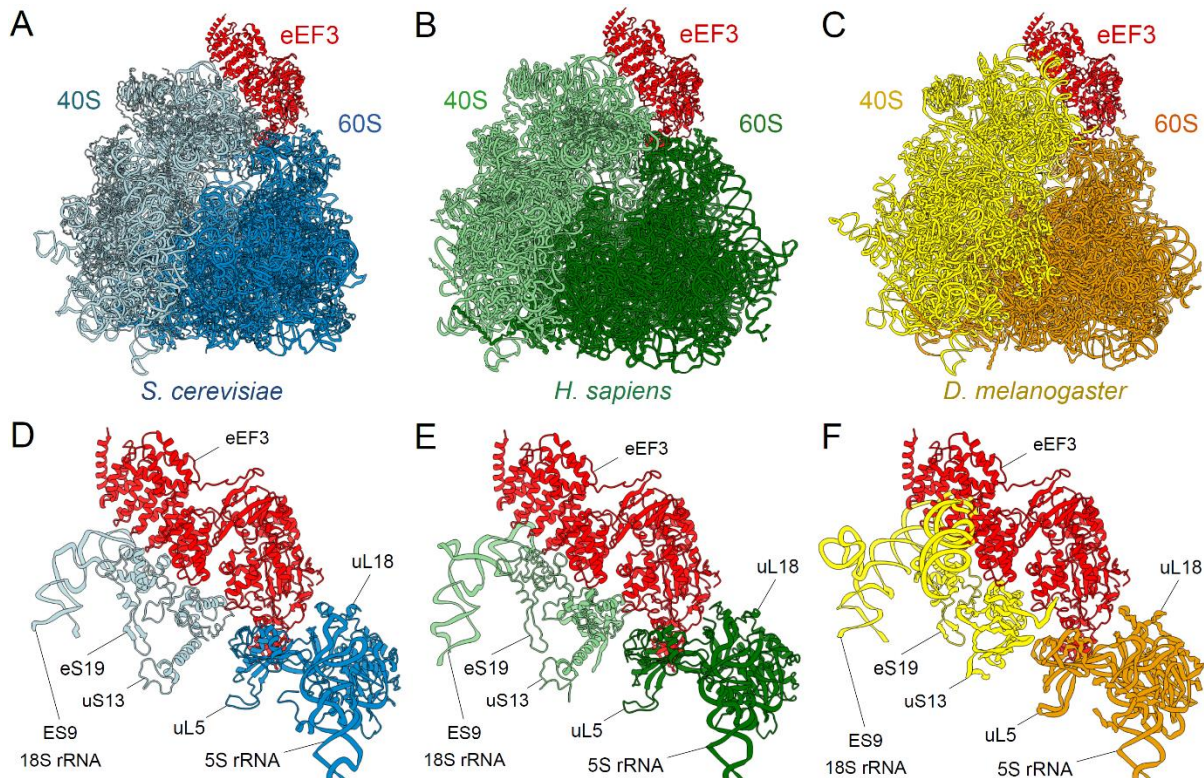


Figure 11. eEF3 in complex with the 80S ribosome. (A) The *S. cerevisiae* (*Sc*) eEF3-80S model is based on the cryo-EM structure of the native eEF3-80S complex at 3.3 Å (Ranjan et al., 2021). (B) Putative eEF3-80S complex bound to the *H. sapiens* (*Hs*) (PDB ID: 6EK0) (Natchiar et al., 2017) and (C) *D. melanogaster* (*Dm*) (PDB ID: 4V6W) (Anger et al., 2013) ribosome. Both ribosome structures were aligned to the cryo-EM structure of the native *S. cerevisiae* eEF3-80S complex shown in (A). (D) Interaction of eEF3 with isolated parts of the *Sc*, (E) *Hs* and (F) *Dm* 80S ribosome.

membrane, e.g. lipids or molecules involved in synthesis pathways (Sturtevant, 2002). Since they feature cross-resistance and show many (partly severe) side effects for organs, targeting distinctive fungal molecules - like eEF3 - would open doors for the design of new potential antifungal agents. Indeed, two compounds were found to target specifically eEF3, aspirochlorine and yefafungin (Monti et al., 1999; Roemer et al., 2011a; Roemer et al., 2011b). Aspirochlorine, a molecule isolated from *Aspergillus* species and a member of epipolythiodioxopiperazines class of compounds (Gardiner et al., 2005), was reported previously to act as a specific and potent inhibitor of fungal translation (IC_{50} of 10 nM) during poly(U)-directed Poly(Phe) synthesis and has a substantially reduced lethal toxicity in mice in comparison to the polyene amphotericin B (100 mg/kg for aspirochlorine vs. 4 mg/kg amphotericin B) (Berg et al., 1976; Monti et al., 1999). Several years ago, Merck took the effort to screen for thousands of various natural products (Roemer et al., 2011b), which have the potential to act as antifungal drugs, leading to the identification of yefafungin, fellutamide C and D (26S proteasome inhibition) (Hines et al., 2008), campafungin (blocks cyclic adenosine monophosphate homeostasis) (Roemer et al., 2011b) and dretamycin (disturbs Fe/S

cluster protein Dre2p) (Wilson et al., 2014), but not even one of these and other molecules could be applied clinically so far (Balibar and Roemer, 2016). A structure of aspirochlorine or yefafungin on the ribosome-bound eEF3 would reveal the compound's mode of action and enable a design of a new, even more potent molecules. Besides eEF3, other essential yeast proteins involved in translation, like eEF2, might represent a target for drug development. Although many of them possess high sequence homology between fungi and human, they do also feature species-specific domains, which may be used for targeting. Furthermore, investigation of 'coupling molecules', which enable an efficient uptake of the compound by the fungi cells, is key.

4.2 The *S. cerevisiae* New1-80S complex

As mentioned previously, New1 is the second closest homologue of eEF3 (Murina et al., 2018). Considering the domain organization, the only difference between New1 and eEF3 is its additional N-terminal prion domain (PD), which does not seem to be conserved between different yeast species (Murina et al., 2018). Besides the fact, that New1 co-sediments with actively translating polysomes and shows cold-sensitivity as well as ribosome assembly defect phenotype in its absence (Li et al., 2009), its functions remained entirely unclear. In Kasari and Pochopien et al. we combined single molecule cryo-EM analysis with *in vitro* genetic and ribo-seq studies to reveal New1's location on the ribosome and suggest a first potential function.

The New1-80S complex was reconstituted *in vitro* from purified yeast 80S and an ATP-hydrolysis deficient EQ₂-mutant version of New1 lacking the PD, and subjected to single particle cryo-EM. The 3.28 Å structure revealed a binding site of New1 to the yeast ribosome, which is similar to that of eEF3, an observation, which is not surprising considering the high sequence homology and nearly identical domain organization. Like for eEF3, the New1's HEAT repeats, ABC2 and the CD are interacting with the 40S head ES9, eS19, uS13 and the 60S CP uL5, uL18 and the 5S rRNA. Within the New1-80S complex, the vacant ribosome adopts a non-rotated state, a conformation, which might be stabilized after binding of the ligand, since the vacant yeast 80S was previously shown to prefer the rotated intersubunit state (Ben-Shem et al., 2011; Spahn et al., 2004b) in contrast to the bacterial ribosome (Munro et al., 2009). The latter observation is also in agreement with our observed remaining ribosomal classes lacking the ligand, which all adopt a predominantly rotated conformation. It can be speculated, that *in vivo*, New1 recognizes a ribosome adopting a non-rotated state, since 40S rotation or head swivel would result in the same destabilization of the HEAT interaction with the 40S head as it is the case for eEF3. Interestingly, New1 possesses a shorter CD compared to eEF3, which does not interact with the L1-stalk in our *in vitro* structure. The missing loop between β4 and β5 (the 'tip' of the CD) was identified in Ranjan, Pochopien and Chih-Chien et al. as the region of eEF3 establishing the majority of the contacts to the lysine dense region on the uL1 protein of the L1-stalk. Especially in PRE-1, PRE-2 and POST-3 states of the eEF3-80S complex, the L1-stalk is in an open position still flexibly interacting with the 'tip' of

eEF3's CD, and it is questionable that the short CD of New1 would be able to interact with the L1-stalk in the same manner due to the distance. Indeed, it is possible, that New1 CD is able to interact with uL1 when the L1-stalk is in a closed position, which is the case during E-site occupation by tRNA or another factor, e.g. eIF5A. Since eIF5A occupation leads to a fully closed conformation of the L1 stalk, similar to that observed for eEF2 (Flis et al., 2018; Spahn et al., 2004a), this L1-state would present an even more preferential case for the 'short' CD interaction of New1 with uL1 due to shorter distance. The performance of a native pull-out and structural elucidation of the *ex-vivo* New1-80S complex would show in detail if or how the New1-CD is interacting with the L1-stalk and if the PD is involved to some extent in ribosome binding.

After the clarification of its binding site, the question remains, which function New1 holds during the translation process. As an eEF3 homologue, is New1 able to fulfil the essential function of eEF3? Yeast genetic experiments revealed that overexpression of New1 rescues a strain lacking the essential eEF3, but considering the long incubation time of 4-5 days for the dot blots, its rescue ability is not very efficient, suggesting another main role of the factor. Ribo-seq analysis uncovered, that New1 is affecting translation termination or recycling, since New1 loss leads to upstream queuing at 3'-terminal lysine and arginine codons. Further studies need to clarify the question how New1 is involved in termination and/or recycling and resolve if New1 is also simultaneously and directly involved in ribosome assembly, as previously suggested (Li et al., 2009).

Since eEF3 is encoded by two paralogous genes, *YEF3* (essential) and *HEF3* (non-essential) (Kellis et al., 2004; Maurice et al., 1998; Murina et al., 2018), the role of Hef3 is also of interest. Recent studies revealed that the closest eEF3 homologue is involved in the selective production of proteins, which defend the yeast cell against reactive oxygen species after H₂O₂ treatment and the induction of oxidative stress (Goscinska et al., 2020). In contrast to eEF3, New1 and Hef3 are non-essential and identified so far only in fungi species, hence the factors probably have no further implication for higher eukaryotes, like humans, for the development of new antifungal targets.

4.3 The *S. cerevisiae* Gcn1-Disome complex

The ISR enables eukaryotic cells to adapt to a variety of environmental stress conditions in a fast and efficient way. In metazoans, four specialized kinases are responsible for sensing different stresses, whereas the yeast system comprises only one of the kinases, the highly conserved protein Gcn2. The prevailing model of ISR activation in yeast postulates, that starvation for one or several amino acids leads to accumulation of tRNA^{deacyl} within the ribosomal A-site, which in turn is the signal for Gcn2, together with its modulators Gcn1 and Gcn20, to get activated, leading to phosphorylation of its target eIF2 α , which results in a subsequent reprogramming of the global gene expression and adaptation to stress (Castilho et al., 2014; Hinnebusch, 2005). The quantity of emerging *in vitro* and *in vivo* studies on the Gcn system reflects its importance, since its

deregulation results in numerous and severe human diseases (Castilho et al., 2014; Kim et al., 2020; Lehman et al., 2015; Ma et al., 2013; Philips and Khan, 2021; Ye et al., 2010). Several crystal and NMR structures of distinct domains of the eukaryotic Gcn2 protein provided valuable insights into its domain architecture (He et al., 2014; Hei et al., 2021; Nameki et al., 2004; Padyana et al., 2005), however a structural basis of the functional 80S-bound Gcn complex still lacks.

In our publication Pochopien and Beckert et al. we performed a native pull-out on an exponentially growing Gcn20-TAP tagged yeast strain, and visualized the *ex vivo* complex by cryo-EM. The structure revealed a remarkable composition of a disome (consisting of the first leading stalled ribosome and a second ribosome, which collided into it) bound by Gcn1 together with Rbg2-Gir2 and Mbf1. The leading stalled ribosome (LSR) is in a non-rotated state occupied by an A- and P-tRNA as well as eIF5A within the E-site (PRE state), whereas the colliding ribosome (CR) is rotated, bearing hybrid A/P- and P/E-tRNAs (HYBRID state). Gcn1 establishes five extensive contacts with both ribosomes within the disome: the Gcn1 N-terminus tightly interacts with the P-stalk proteins (1) and the 40S head (2) on the CR, and spans the LSR, where its middle portion (eEF3-like HEAT) binds the ribosomal site similar to that of eEF3 (3) and the C-terminus reaches the 40S head (4) and the P-stalk region (5). On its termini, Gcn1 interacts with both ribosomal P-stalks of the LSR and CR. In this manner the P-stalks are potentially 'trapped' and cannot fulfil their function in recruiting and stimulating canonical trGTPases (Choi et al., 2015; Tchorzewski, 2002) - an observation, which explains why loss of P-stalk proteins impairs Gcn2-dependent eIF2 α -P in mammals (Harding et al., 2019).

Simultaneously, Gcn1 also binds both 40S heads of the LSR and CR, which might prevent the normally occurring spontaneous rotation and/or head swivel of the 40S (Agirrezabala et al., 2008; Blanchard et al., 2004; Budkevich et al., 2011; Cornish et al., 2008; Julian et al., 2008; Moazed and Noller, 1989), and thus results in stabilization of both ribosomal states. By interacting with both, P-stalks and 40S heads, on the LSR and the CR, Gcn1 potentially recognizes and 'traps' the disome in a rigid and translation impotent state, and this defined structural unit in turn acts as a distinct signal, leading to activation of a specific downstream signaling pathway. The main question is, under which conditions Gcn1 recognizes the PRE-HYBRID disome, which forms a specific 40S-40S interaction interface, including Asc1 (Rack1), and if it is able to also sense other disome or ribosome species, since a recent publication reports that activation of the ISR is favouring a ribosome with an empty A-site (POST state) (Yan and Zaher, 2021).

Previous *in vitro* studies showed that overexpression of eEF3 represses Gcn2 activity, and thus suggested an overlapping binding site of Gcn1 (eEF3-like HEAT) and eEF3 (HEAT) on the ribosome (Visweswaraiah et al., 2012). Based on Gcn1's interaction with the 40S head and the 60S CP of the LSR, our structure reveals that this is indeed the case. The human Gcn1 might bind the LSR in the same manner as the yeast protein due to the high sequence conservation (Castilho et al., 2014) (47% sequence identity of the eEF3-like HEAT region). Another point supporting this

suggestion is the structural comparison in 4.1 (Fig. 11 B, E), which illustrates a potential binding ability of eEF3-HEAT (or in this case: eEF3-like HEAT in Gcn1) to the human ribosome. Interestingly, large scale interaction studies of the yeast proteome could not show even one of the so far known Gcn1 interaction partner (Krogan et al., 2006), suggesting its transient or weak interactions (Castilho et al., 2014) and illustrating the 'hidden' potential of Gcn1. Intriguingly, Gcn1 is able to also bind to monosomes after a full induction of the ISR, as we observe from our sucrose density gradients of lysates from starved cells, showing a monosome peak and no disomes, which is in line with previous results (Marton et al., 1993). The interaction of Gcn1 with the 80S ribosome is potentially less stable compared to its interaction with a disome, however the possibility of a so far unknown conformational change of Gcn1 on the monosome cannot be excluded.

The middle portion (~ 500 residues) of Gcn1, including eEF3-like HEAT and an additional region in the N-terminal direction, is not involved in any ribosome binding, but potentially interacts with the N-terminal Gcn20, however the resolution of Gcn20 is not sufficient for a clear confirmation. The location of the Gcn20 N-terminus is supported by previous *in vitro* studies, in which Gcn20 was shown to neither interact with the ribosome, nor with Gcn2, but its N-terminus interacts with the Gcn1 eEF3-like HEAT region, which was suggested to stabilize Gcn1's binding to the ribosome and lead to enhanced Gcn2 activation (Vazquez de Aldana et al., 1995). From our structural observation we can speculate, that the binding of the Gcn20 N-terminus induces a 'kink' and might act as a 'clamp', compacting Gcn1's elongated and flexible structure and thus leading to the previously suggested stabilization on the ribosome. Interestingly, the activity of Gcn20 can be directly modulated by Gcn2 itself (phosphorylation inactivates Gcn20 and disrupts its interaction with Gcn1) as part of a negative feedback loop (Dokladal et al., 2021).

The noncanonical GTPase Rbg2 is located near the A-site on the LSR, directly interacting with the 40S, 60S and the A-tRNA via its N-terminal helix-turn-helix (HTH), ribosomal proteins S5 domain 2-like (S5D2L) and C-terminal TGS (ThrRS, GT Pase, and SpoT) domain. The simultaneous occupation of the ribosomal E-site by the elongation factor eIF5A, which was shown to bind in presence of problematic polypeptide stretches (Gutierrez et al., 2013; Schuller et al., 2017), leads to the suggestion, that Rbg2 and eIF5A stabilize the A- and P-site tRNAs, respectively. In this manner they potentially enhance peptide bond formation at the PTC to restore translation. Although we cannot confirm the presence of problematic polypeptide motifs due to insufficient resolution of the mRNA on the LSR, recent studies report, that Rbg2 (and Rbg1) indeed enhance translation in presence of problematic polybasic motifs (Zeng et al., 2021). However, conditions, under which the Gcn1-disome complex bound by Rbg2-Gir2 and Mbf1 is formed, need to be clarified via future experiments.

On the other hand, the central GT Pase domain (G-domain) of Rbg2 is interacting with Gir2, a protein, which possesses a N-terminal RWD similar to Gcn2 and was shown to repress Gcn2 activation under certain conditions by competing for Gcn1 binding (Ishikawa et al., 2013; Wout et

al., 2009). Starvation and the simultaneous presence of GTP lead to increased formation of the Rbg2-Gir2 complex binding to Gcn1 (Ishikawa et al., 2013), so Castilho et al. speculate, that the Rbg2-Gir2 complex adjusts the threshold levels for Gcn2 activation to the energetic state of the cell in the manner, that high cellular GTP levels signal enough available energy to continue translation under certain starvation conditions, leading to a dampened Gcn2 activation (Castilho et al., 2014).

During ribosomal collisions, the CR exerts a pulling force on the mRNA during translocation - an event, which leads to slippage of the mRNA and thus to frameshifting on the LSR (Simms et al., 2019). The multiprotein bridging factor (Mbf1) is binding the 40S at the interface between the head and body on the CR, and in this manner stabilizes a non-swivelled conformation of the 40S head, preventing frameshifting on the LSR (Sinha et al., 2020; Wang et al., 2018).

Based on our Gcn1-disome structure, together with available biochemical studies, we propose a model, in which the bound complex is responsible for resolving the collided ribosomes to resume translation: Rbg2 together with eIF5A enhance peptide bond formation, Mbf1 prevents frameshifting and Gir2 ensures a suppression of Gcn2 activation by binding to Gcn1 via its RWD domain. On the other hand, our structure presents some first insights into Gcn1 binding a disome, and thus allows a conclusion on how Gcn1 potentially activates Gcn2. During amino acid starvation, the binding of tRNA^{deacyl} to the ribosomal A-site leads to slower translation and hence ribosome collisions (Darnell et al., 2018; Meydan and Guydosh, 2020). Gcn1 (together with Gcn20) is able to sense these disomes and recruit Gcn2 by placing residues ~2000-2200 near the ribosomal A-site, which are exposed for Gcn2-RWD binding and Gcn2 activation - a potential structure that presents the main, albeit challenging goal for future structural studies. Our co-IP study was performed with cells, which were grown and harvested at the mid log phase (OD₆₀₀=2.5). Since the rate of eIF2 α -P is low during the exponential growth of yeast wild-type cells, but notably increased in the stationary phase (Jimenez-Diaz et al., 2013), another straight-forward possibility to gain the Gcn2-bound ribosomal complex would be to perform the native pull-out under stationary phase conditions.

Although starvation and tRNA^{deacyl} lead to ribosomal collisions, the disome, as a Gcn1 substrate, is probably a very short-lived species, reflected by the fact that mono- and polysome fractions from exponentially growing cells combine to one monosome peak in starved cells treated with 3-AT, which we could observe in our sucrose density gradients. In the latter case, Gcn1 substrates (disomes) disappear as soon as the ISR is fully activated by Gcn2, since the general translation shuts down. Once the ISR is activated, there is no requirement for the Gcn2 kinase to continuously phosphorylate eIF2, because the induced transcriptional activators can be reused for every round of transcription to reprogram the cellular gene expression profile. The challenge for the future is to trap the Gcn2-80S complex after an efficient Gcn2 activation, but during early stages of the ISR induction. This could be obtained by a very short 3-AT treatment of the cells before harvesting or by titration of 3-AT and monitoring the ribosome profile through a sucrose density gradient to

determine the 3-AT concentration, which efficiently activates Gcn2, but simultaneously keeps as many disomes as possible.

Another possibility to 'save' disomes during starvation is the application of a Gcn2 mutant version, e.g. Ser51Ala mutation, which prevents eIF2 α -P and inhibits the global translation shutdown. In this context, a further possible difficulty for trapping the Gcn2-80S complex is the low abundance of the Gcn2 protein within the cell (279 Gcn2 molecules/cell) (Ghaemmaghami et al., 2003). In the course of sample preparation, this might result in an insufficient amount of Gcn2-bound ribosomal species needed for a high-resolution 3D reconstruction of the complex, especially considering the already challenging reconstruction of the Gcn1-bound disomes (7330 Gcn1 molecules/cell), which represented 4.9% of the total particle number (starting with ~ 1 Mio. particles). Furthermore, the binding of the Gcn2 kinase to the disome complex might be transient. To support and potentially increase the amount of Gcn2-bound ribosomal species, overexpression of Gcn2 is reasonable.

The four specialized mammalian kinases PKR, PERK, HRI and Gcn2 exhibit an overlapping activation (Pakos-Zebrucka et al., 2016; Staschke and Wek, 2019; Taniuchi et al., 2016). Based on this observation, the yeast ISR response was shown to be not only activated by nutrient deprivation, but via other stresses, e.g. UV irradiation, oxidative stress, viral mRNAs, high salinity or acidic stress (Anda et al., 2017; Castilho et al., 2014; Pakos-Zebrucka et al., 2016). These conditions might also represent an interesting source for stress treatment of cells for Gcn2-ribosomal complex isolation. An interesting question for the future is how the four kinases are able to overlap in their activation, although they feature very different regulatory domains.

Since ribosome collisions are well-known to activate the RQC, one of the main questions is, how the ISR and RQC machineries interplay with each other and define, from which point one specific pathway is activated, since both pathways were shown to antagonize each other (Yan and Zaher, 2021). The connection between the ISR and RQC is illustrated by the fact, that double deletion of Rbg1, Rbg2 and the helicase Slh1 leads to impaired translation and cell growth (Daugeron et al., 2011). Notably, one of the main RQC players, the E3 ubiquitin ligase Listerin (Ltn1), features a C-terminal RWD domain (Shao et al., 2015) and its potential to compete with Gcn2 for Gcn1 binding would be an interesting point to investigate. Recently, RQC was shown to be more sensitive to translational changes and respond quicker to collisions with lower frequency, whereas Gcn2 responds to a high frequency of stalled ribosomes (Yan and Zaher, 2021), which again reflects how important the timing for the 'trapping' of the Gcn2-80S complex is. Furthermore, the rescue efficiency was shown to depend on collision frequency and the length of the ribosome queue (Goldman et al., 2021). Answering that question will be challenging, since Gcn2 activation and the ISR pathway are very complex, as already described in section 1.5.2. The pathway is not only interfering with numerous mentioned modulators, but was shown to depend on the identity of the deficient amino acid itself (Mazor et al., 2018).

5 References

- Adio, S., Senyushkina, T., Peske, F., Fischer, N., Wintermeyer, W., and Rodnina, M.V. (2015). Fluctuations between multiple EF-G-induced chimeric tRNA states during translocation on the ribosome. *Nature communications* 6, 7442.
- Agirrezabala, X., Lei, J., Brunelle, J.L., Ortiz-Meoz, R.F., Green, R., and Frank, J. (2008). Visualization of the hybrid state of tRNA binding promoted by spontaneous ratcheting of the ribosome. *Molecular cell* 32, 190-197.
- Agrawal, R.K., Penczek, P., Grassucci, R.A., Li, Y., Leith, A., Nierhaus, K.H., and Frank, J. (1996). Direct visualization of A-, P-, and E-site transfer RNAs in the Escherichia coli ribosome. *Science* 271, 1000-1002.
- Agrawal, R.K., Sharma, M.R., Kiel, M.C., Hirokawa, G., Booth, T.M., Spahn, C.M., Grassucci, R.A., Kaji, A., and Frank, J. (2004). Visualization of ribosome-recycling factor on the Escherichia coli 70S ribosome: functional implications. *Proceedings of the National Academy of Sciences of the United States of America* 101, 8900-8905.
- Aitken, C.E., and Lorsch, J.R. (2012). A mechanistic overview of translation initiation in eukaryotes. *Nature structural & molecular biology* 19, 568-576.
- Alkalaeva, E.Z., Pisarev, A.V., Frolova, L.Y., Kisselev, L.L., and Pestova, T.V. (2006). In vitro reconstitution of eukaryotic translation reveals cooperativity between release factors eRF1 and eRF3. *Cell* 125, 1125-1136.
- Almeida, F., Rodrigues, M.L., and Coelho, C. (2019). The Still Underestimated Problem of Fungal Diseases Worldwide. *Front Microbiol* 10, 214.
- Alves, V.S., and Castilho, B.A. (2005). Gir2 is an intrinsically unstructured protein that is present in *Saccharomyces cerevisiae* as a group of heterogeneously electrophoretic migrating forms. *Biochem Biophys Res Commun* 332, 450-455.
- Anand, M., Balar, B., Ulloque, R., Gross, S.R., and Kinzy, T.G. (2006). Domain and nucleotide dependence of the interaction between *Saccharomyces cerevisiae* translation elongation factors 3 and 1A. *The Journal of biological chemistry* 281, 32318-32326.
- Anand, M., Chakraborty, K., Marton, M.J., Hinnebusch, A.G., and Kinzy, T.G. (2003). Functional interactions between yeast translation eukaryotic elongation factor (eEF) 1A and eEF3. *The Journal of biological chemistry* 278, 6985-6991.
- Anda, S., Zach, R., and Grallert, B. (2017). Activation of Gcn2 in response to different stresses. *PLoS One* 12, e0182143.
- Andersen, C.B., Becker, T., Blau, M., Anand, M., Halic, M., Balar, B., Mielke, T., Boesen, T., Pedersen, J.S., Spahn, C.M., *et al.* (2006). Structure of eEF3 and the mechanism of transfer RNA release from the E-site. *Nature* 443, 663-668.

- Andersen, D.S., and Leever, S.J. (2007). The essential *Drosophila* ATP-binding cassette domain protein, *pixie*, binds the 40 S ribosome in an ATP-dependent manner and is required for translation initiation. *The Journal of biological chemistry* 282, 14752-14760.
- Andrade, M.A., and Bork, P. (1995). HEAT repeats in the Huntington's disease protein. *Nat Genet* 11, 115-116.
- Andrade, M.A., Petosa, C., O'Donoghue, S.I., Muller, C.W., and Bork, P. (2001). Comparison of ARM and HEAT protein repeats. *J Mol Biol* 309, 1-18.
- Anger, A.M., Armache, J.P., Berninghausen, O., Habeck, M., Subklewe, M., Wilson, D.N., and Beckmann, R. (2013). Structures of the human and *Drosophila* 80S ribosome. *Nature* 497, 80-85.
- Arenz, S., Abdelshahid, M., Sohmen, D., Payoe, R., Starosta, A.L., Berninghausen, O., Hauryliuk, V., Beckmann, R., and Wilson, D.N. (2016). The stringent factor RelA adopts an open conformation on the ribosome to stimulate ppGpp synthesis. *Nucleic acids research* 44, 6471-6481.
- Averous, J., Lambert-Langlais, S., Mesclon, F., Carraro, V., Parry, L., Jousse, C., Bruhat, A., Maurin, A.C., Pierre, P., Proud, C.G., *et al.* (2016). GCN2 contributes to mTORC1 inhibition by leucine deprivation through an ATF4 independent mechanism. *Sci Rep* 6, 27698.
- Aylett, C.H., and Ban, N. (2017). Eukaryotic aspects of translation initiation brought into focus. *Philos Trans R Soc Lond B Biol Sci* 372.
- Baird, T.D., and Wek, R.C. (2012). Eukaryotic initiation factor 2 phosphorylation and translational control in metabolism. *Adv Nutr* 3, 307-321.
- Balagopal, V., and Parker, R. (2011). Stm1 modulates translation after 80S formation in *Saccharomyces cerevisiae*. *RNA* 17, 835-842.
- Balibar, C.J., and Roemer, T. (2016). Yeast: a microbe with macro-implications to antimicrobial drug discovery. *Brief Funct Genomics* 15, 147-154.
- Ban, N., Nissen, P., Hansen, J., Moore, P.B., and Steitz, T.A. (2000). The complete atomic structure of the large ribosomal subunit at 2.4 Å resolution. *Science* 289, 905-920.
- Banaszynski, L.A., Liu, C.W., and Wandless, T.J. (2005). Characterization of the FKBP.rapamycin.FRB ternary complex. *J Am Chem Soc* 127, 4715-4721.
- Barford, D. (1995). Protein phosphatases. *Curr Opin Struct Biol* 5, 728-734.
- Bargis-Surgey, P., Lavergne, J.P., Gonzalo, P., Vard, C., Filhol-Cochet, O., and Reboud, J.P. (1999). Interaction of elongation factor eEF-2 with ribosomal P proteins. *Eur J Biochem* 262, 606-611.
- Barthelme, D., Dinkelaker, S., Albers, S.V., Londei, P., Ermler, U., and Tampe, R. (2011). Ribosome recycling depends on a mechanistic link between the FeS cluster domain and a conformational switch of the twin-ATPase ABCE1. *Proceedings of the National Academy of Sciences of the United States of America* 108, 3228-3233.
- Bassett, D.E., Jr., Boguski, M.S., and Hieter, P. (1996). Yeast genes and human disease. *Nature* 379, 589-590.

- Becker, T., Armache, J.P., Jarasch, A., Anger, A.M., Villa, E., Sieber, H., Motaal, B.A., Mielke, T., Berninghausen, O., and Beckmann, R. (2011). Structure of the no-go mRNA decay complex Dom34-Hbs1 bound to a stalled 80S ribosome. *Nature structural & molecular biology* *18*, 715-720.
- Behrmann, E., Loerke, J., Budkevich, T.V., Yamamoto, K., Schmidt, A., Penczek, P.A., Vos, M.R., Burger, J., Mielke, T., Scheerer, P., *et al.* (2015). Structural snapshots of actively translating human ribosomes. *Cell* *161*, 845-857.
- Belfield, G.P., and Tuite, M.F. (1993). Translation elongation factor 3: a fungus-specific translation factor? *Mol Microbiol* *9*, 411-418.
- Ben-Shem, A., Garreau de Loubresse, N., Melnikov, S., Jenner, L., Yusupova, G., and Yusupov, M. (2011). The structure of the eukaryotic ribosome at 3.0 Å resolution. *Science* *334*, 1524-1529.
- Ben-Shem, A., Jenner, L., Yusupova, G., and Yusupov, M. (2010). Crystal structure of the eukaryotic ribosome. *Science* *330*, 1203-1209.
- Bengtson, M.H., and Joazeiro, C.A. (2010). Role of a ribosome-associated E3 ubiquitin ligase in protein quality control. *Nature* *467*, 470-473.
- Berg, D.H., Massing, R.P., Hoehn, M.M., Boeck, L.D., and Hamill, R.L. (1976). A30641, a new epidithiodiketopiperazine with antifungal activity. *The Journal of antibiotics* *29*, 394-397.
- Berg, P., and Offengand, E.J. (1958). An Enzymatic Mechanism for Linking Amino Acids to RNA. *Proceedings of the National Academy of Sciences of the United States of America* *44*, 78-86.
- Berlanga, J.J., Ventoso, I., Harding, H.P., Deng, J., Ron, D., Sonenberg, N., Carrasco, L., and de Haro, C. (2006). Antiviral effect of the mammalian translation initiation factor 2α kinase GCN2 against RNA viruses. *EMBO J* *25*, 1730-1740.
- Bittencourt, S., Pereira, C.M., Avedissian, M., Delamano, A., Mello, L.E., and Castilho, B.A. (2008). Distribution of the protein IMPACT, an inhibitor of GCN2, in the mouse, rat, and marmoset brain. *J Comp Neurol* *507*, 1811-1830.
- Blanchard, S.C., Kim, H.D., Gonzalez, R.L., Jr., Puglisi, J.D., and Chu, S. (2004). tRNA dynamics on the ribosome during translation. *Proceedings of the National Academy of Sciences of the United States of America* *101*, 12893-12898.
- Bock, L.V., Blau, C., Schroder, G.F., Davydov, I.I., Fischer, N., Stark, H., Rodnina, M.V., Vaiana, A.C., and Grubmuller, H. (2013). Energy barriers and driving forces in tRNA translocation through the ribosome. *Nature structural & molecular biology* *20*, 1390-1396.
- Boel, G., Smith, P.C., Ning, W., Englander, M.T., Chen, B., Hashem, Y., Testa, A.J., Fischer, J.J., Wieden, H.J., Frank, J., *et al.* (2014). The ABC-F protein EttA gates ribosome entry into the translation elongation cycle. *Nature structural & molecular biology* *21*, 143-151.
- Boudeau, J., Miranda-Saavedra, D., Barton, G.J., and Alessi, D.R. (2006). Emerging roles of pseudokinases. *Trends Cell Biol* *16*, 443-452.
- Brandman, O., and Hegde, R.S. (2016). Ribosome-associated protein quality control. *Nature structural & molecular biology* *23*, 7-15.

- Brandman, O., Stewart-Ornstein, J., Wong, D., Larson, A., Williams, C.C., Li, G.W., Zhou, S., King, D., Shen, P.S., Weibezahn, J., *et al.* (2012). A ribosome-bound quality control complex triggers degradation of nascent peptides and signals translation stress. *Cell* *151*, 1042-1054.
- Brehm, A., Tufteland, K.R., Aasland, R., and Becker, P.B. (2004). The many colours of chromodomains. *Bioessays* *26*, 133-140.
- Breitkreutz, A., Choi, H., Sharom, J.R., Boucher, L., Neduva, V., Larsen, B., Lin, Z.Y., Breitkreutz, B.J., Stark, C., Liu, G., *et al.* (2010). A global protein kinase and phosphatase interaction network in yeast. *Science* *328*, 1043-1046.
- Brown, A., Shao, S., Murray, J., Hegde, R.S., and Ramakrishnan, V. (2015). Structural basis for stop codon recognition in eukaryotes. *Nature* *524*, 493-496.
- Brown, G.D., Denning, D.W., Gow, N.A., Levitz, S.M., Netea, M.G., and White, T.C. (2012). Hidden killers: human fungal infections. *Sci Transl Med* *4*, 165rv113.
- Brundin, P., Melki, R., and Kopito, R. (2010). Prion-like transmission of protein aggregates in neurodegenerative diseases. *Nat Rev Mol Cell Biol* *11*, 301-307.
- Budkevich, T., Giesebrecht, J., Altman, R.B., Munro, J.B., Mielke, T., Nierhaus, K.H., Blanchard, S.C., and Spahn, C.M. (2011). Structure and dynamics of the mammalian ribosomal pretranslocation complex. *Molecular cell* *44*, 214-224.
- Budkevich, T.V., Giesebrecht, J., Behrmann, E., Loerke, J., Ramrath, D.J., Mielke, T., Ismer, J., Hildebrand, P.W., Tung, C.S., Nierhaus, K.H., *et al.* (2014). Regulation of the mammalian elongation cycle by subunit rolling: a eukaryotic-specific ribosome rearrangement. *Cell* *158*, 121-131.
- Buskirk, A.R., and Green, R. (2017). Ribosome pausing, arrest and rescue in bacteria and eukaryotes. *Philos Trans R Soc Lond B Biol Sci* *372*.
- Carter, A.P., Clemons, W.M., Brodersen, D.E., Morgan-Warren, R.J., Wimberly, B.T., and Ramakrishnan, V. (2000). Functional insights from the structure of the 30S ribosomal subunit and its interactions with antibiotics. *Nature* *407*, 340-348.
- Castilho, B.A., Shanmugam, R., Silva, R.C., Ramesh, R., Himme, B.M., and Sattlegger, E. (2014). Keeping the eIF2 alpha kinase Gcn2 in check. *Biochim Biophys Acta* *1843*, 1948-1968.
- Chakraburttty, K., and Kamath, A. (1988). Protein synthesis in yeast. *Int J Biochem* *20*, 581-590.
- Chakraburttty, K., and Triana-Alonso, F.J. (1998). Yeast elongation factor 3: structure and function. *Biol Chem* *379*, 831-840.
- Chandrasekaran, V., Juszkievicz, S., Choi, J., Puglisi, J.D., Brown, A., Shao, S., Ramakrishnan, V., and Hegde, R.S. (2019). Mechanism of ribosome stalling during translation of a poly(A) tail. *Nature structural & molecular biology* *26*, 1132-1140.
- Chaveroux, C., Lambert-Langlais, S., Cherasse, Y., Averous, J., Parry, L., Carraro, V., Jousse, C., Maurin, A.C., Bruhat, A., and Fafournoux, P. (2010). Molecular mechanisms involved in the adaptation to amino acid limitation in mammals. *Biochimie* *92*, 736-745.

- Chen, B., Boel, G., Hashem, Y., Ning, W., Fei, J., Wang, C., Gonzalez, R.L., Jr., Hunt, J.F., and Frank, J. (2014). EttA regulates translation by binding the ribosomal E site and restricting ribosome-tRNA dynamics. *Nature structural & molecular biology* *21*, 152-159.
- Chen, C., Stevens, B., Kaur, J., Smilansky, Z., Cooperman, B.S., and Goldman, Y.E. (2011). Allosteric vs. spontaneous exit-site (E-site) tRNA dissociation early in protein synthesis. *Proceedings of the National Academy of Sciences of the United States of America* *108*, 16980-16985.
- Chen, J.J. (2014). Translational control by heme-regulated eIF2alpha kinase during erythropoiesis. *Curr Opin Hematol* *21*, 172-178.
- Cheng, G., Feng, Z., and He, B. (2005). Herpes simplex virus 1 infection activates the endoplasmic reticulum resident kinase PERK and mediates eIF-2alpha dephosphorylation by the gamma(1)34.5 protein. *J Virol* *79*, 1379-1388.
- Cheng, Y. (2015). Single-Particle Cryo-EM at Crystallographic Resolution. *Cell* *161*, 450-457.
- Cherkasova, V.A., and Hinnebusch, A.G. (2003). Translational control by TOR and TAP42 through dephosphorylation of eIF2alpha kinase GCN2. *Genes Dev* *17*, 859-872.
- Choe, Y.J., Park, S.H., Hassemer, T., Korner, R., Vincenz-Donnelly, L., Hayer-Hartl, M., and Hartl, F.U. (2016). Failure of RQC machinery causes protein aggregation and proteotoxic stress. *Nature* *531*, 191-195.
- Choi, A.K., Wong, E.C., Lee, K.M., and Wong, K.B. (2015). Structures of eukaryotic ribosomal stalk proteins and its complex with trichosanthin, and their implications in recruiting ribosome-inactivating proteins to the ribosomes. *Toxins (Basel)* *7*, 638-647.
- Choi, J., and Puglisi, J.D. (2017). Three tRNAs on the ribosome slow translation elongation. *Proceedings of the National Academy of Sciences of the United States of America* *114*, 13691-13696.
- Chu, J., Hong, N.A., Masuda, C.A., Jenkins, B.V., Nelms, K.A., Goodnow, C.C., Glynne, R.J., Wu, H., Masliah, E., Joazeiro, C.A., *et al.* (2009). A mouse forward genetics screen identifies LISTERIN as an E3 ubiquitin ligase involved in neurodegeneration. *Proceedings of the National Academy of Sciences of the United States of America* *106*, 2097-2103.
- Cornish, P.V., Ermolenko, D.N., Noller, H.F., and Ha, T. (2008). Spontaneous intersubunit rotation in single ribosomes. *Molecular cell* *30*, 578-588.
- Cornish, P.V., Ermolenko, D.N., Staple, D.W., Hoang, L., Hickerson, R.P., Noller, H.F., and Ha, T. (2009). Following movement of the L1 stalk between three functional states in single ribosomes. *Proceedings of the National Academy of Sciences of the United States of America* *106*, 2571-2576.
- Costa-Mattioli, M., and Walter, P. (2020). The integrated stress response: From mechanism to disease. *Science* *368*.
- Crepin, T., Shalak, V.F., Yaremchuk, A.D., Vlasenko, D.O., McCarthy, A., Negrutskii, B.S., Tukalo, M.A., and El'skaya, A.V. (2014). Mammalian translation elongation factor eEF1A2: X-ray structure

and new features of GDP/GTP exchange mechanism in higher eukaryotes. *Nucleic acids research* 42, 12939-12948.

Crick, F. (1970). Central dogma of molecular biology. *Nature* 227, 561-563.

Crick, F.H. (1958). On protein synthesis. *Symp Soc Exp Biol* 12, 138-163.

Crick, F.H. (1966). Codon--anticodon pairing: the wobble hypothesis. *J Mol Biol* 19, 548-555.

Crick, F.H., Barnett, L., Brenner, S., and Watts-Tobin, R.J. (1961). General nature of the genetic code for proteins. *Nature* 192, 1227-1232.

Cridge, A.G., Crowe-McAuliffe, C., Mathew, S.F., and Tate, W.P. (2018). Eukaryotic translational termination efficiency is influenced by the 3' nucleotides within the ribosomal mRNA channel. *Nucleic acids research* 46, 1927-1944.

Crowe-McAuliffe, C., Graf, M., Huter, P., Takada, H., Abdelshahid, M., Novacek, J., Murina, V., Atkinson, G.C., Hauryliuk, V., and Wilson, D.N. (2018). Structural basis for antibiotic resistance mediated by the *Bacillus subtilis* ABCF ATPase VmlR. *Proceedings of the National Academy of Sciences of the United States of America* 115, 8978-8983.

Crowe-McAuliffe, C., Takada, H., Murina, V., Polte, C., Kasvandik, S., Tenson, T., Ignatova, Z., Atkinson, G.C., Wilson, D.N., and Hauryliuk, V. (2021). Structural Basis for Bacterial Ribosome-Associated Quality Control by RqcH and RqcP. *Molecular cell* 81, 115-126 e117.

Dar, A.C., Dever, T.E., and Sicheri, F. (2005). Higher-order substrate recognition of eIF2alpha by the RNA-dependent protein kinase PKR. *Cell* 122, 887-900.

Darnell, A.M., Subramaniam, A.R., and O'Shea, E.K. (2018). Translational Control through Differential Ribosome Pausing during Amino Acid Limitation in Mammalian Cells. *Molecular cell* 71, 229-243 e211.

Daugeron, M.C., Prouteau, M., Lacroute, F., and Seraphin, B. (2011). The highly conserved eukaryotic DRG factors are required for efficient translation in a manner redundant with the putative RNA helicase Slh1. *Nucleic acids research* 39, 2221-2233.

Davidson, A.L., Dassa, E., Orelle, C., and Chen, J. (2008). Structure, function, and evolution of bacterial ATP-binding cassette systems. *Microbiol Mol Biol Rev* 72, 317-364, table of contents.

de la Cadena, S.G., Hernandez-Fonseca, K., Camacho-Arroyo, I., and Massieu, L. (2014). Glucose deprivation induces reticulum stress by the PERK pathway and caspase-7- and calpain-mediated caspase-12 activation. *Apoptosis* 19, 414-427.

Dean, M., Rzhetsky, A., and Allikmets, R. (2001). The human ATP-binding cassette (ABC) transporter superfamily. *Genome Res* 11, 1156-1166.

Decottignies, A., and Goffeau, A. (1997). Complete inventory of the yeast ABC proteins. *Nat Genet* 15, 137-145.

Defenouillere, Q., Yao, Y., Mouaikel, J., Namane, A., Galopier, A., Decourty, L., Doyen, A., Malabat, C., Saveanu, C., Jacquier, A., et al. (2013). Cdc48-associated complex bound to 60S particles is

required for the clearance of aberrant translation products. *Proceedings of the National Academy of Sciences of the United States of America* *110*, 5046-5051.

Defenouillere, Q., Zhang, E., Namane, A., Mouaikel, J., Jacquier, A., and Fromont-Racine, M. (2016). Rqc1 and Ltn1 Prevent C-terminal Alanine-Threonine Tail (CAT-tail)-induced Protein Aggregation by Efficient Recruitment of Cdc48 on Stalled 60S Subunits. *The Journal of biological chemistry* *291*, 12245-12253.

del Pino, J., Jimenez, J.L., Ventoso, I., Castello, A., Munoz-Fernandez, M.A., de Haro, C., and Berlanga, J.J. (2012). GCN2 has inhibitory effect on human immunodeficiency virus-1 protein synthesis and is cleaved upon viral infection. *PLoS One* *7*, e47272.

Deloche, O., de la Cruz, J., Kressler, D., Doere, M., and Linder, P. (2004). A membrane transport defect leads to a rapid attenuation of translation initiation in *Saccharomyces cerevisiae*. *Molecular cell* *13*, 357-366.

Demeshkina, N., Jenner, L., Westhof, E., Yusupov, M., and Yusupova, G. (2012). A new understanding of the decoding principle on the ribosome. *Nature* *484*, 256-259.

Dever, T.E., and Green, R. (2012). The elongation, termination, and recycling phases of translation in eukaryotes. *Cold Spring Harb Perspect Biol* *4*, a013706.

Dey, M., Cao, C., Sicheri, F., and Dever, T.E. (2007). Conserved intermolecular salt bridge required for activation of protein kinases PKR, GCN2, and PERK. *The Journal of biological chemistry* *282*, 6653-6660.

Dey, M., Velyvis, A., Li, J.J., Chiu, E., Chiovitti, D., Kay, L.E., Sicheri, F., and Dever, T.E. (2011). Requirement for kinase-induced conformational change in eukaryotic initiation factor 2alpha (eIF2alpha) restricts phosphorylation of Ser51. *Proceedings of the National Academy of Sciences of the United States of America* *108*, 4316-4321.

Di Giacco, V., Marquez, V., Qin, Y., Pech, M., Triana-Alonso, F.J., Wilson, D.N., and Nierhaus, K.H. (2008). Shine-Dalgarno interaction prevents incorporation of noncognate amino acids at the codon following the AUG. *Proceedings of the National Academy of Sciences of the United States of America* *105*, 10715-10720.

Diaconu, M., Kothe, U., Schlunzen, F., Fischer, N., Harms, J.M., Tonevitsky, A.G., Stark, H., Rodnina, M.V., and Wahl, M.C. (2005). Structural basis for the function of the ribosomal L7/12 stalk in factor binding and GTPase activation. *Cell* *121*, 991-1004.

Dokladal, L., Stumpe, M., Pillet, B., Hu, Z., Garcia Osuna, G.M., Kressler, D., Dengjel, J., and De Virgilio, C. (2021). Global phosphoproteomics pinpoints uncharted Gcn2-mediated mechanisms of translational control. *Molecular cell*.

Dong, J., Lai, R., Jennings, J.L., Link, A.J., and Hinnebusch, A.G. (2005). The novel ATP-binding cassette protein ARB1 is a shuttling factor that stimulates 40S and 60S ribosome biogenesis. *Molecular and cellular biology* *25*, 9859-9873.

- Dong, J., Lai, R., Nielsen, K., Fekete, C.A., Qiu, H., and Hinnebusch, A.G. (2004). The essential ATP-binding cassette protein RLI1 functions in translation by promoting preinitiation complex assembly. *The Journal of biological chemistry* 279, 42157-42168.
- Dong, J., Qiu, H., Garcia-Barrio, M., Anderson, J., and Hinnebusch, A.G. (2000). Uncharged tRNA activates GCN2 by displacing the protein kinase moiety from a bipartite tRNA-binding domain. *Molecular cell* 6, 269-279.
- Donnelly, N., Gorman, A.M., Gupta, S., and Samali, A. (2013). The eIF2alpha kinases: their structures and functions. *Cell Mol Life Sci* 70, 3493-3511.
- Donze, O., and Picard, D. (1999). Hsp90 binds and regulates Gcn2, the ligand-inducible kinase of the alpha subunit of eukaryotic translation initiation factor 2 [corrected]. *Molecular and cellular biology* 19, 8422-8432.
- Drummond, D.A., and Wilke, C.O. (2008). Mistranslation-induced protein misfolding as a dominant constraint on coding-sequence evolution. *Cell* 134, 341-352.
- Du, T.G., Jellbauer, S., Muller, M., Schmid, M., Niessing, D., and Jansen, R.P. (2008). Nuclear transit of the RNA-binding protein She2 is required for translational control of localized ASH1 mRNA. *EMBO Rep* 9, 781-787.
- Ermolenko, D.N., and Noller, H.F. (2011). mRNA translocation occurs during the second step of ribosomal intersubunit rotation. *Nature structural & molecular biology* 18, 457-462.
- Ero, R., Kumar, V., Su, W., and Gao, Y.G. (2019). Ribosome protection by ABC-F proteins-Molecular mechanism and potential drug design. *Protein science : a publication of the Protein Society* 28, 684-693.
- Fei, J., Bronson, J.E., Hofman, J.M., Srinivas, R.L., Wiggins, C.H., and Gonzalez, R.L., Jr. (2009). Allosteric collaboration between elongation factor G and the ribosomal L1 stalk directs tRNA movements during translation. *Proceedings of the National Academy of Sciences of the United States of America* 106, 15702-15707.
- Fei, J., Kosuri, P., MacDougall, D.D., and Gonzalez, R.L., Jr. (2008). Coupling of ribosomal L1 stalk and tRNA dynamics during translation elongation. *Molecular cell* 30, 348-359.
- Feng, Z.H., Wilson, S.E., Peng, Z.Y., Schlender, K.K., Reimann, E.M., and Trumbly, R.J. (1991). The yeast GLC7 gene required for glycogen accumulation encodes a type 1 protein phosphatase. *The Journal of biological chemistry* 266, 23796-23801.
- Fingar, D.C., Salama, S., Tsou, C., Harlow, E., and Blenis, J. (2002). Mammalian cell size is controlled by mTOR and its downstream targets S6K1 and 4EBP1/eIF4E. *Genes Dev* 16, 1472-1487.
- Flis, J., Holm, M., Rundlet, E.J., Loerke, J., Hilal, T., Dabrowski, M., Burger, J., Mielke, T., Blanchard, S.C., Spahn, C.M.T., et al. (2018). tRNA Translocation by the Eukaryotic 80S Ribosome and the Impact of GTP Hydrolysis. *Cell reports* 25, 2676-2688 e2677.
- Fostier, C.R., Monlezun, L., Ousalem, F., Singh, S., Hunt, J.F., and Boel, G. (2020). ABC-F translation factors: from antibiotic resistance to immune response. *FEBS letters*.

- Francis, S.M., Gas, M.E., Daugeron, M.C., Bravo, J., and Seraphin, B. (2012). Rbg1-Tma46 dimer structure reveals new functional domains and their role in polysome recruitment. *Nucleic acids research* *40*, 11100-11114.
- Frank, J., and Agrawal, R.K. (2000). A ratchet-like inter-subunit reorganization of the ribosome during translocation. *Nature* *406*, 318-322.
- Frank, J., Zhu, J., Penczek, P., Li, Y., Srivastava, S., Verschoor, A., Radermacher, M., Grassucci, R., Lata, R.K., and Agrawal, R.K. (1995). A model of protein synthesis based on cryo-electron microscopy of the *E. coli* ribosome. *Nature* *376*, 441-444.
- Gardiner, D.M., Waring, P., and Howlett, B.J. (2005). The epipolythiodioxopiperazine (ETP) class of fungal toxins: distribution, mode of action, functions and biosynthesis. *Microbiology (Reading)* *151*, 1021-1032.
- Garrigues, A., Escargueil, A.E., and Orłowski, S. (2002). The multidrug transporter, P-glycoprotein, actively mediates cholesterol redistribution in the cell membrane. *Proceedings of the National Academy of Sciences of the United States of America* *99*, 10347-10352.
- Garzia, A., Jafarnejad, S.M., Meyer, C., Chapat, C., Gogakos, T., Morozov, P., Amiri, M., Shapiro, M., Molina, H., Tuschl, T., *et al.* (2017). The E3 ubiquitin ligase and RNA-binding protein ZNF598 orchestrates ribosome quality control of premature polyadenylated mRNAs. *Nature communications* *8*, 16056.
- Gerovac, M., and Tampe, R. (2019). Control of mRNA Translation by Versatile ATP-Driven Machines. *Trends Biochem Sci* *44*, 167-180.
- Ghaemmaghami, S., Huh, W.K., Bower, K., Howson, R.W., Belle, A., Dephoure, N., O'Shea, E.K., and Weissman, J.S. (2003). Global analysis of protein expression in yeast. *Nature* *425*, 737-741.
- Gnrke, A., Geigenmuller, U., Rheinberger, H.J., and Nierhaus, L.H. (1989). The allosteric three-site model for the ribosomal elongation cycle. Analysis with a heteropolymeric mRNA. *The Journal of biological chemistry* *264*, 7291-7301.
- Goldman, D.H., Livingston, N.M., Movsik, J., Wu, B., and Green, R. (2021). Live-cell imaging reveals kinetic determinants of quality control triggered by ribosome stalling. *Molecular cell*.
- Gomez-Gutierrez, R., and Morales, R. (2020). The prion-like phenomenon in Alzheimer's disease: Evidence of pathology transmission in humans. *PLoS Pathog* *16*, e1009004.
- Goossens, A., Dever, T.E., Pascual-Ahuir, A., and Serrano, R. (2001). The protein kinase Gcn2p mediates sodium toxicity in yeast. *The Journal of biological chemistry* *276*, 30753-30760.
- Goscinska, K., Shahmoradi Ghahe, S., Domogala, S., and Topf, U. (2020). Eukaryotic Elongation Factor 3 Protects *Saccharomyces cerevisiae* Yeast from Oxidative Stress. *Genes (Basel)* *11*.
- Grousl, T., Ivanov, P., Malcova, I., Pompach, P., Frydlova, I., Slaba, R., Senohrabkova, L., Novakova, L., and Hasek, J. (2013). Heat shock-induced accumulation of translation elongation and termination factors precedes assembly of stress granules in *S. cerevisiae*. *PLoS One* *8*, e57083.

- Gunisova, S., Hronova, V., Mohammad, M.P., Hinnebusch, A.G., and Valasek, L.S. (2018). Please do not recycle! Translation reinitiation in microbes and higher eukaryotes. *FEMS Microbiol Rev* 42, 165-192.
- Guo, X., Aviles, G., Liu, Y., Tian, R., Unger, B.A., Lin, Y.T., Wiita, A.P., Xu, K., Correia, M.A., and Kampmann, M. (2020). Mitochondrial stress is relayed to the cytosol by an OMA1-DELE1-HRI pathway. *Nature* 579, 427-432.
- Gutierrez, E., Shin, B.S., Woolstenhulme, C.J., Kim, J.R., Saini, P., Buskirk, A.R., and Dever, T.E. (2013). eIF5A promotes translation of polyproline motifs. *Molecular cell* 51, 35-45.
- Han, A.P., Yu, C., Lu, L., Fujiwara, Y., Browne, C., Chin, G., Fleming, M., Leboulch, P., Orkin, S.H., and Chen, J.J. (2001). Heme-regulated eIF2alpha kinase (HRI) is required for translational regulation and survival of erythroid precursors in iron deficiency. *EMBO J* 20, 6909-6918.
- Hao, S., Sharp, J.W., Ross-Inta, C.M., McDaniel, B.J., Anthony, T.G., Wek, R.C., Cavener, D.R., McGrath, B.C., Rudell, J.B., Koehnle, T.J., *et al.* (2005). Uncharged tRNA and sensing of amino acid deficiency in mammalian piriform cortex. *Science* 307, 1776-1778.
- Harding, H.P., Novoa, I., Zhang, Y., Zeng, H., Wek, R., Schapira, M., and Ron, D. (2000). Regulated translation initiation controls stress-induced gene expression in mammalian cells. *Molecular cell* 6, 1099-1108.
- Harding, H.P., Ordonez, A., Allen, F., Parts, L., Inglis, A.J., Williams, R.L., and Ron, D. (2019). The ribosomal P-stalk couples amino acid starvation to GCN2 activation in mammalian cells. *eLife* 8.
- Harding, H.P., Zhang, Y., Zeng, H., Novoa, I., Lu, P.D., Calfon, M., Sadri, N., Yun, C., Popko, B., Paules, R., *et al.* (2003). An integrated stress response regulates amino acid metabolism and resistance to oxidative stress. *Molecular cell* 11, 619-633.
- Harjes, E., Jameson, G.B., Tu, Y.H., Burr, N., Loo, T.S., Goroncy, A.K., Edwards, P.J.B., Harjes, S., Munro, B., Gobl, C., *et al.* (2021). Experimentally based structural model of Yih1 provides insight into its function in controlling the key translational regulator Gcn2. *FEBS letters* 595, 324-340.
- Haurlyuk, V., Atkinson, G.C., Murakami, K.S., Tenson, T., and Gerdes, K. (2015). Recent functional insights into the role of (p)ppGpp in bacterial physiology. *Nat Rev Microbiol* 13, 298-309.
- He, H., Singh, I., Wek, S.A., Dey, S., Baird, T.D., Wek, R.C., and Georgiadis, M.M. (2014). Crystal structures of GCN2 protein kinase C-terminal domains suggest regulatory differences in yeast and mammals. *The Journal of biological chemistry* 289, 15023-15034.
- Hei, Z., Wu, S., Zheng, L., Zhou, J., Liu, Z., Wang, J., and Fang, P. (2021). Crystal structures reveal a novel dimer of the RWD domain of human general control nonderepressible 2. *Biochem Biophys Res Commun* 549, 164-170.
- Heitman, J., Movva, N.R., and Hall, M.N. (1991). Targets for cell cycle arrest by the immunosuppressant rapamycin in yeast. *Science* 253, 905-909.
- Hellen, C.U.T. (2018). Translation Termination and Ribosome Recycling in Eukaryotes. *Cold Spring Harb Perspect Biol* 10.

- Heuer, A., Gerovac, M., Schmidt, C., Trowitzsch, S., Preis, A., Kotter, P., Berninghausen, O., Becker, T., Beckmann, R., and Tampe, R. (2017). Structure of the 40S-ABCE1 post-splitting complex in ribosome recycling and translation initiation. *Nature structural & molecular biology* *24*, 453-460.
- Higgins, C.F. (1992). ABC transporters: from microorganisms to man. *Annu Rev Cell Biol* *8*, 67-113.
- Higgins, C.F., and Linton, K.J. (2004). The ATP switch model for ABC transporters. *Nature structural & molecular biology* *11*, 918-926.
- Hilal, T., Yamamoto, H., Loerke, J., Burger, J., Mielke, T., and Spahn, C.M. (2016). Structural insights into ribosomal rescue by Dom34 and Hbs1 at near-atomic resolution. *Nature communications* *7*, 13521.
- Himeno, H., Kurita, D., and Muto, A. (2014). tmRNA-mediated trans-translation as the major ribosome rescue system in a bacterial cell. *Front Genet* *5*, 66.
- Hines, J., Groll, M., Fahnestock, M., and Crews, C.M. (2008). Proteasome inhibition by fellutamide B induces nerve growth factor synthesis. *Chem Biol* *15*, 501-512.
- Hinnebusch, A.G. (2005). Translational regulation of GCN4 and the general amino acid control of yeast. *Annu Rev Microbiol* *59*, 407-450.
- Hinnebusch, A.G., and Lorsch, J.R. (2012). The mechanism of eukaryotic translation initiation: new insights and challenges. *Cold Spring Harb Perspect Biol* *4*.
- Hirashima, A., and Kaji, A. (1973). Role of elongation factor G and a protein factor on the release of ribosomes from messenger ribonucleic acid. *The Journal of biological chemistry* *248*, 7580-7587.
- Ho, Y., Gruhler, A., Heilbut, A., Bader, G.D., Moore, L., Adams, S.L., Millar, A., Taylor, P., Bennett, K., Boutilier, K., *et al.* (2002). Systematic identification of protein complexes in *Saccharomyces cerevisiae* by mass spectrometry. *Nature* *415*, 180-183.
- Hoernes, T.P., Clementi, N., Juen, M.A., Shi, X., Faserl, K., Willi, J., Gasser, C., Kreutz, C., Joseph, S., Lindner, H., *et al.* (2018). Atomic mutagenesis of stop codon nucleotides reveals the chemical prerequisites for release factor-mediated peptide release. *Proceedings of the National Academy of Sciences of the United States of America* *115*, E382-E389.
- Hopfield, J.J. (1974). Kinetic proofreading: a new mechanism for reducing errors in biosynthetic processes requiring high specificity. *Proceedings of the National Academy of Sciences of the United States of America* *71*, 4135-4139.
- Hueso, G., Aparicio-Sanchis, R., Montesinos, C., Lorenz, S., Murguia, J.R., and Serrano, R. (2012). A novel role for protein kinase Gcn2 in yeast tolerance to intracellular acid stress. *Biochem J* *441*, 255-264.
- Hunter, S., Jones, P., Mitchell, A., Apweiler, R., Attwood, T.K., Bateman, A., Bernard, T., Binns, D., Bork, P., Burge, S., *et al.* (2012). InterPro in 2011: new developments in the family and domain prediction database. *Nucleic acids research* *40*, D306-312.

- Hutchison, J.S., Feinberg, B., Rothwell, T.C., and Moldave, K. (1984). Monoclonal antibody specific for yeast elongation factor 3. *Biochemistry* 23, 3055-3063.
- Ikeuchi, K., Tesina, P., Matsuo, Y., Sugiyama, T., Cheng, J., Saeki, Y., Tanaka, K., Becker, T., Beckmann, R., and Inada, T. (2019). Collided ribosomes form a unique structural interface to induce Hel2-driven quality control pathways. *EMBO J* 38.
- Ikeuchi, K., Yazaki, E., Kudo, K., and Inada, T. (2016). Conserved functions of human Pelota in mRNA quality control of nonstop mRNA. *FEBS letters* 590, 3254-3263.
- Imseeng, S., Aylett, C.H., and Maier, T. (2018). Architecture and activation of phosphatidylinositol 3-kinase related kinases. *Curr Opin Struct Biol* 49, 177-189.
- Inglis, A.J., Masson, G.R., Shao, S., Perisic, O., McLaughlin, S.H., Hegde, R.S., and Williams, R.L. (2019). Activation of GCN2 by the ribosomal P-stalk. *Proceedings of the National Academy of Sciences of the United States of America* 116, 4946-4954.
- Ishikawa, K., Azuma, S., Ikawa, S., Semba, K., and Inoue, J. (2005). Identification of DRG family regulatory proteins (DFRPs): specific regulation of DRG1 and DRG2. *Genes Cells* 10, 139-150.
- Ishikawa, K., Ito, K., Inoue, J., and Semba, K. (2013). Cell growth control by stable Rbg2/Gir2 complex formation under amino acid starvation. *Genes Cells* 18, 859-872.
- Ishimura, R., Nagy, G., Dotu, I., Chuang, J.H., and Ackerman, S.L. (2016). Activation of GCN2 kinase by ribosome stalling links translation elongation with translation initiation. *eLife* 5.
- Ishimura, R., Nagy, G., Dotu, I., Zhou, H., Yang, X.L., Schimmel, P., Senju, S., Nishimura, Y., Chuang, J.H., and Ackerman, S.L. (2014). RNA function. Ribosome stalling induced by mutation of a CNS-specific tRNA causes neurodegeneration. *Science* 345, 455-459.
- Ito, K., Honda, T., Suzuki, T., Miyoshi, T., Murakami, R., Yao, M., and Uchiumi, T. (2014). Molecular insights into the interaction of the ribosomal stalk protein with elongation factor 1alpha. *Nucleic acids research* 42, 14042-14052.
- Jackson, R.J., Hellen, C.U., and Pestova, T.V. (2010). The mechanism of eukaryotic translation initiation and principles of its regulation. *Nat Rev Mol Cell Biol* 11, 113-127.
- Jackson, R.J., Hellen, C.U., and Pestova, T.V. (2012). Termination and post-termination events in eukaryotic translation. *Adv Protein Chem Struct Biol* 86, 45-93.
- Janssen, B.D., and Hayes, C.S. (2012). The tmRNA ribosome-rescue system. *Adv Protein Chem Struct Biol* 86, 151-191.
- Jimenez-Diaz, A., Remacha, M., Ballesta, J.P., and Berlanga, J.J. (2013). Phosphorylation of initiation factor eIF2 in response to stress conditions is mediated by acidic ribosomal P1/P2 proteins in *Saccharomyces cerevisiae*. *PLoS One* 8, e84219.
- Joazeiro, C.A.P. (2017). Ribosomal Stalling During Translation: Providing Substrates for Ribosome-Associated Protein Quality Control. *Annu Rev Cell Dev Biol* 33, 343-368.
- Joazeiro, C.A.P. (2019). Mechanisms and functions of ribosome-associated protein quality control. *Nat Rev Mol Cell Biol* 20, 368-383.

- Jones, P.M., and George, A.M. (2013). Mechanism of the ABC transporter ATPase domains: catalytic models and the biochemical and biophysical record. *Crit Rev Biochem Mol Biol* 48, 39-50.
- Jousse, C., Oyadomari, S., Novoa, I., Lu, P., Zhang, Y., Harding, H.P., and Ron, D. (2003). Inhibition of a constitutive translation initiation factor 2alpha phosphatase, CReP, promotes survival of stressed cells. *J Cell Biol* 163, 767-775.
- Julian, P., Konevega, A.L., Scheres, S.H., Lazaro, M., Gil, D., Wintermeyer, W., Rodnina, M.V., and Valle, M. (2008). Structure of ratcheted ribosomes with tRNAs in hybrid states. *Proceedings of the National Academy of Sciences of the United States of America* 105, 16924-16927.
- Juzskiewicz, S., and Hegde, R.S. (2017). Initiation of Quality Control during Poly(A) Translation Requires Site-Specific Ribosome Ubiquitination. *Molecular cell* 65, 743-750 e744.
- Kamath, A., and Chakraburttty, K. (1989). Role of yeast elongation factor 3 in the elongation cycle. *The Journal of biological chemistry* 264, 15423-15428.
- Kambampati, R., Pellegrino, C., Paiva, A., Huang, L., Mende-Mueller, L., and Chakraburttty, K. (2000). Limited proteolysis of yeast elongation factor 3. Sequence and location of the subdomains. *The Journal of biological chemistry* 275, 16963-16968.
- Kaminishi, T., Wilson, D.N., Takemoto, C., Harms, J.M., Kawazoe, M., Schluenzen, F., Hanawa-Suetsugu, K., Shirouzu, M., Fucini, P., and Yokoyama, S. (2007). A snapshot of the 30S ribosomal subunit capturing mRNA via the Shine-Dalgarno interaction. *Structure* 15, 289-297.
- Karimi, R., Pavlov, M.Y., Buckingham, R.H., and Ehrenberg, M. (1999). Novel roles for classical factors at the interface between translation termination and initiation. *Molecular cell* 3, 601-609.
- Kasari, V., Margus, T., Atkinson, G.C., Johansson, M.J.O., and Hauryliuk, V. (2019). Ribosome profiling analysis of eEF3-depleted *Saccharomyces cerevisiae*. *Sci Rep* 9, 3037.
- Keedy, H.E., Thomas, E.N., and Zaher, H.S. (2018). Decoding on the ribosome depends on the structure of the mRNA phosphodiester backbone. *Proceedings of the National Academy of Sciences of the United States of America* 115, E6731-E6740.
- Kellis, M., Birren, B.W., and Lander, E.S. (2004). Proof and evolutionary analysis of ancient genome duplication in the yeast *Saccharomyces cerevisiae*. *Nature* 428, 617-624.
- Kim, E. (2009). Mechanisms of amino acid sensing in mTOR signaling pathway. *Nutr Res Pract* 3, 64-71.
- Kim, J., Daniel, J., Espejo, A., Lake, A., Krishna, M., Xia, L., Zhang, Y., and Bedford, M.T. (2006). Tudor, MBT and chromo domains gauge the degree of lysine methylation. *EMBO Rep* 7, 397-403.
- Kim, K., Park, J.E., Yeom, J., Park, N., Tran, T.T., and Kang, M.J. (2020). Tissue-specific roles of GCN2 in aging and autosomal dominant retinitis pigmentosa. *Biochem Biophys Res Commun* 533, 1054-1060.
- Kisselev, L., Ehrenberg, M., and Frolova, L. (2003). Termination of translation: interplay of mRNA, rRNAs and release factors? *EMBO J* 22, 175-182.

- Ko, M.S., Lee, U.H., Kim, S.I., Kim, H.J., Park, J.J., Cha, S.J., Kim, S.B., Song, H., Chung, D.K., Han, I.S., *et al.* (2004). Overexpression of DRG2 suppresses the growth of Jurkat T cells but does not induce apoptosis. *Arch Biochem Biophys* 422, 137-144.
- Kobe, B., Gleichmann, T., Horne, J., Jennings, I.G., Scotney, P.D., and Teh, T. (1999). Turn up the HEAT. *Structure* 7, R91-97.
- Koehn, J., Fountoulakis, M., and Krapfenbauer, K. (2008). Multiple drug resistance associated with function of ABC-transporters in diabetes mellitus: molecular mechanism and clinical relevance. *Infect Disord Drug Targets* 8, 109-118.
- Kojima, E., Takeuchi, A., Haneda, M., Yagi, A., Hasegawa, T., Yamaki, K., Takeda, K., Akira, S., Shimokata, K., and Isobe, K. (2003). The function of GADD34 is a recovery from a shutoff of protein synthesis induced by ER stress: elucidation by GADD34-deficient mice. *FASEB J* 17, 1573-1575.
- Korostelev, A., Trakhanov, S., Asahara, H., Laurberg, M., Lancaster, L., and Noller, H.F. (2007). Interactions and dynamics of the Shine Dalgarno helix in the 70S ribosome. *Proceedings of the National Academy of Sciences of the United States of America* 104, 16840-16843.
- Korostelev, A.A. (2011). Structural aspects of translation termination on the ribosome. *RNA* 17, 1409-1421.
- Kostova, K.K., Hickey, K.L., Osuna, B.A., Hussmann, J.A., Frost, A., Weinberg, D.E., and Weissman, J.S. (2017). CAT-tailing as a fail-safe mechanism for efficient degradation of stalled nascent polypeptides. *Science* 357, 414-417.
- Kovalchuk, O., and Chakraburty, K. (1994). Comparative analysis of ribosome-associated adenosinetriphosphatase (ATPase) from pig liver and the ATPase of elongation factor 3 from *Saccharomyces cerevisiae*. *Eur J Biochem* 226, 133-140.
- Krogan, N.J., Cagney, G., Yu, H., Zhong, G., Guo, X., Ignatchenko, A., Li, J., Pu, S., Datta, N., Tikuisis, A.P., *et al.* (2006). Global landscape of protein complexes in the yeast *Saccharomyces cerevisiae*. *Nature* 440, 637-643.
- Kryuchkova, P., Grishin, A., Eliseev, B., Karyagina, A., Frolova, L., and Alkalaeva, E. (2013). Two-step model of stop codon recognition by eukaryotic release factor eRF1. *Nucleic acids research* 41, 4573-4586.
- Kubota, H., Obata, T., Ota, K., Sasaki, T., and Ito, T. (2003). Rapamycin-induced translational derepression of GCN4 mRNA involves a novel mechanism for activation of the eIF2 alpha kinase GCN2. *The Journal of biological chemistry* 278, 20457-20460.
- Kubota, H., Ota, K., Sakaki, Y., and Ito, T. (2001). Budding yeast GCN1 binds the GI domain to activate the eIF2alpha kinase GCN2. *The Journal of biological chemistry* 276, 17591-17596.
- Kubota, H., Sakaki, Y., and Ito, T. (2000). GI domain-mediated association of the eukaryotic initiation factor 2alpha kinase GCN2 with its activator GCN1 is required for general amino acid control in budding yeast. *The Journal of biological chemistry* 275, 20243-20246.

- Kurata, S., Nielsen, K.H., Mitchell, S.F., Lorsch, J.R., Kaji, A., and Kaji, H. (2010). Ribosome recycling step in yeast cytoplasmic protein synthesis is catalyzed by eEF3 and ATP. *Proceedings of the National Academy of Sciences of the United States of America* *107*, 10854-10859.
- Kurata, S., Shen, B., Liu, J.O., Takeuchi, N., Kaji, A., and Kaji, H. (2013). Possible steps of complete disassembly of post-termination complex by yeast eEF3 deduced from inhibition by translocation inhibitors. *Nucleic acids research* *41*, 264-276.
- Lageix, S., Rothenburg, S., Dever, T.E., and Hinnebusch, A.G. (2014). Enhanced interaction between pseudokinase and kinase domains in Gcn2 stimulates eIF2alpha phosphorylation in starved cells. *PLoS Genet* *10*, e1004326.
- Lageix, S., Zhang, J., Rothenburg, S., and Hinnebusch, A.G. (2015). Interaction between the tRNA-binding and C-terminal domains of Yeast Gcn2 regulates kinase activity in vivo. *PLoS Genet* *11*, e1004991.
- Laplante, M., and Sabatini, D.M. (2012). mTOR signaling in growth control and disease. *Cell* *149*, 274-293.
- Lee, K.M., Yu, C.W., Chan, D.S., Chiu, T.Y., Zhu, G., Sze, K.H., Shaw, P.C., and Wong, K.B. (2010). Solution structure of the dimerization domain of ribosomal protein P2 provides insights for the structural organization of eukaryotic stalk. *Nucleic acids research* *38*, 5206-5216.
- Lee, K.M., Yu, C.W., Chiu, T.Y., Sze, K.H., Shaw, P.C., and Wong, K.B. (2012). Solution structure of the dimerization domain of the eukaryotic stalk P1/P2 complex reveals the structural organization of eukaryotic stalk complex. *Nucleic acids research* *40*, 3172-3182.
- Lee, S.J., Swanson, M.J., and Sattlegger, E. (2015). Gcn1 contacts the small ribosomal protein Rps10, which is required for full activation of the protein kinase Gcn2. *Biochem J* *466*, 547-559.
- Lehman, S.L., Ryeom, S., and Koumenis, C. (2015). Signaling through alternative Integrated Stress Response pathways compensates for GCN2 loss in a mouse model of soft tissue sarcoma. *Sci Rep* *5*, 11781.
- Letzring, D.P., Wolf, A.S., Brule, C.E., and Grayhack, E.J. (2013). Translation of CGA codon repeats in yeast involves quality control components and ribosomal protein L1. *RNA* *19*, 1208-1217.
- Leung, E.K., Suslov, N., Tuttle, N., Sengupta, R., and Piccirilli, J.A. (2011). The mechanism of peptidyl transfer catalysis by the ribosome. *Annu Rev Biochem* *80*, 527-555.
- Li, M.W., AuYeung, W.K., and Lam, H.M. (2013). The GCN2 homologue in *Arabidopsis thaliana* interacts with uncharged tRNA and uses *Arabidopsis* eIF2alpha molecules as direct substrates. *Plant Biol (Stuttg)* *15*, 13-18.
- Li, Z., Lee, I., Moradi, E., Hung, N.J., Johnson, A.W., and Marcotte, E.M. (2009). Rational extension of the ribosome biogenesis pathway using network-guided genetics. *PLoS Biol* *7*, e1000213.
- Liebman, S.W., and Chernoff, Y.O. (2012). Prions in yeast. *Genetics* *191*, 1041-1072.
- Lill, R., and Wintermeyer, W. (1987). Destabilization of codon-anticodon interaction in the ribosomal exit site. *J Mol Biol* *196*, 137-148.

- Locher, K.P. (2016). Mechanistic diversity in ATP-binding cassette (ABC) transporters. *Nature structural & molecular biology* 23, 487-493.
- Loveland, A.B., Demo, G., and Korostelev, A.A. (2020). Cryo-EM of elongating ribosome with EF-Tu*GTP elucidates tRNA proofreading. *Nature* 584, 640-645.
- Lu, L., Han, A.P., and Chen, J.J. (2001). Translation initiation control by heme-regulated eukaryotic initiation factor 2alpha kinase in erythroid cells under cytoplasmic stresses. *Molecular and cellular biology* 21, 7971-7980.
- Lu, W., Laszlo, C.F., Miao, Z., Chen, H., and Wu, S. (2009). The role of nitric-oxide synthase in the regulation of UVB light-induced phosphorylation of the alpha subunit of eukaryotic initiation factor 2. *The Journal of biological chemistry* 284, 24281-24288.
- Ma, T., Trinh, M.A., Wexler, A.J., Bourbon, C., Gatti, E., Pierre, P., Cavener, D.R., and Klann, E. (2013). Suppression of eIF2alpha kinases alleviates Alzheimer's disease-related plasticity and memory deficits. *Nat Neurosci* 16, 1299-1305.
- Maia de Oliveira, T., Korboukh, V., Caswell, S., Winter Holt, J.J., Lamb, M., Hird, A.W., and Overman, R. (2020). The structure of human GCN2 reveals a parallel, back-to-back kinase dimer with a plastic DFG activation loop motif. *Biochem J* 477, 275-284.
- Maracci, C., and Rodnina, M.V. (2016). Review: Translational GTPases. *Biopolymers* 105, 463-475.
- Marton, M.J., Crouch, D., and Hinnebusch, A.G. (1993). GCN1, a translational activator of GCN4 in *Saccharomyces cerevisiae*, is required for phosphorylation of eukaryotic translation initiation factor 2 by protein kinase GCN2. *Molecular and cellular biology* 13, 3541-3556.
- Marton, M.J., Vazquez de Aldana, C.R., Qiu, H., Chakraborty, K., and Hinnebusch, A.G. (1997). Evidence that GCN1 and GCN20, translational regulators of GCN4, function on elongating ribosomes in activation of eIF2alpha kinase GCN2. *Molecular and cellular biology* 17, 4474-4489.
- Masson, G.R. (2019). Towards a model of GCN2 activation. *Biochem Soc Trans*.
- Mateyak, M.K., Pupek, J.K., Garino, A.E., Knapp, M.C., Colmer, S.F., Kinzy, T.G., and Dunaway, S. (2018). Demonstration of translation elongation factor 3 activity from a non-fungal species, *Phytophthora infestans*. *PLoS One* 13, e0190524.
- Matheisl, S., Berninghausen, O., Becker, T., and Beckmann, R. (2015). Structure of a human translation termination complex. *Nucleic acids research* 43, 8615-8626.
- Matsuo, Y., Ikeuchi, K., Saeki, Y., Iwasaki, S., Schmidt, C., Udagawa, T., Sato, F., Tsuchiya, H., Becker, T., Tanaka, K., *et al.* (2017). Ubiquitination of stalled ribosome triggers ribosome-associated quality control. *Nature communications* 8, 159.
- Matsuo, Y., and Inada, T. (2021). The ribosome collision sensor Hel2 functions as preventive quality control in the secretory pathway. *Cell reports* 34, 108877.
- Matzov, D., Eyal, Z., Benhamou, R.I., Shalev-Benami, M., Halfon, Y., Krupkin, M., Zimmerman, E., Rozenberg, H., Bashan, A., Fridman, M., *et al.* (2017). Structural insights of lincosamides targeting the ribosome of *Staphylococcus aureus*. *Nucleic acids research* 45, 10284-10292.

- Maurice, T.C., Mazzucco, C.E., Ramanathan, C.S., Ryan, B.M., Warr, G.A., and Puziss, J.W. (1998). A highly conserved intraspecies homolog of the *Saccharomyces cerevisiae* elongation factor-3 encoded by the HEF3 gene. *Yeast* *14*, 1105-1113.
- Mazor, K.M., Dong, L., Mao, Y., Swanda, R.V., Qian, S.B., and Stipanuk, M.H. (2018). Effects of single amino acid deficiency on mRNA translation are markedly different for methionine versus leucine. *Sci Rep* *8*, 8076.
- McCormick, J.W., Vogel, P.D., and Wise, J.G. (2015). Multiple Drug Transport Pathways through Human P-Glycoprotein. *Biochemistry* *54*, 4374-4390.
- McFarland, M.R., Keller, C.D., Childers, B.M., Adeniyi, S.A., Corrigan, H., Raguin, A., Romano, M.C., and Stansfield, I. (2020). The molecular aetiology of tRNA synthetase depletion: induction of a GCN4 amino acid starvation response despite homeostatic maintenance of charged tRNA levels. *Nucleic acids research* *48*, 3071-3088.
- Melnikov, S., Ben-Shem, A., Garreau de Loubresse, N., Jenner, L., Yusupova, G., and Yusupov, M. (2012). One core, two shells: bacterial and eukaryotic ribosomes. *Nature structural & molecular biology* *19*, 560-567.
- Merrick, W.C. (2015). eIF4F: a retrospective. *The Journal of biological chemistry* *290*, 24091-24099.
- Meydan, S., and Guydosh, N.R. (2020). Disome and Trisome Profiling Reveal Genome-wide Targets of Ribosome Quality Control. *Molecular cell*.
- Michelitsch, M.D., and Weissman, J.S. (2000). A census of glutamine/asparagine-rich regions: implications for their conserved function and the prediction of novel prions. *Proceedings of the National Academy of Sciences of the United States of America* *97*, 11910-11915.
- Miyazaki, M., Uritani, M., and Kagiyama, H. (1988). The yeast peptide elongation factor 3 (EF-3) carries an active site for ATP hydrolysis which can interact with various nucleoside triphosphates in the absence of ribosomes. *J Biochem* *104*, 445-450.
- Moazed, D., and Noller, H.F. (1989). Intermediate states in the movement of transfer RNA in the ribosome. *Nature* *342*, 142-148.
- Mohan, S., and Noller, H.F. (2017). Recurring RNA structural motifs underlie the mechanics of L1 stalk movement. *Nature communications* *8*, 14285.
- Moldave, K. (1985). Eukaryotic protein synthesis. *Annu Rev Biochem* *54*, 1109-1149.
- Monti, F., Ripamonti, F., Hawser, S.P., and Islam, K. (1999). Aspirochlorine: a highly selective and potent inhibitor of fungal protein synthesis. *The Journal of antibiotics* *52*, 311-318.
- Moore, S.D., and Sauer, R.T. (2007). The tmRNA system for translational surveillance and ribosome rescue. *Annu Rev Biochem* *76*, 101-124.
- Muhs, M., Hilal, T., Mielke, T., Skabkin, M.A., Sanbonmatsu, K.Y., Pestova, T.V., and Spahn, C.M. (2015). Cryo-EM of ribosomal 80S complexes with termination factors reveals the translocated cricket paralysis virus IRES. *Molecular cell* *57*, 422-432.

- Muller, C., Crowe-McAuliffe, C., and Wilson, D.N. (2021). Ribosome Rescue Pathways in Bacteria. *Front Microbiol* *12*, 652980.
- Munro, J.B., Sanbonmatsu, K.Y., Spahn, C.M., and Blanchard, S.C. (2009). Navigating the ribosome's metastable energy landscape. *Trends Biochem Sci* *34*, 390-400.
- Murina, V., Kasari, M., Takada, H., Hinnu, M., Saha, C.K., Grimshaw, J.W., Seki, T., Reith, M., Putrins, M., Tenson, T., *et al.* (2018). ABCF ATPases Involved in Protein Synthesis, Ribosome Assembly and Antibiotic Resistance: Structural and Functional Diversification across the Tree of Life. *J Mol Biol*.
- Myasnikov, A.G., Simonetti, A., Marzi, S., and Klaholz, B.P. (2009). Structure-function insights into prokaryotic and eukaryotic translation initiation. *Curr Opin Struct Biol* *19*, 300-309.
- Nakane, T., Kotecha, A., Sente, A., McMullan, G., Masiulis, S., Brown, P., Grigoras, I.T., Malinauskaite, L., Malinauskas, T., Miehl, J., *et al.* (2020). Single-particle cryo-EM at atomic resolution. *Nature* *587*, 152-156.
- Nameki, N., Yoneyama, M., Koshiya, S., Tochio, N., Inoue, M., Seki, E., Matsuda, T., Tomo, Y., Harada, T., Saito, K., *et al.* (2004). Solution structure of the RWD domain of the mouse GCN2 protein. *Protein science : a publication of the Protein Society* *13*, 2089-2100.
- Nanayakkara, A.K., Follit, C.A., Chen, G., Williams, N.S., Vogel, P.D., and Wise, J.G. (2018). Targeted inhibitors of P-glycoprotein increase chemotherapeutic-induced mortality of multidrug resistant tumor cells. *Sci Rep* *8*, 967.
- Natarajan, K., Meyer, M.R., Jackson, B.M., Slade, D., Roberts, C., Hinnebusch, A.G., and Marton, M.J. (2001). Transcriptional profiling shows that Gcn4p is a master regulator of gene expression during amino acid starvation in yeast. *Molecular and cellular biology* *21*, 4347-4368.
- Natchiar, S.K., Myasnikov, A.G., Kratzat, H., Hazemann, I., and Klaholz, B.P. (2017). Visualization of chemical modifications in the human 80S ribosome structure. *Nature* *551*, 472-477.
- Nielsen, P.R., Nietlispach, D., Mott, H.R., Callaghan, J., Bannister, A., Kouzarides, T., Murzin, A.G., Murzina, N.V., and Laue, E.D. (2002). Structure of the HP1 chromodomain bound to histone H3 methylated at lysine 9. *Nature* *416*, 103-107.
- Nierhaus, K.H. (1990). The allosteric three-site model for the ribosomal elongation cycle: features and future. *Biochemistry* *29*, 4997-5008.
- Nierhaus, K.H., Beyer, D., Dabrowski, M., Schafer, M.A., Spahn, C.M., Wadzack, J., Bittner, J.U., Burkhardt, N., Diedrich, G., Junemann, R., *et al.* (1995). The elongating ribosome: structural and functional aspects. *Biochem Cell Biol* *73*, 1011-1021.
- Nikaido, K., and Ames, G.F. (1999). One intact ATP-binding subunit is sufficient to support ATP hydrolysis and translocation in an ABC transporter, the histidine permease. *The Journal of biological chemistry* *274*, 26727-26735.
- Nikonorova, I.A., Mirek, E.T., Signore, C.C., Goudie, M.P., Wek, R.C., and Anthony, T.G. (2018). Time-resolved analysis of amino acid stress identifies eIF2 phosphorylation as necessary to inhibit mTORC1 activity in liver. *The Journal of biological chemistry* *293*, 5005-5015.

- Ning, W., Fei, J., and Gonzalez, R.L., Jr. (2014). The ribosome uses cooperative conformational changes to maximize and regulate the efficiency of translation. *Proceedings of the National Academy of Sciences of the United States of America* *111*, 12073-12078.
- Nogales, E., and Scheres, S.H. (2015). Cryo-EM: A Unique Tool for the Visualization of Macromolecular Complexity. *Molecular cell* *58*, 677-689.
- Novoa, I., Zhang, Y., Zeng, H., Jungreis, R., Harding, H.P., and Ron, D. (2003). Stress-induced gene expression requires programmed recovery from translational repression. *EMBO J* *22*, 1180-1187.
- Ogle, J.M., Brodersen, D.E., Clemons, W.M., Jr., Tarry, M.J., Carter, A.P., and Ramakrishnan, V. (2001). Recognition of cognate transfer RNA by the 30S ribosomal subunit. *Science* *292*, 897-902.
- Osherovich, L.Z., and Weissman, J.S. (2001). Multiple Gln/Asn-rich prion domains confer susceptibility to induction of the yeast [PSI(+)] prion. *Cell* *106*, 183-194.
- Oswald, C., Holland, I.B., and Schmitt, L. (2006). The motor domains of ABC-transporters. What can structures tell us? *Naunyn Schmiedebergs Arch Pharmacol* *372*, 385-399.
- Ousalem, F., Singh, S., Chesneau, O., Hunt, J.F., and Boel, G. (2019). ABC-F proteins in mRNA translation and antibiotic resistance. *Res Microbiol* *170*, 435-447.
- Padyana, A.K., Qiu, H., Roll-Mecak, A., Hinnebusch, A.G., and Burley, S.K. (2005). Structural basis for autoinhibition and mutational activation of eukaryotic initiation factor 2alpha protein kinase GCN2. *The Journal of biological chemistry* *280*, 29289-29299.
- Pakos-Zebrucka, K., Koryga, I., Mnich, K., Ljubic, M., Samali, A., and Gorman, A.M. (2016). The integrated stress response. *EMBO Rep* *17*, 1374-1395.
- Park, Y., Reyna-Neyra, A., Philippe, L., and Thoreen, C.C. (2017). mTORC1 Balances Cellular Amino Acid Supply with Demand for Protein Synthesis through Post-transcriptional Control of ATF4. *Cell reports* *19*, 1083-1090.
- Paytubi, S., Wang, X., Lam, Y.W., Izquierdo, L., Hunter, M.J., Jan, E., Hundal, H.S., and Proud, C.G. (2009). ABC50 promotes translation initiation in mammalian cells. *The Journal of biological chemistry* *284*, 24061-24073.
- Pereira, C.M., Filev, R., Dubiela, F.P., Brandao, B.B., Queiroz, C.M., Ludwig, R.G., Hipolide, D., Longo, B.M., Mello, L.E., Mori, M.A., *et al.* (2019). The GCN2 inhibitor IMPACT contributes to diet-induced obesity and body temperature control. *PLoS One* *14*, e0217287.
- Pereira, C.M., Sattlegger, E., Jiang, H.Y., Longo, B.M., Jaqueta, C.B., Hinnebusch, A.G., Wek, R.C., Mello, L.E., and Castilho, B.A. (2005). IMPACT, a protein preferentially expressed in the mouse brain, binds GCN1 and inhibits GCN2 activation. *The Journal of biological chemistry* *280*, 28316-28323.
- Perona, J.J., and Gruic-Sovulj, I. (2014). Synthetic and editing mechanisms of aminoacyl-tRNA synthetases. *Top Curr Chem* *344*, 1-41.
- Peske, F., Rodnina, M.V., and Wintermeyer, W. (2005). Sequence of steps in ribosome recycling as defined by kinetic analysis. *Molecular cell* *18*, 403-412.

- Philips, A.M., and Khan, N. (2021). Amino acid sensing pathway: A major check point in the pathogenesis of obesity and COVID-19. *Obes Rev*, e13221.
- Pisarev, A.V., Skabkin, M.A., Pisareva, V.P., Skabkina, O.V., Rakotondrifara, A.M., Hentze, M.W., Hellen, C.U., and Pestova, T.V. (2010). The role of ABCE1 in eukaryotic posttermination ribosomal recycling. *Molecular cell* 37, 196-210.
- Pisareva, V.P., Skabkin, M.A., Hellen, C.U., Pestova, T.V., and Pisarev, A.V. (2011). Dissociation by Pelota, Hbs1 and ABCE1 of mammalian vacant 80S ribosomes and stalled elongation complexes. *EMBO J* 30, 1804-1817.
- Preis, A., Heuer, A., Barrio-Garcia, C., Hauser, A., Eyler, D.E., Berninghausen, O., Green, R., Becker, T., and Beckmann, R. (2014). Cryoelectron microscopic structures of eukaryotic translation termination complexes containing eRF1-eRF3 or eRF1-ABCE1. *Cell reports* 8, 59-65.
- Priess, M., Goddeke, H., Groenhof, G., and Schafer, L.V. (2018). Molecular Mechanism of ATP Hydrolysis in an ABC Transporter. *ACS central science* 4, 1334-1343.
- Proud, C.G. (2014). Control of the translational machinery by amino acids. *Am J Clin Nutr* 99, 231S-236S.
- Qiu, H., Dong, J., Hu, C., Francklyn, C.S., and Hinnebusch, A.G. (2001). The tRNA-binding moiety in GCN2 contains a dimerization domain that interacts with the kinase domain and is required for tRNA binding and kinase activation. *EMBO J* 20, 1425-1438.
- Qiu, H., Garcia-Barrio, M.T., and Hinnebusch, A.G. (1998). Dimerization by translation initiation factor 2 kinase GCN2 is mediated by interactions in the C-terminal ribosome-binding region and the protein kinase domain. *Molecular and cellular biology* 18, 2697-2711.
- Rabl, J., Leibundgut, M., Ataide, S.F., Haag, A., and Ban, N. (2011). Crystal structure of the eukaryotic 40S ribosomal subunit in complex with initiation factor 1. *Science* 331, 730-736.
- Ramesh, R., and Sattlegger, E. (2020). Domain II of the translation elongation factor eEF1A is required for Gcn2 kinase inhibition. *FEBS letters* 594, 2266-2281.
- Ramirez, M., Wek, R.C., and Hinnebusch, A.G. (1991). Ribosome association of GCN2 protein kinase, a translational activator of the GCN4 gene of *Saccharomyces cerevisiae*. *Molecular and cellular biology* 11, 3027-3036.
- Ramrath, D.J., Lancaster, L., Sprink, T., Mielke, T., Loerke, J., Noller, H.F., and Spahn, C.M. (2013). Visualization of two transfer RNAs trapped in transit during elongation factor G-mediated translocation. *Proceedings of the National Academy of Sciences of the United States of America* 110, 20964-20969.
- Ranjan, N., Pochopien, A.A., Chih-Chien Wu, C., Beckert, B., Blanchet, S., Green, R., M, V.R., and Wilson, D.N. (2021). Yeast translation elongation factor eEF3 promotes late stages of tRNA translocation. *EMBO J* 40, e106449.
- Rees, D.C., Johnson, E., and Lewinson, O. (2009). ABC transporters: the power to change. *Nat Rev Mol Cell Biol* 10, 218-227.

- Rheinberger, H.J., Sternbach, H., and Nierhaus, K.H. (1981). Three tRNA binding sites on Escherichia coli ribosomes. *Proceedings of the National Academy of Sciences of the United States of America* 78, 5310-5314.
- Rodland, G.E., Tvegard, T., Boye, E., and Grallert, B. (2014). Crosstalk between the Tor and Gcn2 pathways in response to different stresses. *Cell Cycle* 13, 453-461.
- Rodnina, M.V., Serebryanik, A.I., Ovcharenko, G.V., and El'Skaya, A.V. (1994). ATPase strongly bound to higher eukaryotic ribosomes. *Eur J Biochem* 225, 305-310.
- Roemer, T., Davies, J., Giaever, G., and Nislow, C. (2011a). Bugs, drugs and chemical genomics. *Nat Chem Biol* 8, 46-56.
- Roemer, T., Xu, D., Singh, S.B., Parish, C.A., Harris, G., Wang, H., Davies, J.E., and Bills, G.F. (2011b). Confronting the challenges of natural product-based antifungal discovery. *Chem Biol* 18, 148-164.
- Rojas, M., Gingras, A.C., and Dever, T.E. (2014). Protein phosphatase PP1/GLC7 interaction domain in yeast eIF2gamma bypasses targeting subunit requirement for eIF2alpha dephosphorylation. *Proceedings of the National Academy of Sciences of the United States of America* 111, E1344-1353.
- Rolfes, R.J., and Hinnebusch, A.G. (1993). Translation of the yeast transcriptional activator GCN4 is stimulated by purine limitation: implications for activation of the protein kinase GCN2. *Molecular and cellular biology* 13, 5099-5111.
- Romano, P.R., Garcia-Barrio, M.T., Zhang, X., Wang, Q., Taylor, D.R., Zhang, F., Herring, C., Mathews, M.B., Qin, J., and Hinnebusch, A.G. (1998). Autophosphorylation in the activation loop is required for full kinase activity in vivo of human and yeast eukaryotic initiation factor 2alpha kinases PKR and GCN2. *Molecular and cellular biology* 18, 2282-2297.
- Roobol, A., Roobol, J., Bastide, A., Knight, J.R., Willis, A.E., and Smales, C.M. (2015). p58IPK is an inhibitor of the eIF2alpha kinase GCN2 and its localization and expression underpin protein synthesis and ER processing capacity. *Biochem J* 465, 213-225.
- Ruff, M., Krishnaswamy, S., Boeglin, M., Poterszman, A., Mitschler, A., Podjarny, A., Rees, B., Thierry, J.C., and Moras, D. (1991). Class II aminoacyl transfer RNA synthetases: crystal structure of yeast aspartyl-tRNA synthetase complexed with tRNA(Asp). *Science* 252, 1682-1689.
- Sanders, C.L., and Curran, J.F. (2007). Genetic analysis of the E site during RF2 programmed frameshifting. *RNA* 13, 1483-1491.
- Santoso, A., Chien, P., Osherovich, L.Z., and Weissman, J.S. (2000). Molecular basis of a yeast prion species barrier. *Cell* 100, 277-288.
- Sarkar, A., Thoms, M., Barrio-Garcia, C., Thomson, E., Flemming, D., Beckmann, R., and Hurt, E. (2017). Preribosomes escaping from the nucleus are caught during translation by cytoplasmic quality control. *Nature structural & molecular biology* 24, 1107-1115.

- Sasikumar, A.N., and Kinzy, T.G. (2014). Mutations in the chromodomain-like insertion of translation elongation factor 3 compromise protein synthesis through reduced ATPase activity. *The Journal of biological chemistry* 289, 4853-4860.
- Sattlegger, E., Barbosa, J.A., Moraes, M.C., Martins, R.M., Hinnebusch, A.G., and Castilho, B.A. (2011). Gcn1 and actin binding to Yih1: implications for activation of the eIF2 kinase GCN2. *The Journal of biological chemistry* 286, 10341-10355.
- Sattlegger, E., and Hinnebusch, A.G. (2000). Separate domains in GCN1 for binding protein kinase GCN2 and ribosomes are required for GCN2 activation in amino acid-starved cells. *EMBO J* 19, 6622-6633.
- Sattlegger, E., and Hinnebusch, A.G. (2005). Polyribosome binding by GCN1 is required for full activation of eukaryotic translation initiation factor 2 α kinase GCN2 during amino acid starvation. *The Journal of biological chemistry* 280, 16514-16521.
- Sattlegger, E., Swanson, M.J., Ashcraft, E.A., Jennings, J.L., Fekete, R.A., Link, A.J., and Hinnebusch, A.G. (2004). YIH1 is an actin-binding protein that inhibits protein kinase GCN2 and impairs general amino acid control when overexpressed. *The Journal of biological chemistry* 279, 29952-29962.
- Savary, S., and Willocquet, L. (2020). Modeling the Impact of Crop Diseases on Global Food Security. *Annu Rev Phytopathol* 58, 313-341.
- Saxton, R.A., and Sabatini, D.M. (2017). mTOR Signaling in Growth, Metabolism, and Disease. *Cell* 168, 960-976.
- Schellhaus, A.K., Moreno-Andres, D., Chugh, M., Yokoyama, H., Moschopoulou, A., De, S., Bono, F., Hipp, K., Schaffer, E., and Antonin, W. (2017). Developmentally Regulated GTP binding protein 1 (DRG1) controls microtubule dynamics. *Sci Rep* 7, 9996.
- Scheper, G.C., van der Knaap, M.S., and Proud, C.G. (2007). Translation matters: protein synthesis defects in inherited disease. *Nat Rev Genet* 8, 711-723.
- Schluzen, F., Tocilj, A., Zarivach, R., Harms, J., Gluehmann, M., Janell, D., Bashan, A., Bartels, H., Agmon, I., Franceschi, F., *et al.* (2000). Structure of functionally activated small ribosomal subunit at 3.3 angstroms resolution. *Cell* 102, 615-623.
- Schmidt, C., Kowalinski, E., Shanmuganathan, V., Defenouillere, Q., Braunger, K., Heuer, A., Pech, M., Namane, A., Berninghausen, O., Fromont-Racine, M., *et al.* (2016). The cryo-EM structure of a ribosome-Ski2-Ski3-Ski8 helicase complex. *Science* 354, 1431-1433.
- Schuller, A.P., Wu, C.C., Dever, T.E., Buskirk, A.R., and Green, R. (2017). eIF5A Functions Globally in Translation Elongation and Termination. *Molecular cell* 66, 194-205 e195.
- Schwarz, S., Shen, J., Kadlec, K., Wang, Y., Brenner Michael, G., Fessler, A.T., and Vester, B. (2016). Lincosamides, Streptogramins, Phenicol, and Pleuromutilins: Mode of Action and Mechanisms of Resistance. *Cold Spring Harb Perspect Med* 6.

- Selmer, M., Dunham, C.M., Murphy, F.V.t., Weixlbaumer, A., Petry, S., Kelley, A.C., Weir, J.R., and Ramakrishnan, V. (2006). Structure of the 70S ribosome complexed with mRNA and tRNA. *Science* 313, 1935-1942.
- Semenkov, Y.P., Rodnina, M.V., and Wintermeyer, W. (1996). The "allosteric three-site model" of elongation cannot be confirmed in a well-defined ribosome system from *Escherichia coli*. *Proceedings of the National Academy of Sciences of the United States of America* 93, 12183-12188.
- Sengupta, S., Peterson, T.R., and Sabatini, D.M. (2010). Regulation of the mTOR complex 1 pathway by nutrients, growth factors, and stress. *Molecular cell* 40, 310-322.
- Shao, S., Brown, A., Santhanam, B., and Hegde, R.S. (2015). Structure and assembly pathway of the ribosome quality control complex. *Molecular cell* 57, 433-444.
- Shao, S., Murray, J., Brown, A., Taunton, J., Ramakrishnan, V., and Hegde, R.S. (2016). Decoding Mammalian Ribosome-mRNA States by Translational GTPase Complexes. *Cell* 167, 1229-1240 e1215.
- Shao, S., von der Malsburg, K., and Hegde, R.S. (2013). Listerin-dependent nascent protein ubiquitination relies on ribosome subunit dissociation. *Molecular cell* 50, 637-648.
- Sharkey, L.K.R., and O'Neill, A.J. (2018). Antibiotic Resistance ABC-F Proteins: Bringing Target Protection into the Limelight. *ACS Infect Dis* 4, 239-246.
- Shen, P.S., Park, J., Qin, Y., Li, X., Parsawar, K., Larson, M.H., Cox, J., Cheng, Y., Lambowitz, A.M., Weissman, J.S., *et al.* (2015). Protein synthesis. Rqc2p and 60S ribosomal subunits mediate mRNA-independent elongation of nascent chains. *Science* 347, 75-78.
- Shimizu, T., Nakagaki, M., Nishi, Y., Kobayashi, Y., Hachimori, A., and Uchiumi, T. (2002). Interaction among silkworm ribosomal proteins P1, P2 and P0 required for functional protein binding to the GTPase-associated domain of 28S rRNA. *Nucleic acids research* 30, 2620-2627.
- Shine, J., and Dalgarno, L. (1974). The 3'-terminal sequence of *Escherichia coli* 16S ribosomal RNA: complementarity to nonsense triplets and ribosome binding sites. *Proceedings of the National Academy of Sciences of the United States of America* 71, 1342-1346.
- Shoemaker, C.J., Eyler, D.E., and Green, R. (2010). Dom34:Hbs1 promotes subunit dissociation and peptidyl-tRNA drop-off to initiate no-go decay. *Science* 330, 369-372.
- Shoemaker, C.J., and Green, R. (2011). Kinetic analysis reveals the ordered coupling of translation termination and ribosome recycling in yeast. *Proceedings of the National Academy of Sciences of the United States of America* 108, E1392-1398.
- Silva, R.C., Dautel, M., Di Genova, B.M., Amberg, D.C., Castilho, B.A., and Sattlegger, E. (2015). The Gcn2 Regulator Yih1 Interacts with the Cyclin Dependent Kinase Cdc28 and Promotes Cell Cycle Progression through G2/M in Budding Yeast. *PLoS One* 10, e0131070.
- Simms, C.L., Hudson, B.H., Mosior, J.W., Rangwala, A.S., and Zaher, H.S. (2014). An active role for the ribosome in determining the fate of oxidized mRNA. *Cell reports* 9, 1256-1264.

- Simms, C.L., Yan, L.L., Qiu, J.K., and Zaher, H.S. (2019). Ribosome Collisions Result in +1 Frameshifting in the Absence of No-Go Decay. *Cell reports* 28, 1679-1689 e1674.
- Simms, C.L., Yan, L.L., and Zaher, H.S. (2017). Ribosome Collision Is Critical for Quality Control during No-Go Decay. *Molecular cell* 68, 361-373 e365.
- Sinha, N.K., Ordureau, A., Best, K., Saba, J.A., Zinshteyn, B., Sundaramoorthy, E., Fulzele, A., Garshott, D.M., Denk, T., Thoms, M., *et al.* (2020). EDF1 coordinates cellular responses to ribosome collisions. *eLife* 9.
- Sitron, C.S., and Brandman, O. (2019). CAT tails drive degradation of stalled polypeptides on and off the ribosome. *Nature structural & molecular biology* 26, 450-459.
- Sitron, C.S., Park, J.H., and Brandman, O. (2017). Asc1, Hel2, and Slh1 couple translation arrest to nascent chain degradation. *RNA* 23, 798-810.
- Sitron, C.S., Park, J.H., Giafaglione, J.M., and Brandman, O. (2020). Aggregation of CAT tails blocks their degradation and causes proteotoxicity in *S. cerevisiae*. *PLoS One* 15, e0227841.
- Skabkin, M.A., Skabkina, O.V., Hellen, C.U., and Pestova, T.V. (2013). Reinitiation and other unconventional posttermination events during eukaryotic translation. *Molecular cell* 51, 249-264.
- Skogerson, L., and Engelhardt, D. (1977). Dissimilarity in protein chain elongation factor requirements between yeast and rat liver ribosomes. *The Journal of biological chemistry* 252, 1471-1475.
- Skogerson, L., and Wakatama, E. (1976). A ribosome-dependent GTPase from yeast distinct from elongation factor 2. *Proceedings of the National Academy of Sciences of the United States of America* 73, 73-76.
- Sonenberg, N., and Hinnebusch, A.G. (2009). Regulation of translation initiation in eukaryotes: mechanisms and biological targets. *Cell* 136, 731-745.
- Song, H., Kim, S.I., Ko, M.S., Kim, H.J., Heo, J.C., Lee, H.J., Lee, H.S., Han, I.S., Kwack, K., and Park, J.W. (2004). Overexpression of DRG2 increases G2/M phase cells and decreases sensitivity to nocodazole-induced apoptosis. *J Biochem* 135, 331-335.
- Song, H., Mugnier, P., Das, A.K., Webb, H.M., Evans, D.R., Tuite, M.F., Hemmings, B.A., and Barford, D. (2000). The crystal structure of human eukaryotic release factor eRF1--mechanism of stop codon recognition and peptidyl-tRNA hydrolysis. *Cell* 100, 311-321.
- Spahn, C.M., Gomez-Lorenzo, M.G., Grassucci, R.A., Jorgensen, R., Andersen, G.R., Beckmann, R., Penczek, P.A., Ballesta, J.P., and Frank, J. (2004a). Domain movements of elongation factor eEF2 and the eukaryotic 80S ribosome facilitate tRNA translocation. *EMBO J* 23, 1008-1019.
- Spahn, C.M., Jan, E., Mulder, A., Grassucci, R.A., Sarnow, P., and Frank, J. (2004b). Cryo-EM visualization of a viral internal ribosome entry site bound to human ribosomes: the IRES functions as an RNA-based translation factor. *Cell* 118, 465-475.
- Staschke, K.A., and Wek, R.C. (2019). Adapting to cell stress from inside and out. *Nat Cell Biol* 21, 799-800.

- Stewart, J.D., Cowan, J.L., Perry, L.S., Coldwell, M.J., and Proud, C.G. (2015). ABC50 mutants modify translation start codon selection. *Biochem J* 467, 217-229.
- Sturtevant, J. (2002). Translation elongation-3-like factors: are they rational antifungal targets? *Expert Opin Ther Targets* 6, 545-553.
- Su, T., Izawa, T., Thoms, M., Yamashita, Y., Cheng, J., Berninghausen, O., Hartl, F.U., Inada, T., Neupert, W., and Beckmann, R. (2019). Structure and function of Vms1 and Arb1 in RQC and mitochondrial proteome homeostasis. *Nature* 570, 538-542.
- Sundaramoorthy, E., Leonard, M., Mak, R., Liao, J., Fulzele, A., and Bennett, E.J. (2017). ZNF598 and RACK1 Regulate Mammalian Ribosome-Associated Quality Control Function by Mediating Regulatory 40S Ribosomal Ubiquitylation. *Molecular cell* 65, 751-760 e754.
- Suragani, R.N., Zachariah, R.S., Velazquez, J.G., Liu, S., Sun, C.W., Townes, T.M., and Chen, J.J. (2012). Heme-regulated eIF2alpha kinase activated Atf4 signaling pathway in oxidative stress and erythropoiesis. *Blood* 119, 5276-5284.
- Suraweera, A., Munch, C., Hanssum, A., and Bertolotti, A. (2012). Failure of amino acid homeostasis causes cell death following proteasome inhibition. *Molecular cell* 48, 242-253.
- Svidritskiy, E., Brilot, A.F., Koh, C.S., Grigorieff, N., and Korostelev, A.A. (2014). Structures of yeast 80S ribosome-tRNA complexes in the rotated and nonrotated conformations. *Structure* 22, 1210-1218.
- Szklarczyk, D., Gable, A.L., Lyon, D., Junge, A., Wyder, S., Huerta-Cepas, J., Simonovic, M., Doncheva, N.T., Morris, J.H., Bork, P., *et al.* (2019). STRING v11: protein-protein association networks with increased coverage, supporting functional discovery in genome-wide experimental datasets. *Nucleic acids research* 47, D607-D613.
- Szollosi, D., Chiba, P., Szakacs, G., and Stockner, T. (2020). Conversion of chemical to mechanical energy by the nucleotide binding domains of ABCB1. *Sci Rep* 10, 2589.
- Taniuchi, S., Miyake, M., Tsugawa, K., Oyadomari, M., and Oyadomari, S. (2016). Integrated stress response of vertebrates is regulated by four eIF2alpha kinases. *Sci Rep* 6, 32886.
- Tchorzewski, M. (2002). The acidic ribosomal P proteins. *Int J Biochem Cell Biol* 34, 911-915.
- ter Beek, J., Guskov, A., and Slotboom, D.J. (2014). Structural diversity of ABC transporters. *J Gen Physiol* 143, 419-435.
- Tesina, P., Heckel, E., Cheng, J., Fromont-Racine, M., Buschauer, R., Kater, L., Beatrix, B., Berninghausen, O., Jacquier, A., Becker, T., *et al.* (2019). Structure of the 80S ribosome-Xrn1 nuclease complex. *Nature structural & molecular biology* 26, 275-280.
- Tesina, P., Lessen, L.N., Buschauer, R., Cheng, J., Wu, C.C., Berninghausen, O., Buskirk, A.R., Becker, T., Beckmann, R., and Green, R. (2020). Molecular mechanism of translational stalling by inhibitory codon combinations and poly(A) tracts. *EMBO J* 39, e103365.
- Thomas, C., and Tampe, R. (2018). Multifaceted structures and mechanisms of ABC transport systems in health and disease. *Curr Opin Struct Biol* 51, 116-128.

- Thomas, C., and Tampe, R. (2020). Structural and Mechanistic Principles of ABC Transporters. *Annu Rev Biochem* 89, 605-636.
- Trabuco, L.G., Schreiner, E., Eargle, J., Cornish, P., Ha, T., Luthey-Schulten, Z., and Schulten, K. (2010). The role of L1 stalk-tRNA interaction in the ribosome elongation cycle. *J Mol Biol* 402, 741-760.
- Triana-Alonso, F.J., Chakraborty, K., and Nierhaus, K.H. (1995). The elongation factor 3 unique in higher fungi and essential for protein biosynthesis is an E site factor. *The Journal of biological chemistry* 270, 20473-20478.
- True, H.L., and Lindquist, S.L. (2000). A yeast prion provides a mechanism for genetic variation and phenotypic diversity. *Nature* 407, 477-483.
- Tyzack, J.K., Wang, X., Belsham, G.J., and Proud, C.G. (2000). ABC50 interacts with eukaryotic initiation factor 2 and associates with the ribosome in an ATP-dependent manner. *The Journal of biological chemistry* 275, 34131-34139.
- Uchiumi, T., Honma, S., Nomura, T., Dabbs, E.R., and Hachimori, A. (2002). Translation elongation by a hybrid ribosome in which proteins at the GTPase center of the Escherichia coli ribosome are replaced with rat counterparts. *The Journal of biological chemistry* 277, 3857-3862.
- Uemura, S., Aitken, C.E., Korlach, J., Flusberg, B.A., Turner, S.W., and Puglisi, J.D. (2010). Real-time tRNA transit on single translating ribosomes at codon resolution. *Nature* 464, 1012-1017.
- Uma, S., Hartson, S.D., Chen, J.J., and Matts, R.L. (1997). Hsp90 is obligatory for the heme-regulated eIF-2 α kinase to acquire and maintain an activable conformation. *The Journal of biological chemistry* 272, 11648-11656.
- Uritani, M., and Miyazaki, M. (1988a). Characterization of the ATPase and GTPase activities of elongation factor 3 (EF-3) purified from yeasts. *J Biochem* 103, 522-530.
- Uritani, M., and Miyazaki, M. (1988b). Role of yeast peptide elongation factor 3 (EF-3) at the AA-tRNA binding step. *J Biochem* 104, 118-126.
- Valle, M., Zavialov, A., Sengupta, J., Rawat, U., Ehrenberg, M., and Frank, J. (2003). Locking and unlocking of ribosomal motions. *Cell* 114, 123-134.
- Van Damme, P., Lasa, M., Polevoda, B., Gazquez, C., Elosegui-Artola, A., Kim, D.S., De Juan-Pardo, E., Demeyer, K., Hole, K., Larrea, E., *et al.* (2012). N-terminal acetylome analyses and functional insights of the N-terminal acetyltransferase NatB. *Proceedings of the National Academy of Sciences of the United States of America* 109, 12449-12454.
- van den Elzen, A.M., Schuller, A., Green, R., and Seraphin, B. (2014). Dom34-Hbs1 mediated dissociation of inactive 80S ribosomes promotes restart of translation after stress. *EMBO J* 33, 265-276.
- Van Drie, J.H., and Tong, L. (2020). Cryo-EM as a powerful tool for drug discovery. *Bioorg Med Chem Lett* 30, 127524.

- Van Dyke, N., Pickering, B.F., and Van Dyke, M.W. (2009). Stm1p alters the ribosome association of eukaryotic elongation factor 3 and affects translation elongation. *Nucleic acids research* 37, 6116-6125.
- Vasiliou, V., Vasiliou, K., and Nebert, D.W. (2009). Human ATP-binding cassette (ABC) transporter family. *Hum Genomics* 3, 281-290.
- Vazquez de Aldana, C.R., Marton, M.J., and Hinnebusch, A.G. (1995). GCN20, a novel ATP binding cassette protein, and GCN1 reside in a complex that mediates activation of the eIF-2 alpha kinase GCN2 in amino acid-starved cells. *EMBO J* 14, 3184-3199.
- Verma, R., Reichermeier, K.M., Burroughs, A.M., Oania, R.S., Reitsma, J.M., Aravind, L., and Deshaies, R.J. (2018). Vms1 and ANKZF1 peptidyl-tRNA hydrolases release nascent chains from stalled ribosomes. *Nature* 557, 446-451.
- Verschoor, A., Warner, J.R., Srivastava, S., Grassucci, R.A., and Frank, J. (1998). Three-dimensional structure of the yeast ribosome. *Nucleic acids research* 26, 655-661.
- Vind, A.C., Genzor, A.V., and Bekker-Jensen, S. (2020). Ribosomal stress-surveillance: three pathways is a magic number. *Nucleic acids research* 48, 10648-10661.
- Visweswaraiah, J., Lageix, S., Castilho, B.A., Izotova, L., Kinzy, T.G., Hinnebusch, A.G., and Sattlegger, E. (2011). Evidence that eukaryotic translation elongation factor 1A (eEF1A) binds the Gcn2 protein C terminus and inhibits Gcn2 activity. *The Journal of biological chemistry* 286, 36568-36579.
- Visweswaraiah, J., Lee, S.J., Hinnebusch, A.G., and Sattlegger, E. (2012). Overexpression of eukaryotic translation elongation factor 3 impairs Gcn2 protein activation. *The Journal of biological chemistry* 287, 37757-37768.
- Waller, T., Lee, S.J., and Sattlegger, E. (2012). Evidence that Yih1 resides in a complex with ribosomes. *FEBS J* 279, 1761-1776.
- Wang, J., Zhou, J., Yang, Q., and Grayhack, E.J. (2018). Multi-protein bridging factor 1(Mbf1), Rps3 and Asc1 prevent stalled ribosomes from frameshifting. *eLife* 7.
- Wasserman, M.R., Alejo, J.L., Altman, R.B., and Blanchard, S.C. (2016). Multiperspective smFRET reveals rate-determining late intermediates of ribosomal translocation. *Nature structural & molecular biology* 23, 333-341.
- Wawiora, L., Molestak, E., Szajwaj, M., Michalec-Wawiora, B., Molon, M., Borkiewicz, L., Grela, P., Boguszewska, A., and Tchorzewski, M. (2017). Multiplication of Ribosomal P-Stalk Proteins Contributes to the Fidelity of Translation. *Molecular and cellular biology* 37.
- Webb, K.J., Al-Hadid, Q., Zurita-Lopez, C.I., Young, B.D., Lipson, R.S., and Clarke, S.G. (2011). The ribosomal I1 protuberance in yeast is methylated on a lysine residue catalyzed by a seven-beta-strand methyltransferase. *The Journal of biological chemistry* 286, 18405-18413.
- Wei, D., Yao, J., Yang, X., Cheng, L., Lu, D., and Xue, J. (2004). Molecular cloning and expression of two closely related GTP-binding proteins from zebrafish. *DNA Seq* 15, 246-250.

- Weixlbaumer, A., Jin, H., Neubauer, C., Voorhees, R.M., Petry, S., Kelley, A.C., and Ramakrishnan, V. (2008). Insights into translational termination from the structure of RF2 bound to the ribosome. *Science* *322*, 953-956.
- Wek, R.C., Cannon, J.F., Dever, T.E., and Hinnebusch, A.G. (1992). Truncated protein phosphatase GLC7 restores translational activation of GCN4 expression in yeast mutants defective for the eIF-2 alpha kinase GCN2. *Molecular and cellular biology* *12*, 5700-5710.
- Wek, R.C., Ramirez, M., Jackson, B.M., and Hinnebusch, A.G. (1990). Identification of positive-acting domains in GCN2 protein kinase required for translational activation of GCN4 expression. *Molecular and cellular biology* *10*, 2820-2831.
- Wek, S.A., Zhu, S., and Wek, R.C. (1995). The histidyl-tRNA synthetase-related sequence in the eIF-2 alpha protein kinase GCN2 interacts with tRNA and is required for activation in response to starvation for different amino acids. *Molecular and cellular biology* *15*, 4497-4506.
- Wilkens, S. (2015). Structure and mechanism of ABC transporters. *F1000Prime Rep* *7*, 14.
- Wilson, D.N. (2014). Ribosome-targeting antibiotics and mechanisms of bacterial resistance. *Nat Rev Microbiol* *12*, 35-48.
- Wilson, D.N., and Doudna Cate, J.H. (2012). The structure and function of the eukaryotic ribosome. *Cold Spring Harb Perspect Biol* *4*.
- Wilson, D.N., Hauryliuk, V., Atkinson, G.C., and O'Neill, A.J. (2020). Target protection as a key antibiotic resistance mechanism. *Nat Rev Microbiol* *18*, 637-648.
- Wilson, D.N., and Nierhaus, K.H. (2006). The E-site story: the importance of maintaining two tRNAs on the ribosome during protein synthesis. *Cell Mol Life Sci* *63*, 2725-2737.
- Wilson, D.N., Schlutzenzen, F., Harms, J.M., Starosta, A.L., Connell, S.R., and Fucini, P. (2008). The oxazolidinone antibiotics perturb the ribosomal peptidyl-transferase center and effect tRNA positioning. *Proceedings of the National Academy of Sciences of the United States of America* *105*, 13339-13344.
- Wilson, K.E., Smith, S.K., Kelly, R., Masurekar, P., Xu, D., Parish, C.A., Wang, H., Zink, D.L., Davies, J.E., and Roemer, T. (2014). Discovery, isolation, and structure elucidation of dretamycin. *Journal of natural products* *77*, 1280-1286.
- Wimberly, B.T., Brodersen, D.E., Clemons, W.M., Jr., Morgan-Warren, R.J., Carter, A.P., Vornhein, C., Hartsch, T., and Ramakrishnan, V. (2000). Structure of the 30S ribosomal subunit. *Nature* *407*, 327-339.
- Winz, M.L., Peil, L., Turowski, T.W., Rappsilber, J., and Tollervey, D. (2019). Molecular interactions between Hel2 and RNA supporting ribosome-associated quality control. *Nature communications* *10*, 563.
- Wolff, S., Weissman, J.S., and Dillin, A. (2014). Differential scales of protein quality control. *Cell* *157*, 52-64.

- Won, S., Eidenschenk, C., Arnold, C.N., Siggs, O.M., Sun, L., Brandl, K., Mullen, T.M., Nemerow, G.R., Moresco, E.M., and Beutler, B. (2012). Increased susceptibility to DNA virus infection in mice with a GCN2 mutation. *J Virol* 86, 1802-1808.
- Wout, P.K., Sattlegger, E., Sullivan, S.M., and Maddock, J.R. (2009). *Saccharomyces cerevisiae* Rbg1 protein and its binding partner Gir2 interact on Polyribosomes with Gcn1. *Eukaryot Cell* 8, 1061-1071.
- Wurtmann, E.J., and Wolin, S.L. (2009). RNA under attack: cellular handling of RNA damage. *Crit Rev Biochem Mol Biol* 44, 34-49.
- Yadavalli, S.S., and Ibba, M. (2012). Quality control in aminoacyl-tRNA synthesis its role in translational fidelity. *Adv Protein Chem Struct Biol* 86, 1-43.
- Yamazaki, H., Kasai, S., Mimura, J., Ye, P., Inose-Maruyama, A., Tanji, K., Wakabayashi, K., Mizuno, S., Sugiyama, F., Takahashi, S., *et al.* (2020). Ribosome binding protein GCN1 regulates the cell cycle and cell proliferation and is essential for the embryonic development of mice. *PLoS Genet* 16, e1008693.
- Yan, L.L., and Zaher, H.S. (2019). How do cells cope with RNA damage and its consequences? *The Journal of biological chemistry* 294, 15158-15171.
- Yan, L.L., and Zaher, H.S. (2021). Ribosome quality control antagonizes the activation of the integrated stress response on colliding ribosomes. *Molecular cell* 81, 614-628 e614.
- Yang, H., Hamada, K., Terashima, H., Izuta, M., Yamaguchi-Sihta, E., Kondoh, O., Satoh, H., Miyazaki, M., Arisawa, M., Miyamoto, C., *et al.* (1996). A point mutation within each of two ATP-binding motifs inactivates the functions of elongation factor 3. *Biochim Biophys Acta* 1310, 303-308.
- Yang, H., Rudge, D.G., Koos, J.D., Vaidialingam, B., Yang, H.J., and Pavletich, N.P. (2013). mTOR kinase structure, mechanism and regulation. *Nature* 497, 217-223.
- Yang, R., Wek, S.A., and Wek, R.C. (2000). Glucose limitation induces GCN4 translation by activation of Gcn2 protein kinase. *Molecular and cellular biology* 20, 2706-2717.
- Yap, K.L., and Zhou, M.M. (2011). Structure and mechanisms of lysine methylation recognition by the chromodomain in gene transcription. *Biochemistry* 50, 1966-1980.
- Ye, J., Kumanova, M., Hart, L.S., Sloane, K., Zhang, H., De Panis, D.N., Bobrovnikova-Marjon, E., Diehl, J.A., Ron, D., and Koumenis, C. (2010). The GCN2-ATF4 pathway is critical for tumour cell survival and proliferation in response to nutrient deprivation. *EMBO J* 29, 2082-2096.
- Ye, J., Palm, W., Peng, M., King, B., Lindsten, T., Li, M.O., Koumenis, C., and Thompson, C.B. (2015). GCN2 sustains mTORC1 suppression upon amino acid deprivation by inducing Sestrin2. *Genes Dev* 29, 2331-2336.
- Yerlikaya, A., Kimball, S.R., and Stanley, B.A. (2008). Phosphorylation of eIF2alpha in response to 26S proteasome inhibition is mediated by the haem-regulated inhibitor (HRI) kinase. *Biochem J* 412, 579-588.

- Yonashiro, R., Tahara, E.B., Bengtson, M.H., Khokhrina, M., Lorenz, H., Chen, K.C., Kigoshi-Tansho, Y., Savas, J.N., Yates, J.R., Kay, S.A., *et al.* (2016). The Rqc2/Tae2 subunit of the ribosome-associated quality control (RQC) complex marks ribosome-stalled nascent polypeptide chains for aggregation. *eLife* 5, e11794.
- Youngman, E.M., He, S.L., Nikstad, L.J., and Green, R. (2007). Stop codon recognition by release factors induces structural rearrangement of the ribosomal decoding center that is productive for peptide release. *Molecular cell* 28, 533-543.
- Zaborske, J.M., Narasimhan, J., Jiang, L., Wek, S.A., Dittmar, K.A., Freimoser, F., Pan, T., and Wek, R.C. (2009). Genome-wide analysis of tRNA charging and activation of the eIF2 kinase Gcn2p. *The Journal of biological chemistry* 284, 25254-25267.
- Zaher, H.S., and Green, R. (2009). Fidelity at the molecular level: lessons from protein synthesis. *Cell* 136, 746-762.
- Zavialov, A.V., Hauryliuk, V.V., and Ehrenberg, M. (2005). Splitting of the posttermination ribosome into subunits by the concerted action of RRF and EF-G. *Molecular cell* 18, 675-686.
- Zavialov, A.V., Mora, L., Buckingham, R.H., and Ehrenberg, M. (2002). Release of peptide promoted by the GGQ motif of class 1 release factors regulates the GTPase activity of RF3. *Molecular cell* 10, 789-798.
- Zhang, P., McGrath, B.C., Reinert, J., Olsen, D.S., Lei, L., Gill, S., Wek, S.A., Vattem, K.M., Wek, R.C., Kimball, S.R., *et al.* (2002). The GCN2 eIF2alpha kinase is required for adaptation to amino acid deprivation in mice. *Molecular and cellular biology* 22, 6681-6688.
- Zhou, J., Korostelev, A., Lancaster, L., and Noller, H.F. (2012). Crystal structures of 70S ribosomes bound to release factors RF1, RF2 and RF3. *Curr Opin Struct Biol* 22, 733-742.
- Zhou, J., Lancaster, L., Donohue, J.P., and Noller, H.F. (2019). Spontaneous ribosomal translocation of mRNA and tRNAs into a chimeric hybrid state. *Proceedings of the National Academy of Sciences of the United States of America* 116, 7813-7818.
- Zhu, S., Sobolev, A.Y., and Wek, R.C. (1996). Histidyl-tRNA synthetase-related sequences in GCN2 protein kinase regulate in vitro phosphorylation of eIF-2. *The Journal of biological chemistry* 271, 24989-24994.
- Zurita Rendon, O., Fredrickson, E.K., Howard, C.J., Van Vranken, J., Fogarty, S., Tolley, N.D., Kalia, R., Osuna, B.A., Shen, P.S., Hill, C.P., *et al.* (2018). Vms1p is a release factor for the ribosome-associated quality control complex. *Nature communications* 9, 2197.

6 Publications

2019

Villu Kasari*, **Agnieszka A. Pochopien***, Tõnu Margus, Victoriia Murina, Kathryn Turnbull, Yang Zhou, Tracy Nissan, Michael Graf, Jiří Nováček, Gemma C. Atkinson, Marcus J. O. Johansson, Daniel N. Wilson, Vasili Hauryliuk (2019). A role for the *Saccharomyces cerevisiae* ABCF protein New1 in translation termination/recycling. *Nucleic Acids Research*. 47, 8807-8820.

2021

Namit Ranjan*, **Agnieszka A. Pochopien***, Colin Chih-Chien Wu*, Bertrand Beckert, Sandra Blanchet, Rachel Green, Marina V. Rodnina, Daniel N. Wilson (2021). Yeast translation elongation factor eEF3 promotes late stages of tRNA translocation. *The EMBO Journal*. 10.15252/emj.2020106449.

Agnieszka A Pochopien*, Bertrand Beckert*, Sergo Kasvandik, Otto Berninghausen, Roland Beckmann, Tanel Tenson, Daniel N. Wilson (2021). Structure of Gcn1 bound to stalled and colliding 80S ribosomes. *PNAS*. 10.1073/pnas.2022756118.

*These authors contributed equally to this work.

A role for the *Saccharomyces cerevisiae* ABCF protein New1 in translation termination/recycling

Villu Kasari^{1,2,†}, Agnieszka A. Pochopien^{3,†}, Tõnu Margus^{1,2}, Victoriia Murina^{1,2}, Kathryn Turnbull^{1,2}, Yang Zhou¹, Tracy Nissan^{4,5}, Michael Graf³, Jiří Nováček⁶, Gemma C. Atkinson¹, Marcus J.O. Johansson^{1,*}, Daniel N. Wilson^{3,*} and Vasili Haurlyiuk^{1,2,7,*}

¹Department of Molecular Biology, Umeå University, Building 6K, 6L University Hospital Area, 90187 Umeå, Sweden, ²Laboratory for Molecular Infection Medicine Sweden (MIMS), Umeå University, Building 6K and 6L, University Hospital Area, 90187 Umeå, Sweden, ³Institute for Biochemistry and Molecular Biology, University of Hamburg, Martin-Luther-King-Platz 6, 20146 Hamburg, Germany, ⁴Department of Molecular Biosciences, The Wenner-Gren Institute, Stockholm University, Stockholm, 10691, Sweden, ⁵School of Life Science, University of Sussex, Brighton, BN19RH, UK, ⁶Central European Institute of Technology (CEITEC), Masaryk University, Kamenice 5, 62500 Brno, Czech Republic and ⁷University of Tartu, Institute of Technology, 50411 Tartu, Estonia

Received May 14, 2019; Revised June 14, 2019; Editorial Decision June 17, 2019; Accepted July 11, 2019

ABSTRACT

Translation is controlled by numerous accessory proteins and translation factors. In the yeast *Saccharomyces cerevisiae*, translation elongation requires an essential elongation factor, the ABCF ATPase eEF3. A closely related protein, New1, is encoded by a non-essential gene with cold sensitivity and ribosome assembly defect knock-out phenotypes. Since the exact molecular function of New1 is unknown, it is unclear if the ribosome assembly defect is direct, i.e. New1 is a *bona fide* assembly factor, or indirect, for instance due to a defect in protein synthesis. To investigate this, we employed yeast genetics, cryo-electron microscopy (cryo-EM) and ribosome profiling (Ribo-Seq) to interrogate the molecular function of New1. Overexpression of New1 rescues the inviability of a yeast strain lacking the otherwise strictly essential translation factor eEF3. The structure of the ATPase-deficient (EQ₂) New1 mutant locked on the 80S ribosome reveals that New1 binds analogously to the ribosome as eEF3. Finally, Ribo-Seq analysis revealed that loss of New1 leads to ribosome queuing upstream of 3'-terminal lysine and arginine codons, including those genes encoding proteins of the cytoplasmic translational machinery. Our results suggest that New1 is a translation factor that fine-tunes the

efficiency of translation termination or ribosome recycling.

INTRODUCTION

The ribosome is aided and regulated by accessory factors participating in all stages of the translational cycle: initiation, elongation, termination and recycling (1–4). Translational GTPases are the key players in all these steps and as such have been extensively studied over the past five decades (5,6). Another class of NTPase enzymes has attracted increasing attention in the recent years—the ribosome-associated adenosine triphosphatases (ATPases) belonging to the ATP-binding cassette (ABC) type F (ABCF) protein family. Eukaryotic representatives of this protein family include initiation factor ABCF1/ABC50 (7,8), elongation factor eEF3 (9,10) as well as Gcn20—a key component of general amino acid control pathway (11).

Elongation factor eEF3 is the most well-studied eukaryotic ribosome-associated ABCF ATPase. While early analyses of the evolutionary distribution of eEF3 concluded that it is a fungi-specific translational factor (12) eEF3-like homologues have more recently been found in non-fungal species, such as oomycete *Phytophthora infestans* (13), choanoflagellates and various algae (14). eEF3 is essential both for viability of the yeast *Saccharomyces cerevisiae* (10) and for peptide elongation in a reconstituted yeast translational system (15,16). While biochemical experiments suggest a secondary function for eEF3 in ribosome recycling (17), ribosome profiling analysis of eEF3-

*To whom correspondence should be addressed. Tel: +46 907 850 807; Fax: +46 0 90772630; Email: vasili.haurlyiuk@umu.se
Correspondence may also be addressed to Daniel N. Wilson. Tel: +49 40 42838 2841; Fax: +49 40 42838 2848; Email: Daniel.wilson@chemie.uni-hamburg.de

Correspondence may also be addressed to Marcus J.O. Johansson. Tel: +46 7856 767; Fax: +46 0 90772630; Email: marcus.johansson@umu.se

†The authors wish it to be known that, in their opinion, the first two authors should be regarded as Joint First Authors.

Disclaimer: This article reflects only the author's view and the European Commission is not responsible for any use that may be made of the information it contains.

depleted *S. cerevisiae* suggests that translation elongation is the primary function of eEF3 in the cell (18). A cryo-electron microscopy (cryo-EM) reconstruction of eEF3 on the ribosome localizes the factor within the vicinity of the ribosomal E-site (9), providing a structural explanation for the biochemical observations of E-site tRNA displacement from the ribosome in the presence of eEF3 and ATP (19).

The *S. cerevisiae* genome encodes 29 ABC ATPases, of which five belong to the ABCF subfamily (20). Of these, eEF3, Hef3/eEF3B and New1 together form a group with a distinctive subdomain architecture relative to the other ABCFs (14). Hef3/eEF3B is the closest homologue of eEF3—84% identical on the amino acid level (21)—and is, most likely, a second copy of eEF3 originating from whole-genome duplication in the *Saccharomyces* lineage (22). The second closest homologue is New1 (20)—encoded by a non-essential gene with a cold sensitivity knock-out phenotype (23) (Figure 1A). The molecular function of New1 is unclear. eEF3 and New1 share the same domain architecture, with exception of an additional N-terminal Q/N rich region in New1 that drives the formation of the $[NU^+]$ prion when fused to the C-terminal domains of translation termination factor eRF3 (24,25) (Figure 1A). However, prionogenesis cannot be the sole function of New1 since the very presence of the Q/N motif in New1 is not universal and is limited to *Hemiascomycota* species (26), and is lacking, for instance, in *Schizosaccharomyces pombe* New1 (14) (Figure 1A). Loss of New1 results in a ribosome assembly defect in *S. cerevisiae* and causes cold sensitivity, that is, a growth defect at low temperatures (23). However, it is unclear whether the effect is direct, through participation of New1 in ribosome assembly, or indirect, as perturbation of translation can cause ribosome assembly defects (27). The latter possibility is supported by the detection of New1 in polysomal fractions (23), motivating our current investigation.

Using a combination of ribosome profiling, yeast genetics, molecular biology and cryo-EM, we show that *S. cerevisiae* New1 is a yeast translational factor involved in translation termination/recycling and its loss leads to ribosome queuing at C-terminal lysine and arginine residues that precede stop codons.

MATERIALS AND METHODS

Yeast genetics

Yeast strains and plasmids used in this study are listed in Table 1. Oligonucleotides and synthetic DNA sequences are listed in Supplementary Table S1 and construction of plasmids is described in the *Supplementary information*. Yeast media was prepared as described (28), with the difference that the composition of the drop-out mix was as per Johansson (29). Difco Yeast Nitrogen Base w/o Amino Acids was purchased from Becton Dickinson (291 940), amino acids and other supplements from Sigma-Aldrich. YEPD medium supplemented with 200 μ g/ml GeneticinTM (Gibco 11811-023) was used to select for transformants containing the *kanMX6* marker (30). Strains deleted for *NEW1* were derived from a diploid formed between BY4741 and BY4742, which was transformed with either a *HIS3MX6* or *kanMX6* DNA fragment with the appropriate homologies to the *NEW1* locus. The DNA fragments were ampli-

fied from pFA6a-*HIS3MX6* and pFA6a-*kanMX6* (30) using primers oMJ489 and oMJ490. The two generated heterozygous strains were allowed to sporulate and the *new1* Δ strains (MJY944, MJY945 and MJY1091) were obtained from tetrads. The *new1* Δ ::*kanMX6* strain (MJY1091) was crossed to BY4709 and strains MJY1171 and MJY1173 were obtained from a tetrad. The P_{MET25}-*YEF3 new1* Δ strain (MJY951) was derived from a cross between VKY8 and MJY944. A strain expressing the synthetic LexA-ER-haB112 transcription factor (VHY61) was constructed by integrating the FRP880 plasmid (31) into the *his3* Δ 1 locus of BY4741. To target the plasmid to the *his3* Δ 1 locus, the plasmid was linearized with PacI before transformation.

Polysome profile analyses

Polysome profile analyses and fractionation was performed as described earlier (18). To probe the ribosomal association of New1, the VHY61 strain carrying the β -estradiol-inducible *NEW1-TAP* (VHp262) or *NEW1-EQ₂-TAP* (VHp265) plasmid was grown overnight at 30°C in SC-ura and diluted to OD₆₀₀ \approx 0.05 in the same medium. Cultures were grown until OD₆₀₀ \approx 0.3 at which point β -estradiol was added to a final concentration of 1 μ M. Cells were harvested after 3 h of induction and lysates prepared as previously described (18). The lysis buffer and sucrose gradient were supplemented where appropriate with ATP or AMP-PNP to a final concentration of 1 mM. RNase I treatment was performed for 20 min at room temperature before loading on a 7–45% sucrose gradient in of HEPES:Polymix buffer (20 mM HEPES:KOH pH 7.5, 2 mM dithiothreitol (DTT), 10 mM Mg(OAc)₂, 95 mM KCl, 5 mM NH₄Cl, 0.5 mM CaCl₂, 8 mM putrescine, 1 mM spermidine (32)) and resolving the samples by centrifugation at 35 000 rpm for 3 h at 4°C. Since 1 mM ATP masks the ribosomal absorbance signal at 260 nm, the gradients were analysed with continuous A₂₈₀ measurements. 0.5 ml fractions were collected and stored at –20°C for further analysis.

Immunodetection

The TAP tag was detected using Peroxidase-anti-peroxidase 1:5000 (Sigma, Lot #103M4822), Pgk1 was detected using mouse anti-Pgk1 1:7500 (459250, Invitrogen). Anti-mouse IgG_HRP (AS11 1772, Agrisera) was used as secondary antibody. For western blotting of fractions from polysome profiles, 200 μ l of Polysome Gradient Buffer without sucrose (20 mM Tris-HCl pH 7.5, 50 mM KCl, 10 mM MgCl₂) was added to 200 μ l of each fraction and the samples precipitated by addition of 1.2 ml of 99.5% EtOH and overnight incubation at –20°C. The samples were pelleted by centrifugation at 20 000 \times g for 30 min at 4°C, air dried for 10 min at 50°C and dissolved in 24 μ l of 3 \times Sample Loading Buffer (125 mM Tris-HCl pH6.8, 50% glycerol, 1.43M β -mercaptoethanol (BME), 4% sodium dodecyl sulphate (SDS), 0.025% Bromophenol Blue). A total of 5 μ l of each sample was resolved by 8% SDS-polyacrylamide gel electrophoresis. Since the detection of the TAP-tag is highly specific (see uncut western blots presented on Supplementary Figure S1), we increased throughput by slot blotting. Slot blotting of fractions from polysome profiles was performed using a Minifold II Slot-Blot Manifold (Schleicher

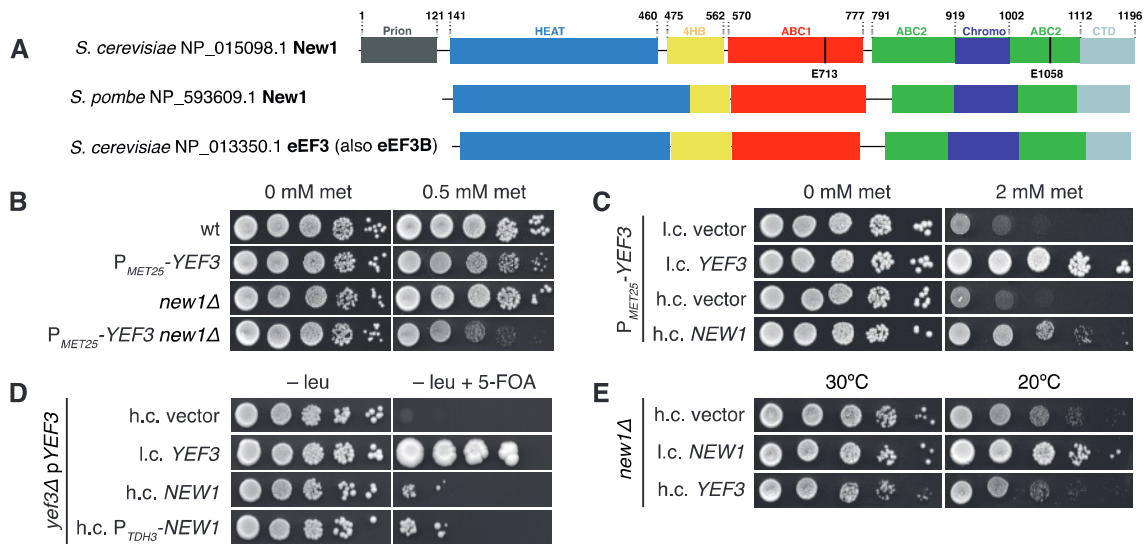


Figure 1. The essential translational factor eEF3 is dispensable upon overexpression of New1. (A) The domain structure of *Saccharomyces cerevisiae* and *Schizosaccharomyces pombe* New1 as well as *S. cerevisiae* eEF3. The location of the catalytic glutamate residues essential for ATPase function is indicated. (B) Loss of *NEW1* increases the growth defect caused by depletion of eEF3. The wild-type (VKY9), P_{MET25} -*YEF3* (VKY8), *new1Δ* (MJY945) and P_{MET25} -*YEF3 new1Δ* (MJY951) strains were grown overnight in liquid SC-met-cys medium, 10-fold serially diluted, spotted on SC-met-cys (0 mM met) and SC-cys (0.5 mM met) plates. The plates were scored after three days incubation at 30°C. (C) Increased dosage of *NEW1* counteracts the growth defect caused by reduced eEF3 levels. The P_{MET25} -*YEF3* strain carrying the indicated low-copy (l.c.) or high-copy (h.c.) *URA3* plasmids was grown overnight in liquid SC-ura-met-cys medium, 10-fold serially diluted, spotted on SC-ura-met-cys (0 mM met) and SC-ura-cys (2 mM met) plates, and incubated at 30°C for 3 days. (D) Increased expression of *NEW1* counteracts the inviability of cells lacking eEF3. The *yef3Δ* strain harbouring the l.c. or h.c. *LEU2* plasmids. The transformants were grown overnight in liquid SC-leu medium, 10-fold serially diluted, spotted onto SC-leu and SC-leu+5-FOA plates, and incubated at 30°C for three (SC-leu) or 5 (SC-leu+5-FOA) days. On 5-FOA containing plates only those cells that have lost the *URA3* plasmid are able to grow (74). (E) Increased dosage of the *YEF3* gene does not suppress the growth defect of *new1Δ* cells. The cells harbouring the indicated plasmids were grown overnight in liquid SC-ura medium, 10-fold serially diluted, spotted on SC-ura plates and incubated at 30°C for 2 or at 20°C for 4 days.

& Schuell) at 30 mbar vacuum. The slots were washed with 150 μ l of Polysome Gradient Buffer, loaded with 150 μ l of the same buffer followed by addition of 10 μ l of each fraction in separate slots. After two washes with 150 μ l of Polysome Gradient Buffer, the membrane was transferred to a hybridization bottle and blocked, using 5% skimmed milk in PBS-T, for 2 h in a hybridization oven set at room temperature. Following antibody incubation (TAP-tag detection), washing and chemiluminescent detection was performed as for western blot (18).

Purification of 80S ribosomes

The *S. cerevisiae* strain PY116 was used for preparation of ribosomes (33). The overnight culture was grown in a fermenter (SP Processum, Domsjö) in 25 L glycerol-lactate medium to OD₆₀₀ of \approx 5, followed by the addition of 25 L of YPD. After 5 h the culture reached the OD₆₀₀ of \approx 5, and it was cooled down to 4°C for several hours, the cells were pelleted by centrifugation, flash-frozen and stored in -80°C. Twenty grams of cell mass was disrupted using a freezer-mill (Spex Freezer Mill, 8 cycles at 14 fps frequency interspersed with 2 min work-rest intervals) and resuspended in 80 ml of ice-cold cell opening buffer (10 mM KCl, 5 mM Mg(OAc)₂, 0.1 mM ethylenediaminetetraacetic acid (EDTA), 10 mM BME, 1 mM PMSF, 0.8 mg/ml heparin, 20 mM Tris:HCl pH 7.5) on ice with stirring. Lysate was clarified by centrifugation for 30 min at 16 000 rpm (Ti 45 rotor, Beckman), the supernatant was loaded onto sucrose cushions (1.1 M su-

crose, 50 mM KCl, 10 mM Mg(OAc)₂, 0.1 mM EDTA, 5 mM BME, 20 mM Tris:HCl, pH 7.5) and centrifuged for 16–18 h at 35 000 rpm. Ribosomal pellets were dissolved in high salt buffer (500 mM NH₄Cl, 250 mM sucrose, 10 mM Mg(OAc)₂, 0.1 mM EDTA, 5 mM BME, 20 mM Tris:HCl pH 7.5 supplemented with 1 mM puromycin), incubated for 1 h at 4°C with gentle mixing and pelleted again (8 h at 35 000 rpm) through 40 ml sucrose cushions. Resultant ribosomal pellets were combined in 15 ml of overlay buffer (50 mM KCl, 5 mM Mg(OAc)₂, 0.1 mM EDTA, 3 mM BME, 10 mM Tris:HCl pH 7.5) and resolved on a 10–40% sucrose gradient in overlay buffer in a zonal rotor (Ti 15, Beckman, 15 h at 21 000 rpm). The peak containing 80S ribosomes was pelleted by centrifugation (19 h at 40 000 rpm) and ribosomes were dissolved in 1 ml of HEPES:Polymix buffer (20 mM HEPES:KOH pH 7.5, 2 mM DTT, 5 mM Mg(OAc)₂, 95 mM KCl, 5 mM NH₄Cl, 0.5 mM CaCl₂, 8 mM putrescine, 1 mM spermidine (32)). The 80S concentration was measured spectrophotometrically (1 A₂₆₀ = 20 nM of 80S). Ribosomes were aliquoted by 50–100 μ l, flash-frozen in liquid nitrogen and stored at -80°C.

Protein expression and purification

The ATPase-deficient New1 construct (VH_p123, Table 1) lacks the aggregation-prone prion domain (New1 Δ Q/N), but contains an N-terminal His₆-tag, and the catalytic glutamic acid residues in the two ATPase active sites are replaced with glutamines (E713Q, E1058Q; New1-EQ₂). The

Table 1. Strains and plasmids used in this study

Name	Description	Reference
Strains		
BY4741	<i>MATα his3Δ1 leu2Δ0 met15Δ0 ura3Δ0</i>	(75)
BY4742	<i>MATα his3Δ1 leu2Δ0 lys2Δ0 ura3Δ0</i>	(75)
BY4709	<i>MATα ura3Δ0</i>	(75)
MJY944	<i>MATα his3Δ1 leu2Δ0 ura3Δ0 new1Δ::HIS3MX6</i>	This study
MJY945	<i>MATα his3Δ1 leu2Δ0 ura3Δ0 new1Δ::HIS3MX6</i>	This study
MJY1091	<i>MATα his3Δ1 leu2Δ0 ura3Δ0 new1Δ::kanMX6</i>	This study
MJY1171	<i>MATα ura3Δ0</i>	This study
MJY1173	<i>MATα ura3Δ0 new1Δ::kanMX6</i>	This study
MJY951	<i>MATα his3 leu2Δ0 ura3Δ0 new1Δ::HIS3MX6 P_{YEF3}::kanMX6-P_{MET25}</i>	This study
PY116	<i>ura3-52 trp1Δ his3-11,15 pep4-4 prb1-1122 prc1-407 leu2-3,112 nuc1::LEU2</i>	(33)
VHY61	<i>MATα leu2Δ0 met15Δ0 ura3Δ0 his3Δ1::FRP880</i>	This study
VKY8	<i>MATα his3 leu2Δ0 ura3Δ0 P_{YEF3}::kanMX6-P_{MET25}</i>	(18)
VKY9	<i>MATα his3 leu2Δ0 ura3Δ0</i>	(18)
VKY20	<i>MATα his3 leu2Δ0 lys2Δ0 ura3Δ0 yef3Δ::kanMX6 /pRS316-YEF3</i>	(18)
YSC1178-202233783	<i>MATα his3Δ1 leu2Δ0 met15Δ0 ura3Δ0 NEW1::TAP-HIS3MX6</i>	(76)
Plasmids		
FRP880	<i>PACTI(-1-520)-LexA-ER-haB112-TCYCI</i>	(31)
FRP1642	<i>PTEF-HygMX-TTEF-insul-(lexA-box)4-PminCYCI</i>	(31)
pDB722	<i>P_{PGKI}-Renilla-CAAC_{cassette}-Firefly-TCYC2, URA3, 2μ ori</i>	(66)
pDB723	<i>P_{PGKI}-Renilla-UAAC_{cassette}-Firefly-TCYC2, URA3, 2μ ori</i>	(66)
pBS1539	<i>CBP-ProtA Kl-URA3 AmpR</i>	(77)
pFA6a-kanMX6	<i>kanMX6 AmpR</i>	(30)
pFA6a-HIS3MX6	<i>HIS3MX6 AmpR</i>	(30)
pRS315	<i>YCp CEN6/ARS4 LEU2 AmpR</i>	(78)
pRS316	<i>YCp CEN6/ARS4 URA3 AmpR</i>	(78)
pRS425	<i>YEpl 2μ ori LEU2 AmpR</i>	(79)
pRS426	<i>YEpl 2μ ori URA3 AmpR</i>	(79)
pRS315-NEW1	<i>NEW1 in pRS315</i>	This study
pRS315-YEF3	<i>YEF3 in pRS315</i>	(18)
pRS316-NEW1	<i>NEW1 in pRS316</i>	This study
pRS316-YEF3	<i>YEF3 in pRS316</i>	(18)
pRS425-NEW1	<i>NEW1 in pRS425</i>	This study
pRS426-YEF3	<i>YEF3 in pRS426</i>	This study
pRS426-NEW1	<i>NEW1 in pRS426</i>	This study
VHp123	<i>6His-NEW1_{ΔQ/N}-EQ2 (ΔP2-P140 E713Q E1058Q, codon optimised to E. coli expression) in pET19b</i>	This study
VHp257	<i>insul-(lexA-box)4-PminCYCI-NEW1_{E713Q}-TAP-T_{synth8} in pRS316</i>	This study
VHp258	<i>insul-(lexA-box)4-PminCYCI-NEW1_{E1058Q}-TAP-T_{synth8} in pRS316</i>	This study
VHp262	<i>insul-(lexA-box)4-PminCYCI-NEW1-TAP-T_{synth8} in pRS316</i>	This study
VHp265	<i>insul-(lexA-box)4-PminCYCI-NEW1-EQ2-TAP-T_{synth8} in pRS316</i>	This study
VHp327	<i>P_{TDH3}-NEW1 in pRS425</i>	This study
VHp603	<i>P_{PGKI}-Renilla-YDR099W(TAA)_{cassette}-Firefly-TCYC2, URA3, 2μ ori</i>	This study
VHp605	<i>P_{PGKI}-Renilla-YNL247W(TAG)_{cassette}-Firefly-TCYC2, URA3, 2μ ori</i>	This study
VHp606	<i>P_{PGKI}-Renilla-YDR099W(CAA)_{cassette}-Firefly-TCYC2, URA3, 2μ ori</i>	This study
VHp607	<i>P_{PGKI}-Renilla-YNL247W(CAG)_{cassette}-Firefly-TCYC2, URA3, 2μ ori</i>	This study

protein was overexpressed in BL21 *Escherichia coli* cells grown at 37°C from an overnight culture in LB medium starting at OD₆₀₀ of 0.06. Cells were grown until OD₆₀₀ of 0.2 and the temperature shifted to 22°C. At OD₆₀₀ = 0.4, the culture was induced with 1 mM Isopropyl β-D-1-thiogalactopyranoside (IPTG). After 1.5 h of expression, the cells were harvested at 8000 × g for 10 min at 4°C. All subsequent steps were performed on ice or at 4°C. The pellet was resuspended in 30 ml of lysis buffer (50 mM Tris–Cl [pH 7.5], 1 mM MgCl₂, 20 mM NaCl, 10 mM Imidazole, protease inhibitor cocktail (cOmplete ULTRA EDTA free, Roche) and lysed using a microfluidizer (Microfluidics M-110L) by passing cells three times at 18 000 p.s.i. The cell debris was removed upon centrifugation in a SS34 rotor at 4°C (27 000 × g for 15 min) and the proteins were purified from the supernatant by His-tag affinity chromatography using Ni-NTA agarose beads (Clontech). The bound proteins were washed with lysis buffer contain-

ing 25 mM imidazole and then eluted with lysis buffer containing 500 mM imidazole. The final eluate was purified by size-exclusion chromatography using HiLoad 16/600 Superdex 75 (GE Healthcare) in gel filtration buffer (50 mM Tris–HCl [pH 7.5], 700 mM NaCl, 10 mM MgCl₂, 2 mM DTT). The aliquots were pooled, snap-frozen in liquid nitrogen and stored at –80°C.

Sample and grid preparation

All following steps were performed in buffer composed of 20 mM HEPES [pH 7.5], 2 mM DTT, 100 mM KOAc and 20 mM Mg(OAc)₂. The purified components and the nucleotide (80S:New1_{ΔQ/N}.EQ₂:ATP) were mixed at a ratio 1:2:2000 and incubated 20 min at 30°C. DDM was added to the sample to a final concentration of 0.01% (v/v). For grid preparation, 5 μl (5 A₂₆₀/ml) of the freshly prepared ribosomal complex was applied to 2 nm precoated Quan-

tifoil R3/3 holey carbon supported grids and vitrified using a Vitrobot Mark IV (FEI, Netherlands).

Cryo-electron microscopy and single-particle reconstruction

Data collection was performed on an FEI Titan Krios transmission electron microscope equipped with a Falcon II direct electron detector (FEI) at 300 kV at a pixel size of 1.063 Å. A total of 3519 Micrographs were collected using an under defocus range from -0.5 to -2.5 μm . Each micrograph was collected as series of 16 frames ($2.7\text{ e}^-/\text{\AA}^2$ pre-exposure; $2.7\text{ e}^-/\text{\AA}^2$ dose per frame). All frames (accumulated dose of $45.9\text{ e}^-/\text{\AA}^2$) were aligned using the Unblur software (34). Power-spectra, defocus values, astigmatism and resolution estimates for each micrograph were determined using Gctf version 1.06 (35). After manual inspection and application of a resolution cut-off which preserved micrographs showing Thon rings beyond 3.5 Å, 1919 micrographs were subjected to the next processing steps. Automated particle picking was performed using Gautomatch version 0.56 (<http://www.mrc-lmb.cam.ac.uk/kzhang/>) resulting in 171 106 particles, which were first processed using RELION-2.1 (36). Manual inspection of 6xbinned 2D particle classes after 2D classification resulted in 144 876 particles that were further used for 3D-refinement using an empty *S. cerevisiae* 80S ribosome (density map was created using the PDB ID: 3j78 with the tRNAs removed) as a reference structure. Subsequently, a 3D classification was performed sorting the particles into five classes (Supplementary Figure S2). The class containing the New1-80S complex (57 226 particles) was subjected to focused-sorting, using a mask encompassing the New1 ligand. The New1-containing population (48 757 particles) was then refined using undecimated particles and additionally focused refined with a spherical mask encompassing the New1 ligand as well as the 40S head (Supplementary Figure S2). Subsequently, the overall refined structure was subjected to contrast-transfer function (CTF) refinement using RELION-3.0 (37). The CTF refined particles were again 3D refined and subsequently multibody refinement was performed. For the multibody refinement, three masks were used: the first one encompassed the first portion of New1 (HEAT and 4HB, residue range 141–549) as well as the SSU Head, the second mask included the remain part of New1 (ABC1-ABC2-CD, residue range 570–1112) and the LSU, and the third mask covered the SSU Body (Supplementary Figures S2 and 3E). The final reconstructions were corrected for the modulation transfer function of the Falcon 2 detector and sharpened by applying a negative B-factor estimated by RELION-3.0 (37). For the sharpening, a mask for the whole New1–80S complex (for the overall refinement) and New1 (for the local refinement) was used, respectively, resulting in a final average reconstruction of 3.28 Å for the New1–80S complex and 3.63 Å for the New1 (Supplementary Figures S2 and 3A). The same was done for each part of the multibody refined volumes, which provided an average resolution of 3.26 Å for the SSU Head-New1 (HEAT, 4HB), 3.06 Å for the LSU-New1 (ABC1, ABC2, CD) and 3.14 Å for the SSU Body. The single multibodies were merged using phenix 1.15 via the phenix.combine_focused_maps command (38). The resolution of the 3.28 Å volume was es-

timated using the ‘gold standard’ criterion (FSC = 0.143) (39). Local-resolution estimation and local filtering of the final volumes was done using Relion-2.1 (Supplementary Figure S3F-N).

Molecular modelling

A homology model of New1 was created using the deposited structure of the eEF3 protein model (PDB ID: 2IX8) (9) as a template for SWISS-MODELLER (40). The homology model was fitted into density with UCSF Chimera 1.12.1 (41) using the command ‘fit in map’: Single domains were manually adjusted with Coot version 0.8.9.2 (42). The chromo domain was built *de novo* based on the secondary structure elements of the chromo domain of HP1 complexed with the histone H3 tail of *Drosophila melanogaster* (PDB ID: 1KNE). The ATP molecules within the ABCs were obtained from the PDB ID: 6HA8 (43). The model of the *S. cerevisiae* 80S ribosome was derived from PDB ID: 4U4R. The proteins of the SSU and LSU were fitted separately into locally filtered electron density maps using UCSF Chimera (41). The rRNA was fitted domain-wise in Coot (42). Afterwards manual adjustments were applied to all fitted molecular models using Coot. The combined molecular model (proteins+rRNA) was then refined into the merged multibody maps using the phenix.real_space_refine command of phenix version 1.14, with restraints that were obtained via the phenix.secondary_structure_restraints command (38). Cross-validation against overfitting was performed as described elsewhere (44) (Supplementary Figure S3B). Statistics for the model were obtained using MolProbity (45) and are represented in Supplementary Table S2.

Figure preparation

Figures showing atomic models and electron densities were generated using either UCSF Chimera (41) or Chimera X (46) and assembled with Inkscape.

Preparation of Ribo-Seq and RNA-Seq libraries and data analysis

Cultures of wild type (MJY1171) and *new1* Δ (MJY1173) strains were grown overnight at 20°C (or, alternatively, at 30°C), diluted to $\text{OD}_{600} \approx 0.05$ in 750 ml of SC medium and incubated in a water bath shaker at 20°C (or 30°C) until $\text{OD}_{600} \approx 0.6$. Cells were harvested by rapid vacuum filtration onto a 0.45 μm nitrocellulose membrane, scraped off, and frozen in liquid nitrogen. Cells were lysed by cryogenic milling and RNA-Seq and Ribo-Seq libraries prepared from the cell extracts. RNA-Seq libraries were prepared using Scriptseq Complete Gold Yeast Kit (Epicentre). Ribo-Seq libraries were prepared essentially as per Ingolia and colleagues (18) with updated enzymes, modifications of rRNA removal and sample purification procedures. Detailed protocols can be found in our GitHub repository https://github.com/GCA-VH-lab/Lab_protocols.

NGS and data analysis

Multiplexed Ribo-Seq and RNA-Seq libraries were sequenced for 51 cycles (single read) on an Illumina

HiSeq2500 platform. The quality of Illumina reads was controlled using FastQC (47) (<http://www.bioinformatics.babraham.ac.uk/projects/fastqc>), and low quality reads (Phred score below 20) were discarded. The adaptor sequence (5'-NNNNCTGTAGGCACCATCAAT-3') was removed using Cutadapt (48). After removing reads mapping to non-coding RNA, reads were mapped to the *S. cerevisiae* reference genome R64-1-1.85 using HISAT2 (49). In the case of Ribo-Seq, out of 36–47 million unprocessed reads after removal of non-coding RNA (rRNA and tRNA) and reads that mapped more than twice 3–8 million reads remained. Pooling resulted in 7.8 (20°C)/9.3 (30°C) million reads total for wild-type and 12.7 (20°C)/5.5 (30°C) million reads for *new1*Δ. RNA-Seq reads were processed similarly, omitting the Cutadapt step; out of 16–32 million unprocessed reads, 12.5–20 million remained after removing non-coding RNA and reads that mapped more than two times. The analysis pipeline was implemented in Python 3 and is available at GitHub repository (<https://github.com/GCA-VH-lab/2019-NAR>). Reads that mapped once to the genome were used for final P-site assignment using read length-specific offsets, as provided in the file readlength_offsets_expert.txt on GitHub. Mapped reads were normalised as reads per million (RPM). The ribosome queuing metric was computed using the Python script compute_queueing.py. Gene coverage was calculated using HTSeq-count (50) and differential gene expression (DE) analyses were performed using the DESeq2 package (51). All four replicates (two at 30°C and two at 20°C) of wild type and *new1*Δ datasets were used in the analyses. Differentially expressed genes were identified based on an adjusted *P*-value cut-off of 0.05 as well as at least 2-fold difference in expression level (Supplementary Table S4). Only the genes that with >10 Ribo-Seq or RNA-Seq were used for analysis. GO enrichment analysis was performed using the Gene Ontology (GO) knowledgebase (<http://geneontology.org/>) (52) implemented in PANTHER (53). The R script used for analyses, as well as both input and output files are available at GitHub repository (https://github.com/GCA-VH-lab/2019-NAR/tree/master/Differential_Expression).

RESULTS

New1 has a function that partially overlaps with that of eEF3

New1's closest homologue in *S. cerevisiae*—the translation factor eEF3 encoded by the *YEF3* gene—is an essential player in translation elongation (15,16) with a putative secondary function in ribosome recycling (17). While deletion of the *NEW1* gene alone causes a pronounced growth defect (40% reduction) at 20°C (23), the growth defect at 30°C is relatively minor (10%) (Supplementary Table S3). To investigate a potential overlap in the functions of New1 and eEF3, we introduced a *new1*Δ allele into cells in which *YEF3* is under the control of the methionine repressible *MET25* promoter (P_{MET25}) (54). We have previously characterized the P_{MET25} -*YEF3* strain and demonstrated that addition of increasing methionine concentrations specifically leads to a decrease in the eEF3 levels, resulting in a gradual slow-down of growth (18) (Supplementary Figure S4A). The methionine-induced growth inhibition of P_{MET25} -*YEF3* cells was more pronounced in the absence of

NEW1, at both 20°C and 30°C (Figure 1B and Supplementary Figure S4BC). While these results are consistent with overlapping functions of New1 and eEF3 in protein synthesis, the additive negative effects on fitness could also be due to the two proteins acting on two sequential steps in gene expression, for example, ribosome assembly (New1) and translation (eEF3). Therefore, we investigated whether New1 can functionally substitute for eEF3's cellular function. To do this, we first tested whether full-length New1 can suppress the growth defect caused by eEF3 depletion. We found that increased *NEW1* gene dosage did, indeed, counteract the growth retardation caused by eEF3 depletion in P_{MET25} -*YEF3* cells (Figure 1C and Supplementary Figure S4D). Second, we investigated whether an increased level of New1 could overcome the essentiality of eEF3. To do so, we constructed a *yef3*Δ strain that was rescued by a wild-type *YEF3* gene on a *URA3* plasmid. Increased dosage of the *NEW1* gene, either under its own or the strong *TDH3* promoter (P_{TDH3}), counteracted the requirement of the *YEF3* plasmid for viability (Figure 1D).

Taken together, our findings demonstrate that New1 can, although with low efficiency, perform the essential molecular function of eEF3 in protein synthesis. On the other hand, increased *YEF3* gene dosage does not suppress the cold sensitivity phenotype of a *new1*Δ strain, suggesting that New1 has a specific molecular function that cannot be performed by eEF3 (Figure 1E).

The ATPase-deficient New1-EQ₂ mutant is locked on translating ribosomes

To characterise the association of New1 with ribosomes, we used ATPase-deficient mutants in which the catalytic glutamic acid residues (E713 and E1058) in the two ATPase active sites (Figure 1A) are replaced by glutamines (Q) (so-called EQ₂ mutants). Locked in the ATP-bound conformation, the EQ₂ mutants of *E. coli* ABCF EttA (55), *Bacillus subtilis* VmlR (43) and human ABCF ABCF1/ABC50 (7) were previously used to trap these ABCF ATPases on ribosomes. We used a tightly controlled β-estradiol-inducible LexA-ER-B112 expression system (31) to drive expression of C-terminally TAP-tagged (56) versions of New1 or New1-EQ₂. While induction of New1-TAP has no effect on growth, the induction of New1-EQ₂-TAP leads to growth inhibition ~3 h after the addition of the inducer β-estradiol (Figure 2A and Supplementary Figure S5AB). At this time point, the level of New1-EQ₂ is about 3-fold higher than those observed in a strain that expresses a C-terminally TAP-tagged New1 from its normal chromosomal location (Supplementary Figure S1). One likely reason for the growth inhibition is the non-productive association of New1-EQ₂ with its ribosomal target, be it ribosome assembly intermediates or mature 80S ribosomes. We directly tested this hypothesis by performing polysome fractionation and immunoblotting. In ATP-supplemented lysates, the bulk of New1-EQ₂—but not wild type New1—localizes to the polysomal fractions, suggesting that translating ribosomes are indeed the cellular target of the factor (Figure 2B and Supplementary Figure S5C). Omitting ATP from the lysis buffer and sucrose gradients leads to loss of New1-EQ₂ from polysomal fractions, suggesting that ATP

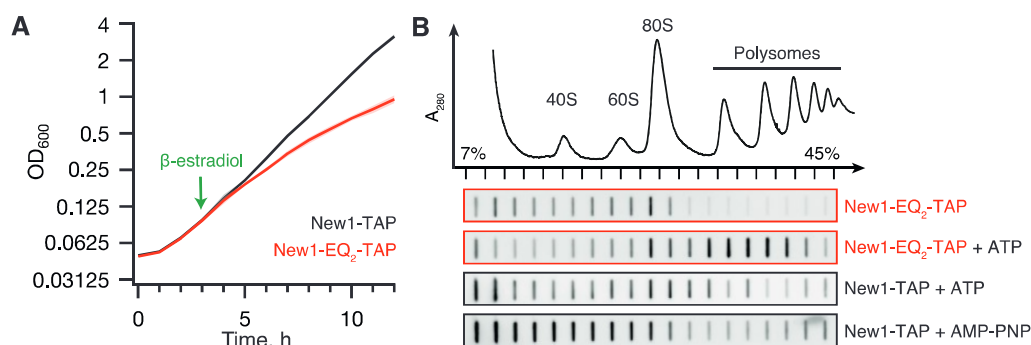


Figure 2. ATPase-deficient New1-EQ₂ inhibits cell growth and stably co-sediments with polysomal fractions. (A) Expression of New1-EQ₂-TAP, but not wild-type New1-TAP causes growth inhibition. The strains were grown in SC-ura medium at 30°C and expression of New1-TAP or New1-EQ₂-TAP was induced by addition of β-estradiol to final concentration of 1 μM as indicated by the green arrow. OD₆₀₀ measurements are presented as geometric means of three independent transformants, and standard error of the mean is indicated with shading. (B) Polysome profile and immunoblot analyses of yeast strains expressing New1-TAP or New1-EQ₂-TAP. The cells were grown at 30°C and at OD₆₀₀ ≈ 0.3 protein expression was induced by 1 μM β-estradiol. The cells were collected after 3 h, clarified lysates resolved on sucrose gradients (either in the absence of nucleotides or supplemented by 1 mM ATP/AMP-PNP), and TAP-tag detected by slot-blotting using rabbit Peroxidase-anti-peroxidase. Full-size Western blots of wild-type and EQ₂ New-TAP are presented on Supplementary Figure S5C.

binding drives the factor's affinity to the ribosome (Figure 2B and Supplementary Figure S5D). The interaction with ribosomes is specific, since collapsing polysomes either by RNase I treatment or preparing yeast lysates under run-off conditions (that is, in the absence of cycloheximide), leads to loss of New1-EQ₂ from the high-sucrose fractions and redistribution into the 80S fraction (Supplementary Figure S5F-G). Unlike native ATP, a commonly used non-hydrolysable analogue AMP-PNP fails to stabilize wild-type New1 binding to polysomes (Supplementary Figure S5H), suggesting that AMP-PNP is a poor substrate for New1 (Figure 2B). Therefore, for solving the structure of New1 locked on the 80S ribosome, we used the EQ₂ mutant and ATP instead of using the wild-type protein and AMP-PNP.

Structure of the New1_{ΔQ/N}-EQ₂ on the 80S ribosome

To determine the binding site of New1 on the ribosome, we incubated *S. cerevisiae* 80S ribosomes with New1_{ΔQ/N}-EQ₂ variant in the presence of ATP, and subjected the assembled New1_{ΔQ/N}-EQ₂-80S complex (hereafter referred to as the New1-80S complex) to single particle cryo-EM (Figure 3A). After 2D classification, a total of 144 876 ribosomal particles were sorted into five distinct ribosomal subpopulations (Supplementary Figure S2). One major population (class 1 containing 57 226 particles, 39.5%) was obtained that contained additional density spanning the head of the 40S subunit and central protuberance of the large 50S subunit, whereas this density was either fragmented (class 2) or absent (class 3–5) in the remaining subpopulations (Supplementary Figure S2). Further local 3D classification of class 1 and the subsequent refinement of the defined New1-80S particles (class 2 containing 48 757 particles) yielded a final reconstruction of the New1-80S complex (Figure 3A), with an average resolution of 3.28 Å (Supplementary Figures S2 and 3). Local resolution calculations reveal that while the core of the ribosomal subunits was well resolved and ex-

tended to 3.0 Å, the peripherally bound New1 ligand was less well-resolved, with local resolution ranging between 4–7 Å (Supplementary Figure S3C-F). To improve the overall resolution of the New1 density, further focussed and multi-body refinement were performed (see 'Materials and Methods' section). The resulting maps showed significant improvements in the local resolution for New1, particularly at the interaction interface between New1 and 80S ribosome where the resolution approached 3 Å (Supplementary Figure S3G-N) and sidechains were clearly visible, whereas the periphery was less well-resolved (4–7 Å) and only large and bulky sidechains could be visualized (Supplementary Figure S6A and B). Together with the high sequence homology to eEF3, this enabled us to generate homology models for each domain of New1 using the crystal structure of eEF3 (9) as a template, which could then be unambiguously fitted and refined into the cryo-EM map of the New1-80S complex (Figure 3B and C; Supplementary Figure S6C). Extra density was also observed for two molecules of ATP bound within each of the active sites of the ABC1 and ABC2 domains of New1 (Supplementary Figure S6D and E). This is consistent with the ability of New1-EQ₂ variant to bind, but not hydrolyse, ATP. The ABC1 and ABC2 nucleotide binding domains (NBDs) were observed in a closed conformation, analogous to the closed conformations adopted in the 70S-bound ABCF protein VmlR from *B. subtilis* (43) and archaeal 40S-ABCE1 complex (57), and distinct from the open conformation observed for the free state of ABCE1 (58) (Supplementary Figure S7A-C). Modelling of an open conformation of New1 on the ribosome suggests that it is incompatible with stable binding, leading to either a clash of the ABC2-CD with the central protuberance of the large 60S subunit (LSU) or dissociation of the ABC1-HEAT-4HB domain from the small 40S subunit (SSU) (Supplementary Figure S7D-G). These observations support the idea that New1 binds to the ribosome in the 'closed' ATP-bound conformation and that ribosome-stimulated hydrolysis of ATP to ADP would promote New1 dissociation.

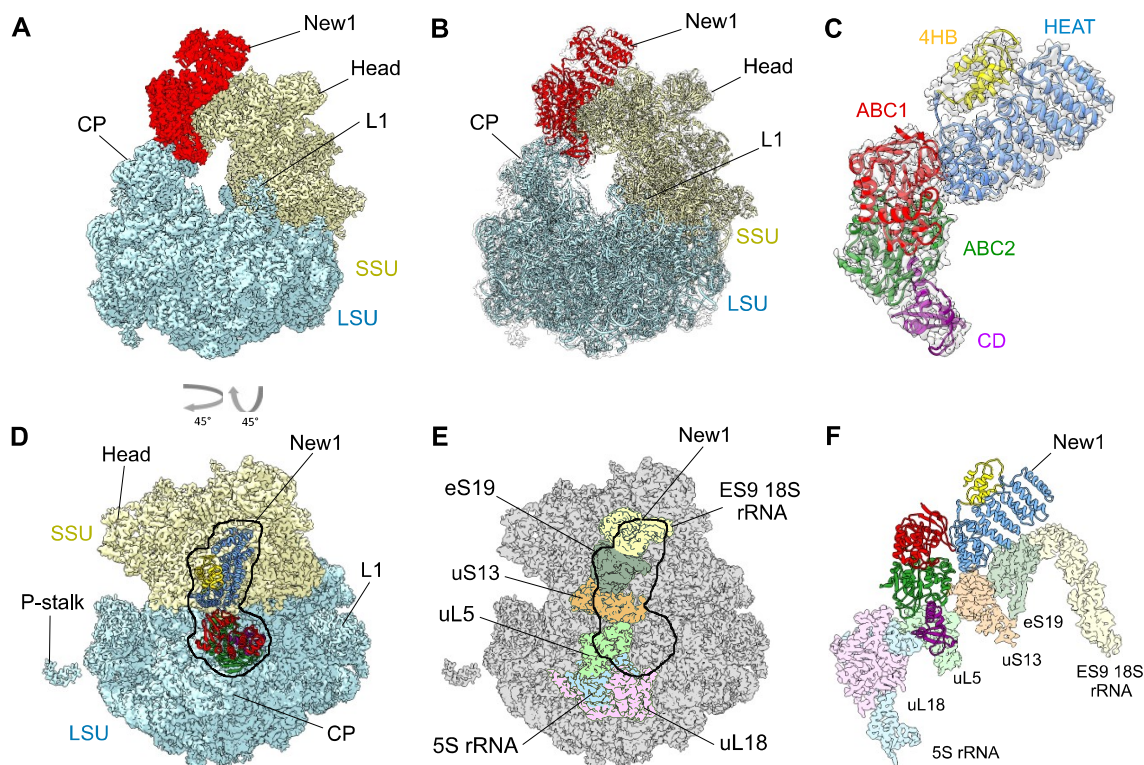


Figure 3. The New1 interaction with the 80S Ribosome in *Saccharomyces cerevisiae*. (A and B) Cryo-EM reconstruction of the New1–80S complex with (A) segmented densities for New1 (red), SSU (yellow) and LSU (cyan) and (B) transparent multibody refined cryo-EM map with fitted molecular models for New1 (red), SSU (yellow) and LSU (cyan). CP, central protuberance. (C) Isolated cryo-EM map density (transparent grey) for New1 from (B) with New1 model colored according to its domain architecture, HEAT (blue), 4HB (yellow), ABC1 (red), ABC2 (green) and CD (magenta). (D) Top view of the New1 (coloured by domain as in (C)) bound to the ribosome with LSU (cyan) and SSU (yellow). (E) Outline of New1 binding site on the 80S ribosome with ribosomal components colored as in (E). (F) Interaction environment of New1 (coloured by domain as in (C)) on the ribosome, with ribosomal components colored as in (E).

Interaction of New1 with the 80S ribosome

To ascertain the contacts between New1 and the 80S ribosome, the crystal structure of the *S. cerevisiae* SSU and LSU was also fitted and refined together with New1 (Figure 3B). Overall, the binding site is globally similar to that observed previously for eEF3; however, with the improved resolution it is now possible to better ascertain which regions of New1 interact with which ribosomal components (Figure 3D–F). The majority of the contacts with the SSU are established between the N-terminal HEAT domain and components of the SSU head, specifically, with the tip of expansion segment 9 (ES9) of the 18S rRNA and ribosomal proteins uS13 and uS19 (Figure 3D–F). The 4HB and ABC1 domains of New1 do not interact with any ribosomal components, whereas ABC2 and CD form extensive interaction with the LSU, mainly with the 5S rRNA and ribosomal protein uL5. Additionally, bridging interactions are formed by ABC2 that contacts uL5 on the LSU and uS13 on the SSU (Figure 3D–F). A more in-depth description of these interactions is found in the *Supplementary Results* section, with an accompanying Supplementary Figure S8. By contrast, the tip of the CD makes no contacts with the ribosome, but rather extends into the vacant E-site in the direction of the L1 stalk (Figure 4A), as observed previously for the eEF3–80S structure (Figure 4B) (9). The CD of eEF3

has been proposed to influence the conformation of the L1 stalk and thereby facilitate release of the E-site tRNA (9). However, compared to eEF3, the CD of New1 is truncated and lacks the $\beta 4$ – $\beta 5$ -hairpin (Figure 4C–D) and therefore the extent by which the CD of New1 reaches towards the L1 stalk is reduced (Figure 4A). We speculate that the $\beta 4$ – $\beta 5$ -hairpin plays an important role in eEF3 function to promote the open conformation of the L1 stalk necessary for E-tRNA release and that the absence of this motif in New1 may explain why New1 overexpression cannot fully rescue the growth defect caused by depletion or loss of eEF3. This raises the question as to whether New1 has acquired another function on the ribosome that is distinct from eEF3.

New1 depletion leads to ribosome queuing upstream of 3'-terminal lysine and arginine codons

To assess the global effects of New1 loss on translation in yeast we used ribosome profiling (Ribo-Seq) (59) of wild-type and *new1* Δ strains both at 20°C and 30°C, with two biological replicates for each condition. We also carried out RNA-seq to enable normalization of translation level for the transcription level effects on expression. We performed differential expression analysis of both RNA-Seq (38 genes with increased coverage and 48 genes with decreased coverage) and Ribo-Seq (26 genes with increased

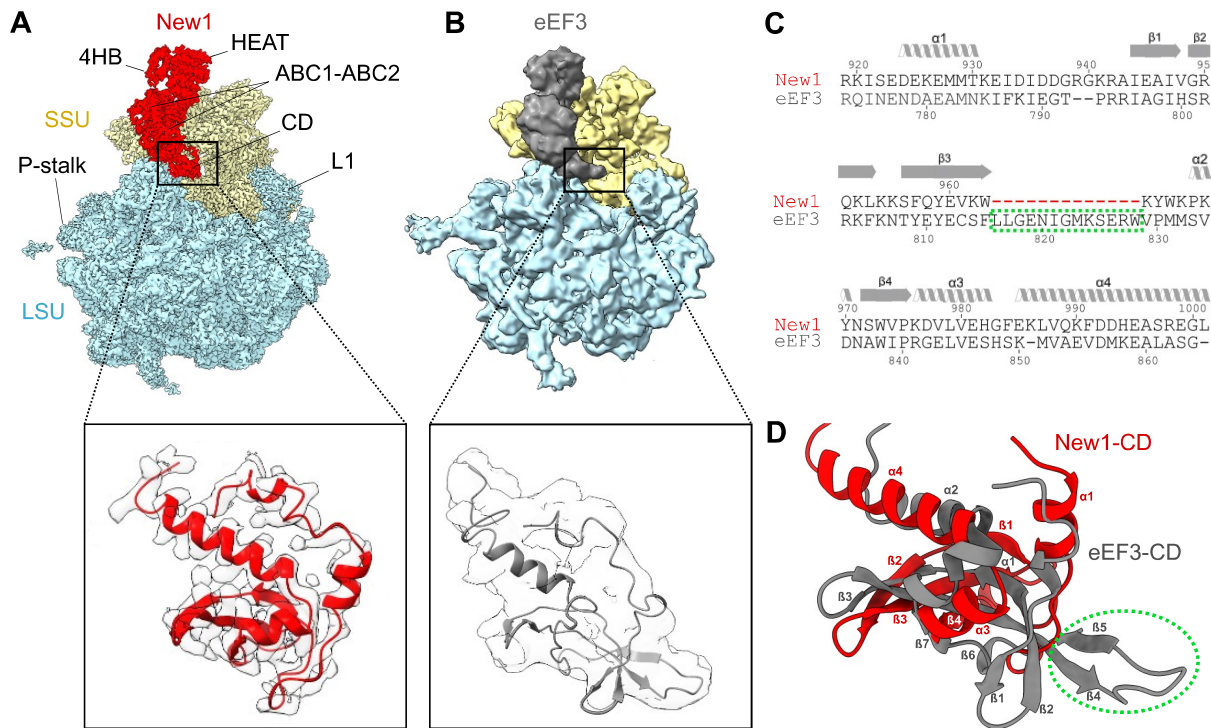


Figure 4. Comparison of the chromodomain region of New1 and eEF3. (A) Cryo-EM reconstructions of the New1–80S and (B) the eEF3–80S (9.9 Å, EMD ID: 1233) complexes as well as zoom showing comparison of the New1–CD (red with grey cryo-EM density) with that of the eEF3 model (grey, PDB ID: 2ix8) (9). (C) Sequence alignment of the CD of New1 and EF3, highlighting truncated region in New1 (red dashes). (D) Comparison of structures of New1–CD (red) with eEF3–CD (grey, PDB ID: 2iw3) (9). The green dashed circle highlights the eEF3 residues, which are missing in the New1p sequence in (C).

coverage and 47 genes with decreased coverage) (Supplementary Table S4, see ‘Materials and Methods’ section for details). Next, we applied Gene Ontology (GO) analysis (52) to identify the biological processes, molecular functions and cellular components enriched in the differentially expressed genes (Supplementary Table S4). Increased RNA-Seq coverage is associated with mitochondrial function and cell energetics, such as ubiquinol to cytochrome c (GO:0006122), ATP synthesis coupled proton transport (GO:0015986), ATP hydrolysis coupled cation transmembrane transport (GO:0099132) and mitochondrion organization (GO:0007005); analysis of the genes with differentially increased Ribo-Seq coverage reveals no GO enrichment. Decreased RNA-Seq coverage is associated with urea cycle (GO:0000050), ethanol biosynthetic process involved in glucose fermentation to ethanol (GO:0043458), arginine biosynthetic process (GO:0006526), NADH oxidation (GO:0006116) and amino acid catabolic process to alcohol via Ehrlich pathway (GO:0000947). The genes with decreased Ribo-Seq coverage are associated with an overlapping set of GO terms, suggesting the effects are predominantly at the mRNA level.

The Ribo-Seq procedure generates two distinct classes of RPFs: ‘short’ (20–22 nucleotides) and ‘long’ (28–30 nucleotides), which originate from ribosomes with vacant or occupied A-sites, respectively (60). The translation elongation inhibitor cycloheximide has previously been a common component in Ribo-Seq library preparation; however, this antibiotic has recently been found to drive near-exclusive

formation of long RPFs (60,61). Therefore, to be able to use the RPF size distribution as an additional insight into the nature of translational perturbation upon the loss of New1, we omitted cycloheximide during cell collection and lysis.

At 30°C the RPF length distributions of wild-type and *new1*Δ are very similar (Supplementary Figure S9A). However, at 20°C, i.e. when New1 absence leads to a significant growth defect (Supplementary Table S2), short RPFs are moderately depleted in the *new1*Δ dataset (Supplementary Figure S9B). While depletion of short RPFs signals a lower abundance of ribosomes with a vacant A-site, the causality is unclear: the lower fraction of the 80S with an empty A-site could reflect a perturbation of translation in the absence of New1 or be a mere consequence of the slower growth rate. Strikingly, the lack of New1 leads to the appearance of periodic (≈30 nt) ‘waves’ of ribosomal density preceding the stop codon (Figure 5A and Supplementary Figure S9C–F). The period of the ‘waves’ corresponds to the size of mRNA fragment protected by a ribosome, suggesting ribosome queuing upstream of the stop codon due to a defect in translation termination or/and ribosome recycling. The effect is more pronounced at 20°C, correlating with the severity of the growth defect (compare Supplementary Figure S9C–F). We compared our Ribo-Seq analysis of the *new1*Δ strain with other yeast strains defective in translation termination, namely, *S. cerevisiae* depleted for eIF5A (62) or Rli1/ABCE (63) (Figure 5B), as well as active eRF3 through formation of Sup35 [*PSI+*] prion (64) (Supplementary Figure S10). The extent of ribosomal queuing in the

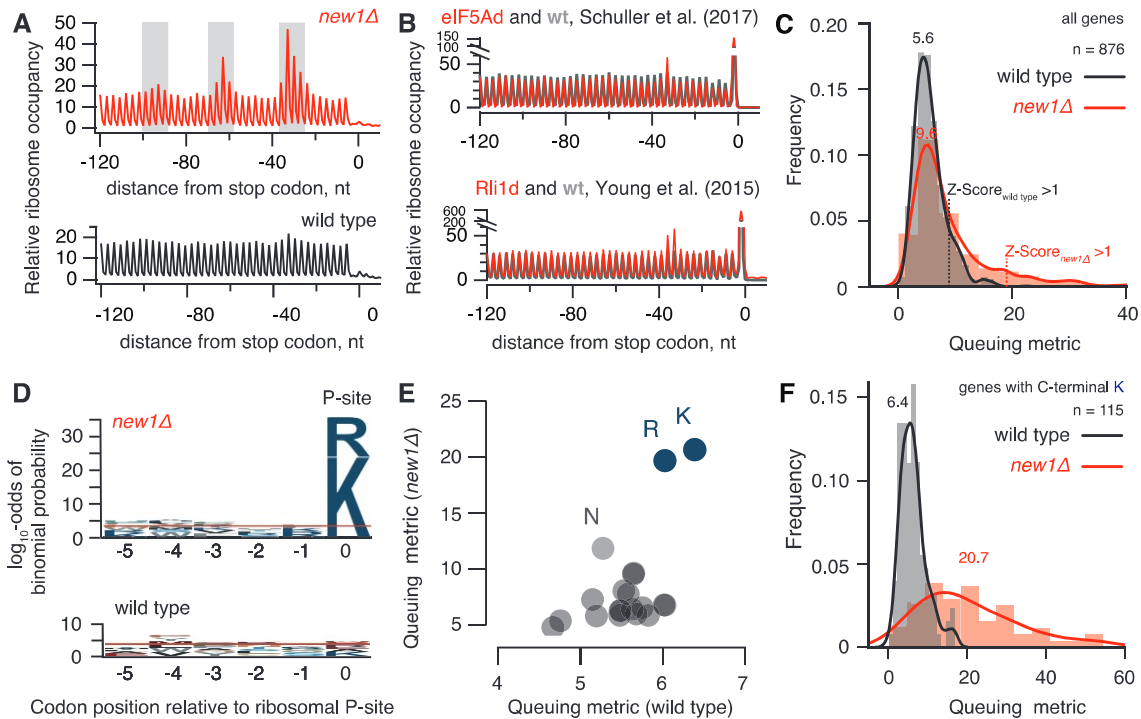


Figure 5. Loss of New1 leads to ribosome queuing at C-terminal lysine and arginine residues. (A) Metagene analysis Ribo-Seq libraries detects ‘waves’ of the ribosomal density preceding the stop codon in the case of *new1Δ* but not wild-type. Note that due to technical reasons the metagene plots lack the pronounced peak at the stop codon both in the case of wild-type and *new1Δ* datasets. (B) Metagene analysis of Rli1-depleted and the corresponding wild-type (62) Ribo-Seq datasets. (C) ‘3-terminal ribosome queuing metric’ (or just ‘queuing metric’ for short) computed for individual ORFs. (D) Sequence conservation analysis for ORFs displaying high degree of ribosomal queuing at the C-terminus (Z-score cut-off of 1) in wild-type and *new1Δ*. Over-representation of specific amino acids at positions relative to the P-site codon was computed using pLogo (67). Horizontal red lines represent significance threshold (the \log_{10} -odds 3.45) corresponding to a Bonferroni corrected *P*-value of 0.05. (E) Mean ribosome queuing distribution for ORFs in wild-type and *new1Δ* sorted by the nature of the C-terminal amino acid. (F) Ribosome queuing metric distribution for genes with C-terminal lysine. All analyses were performed using pooled datasets collected at 20°C. Analyses of individual replicates of both 20°C and 30°C datasets are presented on Supplementary Figure S9C–F.

new1Δ strain is much more dramatic and no queuing is detectable in the [*PSI+*] Ribo-Seq dataset. Our metagene plots lack the pronounced peak at the stop codon, both in the case of wild type and *new1Δ* datasets. This is not unexpected as ribosomal post-termination complexes are more sensitive to ionic strength than elongating ribosomes (62) and require stabilisation by cycloheximide that was specifically omitted in our Ribo-Seq protocol (65).

We next set out to determine whether only a subset of translated mRNAs is affected by New1 loss—and if this is the case, which ORF features correlate with aberrant mRNA translation in the *new1Δ* strain. We defined the ‘C-terminal ribosome queuing metric’ (or just ‘queuing metric’ for short) as a ratio between the sum of the maximal Ribo-Seq counts within the three peaks preceding the stop codon (highlighted with grey shading on Figure 5A) and the average Ribo-Seq density between the peaks. We plotted distributions of the queuing metric values for individual datasets (Figure 5C) as well as for individual ORFs in *new1Δ* against wild-type (Supplementary Figures S11A). While the effect of New1 loss on the mean queuing metric is moderate (5.6 wt versus 9.6 *new1Δ*), the distribution in the *new1Δ* dataset has a clear ‘heavy tail’. While the high queuing metric in *new1Δ* is associated with relatively higher ribosome density after the stop codon (3’ UTR) (Supplementary Figure

S12A–F), the 3’ UTR density in genes displays no codon periodicity suggesting that *new1Δ* does not lead to increased readthrough (Supplementary Figure S12C and F). Consistent with this notion, analyses of readthrough using a dual-luciferase readthrough reporter system (66) detected no apparent difference between the *new1Δ* and wild-type strains (Supplementary Figure S17C).

We selected the ORFs with high queuing metric values using a Z-score cut-off of 1 and applied pLogo (67) to analyse the sequence conservation pattern in the C-terminal region encompassing five codons preceding the stop codon. Strikingly, in the case of *new1Δ* the selected ORFs display a clear conservation signal localized at the C-terminal amino acid, dominated by positively charged lysine (K) and arginine (R) residues (Figure 5D). In the wild-type dataset there is no signal passing the significance cut-off; and no specific C-terminal amino acid signal is detectable in eIF5A (62) or Rli1/ABCE (63) datasets (Supplementary Figure S13), which could be attributed to the relative weakness of the queuing signal in these datasets. Therefore, we tested if the nature of the C-terminal amino acid correlates with the increase in the ribosomal density at the stop codon upon eIF5A and Rli1/ABCE depletion and in [*PSI+*] (Supplementary Figure S14). Our analysis detects no specific increase of the Ribo-Seq density at the stop codons preceded

by C-terminal arginine and lysine residues, further reinforcing the specificity of the effect we observed in the *new1Δ* strain. Finally, we tested if the nature of the stop codon is associated with ribosomal queuing, but detected no signal (Supplementary Figure S15). At the same time, stop codon context analysis readily picks up an over-representation of C-terminal codons encoding lysine (AAA) and arginine (AGA and CGN), consistent with an effect on the amino acid level.

After establishing that the nature of the C-terminal amino acid is the key predictor of ribosomal queuing at the C-terminus, we plotted the mean queuing metric for ORFs grouped by the nature of the different C-terminal amino acid (Figure 5E; note the difference in scale of the X and Y axis). Importantly, in this case we have not pre-selected a subset of ORFs but rather analysed all of the 876 ORFs with sufficient coverage of 3'-terminal 120-nucleotide region (≥ 10 rpm) in all the four conditions (wt and *new1Δ*, 20°C and 30°C). The analysis readily picks up lysine and arginine as outliers in the *new1Δ* background, and detects a weaker signal for asparagine (N). We plotted queuing metric distributions for individual ORFs grouped by the nature of the C-terminal amino acid (Lysine: Figure 5F; distributions for ORFs ending with other amino acids are presented on Supplementary Figure S16). In the case of wild-type, distribution of the queuing metric for ORFs terminating with lysine is similar to that of ORFs in general (compare Figure 5C and F). Conversely, *new1Δ* ORFs terminating with lysine display a broad distribution that is strongly shifted to higher values, consistent with significantly higher ribosomal queuing on mRNAs encoding C-terminal lysine residues (Figure 5E).

After establishing that effect of the New1 loss is clearly mRNA-specific and is not solely determined by the C-terminal residue alone, we re-assessed the stop codon readthrough in *new1Δ* using a modified dual-luciferase reporter system. We chose two ORFs—YDR099W / BMH2 (C-terminal lysine, UAA stop codon) and YNL247 (C-terminal lysine, UAG stop codon)—which in *new1Δ* strain are characterized by possessing high queuing score and increased RiboSeq density in 3' UTR. Additionally, these mRNAs show sufficient RiboSeq coverage as per visual inspection (Supplementary Figure S17A and B). We constructed readthrough reporters containing the four codons immediately preceding and the two codons after the native stop codon present in YDR099W and YNL247. Despite containing C-terminal lysine residues, neither of the two reporters display an increased readthrough level in the *new1Δ* background (Supplementary Figure S17C).

DISCUSSION

Our results show a novel role for New1 in fine-tuning the efficiency of translation termination and/or ribosome recycling in *S. cerevisiae*. Two molecular functions have previously been documented for New1. The first is its necessity for efficient ribosome assembly, which is phenotypically manifested in a pronounced cold-sensitivity of the *new1Δ* strain (23). While New1 loss compromises ribosomal assembly, this phenotype does not necessitate that the direct role of New1 in the process is as a *bona fide* assem-

bly factor. A homologue of New1 and the bacterial ABCF translation factor EttA (55)—Uup—presents an analogous case: while overexpression of Uup suppresses both cold sensitivity and ribosome assembly in *E. coli* caused by knock-out of the translational GTPase BipA (14), it is unclear if Uup is an assembly factor or translation factor. The association of New1 with polysomal fractions (see Figure 2B and (23)) indicate that the effect on ribosome assembly is indirect and is caused by the perturbation of translation in the *new1Δ* strain. Our yeast genetics, cryo-EM and Ribo-Seq results collectively argue that New1, indeed, acts on mature ribosomes, and its loss affects translation termination/recycling, leading to ribosomal pile up in front of stop codons preceded by a lysine or arginine codon. The genes involved in protein biosynthesis display only a mild enrichment in C-terminal arginines and lysines compared to ORFs in general (23 versus 21%, Supplementary Figure S11B). However, the metagene of translation-associated genes displays a clear ribosome stalling pattern (Supplementary Figure S11C). We conclude that the ribosome assembly defect in the *new1Δ* strain could be a knock-on effect of the protein synthesis defect, although it is also possible that New1 is a dual-function factor that is involved both in protein synthesis and ribosome assembly, similarly to Rli1/ABCE1 (68,69), eIF5B/Fun12 (70,71) and eIF6/TIF6 (72). A dedicated follow-up study is necessary to test this hypothesis. The second proposed molecular function of New1 is mediated by its prion-like propensity to aggregate in *S. cerevisiae* (24). When overexpressed, New1 influences formation of the prion state of translation termination factor eEF3/Sup35—[PSI+]—and the effect is strictly dependent on New1's N-terminal Q/N rich region (25,73). Importantly, since the Q/N region is not universal for New1—the distribution of this region is limited to *Hemiascomycota* species (26)—prionogenesis is not a general feature of New1.

Here we demonstrate that New1 binds to ribosomes and plays a role in facilitating translation termination and/or ribosome recycling at stop codons preceded by a codon for the positively charged amino acids lysine or arginine. However, the mechanism by which New1 facilitates this process remains to be elucidated. At present, we can only speculate that binding of New1 to the ribosome in a position analogous to eEF3, exert its influence via the E-site, possibly by affecting the stability of the E-site tRNA and/or the conformation of the L1 stalk, however we also cannot rule out that New1 is involved in recruitment or dissociation of other auxiliary factors from the ribosome that directly influence the termination/recycling process. A systematic follow-up investigation is necessary to establish the connection between the termination / recycling defect caused by New1 loss.

DATA AVAILABILITY

Ribo-Seq and RNA-Seq sequencing data have been deposited in the ArrayExpress database at EMBL-EBI (www.ebi.ac.uk/arrayexpress) under accession number E-MTAB-7763. The cryo-EM maps of the New1–80S complex (including all individual multibody maps) and the associated molecular model have been deposited in the Protein Data

Bank and Electron Microscopy Data Bank with the accession codes 6S47 and EMD-10098, respectively.

SUPPLEMENTARY DATA

Supplementary Data are available at NAR Online.

ACKNOWLEDGEMENTS

We are grateful to Mridula Muppavarapu for help with polysome profiling, Roshani Payoe for constructing plasmid VHp123, Erik Johansson for providing yeast biomass, Akira Kaji for sharing anti-eEF3 antibodies, Jingdong Cheng for help with the initial New1 model, Susi Reider for grid preparation as well as Otto Berninghausen and Roland Beckmann for Spirit cryo-EM data collection. CIISB research infrastructure project LM2015043 funded by MEYS CR is gratefully acknowledged for the financial support of the measurements at the CF Cryo-electron Microscopy and Tomography CEITEC MU.

FUNDING

European Regional Development Fund through the Centre of Excellence for Molecular Cell Technology (to V.H.); Estonian Science Foundation Grants [PRG335 to V.H.]; Molecular Infection Medicine Sweden (MIMS) (to V.H.); Swedish Research council [2017-03783 to V.H., 2015-04746 to G.C.A., 2017-04663 to T.N.]; Ragnar Söderberg foundation (to V.H.); Kempestiftelsernas grants (JCK-1627 to G.C.A., SMK-1349 to V.H.); Magnus Bergvalls Foundation [2017-02098 to M.J.]; Åke Wibergs Foundation [M14-0207 to M.J.]; Deutsche Forschungsgemeinschaft [WI3285/8-1 to D.N.W.]; Horizon 2020 Programme of the European Union, iNEXT project [2643]; MEYS CR [LM2015043]. Funding for open access charge: Vetenskapsrådet [2017-03783 to V.H.].

Conflict of interest statement. None declared.

REFERENCES

- Rodnina, M.V. and Wintermeyer, W. (2016) Protein elongation, co-translational folding and targeting. *J. Mol. Biol.*, **428**, 2165–2185.
- Simonetti, A., Marzi, S., Jenner, L., Myasnikov, A., Romy, P., Yusupova, G., Klaholz, B.P. and Yusupov, M. (2009) A structural view of translation initiation in bacteria. *Cell Mol. Life Sci.*, **66**, 423–436.
- Hinnebusch, A.G. (2014) The scanning mechanism of eukaryotic translation initiation. *Annu. Rev. Biochem.*, **83**, 779–812.
- Dever, T.E. and Green, R. (2012) The elongation, termination, and recycling phases of translation in eukaryotes. *Cold Spring Harb. Perspect. Biol.*, **4**, a013706.
- Atkinson, G.C. (2015) The evolutionary and functional diversity of classical and lesser-known cytoplasmic and organellar translational GTPases across the tree of life. *BMC Genomics*, **16**, 78.
- Maracci, C. and Rodnina, M.V. (2016) Review: translational GTPases. *Biopolymers*, **105**, 463–475.
- Paytubi, S., Wang, X., Lam, Y.W., Izquierdo, L., Hunter, M.J., Jan, E., Hundal, H.S. and Proud, C.G. (2009) ABC50 promotes translation initiation in mammalian cells. *J. Biol. Chem.*, **284**, 24061–24073.
- Qu, L., Jiang, Y., Cheng, C., Wu, D., Meng, B., Chen, Z., Zhu, Y., Shaw, N., Ouyang, S. and Liu, Z.J. (2018) Crystal structure of ATP-bound human ABCF1 demonstrates a unique conformation of ABC proteins. *Structure*, **26**, 1259–1265.
- Andersen, C.B., Becker, T., Blau, M., Anand, M., Halic, M., Balar, B., Mielke, T., Boesen, T., Pedersen, J.S., Spahn, C.M. *et al.* (2006) Structure of eEF3 and the mechanism of transfer RNA release from the E-site. *Nature*, **443**, 663–668.
- Sandbaken, M.G., Lupisella, J.A., DiDomenico, B. and Chakraburty, K. (1990) Protein synthesis in yeast. Structural and functional analysis of the gene encoding elongation factor 3. *J. Biol. Chem.*, **265**, 15838–15844.
- Vazquez de Aldana, C.R., Marton, M.J. and Hinnebusch, A.G. (1995) GCN20, a novel ATP binding cassette protein, and GCN1 reside in a complex that mediates activation of the eIF-2 alpha kinase GCN2 in amino acid-starved cells. *EMBO J.*, **14**, 3184–3199.
- Ross-Smith, N., Tan, P., Belfield, G. and Tuite, M.F. (1995) Translational elongation factor 3 (EF-3): a study of its structural and functional divergence in fungi. *Biochem. Soc. Trans.*, **23**, 132S.
- Mateyak, M.K., Pupek, J.K., Garino, A.E., Knapp, M.C., Colmer, S.F., Kinzy, T.G. and Dunaway, S. (2018) Demonstration of translation elongation factor 3 activity from a non-fungal species, *Phytophthora infestans*. *PLoS One*, **13**, e0190524.
- Murina, V., Kasari, M., Takada, H., Hinnu, M., Saha, C.K., Grimshaw, J.W., Seki, T., Reith, M., Putrinš, M., Tenson, T. *et al.* (2018) ABCF ATPases involved in protein synthesis, ribosome assembly and antibiotic resistance: Structural and functional diversification across the tree of life. *J. Mol. Biol.*, doi:10.1016/j.jmb.2018.12.013.
- Hutchison, J.S., Feinberg, B., Rothwell, T.C. and Moldave, K. (1984) Monoclonal antibody specific for yeast elongation factor 3. *Biochemistry*, **23**, 3055–3063.
- Uritani, M. and Miyazaki, M. (1988) Role of yeast peptide elongation factor 3 (EF-3) at the AA-tRNA binding step. *J. Biochem.*, **104**, 118–126.
- Kurata, S., Nielsen, K.H., Mitchell, S.F., Lorsch, J.R., Kaji, A. and Kaji, H. (2010) Ribosome recycling step in yeast cytoplasmic protein synthesis is catalyzed by eEF3 and ATP. *PNAS*, **107**, 10854–10859.
- Kasari, V., Margus, T., Atkinson, G.C., Johansson, M.J.O. and Hauryliuk, V. (2019) Ribosome profiling analysis of eEF3-depleted *Saccharomyces cerevisiae*. *Sci. Rep.*, **9**, 3037.
- Triana-Alonso, F.J., Chakraburty, K. and Nierhaus, K.H. (1995) The elongation factor 3 unique in higher fungi and essential for protein biosynthesis is an E site factor. *J. Biol. Chem.*, **270**, 20473–20478.
- Decottignies, A. and Goffeau, A. (1997) Complete inventory of the yeast ABC proteins. *Nat. Genet.*, **15**, 137–145.
- Maurice, T.C., Mazzucco, C.E., Ramanathan, C.S., Ryan, B.M., Warr, G.A. and Puziss, J.W. (1998) A highly conserved intraspecies homolog of the *Saccharomyces cerevisiae* elongation factor-3 encoded by the HEF3 gene. *Yeast*, **14**, 1105–1113.
- Kellis, M., Birren, B.W. and Lander, E.S. (2004) Proof and evolutionary analysis of ancient genome duplication in the yeast *Saccharomyces cerevisiae*. *Nature*, **428**, 617–624.
- Li, Z., Lee, I., Moradi, E., Hung, N.J., Johnson, A.W. and Marcotte, E.M. (2009) Rational extension of the ribosome biogenesis pathway using network-guided genetics. *PLoS Biol.*, **7**, e1000213.
- Santoso, A., Chien, P., Osheroovich, L.Z. and Weissman, J.S. (2000) Molecular basis of a yeast prion species barrier. *Cell*, **100**, 277–288.
- Osheroovich, L.Z. and Weissman, J.S. (2001) Multiple Gln/Asn-rich prion domains confer susceptibility to induction of the yeast [PSI(+)] prion. *Cell*, **106**, 183–194.
- Harrison, L.B., Yu, Z., Stajich, J.E., Dietrich, F.S. and Harrison, P.M. (2007) Evolution of budding yeast prion-determinant sequences across diverse fungi. *J. Mol. Biol.*, **368**, 273–282.
- Siibak, T., Peil, L., Donhofer, A., Tats, A., Remm, M., Wilson, D.N., Tenson, T. and Remme, J. (2011) Antibiotic-induced ribosomal assembly defects result from changes in the synthesis of ribosomal proteins. *Mol. Microbiol.*, **80**, 54–67.
- Amberg, D.C., Burke, D. and Strathern, J.N. (2005) In: *Methods in Yeast Genetics: a Cold Spring Harbor Laboratory Course Manual*. CSHL Press, NY.
- Johansson, M.J. (2017) Determining if an mRNA is a substrate of nonsense-mediated mRNA decay in *Saccharomyces cerevisiae*. *Methods Mol. Biol.*, **1507**, 169–177.
- Longtine, M.S., McKenzie, A. 3rd, Demarini, D.J., Shah, N.G., Wach, A., Brachat, A., Philippsen, and Pringle, J.R. (1998) Additional modules for versatile and economical PCR-based gene deletion and modification in *Saccharomyces cerevisiae*. *Yeast*, **14**, 953–961.
- Ottoz, D.S., Rudolf, F. and Stelling, J. (2014) Inducible, tightly regulated and growth condition-independent transcription factor in *Saccharomyces cerevisiae*. *Nucleic Acids Res.*, **42**, e130.

32. Antoun, A., Pavlov, M.Y., Tenson, T. and Ehrenberg, M.M. (2004) Ribosome formation from subunits studied by stopped-flow and Rayleigh light scattering. *Biol. Proceed. Online*, **6**, 35–54.
33. Chilkova, O., Jonsson, B.H. and Johansson, E. (2003) The quaternary structure of DNA polymerase epsilon from *Saccharomyces cerevisiae*. *J. Biol. Chem.*, **278**, 14082–14086.
34. Grant, T. and Grigorieff, N. (2015) Measuring the optimal exposure for single particle cryo-EM using a 2.6 Å reconstruction of rotavirus VP6. *Elife*, **4**, e06980.
35. Zhang, K. (2016) Gctf: Real-time CTF determination and correction. *J. Struct. Biol.*, **193**, 1–12.
36. Kimanius, D., Forsberg, B.O., Scheres, S.H. and Lindahl, E. (2016) Accelerated cryo-EM structure determination with parallelisation using GPUs in RELION-2. *Elife*, **5**, e18722.
37. Zivanov, J., Nakane, T., Forsberg, B.O., Kimanius, D., Hagen, W.J., Lindahl, E. and Scheres, S.H. (2018) New tools for automated high-resolution cryo-EM structure determination in RELION-3. *Elife*, **7**, e42166.
38. Adams, P.D., Afonine, P.V., Bunkoczi, G., Chen, V.B., Davis, I.W., Echols, N., Headd, J.J., Hung, L.W., Kapral, G.J., Grosse-Kunstleve, R.W. *et al.* (2010) PHENIX: a comprehensive Python-based system for macromolecular structure solution. *Acta Crystallogr. Sect. D Biol. Crystallogr.*, **66**, 213–221.
39. Scheres, S.H. and Chen, S. (2012) Prevention of overfitting in cryo-EM structure determination. *Nat. Methods*, **9**, 853–854.
40. Bienert, S., Waterhouse, A., de Beer, T.A., Tauriello, G., Studer, G., Bordoli, L. and Schwede, T. (2017) The SWISS-MODEL repository—new features and functionality. *Nucleic Acids Res.*, **45**, D313–D319.
41. Pettersen, E.F., Goddard, T.D., Huang, C.C., Couch, G.S., Greenblatt, D.M., Meng, E.C. and Ferrin, T.E. (2004) UCSF Chimera—a visualization system for exploratory research and analysis. *J. Comput. Chem.*, **25**, 1605–1612.
42. Emsley, P. and Cowtan, K. (2004) Coot: model-building tools for molecular graphics. *Acta Crystallogr. Sect. D Biol. Crystallogr.*, **60**, 2126–2132.
43. Crowe-McAuliffe, C., Graf, M., Huter, P., Takada, H., Abdelshahid, M., Novacek, J., Murina, V., Atkinson, G.C., Haurlyuk, V. and Wilson, D.N. (2018) Structural basis for antibiotic resistance mediated by the *Bacillus subtilis* ABCF ATPase VmlR. *PNAS*, **115**, 8978–8983.
44. Brown, A., Long, F., Nicholls, R.A., Toots, J., Emsley, P. and Murshudov, G. (2015) Tools for macromolecular model building and refinement into electron cryo-microscopy reconstructions. *Acta Crystallogr. Sect. D Biol. Crystallogr.*, **71**, 136–153.
45. Chen, V.B., Arendall, W.B. 3rd, Headd, J.J., Keedy, D.A., Immormino, R.M., Kapral, G.J., Murray, L.W., Richardson, J.S. and Richardson, D.C. (2010) MolProbity: all-atom structure validation for macromolecular crystallography. *Acta Crystallogr. Sect. D Biol. Crystallogr.*, **66**, 12–21.
46. Goddard, T.D., Huang, C.C., Meng, E.C., Pettersen, E.F., Couch, G.S., Morris, J.H. and Ferrin, T.E. (2018) UCSF ChimeraX: Meeting modern challenges in visualization and analysis. *Protein Sci.*, **27**, 14–25.
47. Andrews, S. (2010) FastQC: a quality control tool for high throughput sequence data. <https://www.bioinformatics.babraham.ac.uk/projects/fastqc/>.
48. Martin, M. (2011) Cutadapt removes adapter sequences from high-throughput sequencing reads. *EMBnet. J.*, **17**, 10–12.
49. Pertea, M., Kim, D., Pertea, G.M., Leek, J.T. and Salzberg, S.L. (2016) Transcript-level expression analysis of RNA-seq experiments with HISAT, StringTie and Ballgown. *Nat. Protoc.*, **11**, 1650–1667.
50. Anders, S., Pyl, P.T. and Huber, W. (2015) HTSeq—a Python framework to work with high-throughput sequencing data. *Bioinformatics*, **31**, 166–169.
51. Love, M.I., Huber, W. and Anders, S. (2014) Moderated estimation of fold change and dispersion for RNA-seq data with DESeq2. *Genome Biol.*, **15**, 550.
52. Ashburner, M., Ball, C.A., Blake, J.A., Botstein, D., Butler, H., Cherry, J.M., Davis, A.P., Dolinski, K., Dwight, S.S., Eppig, J.T. *et al.* (2000) Gene ontology: tool for the unification of biology. The Gene Ontology Consortium. *Nat. Genet.*, **25**, 25–29.
53. Mi, H., Huang, X., Muruganujan, A., Tang, H., Mills, C., Kang, D. and Thomas, P.D. (2017) PANTHER version 11: expanded annotation data from Gene Ontology and Reactome pathways, and data analysis tool enhancements. *Nucleic Acids Res.*, **45**, D183–D189.
54. Mumberg, D., Muller, R. and Funk, M. (1994) Regulatable promoters of *Saccharomyces cerevisiae*: comparison of transcriptional activity and their use for heterologous expression. *Nucleic Acids Res.*, **22**, 5767–5768.
55. Böel, G., Smith, P.C., Ning, W., Englander, M.T., Chen, B., Hashem, Y., Testa, A.J., Fischer, J.J., Wieden, H.J., Frank, J. *et al.* (2014) The ABC-F protein EttA gates ribosome entry into the translation elongation cycle. *Nat. Struct. Mol. Biol.*, **21**, 143–151.
56. Rigaut, G., Shevchenko, A., Rutz, B., Wilm, M., Mann, M. and Seraphin, B. (1999) A generic protein purification method for protein complex characterization and proteome exploration. *Nat. Biotechnol.*, **17**, 1030–1032.
57. Heuer, A., Gerovac, M., Schmidt, C., Trowitzsch, S., Preis, A., Kotter, P., Berninghausen, O., Becker, T., Beckmann, R. and Tampe, R. (2017) Structure of the 40S-ABCE1 post-splitting complex in ribosome recycling and translation initiation. *Nat. Struct. Mol. Biol.*, **24**, 453–460.
58. Karcher, A., Schele, A. and Hopfner, K.P. (2008) X-ray structure of the complete ABC enzyme ABCE1 from *Pyrococcus abyssi*. *J. Biol. Chem.*, **283**, 7962–7971.
59. Ingolia, N.T., Hussmann, J.A. and Weissman, J.S. (2018) Ribosome profiling: global views of translation. *Cold Spring Harb. Perspect. Biol.*, **11**, a032698.
60. Wu, C.C., Zinshteyn, B., Wehner, K.A. and Green, R. (2019) High-Resolution ribosome profiling defines discrete ribosome elongation states and translational regulation during cellular stress. *Mol. Cell*, **73**, 959–970.
61. Lareau, L.F., Hite, D.H., Hogan, G.J. and Brown, P.O. (2014) Distinct stages of the translation elongation cycle revealed by sequencing ribosome-protected mRNA fragments. *Elife*, **3**, e01257.
62. Schuller, A.P., Wu, C.C., Dever, T.E., Buskirk, A.R. and Green, R. (2017) eIF5A functions globally in translation elongation and termination. *Mol. Cell*, **66**, 194–205.
63. Young, D.J., Gudyosh, N.R., Zhang, F., Hinnebusch, A.G. and Green, R. (2015) Rli1/ABCE1 recycles terminating ribosomes and controls translation reinitiation in 3'UTRs in vivo. *Cell*, **162**, 872–884.
64. Baudin-Baillieu, A., Legendre, R., Kuchly, C., Hatin, I., Demais, S., Mestdagh, C., Gautheret, D. and Namy, O. (2014) Genome-wide translational changes induced by the prion [PSI⁺]. *Cell Rep.*, **8**, 439–448.
65. Susorov, D., Mikhailova, T., Ivanov, A., Sokolova, E. and Alkalaeva, E. (2015) Stabilization of eukaryotic ribosomal termination complexes by deacylated tRNA. *Nucleic Acids Res.*, **43**, 3332–3343.
66. Keeling, K.M., Lanier, J., Du, M., Salas-Marco, J., Gao, L., Kaenjak-Angeletti, A. and Bedwell, D.M. (2004) Leaky termination at premature stop codons antagonizes nonsense-mediated mRNA decay in *S. cerevisiae*. *RNA*, **10**, 691–703.
67. O'Shea, J.P., Chou, M.F., Quader, S.A., Ryan, J.K., Church, G.M. and Schwartz, D. (2013) pLogo: a probabilistic approach to visualizing sequence motifs. *Nat. Methods*, **10**, 1211–1212.
68. Kispal, G., Sipos, K., Lange, H., Fekete, Z., Bedekovics, T., Janaky, T., Bassler, J., Aguilar Netz, D.J., Balk, J., Rotte, C. *et al.* (2005) Biogenesis of cytosolic ribosomes requires the essential iron-sulphur protein Rli1p and mitochondria. *EMBO J.*, **24**, 589–598.
69. Pisarev, A.V., Skabkin, M.A., Pisareva, V.P., Skabkina, O.V., Rakotondrafara, A.M., Hentze, M.W., Hellen, C.U. and Pestova, T.V. (2010) The role of ABCE1 in eukaryotic posttermination ribosomal recycling. *Mol. Cell*, **37**, 196–210.
70. Lebaron, S., Schneider, C., van Nues, R.W., Swiatkowska, A., Walsh, D., Botcher, B., Granneman, S., Watkins, N.J. and Tollervey, D. (2012) Proofreading of pre-40S ribosome maturation by a translation initiation factor and 60S subunits. *Nat. Struct. Mol. Biol.*, **19**, 744–753.
71. Pestova, T.V., Lomakin, I.B., Lee, J.H., Choi, S.K., Dever, T.E. and Hellen, C.U. (2000) The joining of ribosomal subunits in eukaryotes requires eIF5B. *Nature*, **403**, 332–335.
72. Miluzio, A., Beugnet, A., Volta, V. and Biffo, S. (2009) Eukaryotic initiation factor 6 mediates a continuum between 60S ribosome biogenesis and translation. *EMBO Rep.*, **10**, 459–465.
73. Inoue, Y., Kawai-Noma, S., Koike-Takeshita, A., Taguchi, H. and Yoshida, M. (2011) Yeast prion protein New1 can break Sup35

- amyloid fibrils into fragments in an ATP-dependent manner. *Genes Cells*, **16**, 545–556.
74. Boeke, J.D., LaCroute, F. and Fink, G.R. (1984) A positive selection for mutants lacking orotidine-5'-phosphate decarboxylase activity in yeast: 5-fluoro-orotic acid resistance. *Mol. Gen. Genet.*, **197**, 345–346.
75. Brachmann, C.B., Davies, A., Cost, G.J., Caputo, E., Li, J., Hieter, P. and Boeke, J.D. (1998) Designer deletion strains derived from *Saccharomyces cerevisiae* S288C: a useful set of strains and plasmids for PCR-mediated gene disruption and other applications. *Yeast*, **14**, 115–132.
76. Ghaemmaghami, S., Huh, W.K., Bower, K., Howson, R.W., Belle, A., Dephoure, N., O'Shea, E.K. and Weissman, J.S. (2003) Global analysis of protein expression in yeast. *Nature*, **425**, 737–741.
77. Puig, O., Caspary, F., Rigaut, G., Rutz, B., Bouveret, E., Bragado-Nilsson, E., Wilm, M. and Seraphin, B. (2001) The tandem affinity purification (TAP) method: a general procedure of protein complex purification. *Methods*, **24**, 218–229.
78. Sikorski, R.S. and Hieter, P. (1989) A system of shuttle vectors and yeast host strains designed for efficient manipulation of DNA in *Saccharomyces cerevisiae*. *Genetics*, **122**, 19–27.
79. Christianson, T.W., Sikorski, R.S., Dante, M., Shero, J.H. and Hieter, P. (1992) Multifunctional yeast high-copy-number shuttle vectors. *Gene*, **110**, 119–122.

SUPPLEMENTARY ONLINE MATERIALS

for

A role for the *Saccharomyces cerevisiae* ABCF protein New1 in translation termination/recycling

Villu Kasari^{1,2,†}, Agnieszka A. Pochopien^{3,†}, Tõnu Margus^{1,2}, Victoriia Murina^{1,2}, Kathryn Turnbull^{1,2}, Yang Zhou¹, Tracy Nissan^{4,5}, Michael Graf³, Jiří Nováček⁶, Gemma C. Atkinson¹, Marcus J.O. Johansson¹, Daniel N. Wilson^{3,*}, Vasili Hauryliuk^{1,2,7,*}

¹Department of Molecular Biology, Umeå University, Building 6K, 6L University Hospital Area, 90187 Umeå, Sweden

²Laboratory for Molecular Infection Medicine Sweden (MIMS), Umeå University, Building 6K and 6L, University Hospital Area, 90187 Umeå, Sweden

³Institute for Biochemistry and Molecular Biology, University of Hamburg, Martin-Luther-King-Platz 6, 20146 Hamburg, Germany

⁴Department of Molecular Biosciences, The Wenner-Gren Institute, Stockholm University, Stockholm, 10691, Sweden

⁵School of Life Science, University of Sussex, Brighton, BN19RH, United Kingdom

⁶Central European Institute of Technology (CEITEC), Masaryk University, Kamenice 5, 62500 Brno, Czech Republic.

⁷University of Tartu, Institute of Technology, 50411 Tartu, Estonia

† these authors contributed equally

* to whom correspondence should be addressed:

Vasili Hauryliuk: vasili.hauryliuk@umu.se, +46 907 850 807

Marcus J.O. Johansson: marcus.johansson@umu.se, +46 7856 767

Daniel N. Wilson: Daniel.wilson@chemie.uni-hamburg.de, +49 40 42838 2841

Supplementary methods

Plasmid construction

Low and high copy plasmids harbouring the *YEF3* gene (pRS315-*YEF3* and pRS426-*YEF3*) were constructed by cloning a *SacI/BamHI* *YEF3* DNA fragment from pRS316-*YEF3* (1) into the corresponding sites of pRS315 and pRS426, respectively (2,3). To construct low and high copy *URA3* plasmids carrying the *NEW1* gene (pRS316-*NEW1* and pRS426-*NEW1*), we cloned an *EcoRI/XhoI* *NEW1* DNA fragment, PCR-amplified from BY4741 using oMJ485 and oMJ486, into the corresponding sites of pRS316 and pRS426 (2,3). Low and high copy *LEU2* plasmids harbouring the *NEW1* gene (pRS315-*NEW1* and pRS425-*NEW1*) were constructed by cloning a *SacI/XhoI* *NEW1* DNA fragment from pRS426-*NEW1* into the *SacI/Sall* (pRS315) or *SacI/XhoI* (pRS425) sites of the respective vector.

The construction of a plasmid in which *NEW1* is under control of the *TDH3* promoter (P_{TDH3}) involved assembly of three DNA fragments. A *NEW1* DNA fragment that lacks the sequence for the promoter and 5'-UTR was PCR amplified from pRS426-*NEW1* using primers V47 and V45. A P_{TDH3} DNA fragment was PCR amplified from genomic BY4741 DNA using primers V42 and V46, and the pRS425 backbone was amplified using primers V40 and V41. The three PCR fragments were assembled into VHp327 (pRS425- P_{TDH3} -*NEW1*) using NEBuilder® HiFi DNA Assembly Master Mix (New England Biolabs).

Construction of *NEW1* $_{\Delta Q/N}$ expression plasmid for protein purification from *E. coli*. Codons 141-1197 of the yeast *NEW1* coding sequence (NCBI Gene ID: 855875) were optimised for *E. coli* K12 expression using IDT Codon optimisation tool <https://eu.idtdna.com/CodonOpt>. The optimised DNA sequence (Ecol-New1 $_{\Delta Q/N}$) was ordered as two synthetic gene blocks (gBlocks) from Integrated DNA Technologies. The pET19b vector was linearised by *NcoI* and *BamHI* double digestion. The linear vector and the two gBlocks were assembled using NEBuilder® HiFi DNA Assembly Master Mix (New England Biolabs). The sequence for the catalytic glutamic acid (E) codons in both ABC ATPase domains of *NEW1* (E713 and E1058) was changed to glutamine (Q) codons to generate the VHp123 construct.

The β -estradiol-inducible *NEW1*-TAP construct used for the LexA-ER-B112 expression system was assembled from four different DNA fragments. First, the backbone of pRS316 (2) was PCR amplified using primers V62 and V63. Second, the insulator-(lexA-box)₄-PminCYC1 DNA fragment was PCR amplified from FRP1642 (4) using primers V64 and V65. Third, the *NEW1* ORF was PCR amplified from genomic DNA of BY4741 using primers V67 and V70. Fourth, the sequence for the TAP-tag was PCR amplified from pBS1539 (5) using primers V72 and V73 of which the latter primer introduces the sequence for the T_{synth8} transcriptional terminator (6). Finally, the plasmid (VHp262) was assembled from the four DNA fragments using NEBuilder® HiFi DNA Assembly Master Mix (New England Biolabs). The sequence for the catalytic glutamic acid (E) codon in one or both of the ABC ATPase domains of *NEW1* was subsequently mutated in VHp262 to a glutamine (Q) codon by the Protein Expertise Platform (Umeå University), generating plasmids VHp257, VHp258 and VHp265.

Dual luciferase reporter plasmids used to assay termination readthrough of biologically significant genes, displaying increased waviness metrics and 3' UTR occupancy in a *new1* Δ background were based upon pDB722 (7). Initially, site directed mutagenesis was used to mutate out the *BamHI*

site upstream of the Renilla luciferase gene in pDB722 using primer KT80. This then allowed for replacement of the original pDB722 reporter cassette with cassettes of interest via insertion into the Sall and BamHI cloning sites flanking the cassette. Staggered, complimentary primer pairs KT18/19, KT22/23, KT24/25 and KT28/29 were annealed to yield dsDNA fragments YDR099W(TAA), YNL247W(TAG), YDR099W(CAA) and YNL247W(CAG), respectively, that each possessed Sall and BamHI sticky ends. Fragments were then cloned into the modified pDB722 vector resulting in VHp603, VHp604, VHp605 and VHp606 respectively. Each readthrough cassette was designed to contain the four codons immediately upstream and the two successive codon downstream of the native stop codon, or, to include the equivalent non-stop codon (TAA-CAA or TAG-CAG).

Growth assays

To assess the effects of New1-TAP, New1^{E713Q}-TAP, New1^{E1058Q}-TAP and New1^{EQ2}-TAP expression on cell growth, the VHY61 strain carrying either pRS316, VHp262, VHp257, VHp258, or VHp265 was grown overnight at 30°C in SC-ura medium, diluted to OD₆₀₀ ≈ 0.05 in the same medium and grown for three hours at 30°C. A 15 mL aliquot of each culture was transferred to a pre-warmed flask and β-estradiol was added to a final concentration of 1 μM. The growth of the both uninduced and induced cultures was monitored by hourly OD₆₀₀ measurements.

Estimation of the relative 3' UTR coverage and dual-luciferase assays

The log₂ ratio of Ribo-Seq footprint densities in the 3' UTR to that in the respective ORFs was used to estimate *the relative 3' UTR coverage*. The 3' UTR coverage was calculated for the 30 nucleotides (nt) following the stop codon, and the ORF coverage was calculated by excluding 60 nt from both 3' and 5' ends and using only genes 150 nt long or longer. Only reads that aligned once were used and genes with multiexon structure were excluded.

Readthrough assays were performed using the dual-luciferase reporter assay system (E1910, Promega) and a GloMax 20/20 luminometer (Promega). The wild type (VKY9) and *new1Δ* (MJY945) strains carrying either pDB722 (CAA C) or pDB723 (UAA C) (7) were grown overnight in SC-ura medium at 20°C or 30°C, diluted to OD₆₀₀ ≈ 0.05 in the same medium and grown until OD₆₀₀ ≈ 0.5 at the respective temperature. 5 μL aliquots (in technical triplicates) from the cultures were assayed as previously described (8). The experiment was repeated three times at each temperature using independent transformants for each experiment.

Supplementary results

Interaction of New1 with the 80S ribosome

The HEAT domain of New1 contains eight HEAT repeats composed of 16 α -helices (α 1- α 16) linked by 8 short loops (loops 1-8). Although the N-terminal region of the HEAT domain consisting of the first two HEAT repeats (α 1- α 4) of New1 is not well-resolved (**Supplementary Figure S3D-N**), the mode of interaction is likely to utilize positively charged residues, such as Lys195 (loop 2) or Lys239 (loop 3), which come into close proximity to the tip of ES9 (**Supplementary Figure S8A**). By contrast, the remaining HEAT repeats are nicely resolved, revealing a network of interactions between the loop residues and components of the SSU. Briefly, within loop 4, Lys280 interacts with the backbone of nucleotides 1359-1363 of ES9 (**Supplementary Figure S8A**) and the backbone carbonyl of Ala279 of New1 is within hydrogen-bonding distance of Arg134 of eS19 (**Supplementary Figure S8B**). In loop 5, T-shaped stacking interaction is observed from the sidechain of Phe321 of New1 with Phe21 of eS19, and the backbone carbonyl of Thr319 of New1 is within hydrogen bonding distance of Arg24 of eS19 (**Supplementary Figure S8B**). Residues (Gln357-Pro359) within loop 6 also approach eS19 with vicinity of Arg24, whereas HEAT repeat loops 7 and 8 of New1 are oriented towards with uS13, where hydrogen bond interactions are possible between Gln401 (loop 7) with the backbone carbonyl of Lys49 of uS13 and in loop 8 between Ser443 and Arg448 with Lys49 and His78, respectively, of uS13 (**Supplementary Figure S8B-C**).

The ABC2 domain of New1 bridges the intersubunit space by forming protein-protein interactions with uS13 on the SSU and uL5 on the LSU. Interactions with the SSU are possible between the sidechains of Gln63 and Glu67 in uS13 which are in hydrogen bond distance with the backbone carbonyls of Leu1006 and Pro1008, respectively (**Supplementary Figure S8D**). Contacts between ABC2 and uL5 are more extensive and involve multiple sidechains located within α -helix (residues 984-1003) of ABC2, including Arg998, Glu999, Tyr1003 and Arg1004, as well as interaction between Lys115 of uL5 with the backbone of Arg1004 of ABC2 (**Supplementary Figure S8D**). In addition, ABC2 interacts with backbone of nucleotides 31-33 of the 5S rRNA, including a potential hydrogen bond between Arg809 and phosphate-oxygen of U33 (**Supplementary Figure S8D**). Arg809 can also form hydrogen bonds with the sidechain of Asp214 of uL18 and backbone interactions are possible between amine of Ala810 and the carbonyl of Asp214 (**Supplementary Figure S8D**).

Interactions are also observed at the base of the CD of New1 with the 5S rRNA and uL5. The loop between β 2- and β 3-strands of the CD contains three Lys residues (Lys 952, Lys954 and Lys955), which are well-resolved and interact with major groove of the stem-loop created by nucleotides 34-40 of the 5S rRNA (**Supplementary Figure S8E**). In addition, potential hydrogen bonding is possible from Gln951 of the CD of New1 with Glu38 and Thr44 of uL5.

Supplementary Table S1. Oligonucleotides and synthetic dsDNA blocks used in this study.

Name	Sequence 5'-3'
Oligonucleotides	
V40	CTGAACTGCCTCGAGGTTAACTGTGGGAATACTCAGGTATCGTAAG
V41	TCTTTGAAATGGCAGACGGTTATCCACAGAATCAGGG
V42	TCTGTGGATAACCGTCTGCCATTTCAAAGAATACGTAAATAATTAATAGTAGTGATTTT
V43	CAAAAATTGAGAGATCATTTTTGTTTGTATGTGTGTTTATTCGAAACTAAGTTCT
V44	CATAAACAAACAAAATGATCTCTCAATTTTTGTCAAAGATACCTGAATGT
V45	ATTCCCACAGTTAACCTCGAGGCAGTTCAGGAG
V46	CTTCTTTGGAGGCATTTTTGTTTGTATGTGTGTTTATTCGAAACTAAGTTCT
V47	CATAAACAAACAAAATGCCTCCAAAGAAGTTTAAGGATCTAAAC
V62	ATGTAGGAATAAAGAGTATCATCTTTCAAACGGTTATCCACAGAATCAG
V63	CAGGTTTATATATTATTGCGGCCGCACTACCGCAGGGTAATAACTGAT
V64	TAGTGCGGCCGCAATAATA
V65	AGAAGTATAGTAATTTATGCTGCAAAGG
V67	GACCTTTGCAGCATAAATTACTATACTTCTAAAAATGCCTCCAAAGAAGTTTAAGG
V70	GAAATCTTTTTCCATCTTCTTTTTCCATATCTTCTTCATCGTCAGTATCAAC
V72	ATGGAAAAGAGAAGATGGAAAAGAATTTTCATAGCCG
V73	TTTCAAAGATGATACTCTTATTCTACATAAGTAAATGAGTTTATATATCAGGTTGACT TCCCCGCG
oMJ485	TTTTGAATTCACGCCAAATTTTCGCTTTCTC
oMJ486	TTTTCTCGAGGCAGTTCAGGAGTTATTTTTGGT
oMJ489	ACTGTAAATACAACGACAATCAGTGCTAATTCAACTCAGGCGGATCCCCGGGTTAATT AA
oMJ490	AAACGAAGTTAGCGAAGATAAAACACTAGCCAGTAGGCTTGAATTCGAGCTCGTTTAA AC
KT18	TCGACGGAACCAACCAATAAGAGCGCG
KT19	GATCCGCGCTCTTATTTGGTTGGTTCCG
KT22	TCGACGGGTGAAGACAAATAGAATACTG
KT23	GATCCAGTATTCTATTTGTCTTCACCCG
KT24	TCGACGGAACCAACCAACAAGAGCGCG
KT25	GATCCGCGCTCTTGTGGTTGGTTCCG
KT28	TCGACGGGTGAAGACAAACAGAATACTG
KT29	GATCCAGTATTCTGTTTGTCTTCACCCG
KT80	CAAATATACCTCGAGCAAGGAACCATGACTTCGAAAGTTT

Synthetic dsDNA blocks (gBlocks®)

NEW1 gBlock1

AAGAAGGAGATATACCATGGGCCACCATCACCATCATCACGGTTCTGGTATCAGCCAG
TTTTTGAGTAAAATCCCGGAGTGCCAATCCATCACAGACTGCAAAAACCAAATCAAATT

GATTATCGAGGAGTTCGGCAAGGAAGGGAAGCTCGACCGGGGAAAAAATTGAAGAATG
GAAGATTGTAGATGTGCTTTCAAAGTTTATCAAGCCTAAAAATCCTTCCTTAGTACGTG
AATCAGCGATGTTAATCATCTCAAACATTGCACAGTTCTTTAGTGGTAAACCTCCTCAA
GAGGCCTATCTTTTACCGTTCTTTAACGTTGCCCTTGATTGCATTAGCGACAAGGAGAA
TACGGTCAAACGTGCCGCTCAGCATGCCATTGATTCTCTGCTGAACTGTTTTCTATG
GAAGCTTTGACATGTTTCGTCTGCCAACGATCTTGGACTACCTTTTCGTCGGGCGCAA
AATGGCAAGCAAAGATGGCCGCTCTTTCCGTAGTGGACCGCATCCGCGAGGACAGTG
CAAATGACCTTTTGGAGCTTACTTTCAAAGATGCTGTACCAGTCCTTACTGATGTTGCT
ACAGATTTTAAGCCGGAGCTGGCAAACAAGGCTATAAACTTTGCTTGACTACGTTT
CTATCTTAGACAATTTGGACCTGAGTCCTCGTTATAAGTTAATCGTCGATACTCTTCAA
GACCCATCAAAGTCCCGGAATCAGTGAAGAGTCTGTCTTCGGTCACCTTTGTCCGG
AAGTGAAGTGAAGCGTCTTTGTGCTTTTGGTGCCAATTCTTAACCGCAGCTTAAACCT
GTCTAGTAGTTCTCAAGAGCAATTACGTCAAACAGTGATTGTGGTGCAGAACCTGACC
CGTCTGGTCAACAATCGCAACGAAATTGAGTCTTTTATCCCTTTGTTGTTGCCAGGTAT
CCAGAAAGTGGTCGATACAGCTTCACTGCCTGAGGTGCGTGAATTGGCTGAAAAAGC
ATTGAACGTCTTAAAGGAGGATGACGAGGCAGACAAAGAGAACAATTCTCGGGGCG
TCTGACCCTGGAAGAAGGGCGCGACTTTTTGCTTGACCATCTGAAAGATATCAAGGCT
GATGACTCTTGTTTTGTAAAGCCGTACATGAATGATGAAACAGTTATTAATATATGTC
GAAGATCCTGACAGTTGACTCTAACGTGAATGATTGGAAACGCTTGGAAAGATTTTCTG
ACGGCAGTCTTTGGGGGGTCAAGTCCCAACGTGAGTTCGTTAAACAGGATTTTCATCC
ACAACCTGCGCGCTTTGTTCTATCAGGAGAAAGAACGTGCGGATGAGGACGAGGGTA
TTGAAATCGTGAATACCGATTTTTCACTGGCGTATGGCAGTCGCATGTTGCTGAACAA
GACAACTTGCGCCTTCTTAAGGGGCACCGCTATGGGCTGTGCGGCCGTAATGGTGC
GGGTAAGTCGACCCTGATGCGTGCT

NEW1 gBlock2

GGTGCGGGTAAGTCGACCCTGATGCGTGCTATCGCCAACGGACAACCTGGATGGTTTT
CCAGACAAAGATACTTTGCGTACCTGTTTCGTGGAACATAAGCTGCAGGGCGAAGAA
GGAGACTTAGACCTGGTATCCTTTATTGCACTTGACGAAGAGTTGCAGTCCACAAGCC
GCGAAGAAATCGCAGCTGCACTTGAATCTGTGGGCTTCGACGAAGAGCGTCGCGCGC
AGACGGTCGGCTCATTGTCTGGCGGCTGGAAGATGAAATTGGAGCTTGCAGCGCGCTA
TGCTTCAAAGGCAGACATTTTACTGTTGGACGAACCGACAAATCACCTTGACGTATC
CAACGTAAAGTGGCTTGAGGAATACTTGTGGAACACACGGACATCACGTCATTGATT
GTCAGCCATGACAGTGGCTTTTTGGACACGGTATGCACAGATATTATCACTATGAAA
ATAAAAAATTGGCTTATTACAAAGGGAATTTAGCAGCGTTTGTAGAACAAAAACCTGAA
GCCAAGTCCTACTATACTTTGACCGACAGCAACGCGCAGATGCGTTTTCCCTCCTCCGG
GTATCCTGACGGGCGTTAAGTCTAATACCGCGCCGTGGCCAAATGACCGATGTCA
CGTTTTCTTACCCTGGAGCCCAGAAGCCGTCTCTTAGCCATGTGTCCTGCTCATTGTC
CTTGTCGTCCCGTGTAGCATGTCTTGACCGAATGGTGCAGGAAAATCCACTTTAATC
AAGTTGCTGACGGGGGAGCTGGTGCCGAACGAAGGCAAAGTCGAAAAACATCCGAAT
TTGCGTATTGGTTACATCGCGCAGCATGCCTTACAGCATGTCAATGAGCATAAAGAGA

AAACAGCTAATCAATACCTGCAATGGCGTTATCAATTCGGGGACGACCGCGAAGTGTT
GTTGAAGGAATCCCGTAAGATCTCGGAAGATGAGAAAGAGATGATGACAAAGGAAATT
GACATTGACGATGGGCGTGGAAAGCGCGCCATCGAGGCCATTGTAGGCCGCCAGAA
ACTTAAAAGAGCTTTCAGTACGAAGTAAAGTGGAAATATTGGAAGCCAAAATACAACA
GTTGGGTACCGAAGGACGTCCTTGTTGAGCACGGCTTCGAAAAGCTGGTTCAAAAATT
CGATGATCACGAGGCTAGTCGCGAGGGATTGGGATACCGCGAGCTTATTCCGAGCGT
TATTACAAAACACTTTGAAGATGTAGGATTGGATAGTGAGATCGCGAACCACACCCCT
CTGGGGTCACTTTCAGGGGGTCAACTTGTAAGGTCGTGATTGCCGGGGCAATGTGG
AATAACCCACACCTTCTTGTTCTTGACGAGCCGACTAACTATTTGGATCGCGACTCCCT
TGGGGCTTTAGCCGTGGCTATTCGTGATTGGTCCGGAGGCGTGGTTATGATTTGCA
CAATAATGAGTTCGTGGGGGCGTTATGCCCTGAACAGTGGATCGTGGAGAATGGGAA
AATGGTACAAAAGGAAGCGCTCAAGTCGATCAATCTAAGTTTGAAGACGGGGGGAA
CGCCGATGCTGTCGGATTGAAAGCCTCCAATCTTGCCAAGCCGAGCGTTGACGATGA
TGATAGTCCTGCCAATATTAAGGTCAAGCAACGTAAGAAACGTCTTACTCGTAATGAAA
AAAAATTGCAAGCTGAGCGTCGTCTTTCGTTACATCGAGTGGTTGTCATCCCCGAA
AGGAACACCGAAACCTGTGGACACTGACGACGAAGAAGACTGATAAGGATCCGGCTG
CTAACAAAGCCCGAAAG

Supplementary Table S2. Cryo-EM data collection, refinement and validation statistics of the New1-80S complex (EMDB ID: XXXX, PDB ID: XXXX)

Data collection

Microscope	FEI Titan Krios
Camera	Falcon II
Magnification	131,703
Voltage (kV)	300
Electron dose (e ⁻ /Å ²)	45.9
Defocus range (μm)	-0.5 to -2.5
Pixel size (Å)	1.063
Initial particles (no.)	171,106
Final particles (no.)	48,757

Model composition

Protein residues	12,065
RNA bases	5,105

Refinement

Resolution range (Å)	3.28
Map CC (around atoms)	0.81
Map CC (whole unit cell)	0.80
Map sharpening <i>B</i> factor (Å ²)	-83.92
R.m.s. deviations	
Bond lengths (Å)	0.0079
Bond angles (°)	0.83

Validation

MolProbity score	1.88
Clashscore	4.95
Poor rotamers (%)	1.32

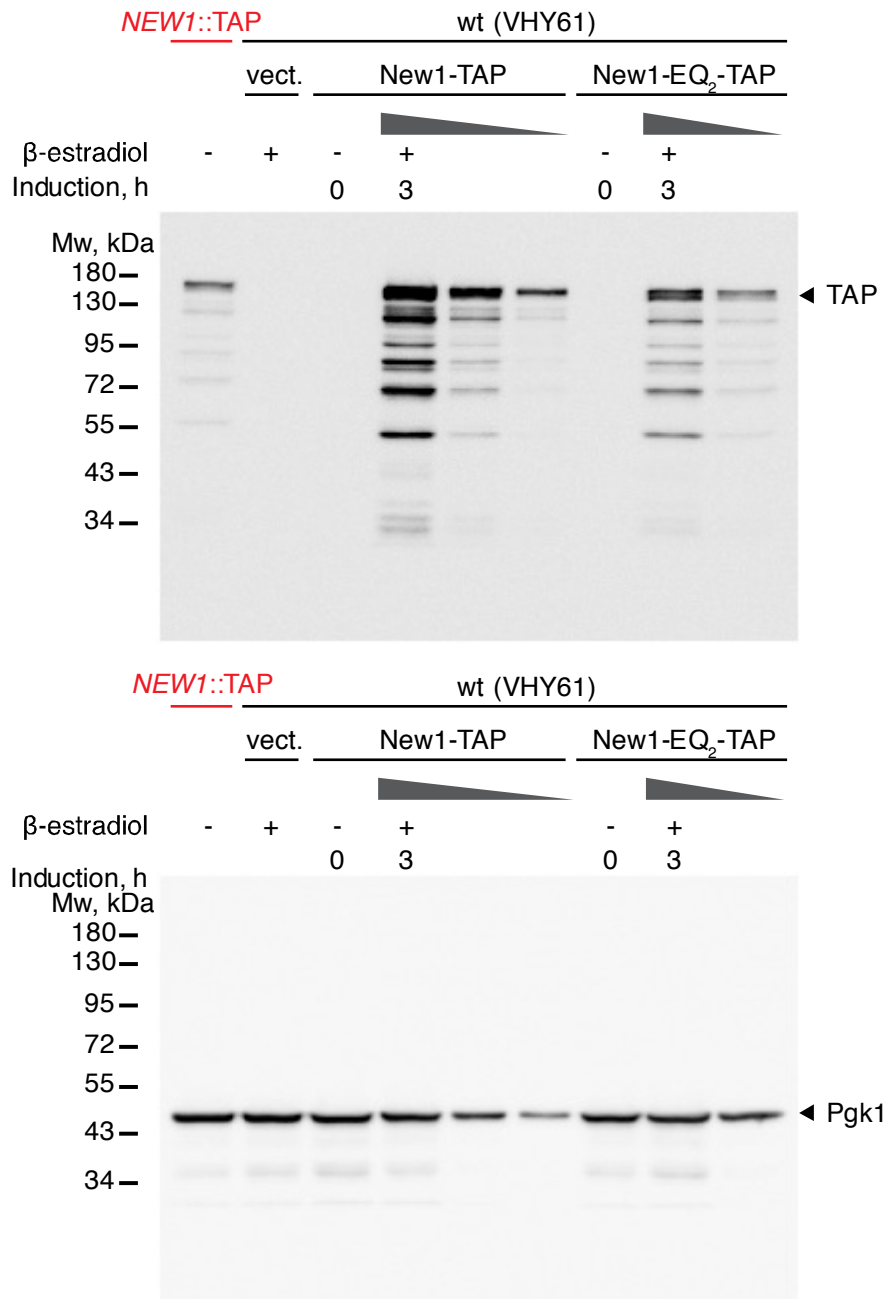
Ramachandran plot

Favored (%)	90.79
Allowed (%)	8.53
Disallowed (%)	0.68

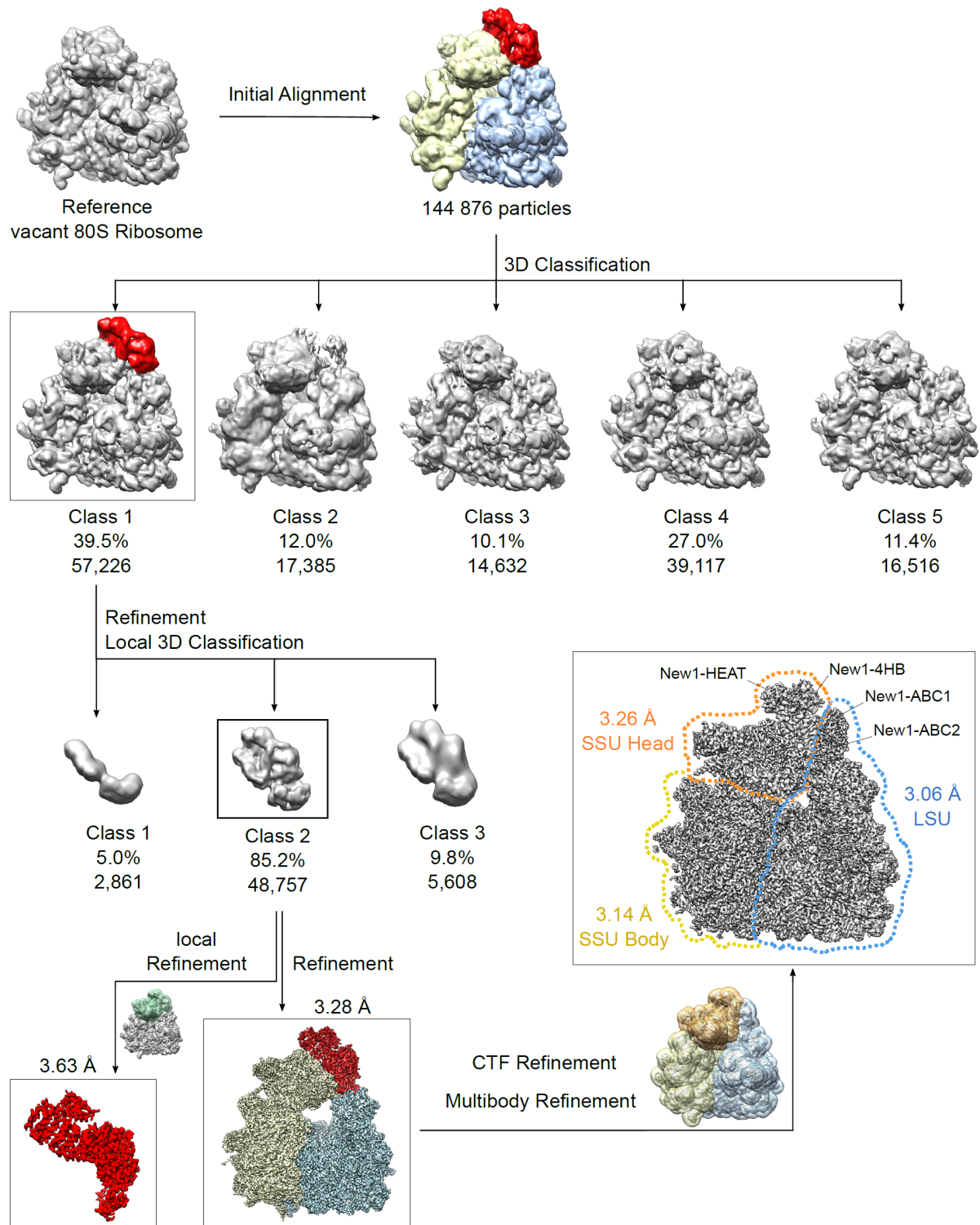
Supplementary Table S3. Generation times of indicated wild-type and *new1Δ* strains.

Strain	Generation time (h) ^a	
	20°C	30°C
wt (VKY9)	3.15 ± 0.20	1.57 ± 0.01
<i>new1Δ::HIS3MX6</i> (MJY945)	4.62 ± 0.41	1.72 ± 0.11
wt (MJY1171)	3.10 ± 0.10	1.55 ± 0.01
<i>new1Δ::kanMX6</i> (MJY1173)	4.40 ± 0.07	1.72 ± 0.01

^a Growth rates were determined in SC medium. The values represent the mean from three independent experiments and their standard deviations.

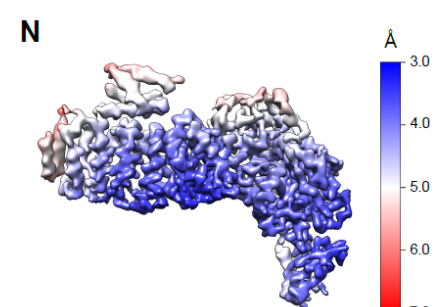
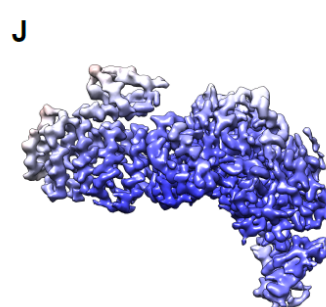
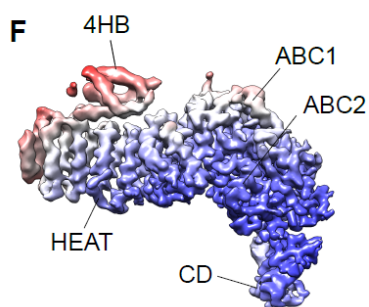
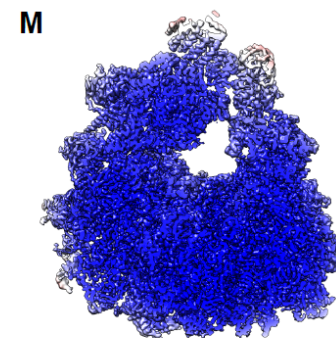
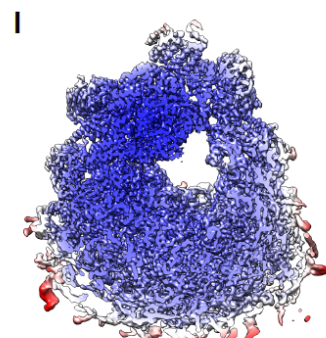
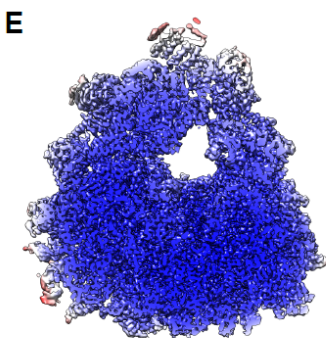
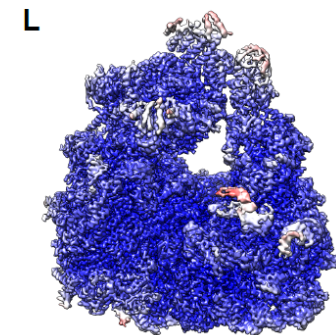
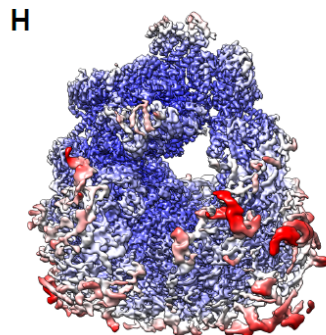
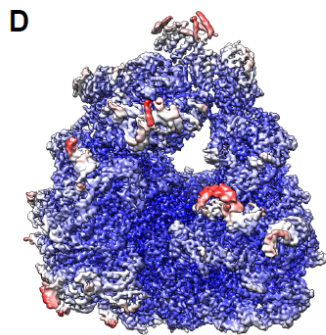
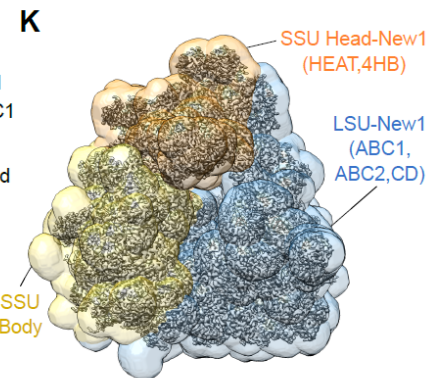
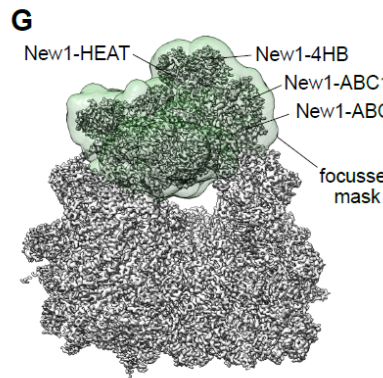
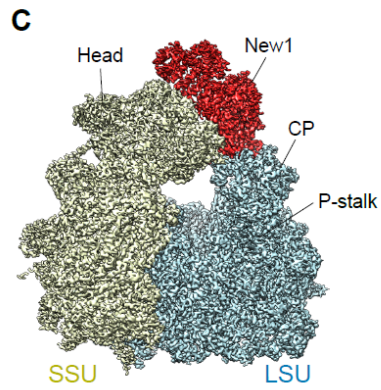
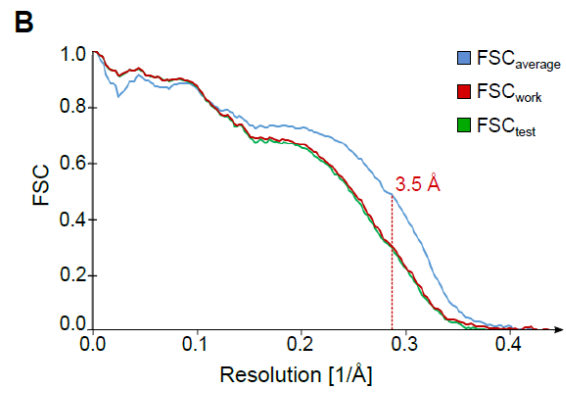
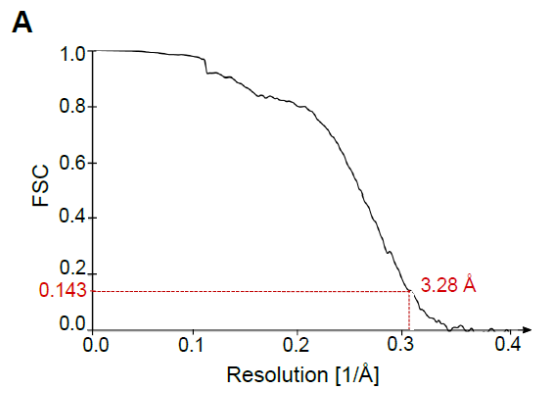


Supplementary Figure S1. Comparison of New1-TAP levels in strains used in this study by anti-TAP Western blotting. The VHY61 strain transformed with either empty vector (pRS316), as well as inducible New1-TAP (VHp262), or New1-EQ₂-TAP (VHp265) plasmids, were grown on SC-ura medium at 30°C until OD₆₀₀ ≈ 0.3, at which point β-estradiol was added to a final concentration of 1 μM. Cells were harvested either immediately prior to addition of β-estradiol (0 h) or 3 hours after (3 h). The *NEW1::TAP* control strain (YSC1178-202233783) was grown in SC medium at 30°C. Approximately 5 μg of total protein was loaded per lane, followed by serial 3-fold dilutions.

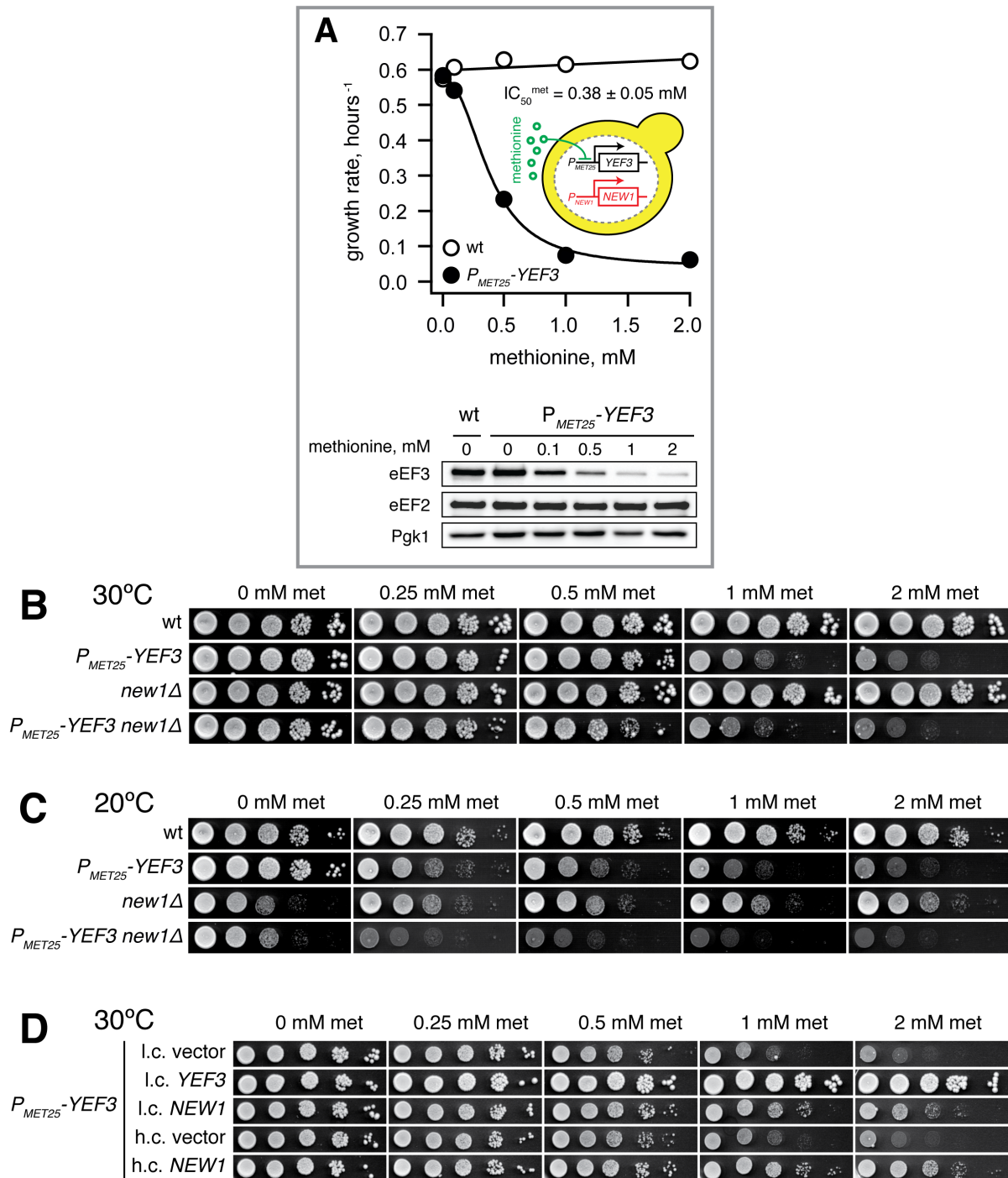


Supplementary Figure S2. 3D classification of the *S. cerevisiae* New1-80S complex. Following 2D classification, 144,876 particles were initially aligned against a vacant *S. cerevisiae* 80S ribosome and subjected to 3D classification with 3x binned images, sorting the particles into five classes. Class 1 contained a highly resolved New1-80S complex, whereas Class 2 was poorly resolved with partial ligand occupation. Furthermore, 80S particles with E-site tRNA (Class 3) could be identified as well as highly resolved 80S (Class 4, Class 5), which differ in the dynamic of the SSU. Focused sorting of 57,226 particles of class1 was implemented using a mask for the ligand only. The particles containing the well-

resolved ligand (class2, 48,757 particles) were further 3D refined yielding a final reconstruction with an average resolution of 3.28 Å. These particles were also locally refined using a (transparent green depicted) mask, which included the whole New1 and the head of the 40S subunit resulting in an improved overall ligand resolution of 3.63 Å. Based on the 3.28 Å resolved map, a CTF refinement was performed. The CTF refined particles were then 3D refined and subjected to multibody refinement using three distinct masks (SSU-New1(HEAT, 4HB), transparent orange; LSU-New1(ABC1, ABC2, CD), transparent blue; SSU Body, transparent yellow). The resulting average resolution for the SSU-New1 part obtained 3.26 Å, the LSU-New1 3.06 Å and the SSU Body 3.14 Å.

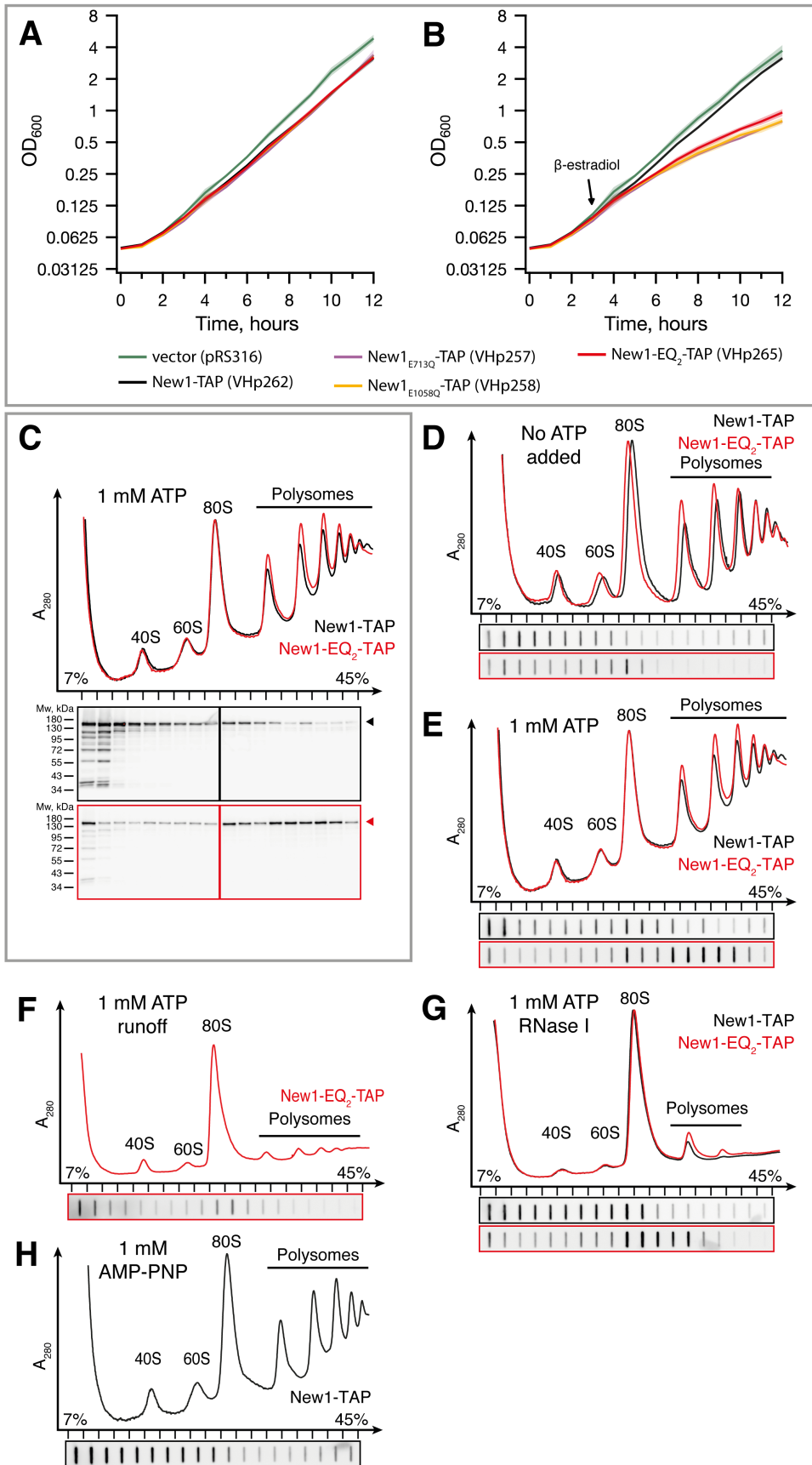


Supplementary Figure S3. Overview of the final refined cryo-EM reconstruction of the New1-80S complex. (A) Fourier shell correlation (FSC) curve of the final refined cryo-EM map of the New1-80S complex, indicating the average resolution of 3.28 Å, according to the gold-standard criterion (FSC=0.143). (B) Fit of models to maps. FSC curves calculated between the refined model and the final map (blue), with the self- and cross-validated correlations in red and green, respectively. The red dashed line shows the resolution limit that was used for the model refinement. (C) Cryo-EM map of the New1-80S complex, segmented and colored according to the small (SSU, yellow) and large (LSU, cyan) ribosomal subunit, as well as for New1 (red). (D) Mask used for the local refinement encompassing New1 and the head of the 40S subunit (transparent green). (E) Masks used for the multibody refinement. SSU-New1(HEAT, 4HB), transparent orange; LSU-New1(ABC1, ABC2, CD), transparent blue; SSU Body, transparent yellow. (F) Same view as in (C) but colored according to local resolution. (G) Cryo-EM map after local refinement colored according to local resolution showing the improvement in the resolution for the ligand and the 40S head region. (H) Merged cryo-EM maps after multibody refinement colored according to local resolution showing the improvement in the resolution for the whole 80S and the interaction interface between 80S and New1. (I-K) Transverse section of (F), (G) and (H), respectively. (L-N) View of the isolated density for New1 (L) from (F) before local refinement, (M) from (G) after local refinement and (N) from (H) after multibody refinement. The scale bar is valid for all showed resolution panels.



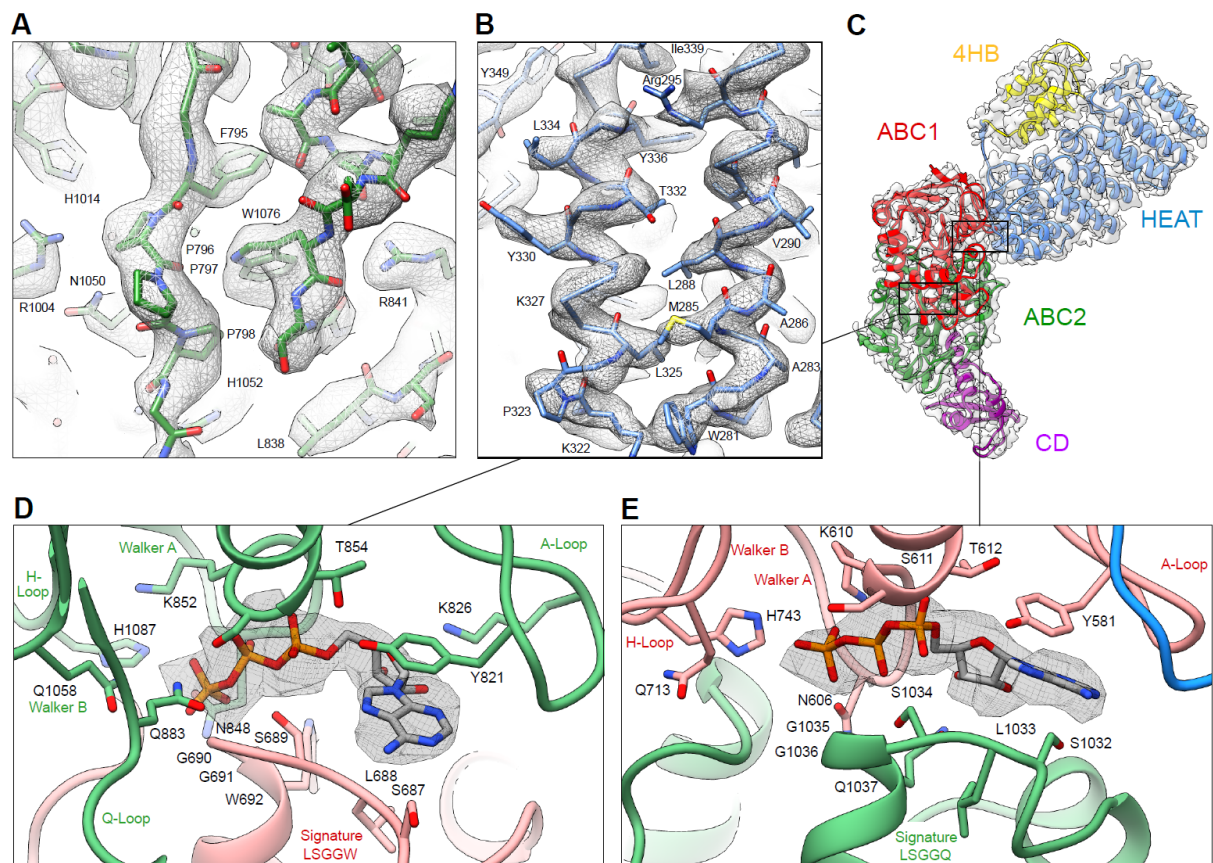
Supplementary Figure S4. The growth defect of eEF3-depleted cells is influenced by the presence or absence of *NEW1*. (A) Tunable repression of eEF3 expression leads to a gradual decrease in growth rate. The P_{MET25} -YEF3 (VKY8) strain was grown at 30°C in liquid synthetic complete medium lacking methionine and cysteine (SC-met-cys) supplemented with methionine at different concentrations (see insert). The growth rate (μ_2) was calculated as the slope of the linear regression of \log_2 -transformed OD₆₀₀ measurements. The addition of increasing concentrations of methionine represses the expression of eEF3 driven by P_{MET25} promoter without affecting the levels of elongation factor 2, eEF2, or 3-phosphoglycerate kinase, Pgk1. (B and C) Growth of the wild-type (VKY9), P_{MET25} -YEF3 (VKY8), *new1*Δ (MJY945) and P_{MET25} -YEF3 *new1*Δ (MJY951) strains on medium containing

different concentrations of methionine. The strains were grown overnight in liquid SC-met-cys medium, 10-fold serially diluted and spotted on SC-met-cys plates supplemented with the indicated concentrations of methionine. The plates were incubated at 30°C (**B**) for three or at 20°C (**C**) for four days. (**D**) Growth of the *P_{MET25}-YEF3* (VKY8) strain harboring the indicated low-copy (l.c.; pRS316, pRS316-*YEF3*, or pRS316-*NEW1*) or high-copy (h.c.; pRS426 or pRS425-*NEW1*) plasmids. Cells were grown overnight in liquid SC-ura-met-cys medium, 10-fold serially diluted and spotted on SC-ura-met-cys plates supplemented with the indicated concentrations of methionine. The plates were incubated at 30°C for three days.

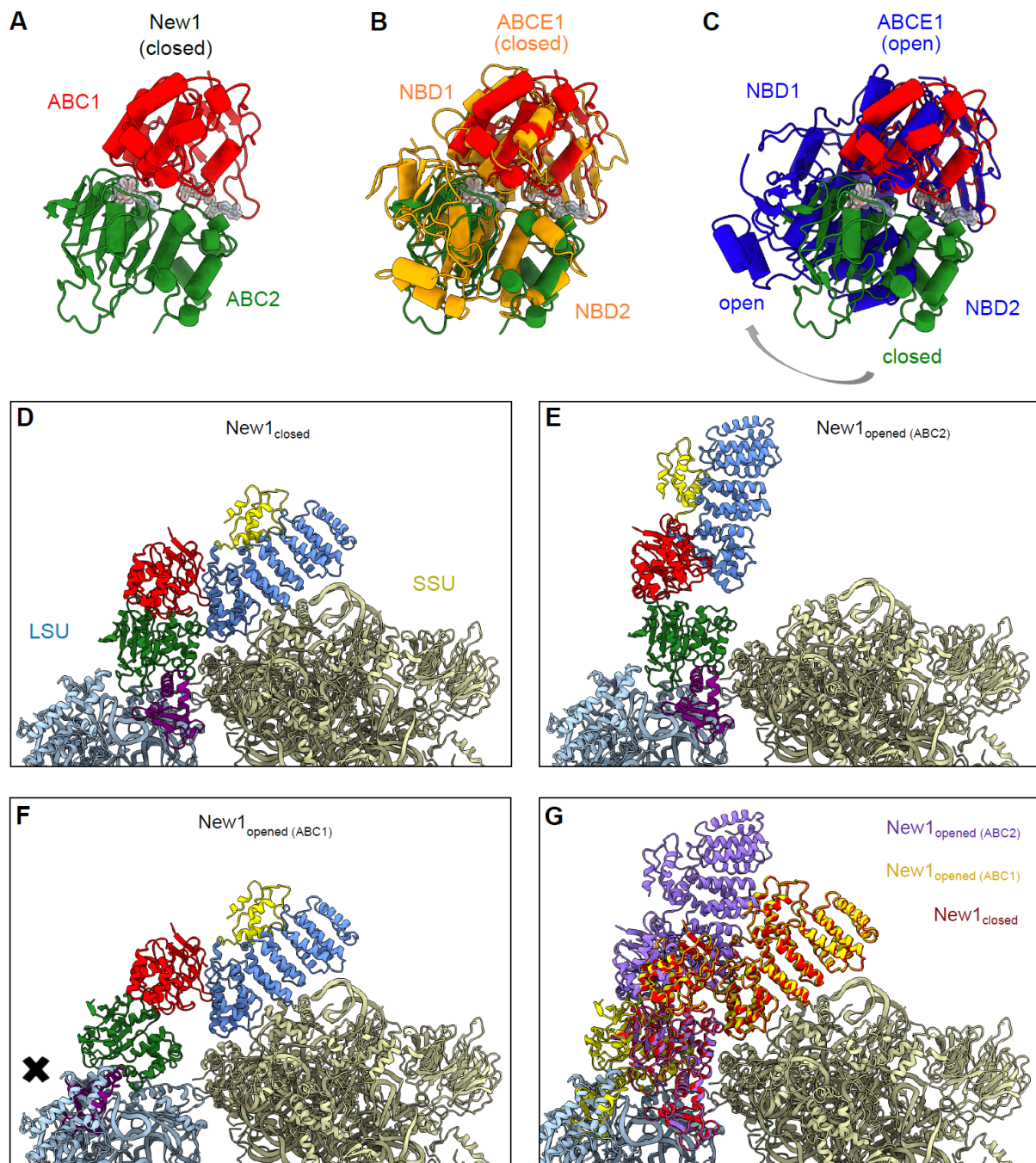


Supplementary Figure S5. New1-EQ₂ cosediments with actively translating ribosomes in the presence of ATP. (A and B) Expression of New1-EQ₂ inhibits cell growth. The VHY61 strain

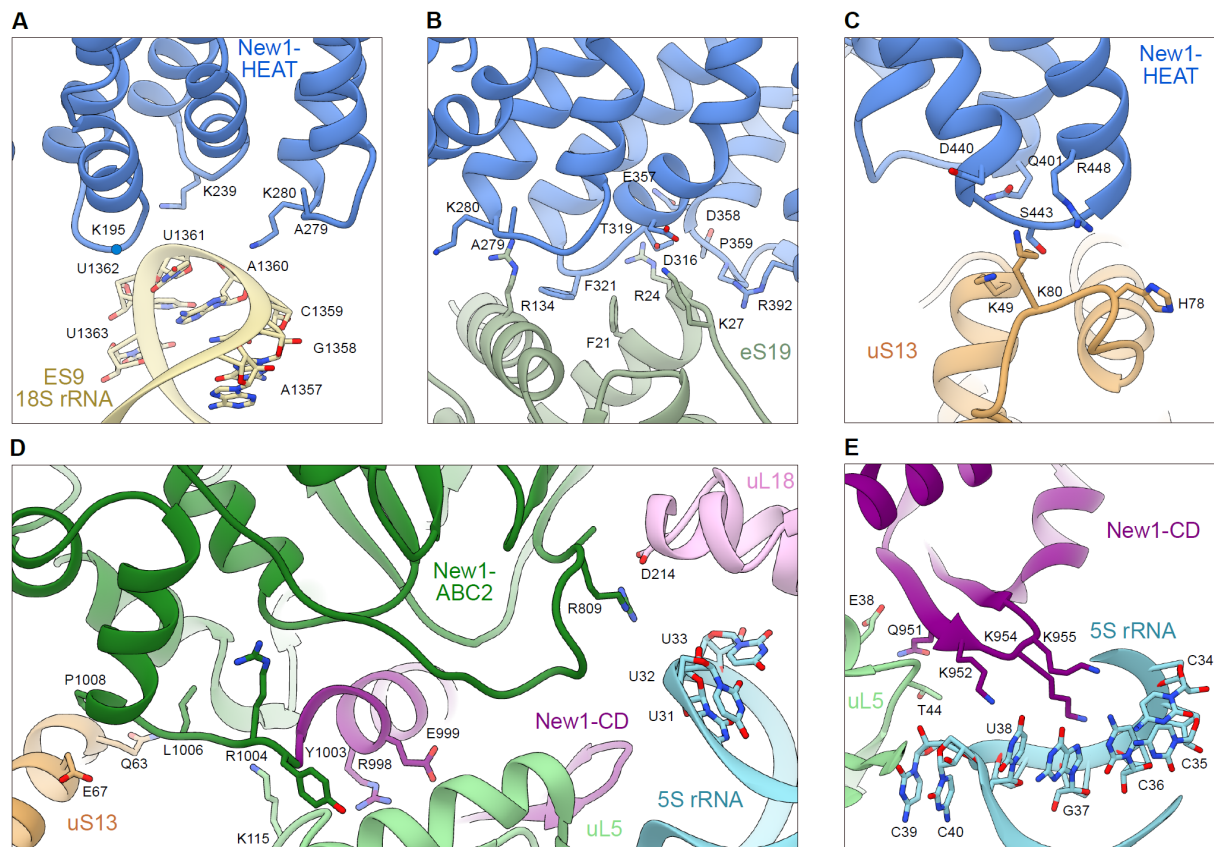
transformed with the indicated inducible expression plasmids were pre-grown overnight in SC-ura medium at 30°C, diluted to $OD_{600} \approx 0.05$ in the same medium and grown for three hours. An aliquot from each culture was then transferred to a prewarmed flask and β -estradiol was added to a concentration of 1 μ M. The growth of uninduced (**A**) and induced (**B**) cultures was monitored by hourly OD_{600} measurements. The data are presented as geometric means of three independent transformants and standard errors of the mean are indicated by shading. (**C-G**) Polysome profile and immunoblot analyses of yeast cells (VHY61) carrying the inducible New1-TAP (VHp262, black lines and boxes) or New1-EQ₂-TAP (VHp265, red lines and boxes) plasmids. Cells were grown at 30°C until $OD_{600} \approx 0.3$, supplemented with 1 μ M β -estradiol and harvested after 3h. Lysates and sucrose gradients were either left unsupplemented (**D**) or supplemented with ATP (**A**, **E-G**) or AMP-PNP (**H**). The ATP-supplemented samples were, where indicated, treated with RNase I (**E**), or derived from cultures not pre-treated with cycloheximide (runoff conditions) (**F**). Fractions from the gradients were analyzed by western (**C**) or slot blotting (**D-H**). The blots were probed for TAP-tag. ◀ and ▶ symbols denote positions of the full-size proteins.



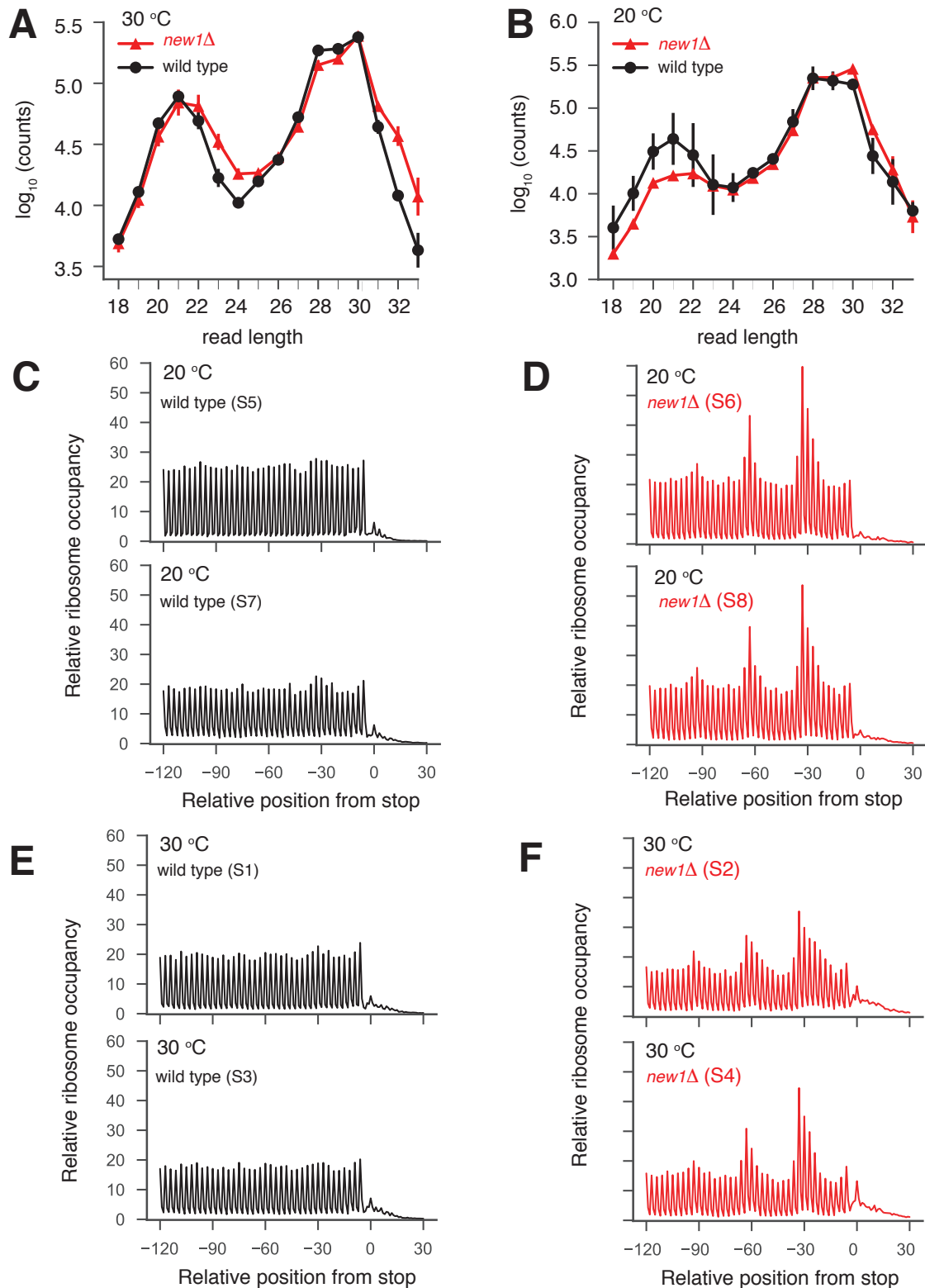
Supplementary Figure S6. Model for *S. cerevisiae* New1 with bound ATP molecules. (A-B) Selected examples illustrating the quality of fit of the molecular model (A) within ABC2 and (B) the HEAT repeats to the unsegmented cryo-EM map (grey mesh). (C) Model of the 80S-bound New1 based on the multibody refined map and colored by domain, HEAT (blue), 4HB (yellow), ABC1 (red), ABC2 (green) and CD (magenta). (D, E) Views of the two closed nucleotide-binding sites created by ABC1 and ABC2. For the bound ATP molecules cryo-EM map densities of the multibody refined map (dark grey mesh) are illustrated. The Walker A and Walker B motifs with the mutated Q1058 (D) and Q713 (E) residues of the signature motif, as well as the ‘switch’ histidine (H1087 (D) and H743 (E)), are shown as sticks and labelled.



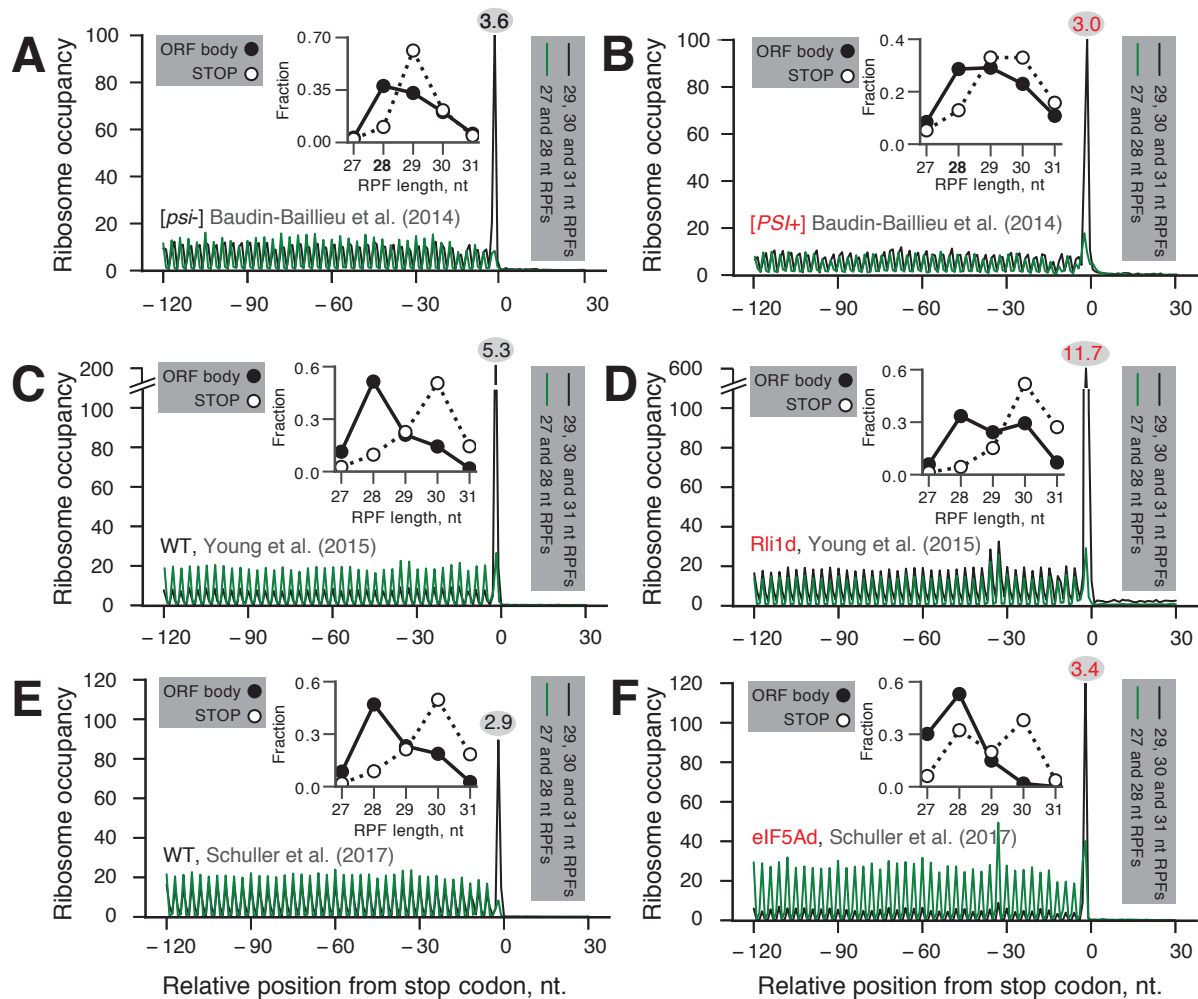
Supplementary Figure S7. The closed conformation of the New1. (A) The ABC1 (red) and ABC2 (green) domain of New1 in the New1-80S complex adopts a closed conformation. (B-C) Conformation of the New1 NBDs with respect to other ABC proteins. Alignment (based on ABC1) of the New1-ABCs with (B) the closed conformation of the NBDs of *S. cerevisiae* ABCE1 (orange, PDB: 5LL6) (9) and (C) the *E. coli* ABCE1 protein observed in the open conformation (blue, PDB ID: 3OZX) (10). (D-G) Incompatibility of New1 to the 80S Ribosome in an open conformation. (D) The New1 model in a closed conformation colored due to the different domain organization. (E) The potential opened New1 aligned to ABC2 or (F) ABC1 of the ABCE1 protein in an opened conformation (PDB ID: 3OZX) (10). (G) Overlay of the closed New1 model (dark red) with the potential opened state models aligned to ABC1 (dark yellow) and ABC2 (violet), respectively.



Supplementary Figure S8. Interactions of New1 with the 80S Ribosome. (A-C) Interactions of the New1-HEAT repeat region (blue) with (A) ES9 of the 18S rRNA (light yellow), (B) eS19 (pale green), and (C) uS13 (light orange) of the SSU. (D) New1-ABC2 (green) bridges the intersubunit space by interacting with the SSU protein uS13 and the LSU proteins uL5 (pastel light green) and uL18 (light pink) as well as by forming protein-RNA intercalations with the 5S rRNA (light blue). (E) Intercation of the lysine dense region of New1-CD (magenta) with the 5S rRNA as well as uL5. Residues with a clear density within the cryo-EM map are shown as sticks whereas the rest is depicted as dots and labeled.

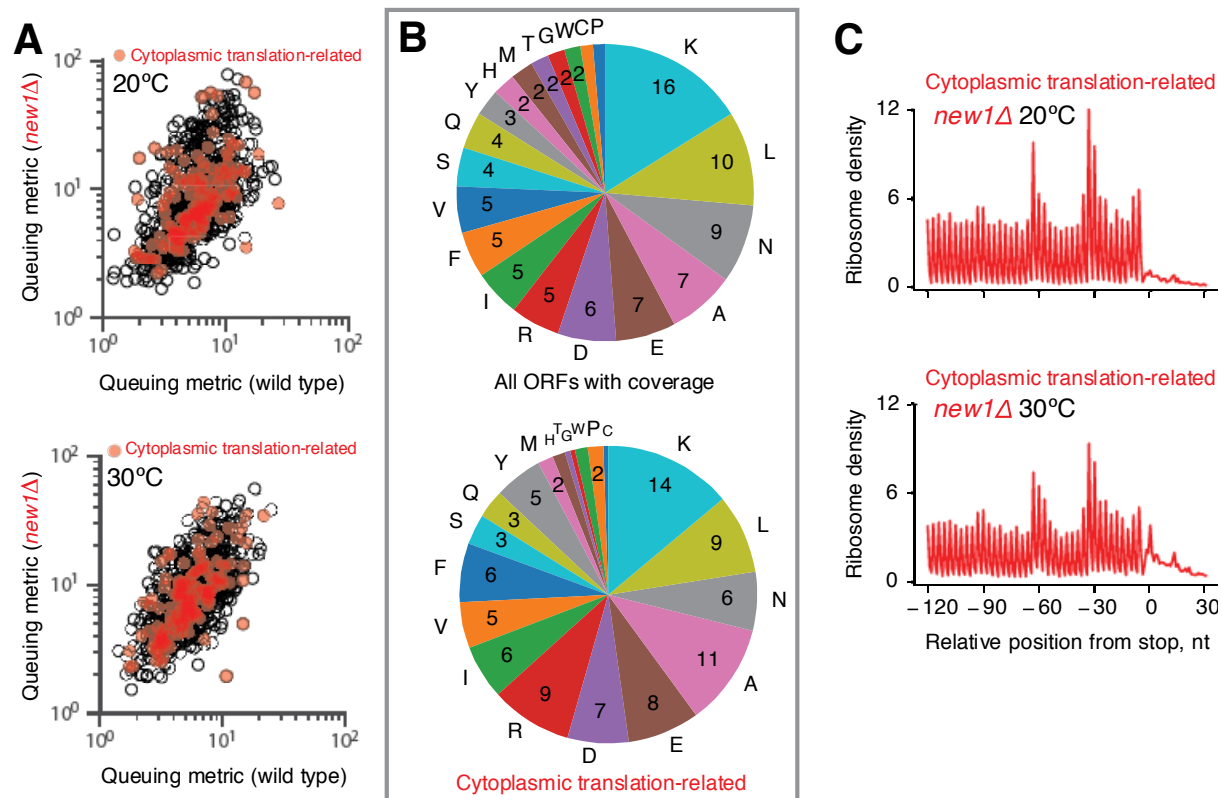


Supplementary Figure S9. RPF read length distributions and metagene analysis of Ribo-Seq data. RPF read length distributions in wild type (wt) and *new1Δ* Ribo-Seq libraries at 30 °C (A) and 20°C (B). Data are presented as the geometric mean of two biological replicates and the error bars represent the standard error of the mean. Metagene plots of ribosome density around start and stop codons, wild type (C and D) and *new1Δ* (E and F) strain. Reads are aligned in respect to the P-site.

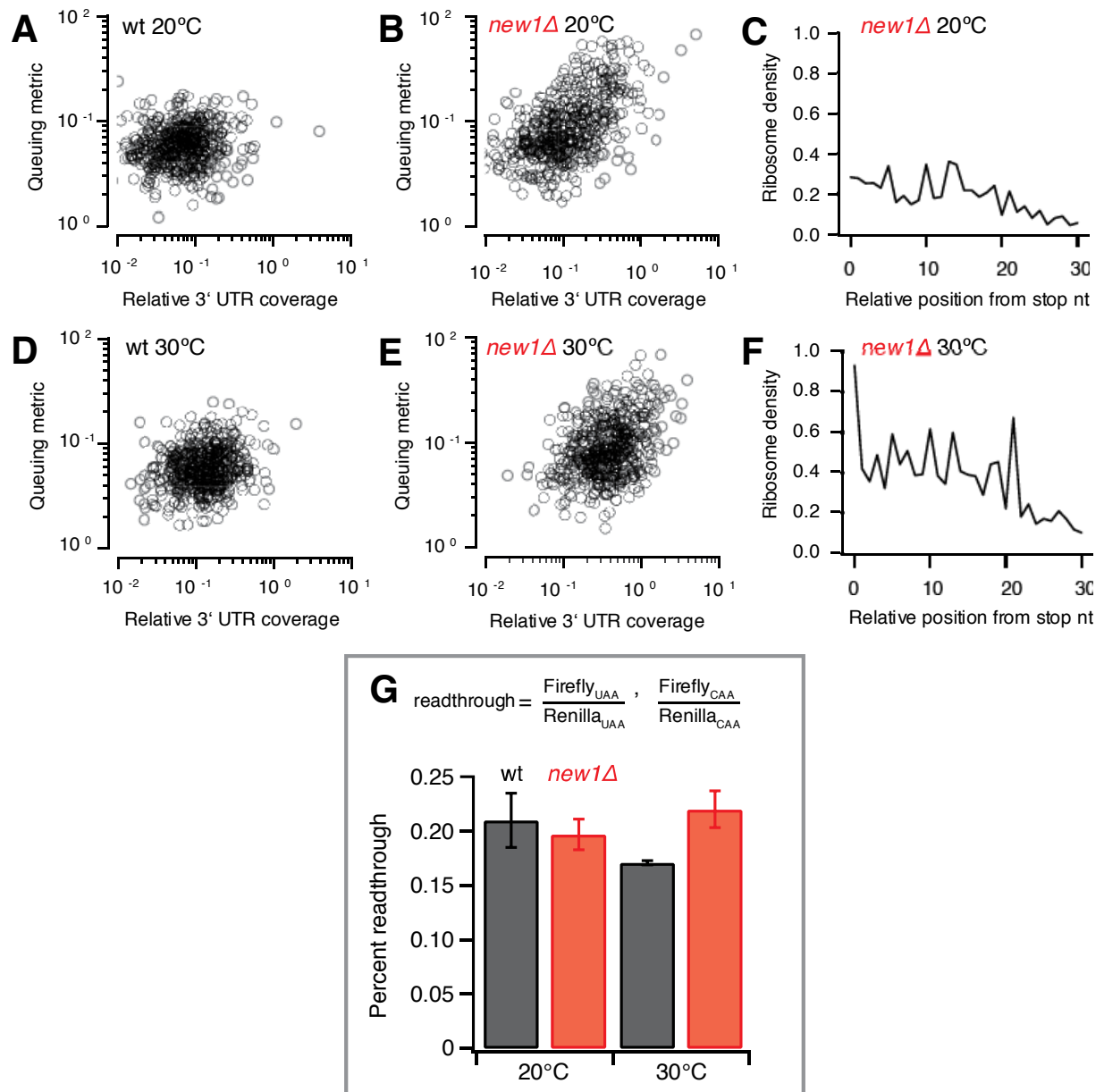


Supplementary Figure S10. Metagenes plots around the stop codon grouped by RPF read length.

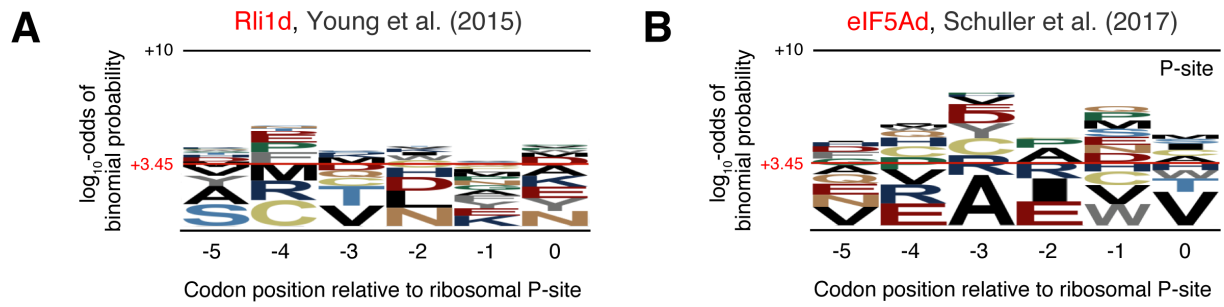
Ribo-Seq metagenes profiles are shown for the following strains: [PSI+] (B) and [psi-] (A) (11), Rli1-depleted (D) and the corresponding wild type (C) (12) and eIF5A-depleted (F) and the corresponding wild type (E) (13). Ribosome densities corresponding to 27-28 nucleotide-long (dominant RPF lengths within the ORF body) and 29-31 nucleotide-long (dominant RPF lengths at the stop codon) RPF reads are plotted respectively as green and black traces. Reads are aligned with respect to the P-site. The frequency of individual RPF read lengths within the ORF body (filled circles; computed for metagenes positions -180 to -90) and at the stop codon (empty circles) are shown as inset graphs. The relative increase of the ribosome density at the stop codon over the average density within the ORF body is indicated over the stop codon peak within a grey oval and is computed for pooled Ribo-Seq data (27-31 nucleotide-long RPFs).



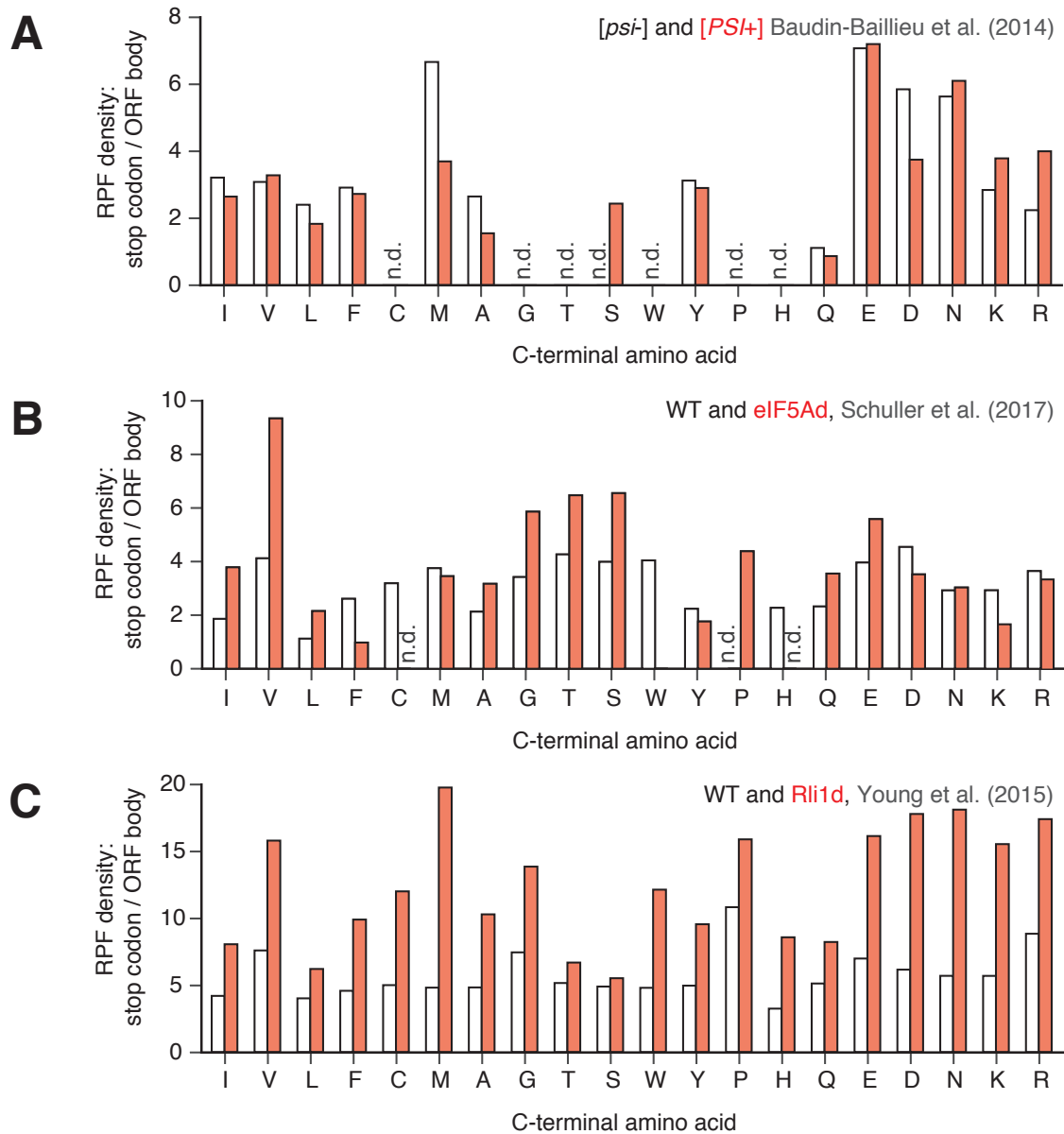
Supplementary Figure S11. C-terminal amino acid composition and ribosome queuing at cytoplasmic translation-related genes in *new1Δ* strain. (A) 3'-terminal ribosome queuing metric ('queuing metric' for short) computed for individual ORFs, wild type and *new1Δ* at 20 °C and 30 °C. (B) C-terminal amino acid fractions (%) were calculated for all genes with sufficient coverage (≥ 5 rpm for positions -120 to 0) (top: 1,492 ORFs) or for cytoplasmic translation-related genes (bottom: 288 ORFs classified by YeastMine Gene Ontology tools (14) with Gene Ontology groups containing 'translation'; RNA and mitochondrial genes are excluded). (C) Metagenes analysis of translation-related ORFs in *new1Δ* 20 °C and 30 °C.



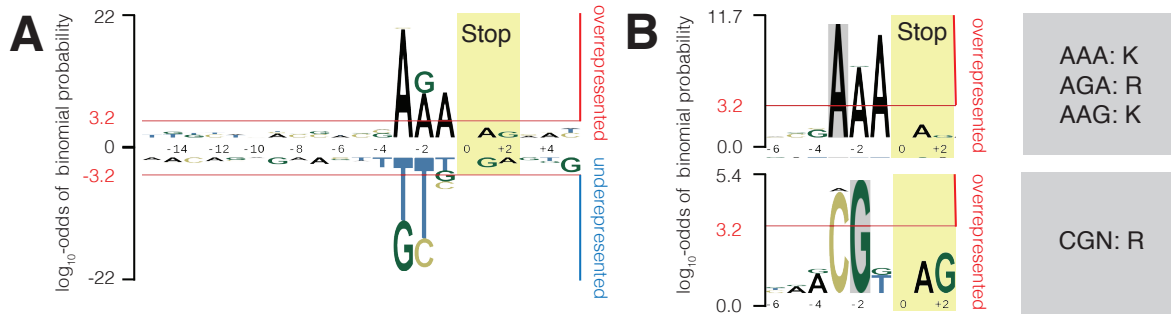
Supplementary Figure S12. Correlation of ribosome queuing and 3' UTR coverage. The ribosome queuing metric versus relative 3' UTR coverage is plotted for wild type (**A** and **D**, 20°C and 30°C) and *new1Δ* (**B** and **E**, 20°C and 30°C) strains. Individual dots represent individual ORFs. Only genes where a queuing metric and relative 3' UTR coverage can be computed in all 4 conditions are included (520 in total). Metagene plots are computed for 100 ORFs with the highest queuing metric values (**C** and **F**). (**G**) The *new1Δ* strain does not display a significant increase in stop codon readthrough. Readthrough levels of the UAA stop codon in the wild type (VKY9) and *new1Δ* (MJY945) strains at 20°C or 30°C are shown. The values represent the mean of three independent experiments. The standard deviation is indicated.



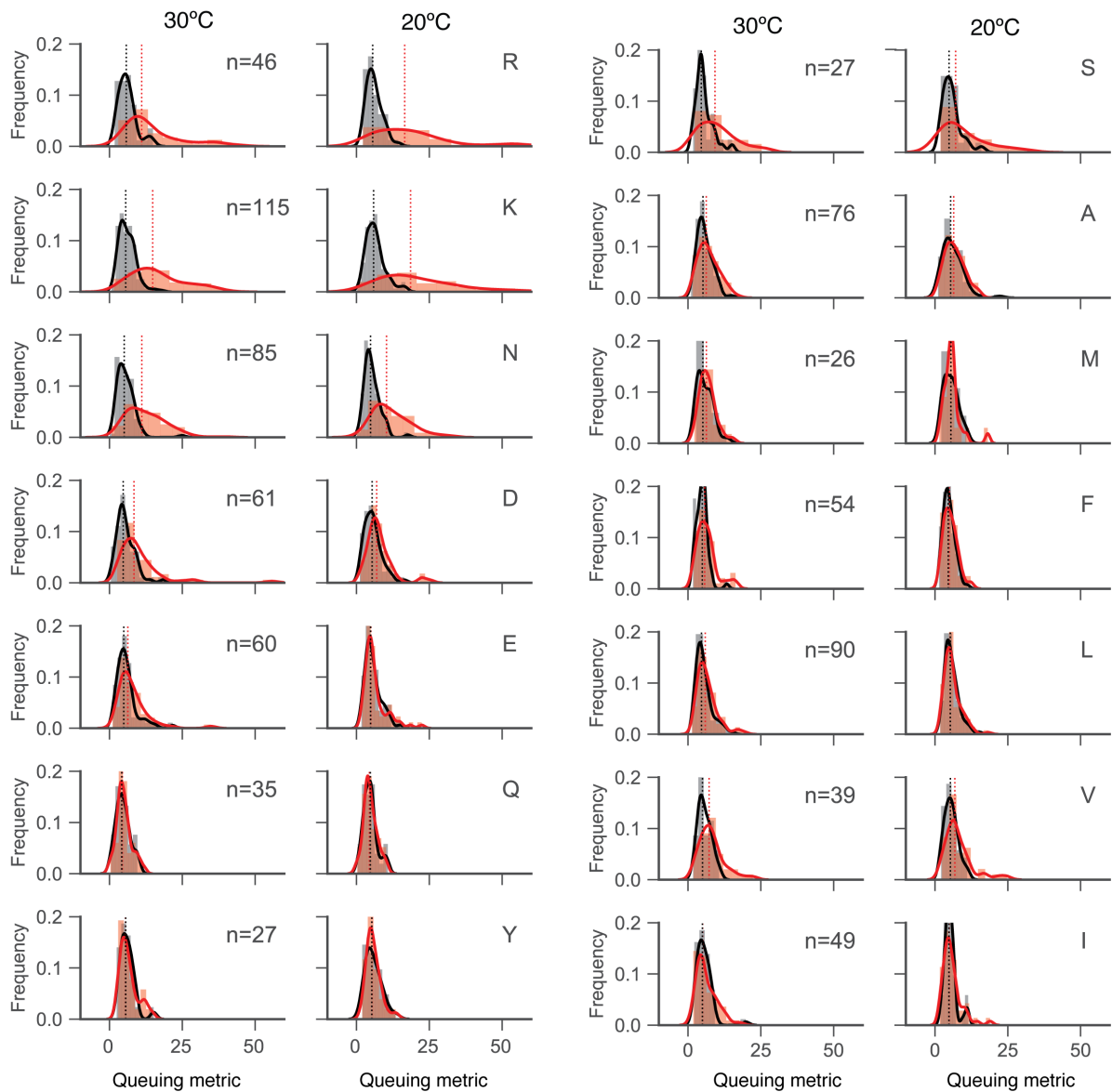
Supplementary Figure S13. Lack of amino acid sequence conservation for ORFs displaying a high degree of ribosomal queuing at the C-terminus for Rli1-depleted (A) (12) and eIF5A-depleted (B) (13) *S. cerevisiae*. pLogo (15) was used to calculate the overrepresentation of specific amino acids at positions relative to the P-site. The 100 top genes based on the queuing score were used as the foreground. Horizontal red lines on the pLogos represent the significance threshold (the log₁₀-odds 3.45) corresponding to a Bonferroni corrected p-value of 0.05.



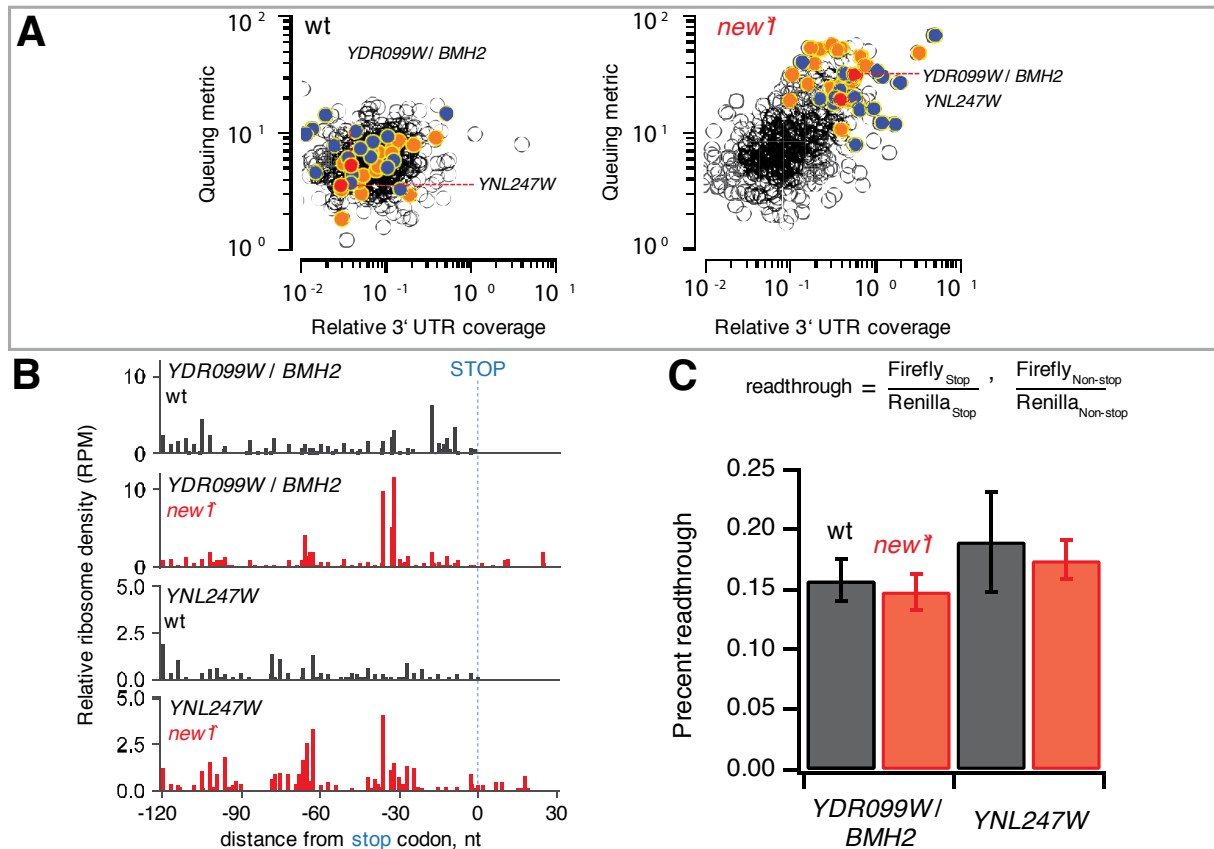
Supplementary Figure S14. The relative increase in ribosome density at the stop codon over the average density within the ORF is shown for individual C-terminal amino acids. Densities are calculated for pooled Ribo-Seq data (27-31 nucleotide-long RPFs) with sufficient entries (≥ 10 instances per individual C-terminal amino acid): *[PSI+]* and *[psi-]* (**A**) (11), *Rli1*-depleted and the corresponding wild type (**B**) (12), and *eIF5A*-depleted and the corresponding wild type (**C**) (13) *S. cerevisiae*.



Supplementary Figure S15. Stop codon context bias is associated with a high ribosome queuing metric in the *new1Δ* strain at 20°C. Overrepresentation (**A**, top, **B** top and bottom) and underrepresentation (**A**, bottom) of specific nucleotides at positions relative to the A-site is calculated using pLogo (15). The position of the stop codon is highlighted with a yellow box (positions 0 to +2). Overrepresentation subpatterns were extracted focusing on a 'fixed' adenine in the -3 position (**B**, top) and guanine in the -2 position (**B**, bottom). To calculate the conditional probabilities, 131 sequences displaying high ribosome queuing at the C-terminus (Z -score>1) were used as the foreground and 1,439 sequences with sufficient Ribo-Seq coverage (including 131 used as the foreground) were used as the background. Horizontal red lines on the pLogos represent the significance threshold (the log₁₀-odds 3.2), corresponding to a Bonferroni corrected p-value of 0.05.



Supplementary Figure S16. Distributions of the ribosome queuing metric for individual ORFs are grouped according to the identity of the C-terminal amino acid. Wild type and *new1Δ* data are shown in black and red, respectively. The same ORFs were used to calculate the queuing metric distributions for wild type and *new1Δ*, both at 20°C and 30°C. Only C-terminal amino acids with more than 20 instances in the dataset were analysed ($n > 20$).



Supplementary Figure S17. 3' ORF regions *YDR099W / BMH2* and *YNL247* do not cause stop codon readthrough in *new1Δ* background. (A) The ribosome queuing metric versus relative 3' UTR coverage is plotted for wild type and *new1Δ* (20°C) strains. Individual dots represent individual ORFs. Top 20 ORFs with highest queuing metric shift and top 20 ORFs with the highest relative 3' UTR coverage are highlighted in orange and blue, respectively. The two genes selected for experimental testing are in red: *YDR099W / BMH2* (C-terminal K residue, UAA stop codon) and *YNL247* (C-terminal K residue, UAG stop codon). (B) Ribosome footprint density along *YDR099W / BMH2* and *YNL247* genes. The first nucleotide of the stop codon corresponds to 0. (C) Stop codon readthrough assays using modified dual-luciferase reporters based on the *YDR099W / BMH2* and *YNL247* ORFs. Readthrough percentage was calculated based on the given formula ('Stop' corresponds to UAA or UAG and 'non-stop' corresponds to CAA or CAG). Experiments were carried out in wild type (VKY9) and *new1Δ* (MJY945) strains at 20°C. The values represent the arithmetic mean of three independent experiments and the error bars indicate the standard deviation.

Supplementary references:

1. Kasari, V., Margus, T., Atkinson, G.C., Johansson, M.J.O. and Hauryliuk, V. (2019) Ribosome profiling analysis of eEF3-depleted *Saccharomyces cerevisiae*. *Sci Rep*, **9**, 3037.
2. Sikorski, R.S. and Hieter, P. (1989) A system of shuttle vectors and yeast host strains designed for efficient manipulation of DNA in *Saccharomyces cerevisiae*. *Genetics*, **122**, 19-27.
3. Christianson, T.W., Sikorski, R.S., Dante, M., Shero, J.H. and Hieter, P. (1992) Multifunctional yeast high-copy-number shuttle vectors. *Gene*, **110**, 119-122.
4. Ottoz, D.S., Rudolf, F. and Stelling, J. (2014) Inducible, tightly regulated and growth condition-independent transcription factor in *Saccharomyces cerevisiae*. *Nucleic acids research*, **42**, e130.
5. Puig, O., Caspary, F., Rigaut, G., Rutz, B., Bouveret, E., Bragado-Nilsson, E., Wilm, M. and Seraphin, B. (2001) The tandem affinity purification (TAP) method: a general procedure of protein complex purification. *Methods*, **24**, 218-229.
6. Curran, K.A., Morse, N.J., Markham, K.A., Wagman, A.M., Gupta, A. and Alper, H.S. (2015) Short Synthetic Terminators for Improved Heterologous Gene Expression in Yeast. *ACS Synth Biol*, **4**, 824-832.
7. Keeling, K.M., Lanier, J., Du, M., Salas-Marco, J., Gao, L., Kaenjak-Angeletti, A. and Bedwell, D.M. (2004) Leaky termination at premature stop codons antagonizes nonsense-mediated mRNA decay in *S. cerevisiae*. *RNA*, **10**, 691-703.
8. Johansson, M.J. and Jacobson, A. (2010) Nonsense-mediated mRNA decay maintains translational fidelity by limiting magnesium uptake. *Genes Dev*, **24**, 1491-1495.
9. Heuer, A., Gerovac, M., Schmidt, C., Trowitzsch, S., Preis, A., Kotter, P., Berninghausen, O., Becker, T., Beckmann, R. and Tampe, R. (2017) Structure of the 40S-ABCE1 post-splitting complex in ribosome recycling and translation initiation. *Nature structural & molecular biology*, **24**, 453-460.
10. Barthelme, D., Dinkelaker, S., Albers, S.V., Londei, P., Ermler, U. and Tampe, R. (2011) Ribosome recycling depends on a mechanistic link between the FeS cluster domain and a conformational switch of the twin-ATPase ABCE1. *Proceedings of the National Academy of Sciences of the United States of America*, **108**, 3228-3233.
11. Baudin-Baillieu, A., Legendre, R., Kuchly, C., Hatin, I., Demais, S., Mestdagh, C., Gautheret, D. and Namy, O. (2014) Genome-wide translational changes induced by the prion [PSI⁺]. *Cell Rep*, **8**, 439-448.
12. Young, D.J., Guydosh, N.R., Zhang, F., Hinnebusch, A.G. and Green, R. (2015) Rli1/ABCE1 Recycles Terminating Ribosomes and Controls Translation Reinitiation in 3'UTRs In Vivo. *Cell*, **162**, 872-884.
13. Schuller, A.P., Wu, C.C., Dever, T.E., Buskirk, A.R. and Green, R. (2017) eIF5A Functions Globally in Translation Elongation and Termination. *Molecular cell*, **66**, 194-205 e195.
14. Balakrishnan, R., Park, J., Karra, K., Hitz, B.C., Binkley, G., Hong, E.L., Sullivan, J., Micklem, G. and Cherry, J.M. (2012) YeastMine--an integrated data warehouse for *Saccharomyces cerevisiae* data as a multipurpose tool-kit. *Database (Oxford)*, **2012**, bar062.

15. O'Shea, J.P., Chou, M.F., Quader, S.A., Ryan, J.K., Church, G.M. and Schwartz, D. (2013) pLogo: a probabilistic approach to visualizing sequence motifs. *Nat Methods*, **10**, 1211-1212.



Yeast translation elongation factor eEF3 promotes late stages of tRNA translocation

Namit Ranjan^{1,*†} , Agnieszka A Pochopien^{2,3,†}, Colin Chih-Chien Wu^{4,†}, Bertrand Beckert³, Sandra Blanchet¹, Rachel Green^{4,5,**} , Marina V Rodnina^{1,***}  & Daniel N Wilson^{2,3,****} 

Abstract

In addition to the conserved translation elongation factors eEF1A and eEF2, fungi require a third essential elongation factor, eEF3. While eEF3 has been implicated in tRNA binding and release at the ribosomal A and E sites, its exact mechanism of action is unclear. Here, we show that eEF3 acts at the mRNA–tRNA translocation step by promoting the dissociation of the tRNA from the E site, but independent of aminoacyl-tRNA recruitment to the A site. Depletion of eEF3 *in vivo* leads to a general slowdown in translation elongation due to accumulation of ribosomes with an occupied A site. Cryo-EM analysis of native eEF3–ribosome complexes shows that eEF3 facilitates late steps of translocation by favoring non-rotated ribosomal states, as well as by opening the L1 stalk to release the E-site tRNA. Additionally, our analysis provides structural insights into novel translation elongation states, enabling presentation of a revised yeast translation elongation cycle.

Keywords ABC ATPase; cryo-EM; eEF3; E-site tRNA; L1 stalk

Subject Category Translation & Protein Quality

DOI 10.15252/embj.2020106449 | Received 6 August 2020 | Revised 10 December 2020 | Accepted 21 December 2020 | Published online 8 February 2021

The EMBO Journal (2021) 40: e106449

Introduction

Protein synthesis is an evolutionary conserved process. Translation elongation entails the same repetitive steps of decoding, peptide bond formation, and translocation in all living organisms, catalyzed by highly homologous translation elongation factors eEF1A/EF-Tu and eEF2/EF-G in eukaryotes and bacteria, respectively, assisted by eEF1B/EF-Ts and eIF5A/EF-P (Dever & Green, 2012; Rodnina, 2018). It is therefore particularly surprising that some fungi, such as

Saccharomyces cerevisiae, *Candida albicans*, and *Pneumocystis carinii* have an additional essential, abundant elongation factor, eEF3 (Skogerson & Wakatama, 1976; Uritani & Miyazaki, 1988; Kamath & Chakraburty, 1989; Colthurst *et al*, 1991). Moreover, recent bioinformatic analyses indicate that eEF3-like proteins exist more broadly in unicellular eukaryotes, not just in fungi (Mateyak *et al*, 2018). Some organisms, e.g., *S. cerevisiae*, also contains an eEF3 homologue, termed New1p, which when overexpressed can rescue strains depleted for eEF3 (Kasari *et al*, 2019b). In exponentially growing *S. cerevisiae* cells, eEF3, eEF1A, eEF2, and eRF1 exert the strongest control over the rate of translation (Firczuk *et al*, 2013). In yeast, the amount of eEF3 per cell is comparable to that of ribosomes, eEF2, and eEF1B, 10 times lower than that of eEF1A, and 5–10 times higher than of the termination factors and the majority of initiation factors (Firczuk *et al*, 2013). These data suggest that there is sufficient eEF3 to participate in every round of translation elongation.

eEF3 is a cytoplasmic protein that belongs to the superfamily of ATP-binding cassette (ABC) proteins, specifically, of the F subtype (Murina *et al*, 2018). In *S. cerevisiae*, eEF3 consists of a single polypeptide chain of 1,044 amino acids comprising several domains: a HEAT repeat domain, a four-helix bundle domain (4HB domain), two ATP-binding domains, ABC1 and ABC2, with a chromodomain (CD) insertion within ABC2, as well as eEF3-specific C-terminal domain (Kambampati *et al*, 2000; Murina *et al*, 2018). A low-resolution (9.9 Å) cryo-electron microscopy (cryo-EM) structure of the ribosome–eEF3 complex revealed that eEF3 binds to the ribosome, spanning across the boundary between the head of the 40S subunit and the central protuberance of the 60S subunit, where it contacts ribosomal RNA (rRNA) and proteins, but should not interfere with the binding of eEF1A or eEF2 (Andersen *et al*, 2006). Despite these structural clues, the function of eEF3 remains poorly understood. Early studies reported that eEF3 facilitates binding of the ternary complex eEF1A–GTP–aminoacyl-tRNA to the decoding site (A site) of the ribosome, thus increasing the fidelity of translation (Uritani & Miyazaki, 1988); genetic and physical interactions between eEF1A

1 Department of Physical Biochemistry, Max Planck Institute for Biophysical Chemistry, Göttingen, Germany

2 Gene Center, Department for Biochemistry and Center for Integrated Protein Science Munich (CiPSM), University of Munich, Munich, Germany

3 Institute for Biochemistry and Molecular Biology, University of Hamburg, Hamburg, Germany

4 Department of Molecular Biology and Genetics, Johns Hopkins University School of Medicine, Baltimore, MD, USA

5 Howard Hughes Medical Institute, Johns Hopkins University School of Medicine, Baltimore, MD, USA

*Corresponding author. Tel: +49 551 2012958; E-mail: namit.ranjan@mpiibpc.mpg.de

**Corresponding author. Tel: +1 410 614 4928; E-mail: ragreen@jhmi.edu

***Corresponding author. Tel: +49 551 2012900; E-mail: rodnina@mpiibpc.mpg.de

****Corresponding author. Tel: +49 40 42838 2847; E-mail: daniel.wilson@chemie.uni-hamburg.de

†These authors contributed equally to this work

and eEF3 appear to support this hypothesis (Anand *et al*, 2003; Anand *et al*, 2006). An *in vitro* study of tRNA binding to the ribosome argued that eEF3 accelerates dissociation of tRNA from the exit site (E site) independent of translocation and is required for aminoacyl-tRNA binding to the A site when the E site is occupied (Triana-Alonso *et al*, 1995); thus, according to this model, eEF3 regulates decoding. By contrast, another study proposed that eEF3 facilitates the release of tRNA from the P site during the disassembly of post-termination complexes at the ribosome recycling step of translation (Kurata *et al*, 2013).

eEF3 has also been implicated in translational control in response to environmental stress. Expression of eEF3 is altered during morphogenesis in *Aspergillus fumigatus* and upon starvation in *S. cerevisiae* (Grousl *et al*, 2013; Kubitschek-Barreira *et al*, 2013). Interaction of eEF3 with the ribosome in *S. cerevisiae* is affected by Stm1, a protein that binds to the mRNA entry tunnel of the ribosome (Ben-Shem *et al*, 2011), inhibits translation at the onset of the elongation cycle, and promotes decapping of a subclass of mRNAs (Van Dyke *et al*, 2009; Balagopal & Parker, 2011). In yeast lacking Stm1, eEF3 binding to ribosomes is enhanced and overexpression of eEF3 impairs growth (Van Dyke *et al*, 2009). On the other hand, eEF3 affects the function of Gcn1, thereby modulating the kinase activity of Gcn2 (Sattlegger & Hinnebusch, 2005). In addition to these functional interactions, the *Saccharomyces* genome and the STRING databases suggest that eEF3 interacts with a number of proteins that may affect the efficiency of translation (Cherry *et al*, 2012; Szklarczyk *et al*, 2019), including eEF2, heat shock proteins, or She2 and She3, the adaptor proteins that facilitate targeted transport of distinct mRNAs (Heym & Niessing, 2012). Together these data raise the possibility that eEF3 may act as a hub for translational control, but insight into the role that eEF3 plays within these regulatory networks is hampered by the lack of understanding of its basic function.

Here, we address the function of eEF3 using a combination of rapid kinetics in a fully reconstituted yeast *in vitro* translation system, ribosome profiling, and cryo-EM. First, we show using biochemical and kinetic approaches that eEF3 helps eEF2 to complete tRNA–mRNA translocation by accelerating the late stages of the process. While eEF3 facilitates E-site tRNA release, this activity is not dependent on the binding of ternary complex to the A site, as previously reported (Triana-Alonso *et al*, 1995). Ribosome profiling of strains conditionally depleted of eEF3 reveals global changes in ribosome state in the cell wherein ribosomes accumulate with an occupied A site (typical of ribosomes in a pre-translocation state). These data are consistent with the presence of a new rate-limiting step in elongation where ribosomes cannot undergo translocation due to the presence of deacylated tRNA in the E site. Cryo-EM of native eEF3-ribosome complexes provides a structural basis for the mechanism of action of eEF3 to promote late steps of translocation as well as facilitate E-site tRNA release.

Results

eEF3 promotes late steps of tRNA–mRNA translocation

To understand the function of eEF3, we used a fully reconstituted translation system from yeast components (Appendix Fig S1A). We

assembled an 80S initiation complex (80S IC) using purified 40S and 60S subunits, mRNA, and initiator tRNA ($[^3\text{H}]\text{Met-tRNA}_i^{\text{Met}}$) in the presence of initiation factors eIF1, eIF1A, eIF2, eIF3, eIF5, and eIF5B (Appendix Fig S1B). Addition of $[^{14}\text{C}]\text{Phe-tRNA}^{\text{Phe}}$ in the ternary complex with eEF1A and GTP (TC-Phe), and eIF5A resulted in decoding of the next codon UUU and formation of the dipeptide MetPhe (Fig 1A). Using a fully reconstituted translation system allows us to study each step of translation in a codon-resolved manner and to identify the reactions that are promoted by eEF3. To test whether eEF3 affects the first round of translation elongation, we monitored the dipeptide formation in real time. As the reaction is rapid, we carried out experiments in a quench-flow apparatus. We separated dipeptides from unreacted amino acids by HPLC and quantified the extent of dipeptide formation by radioactivity counting. The rate of MetPhe formation (0.15 s^{-1}) was not affected by the addition of eEF3 (Fig 1B), and only slightly at very high eEF3 concentration (Fig EV1A). Similarly, formation of the MetVal peptide measured on an mRNA with Val (GUU) codon was not affected by the presence of eEF3 (Fig EV1B). These results indicate that eEF3 is not essential for the first round of decoding or peptide bond formation. Next, we tested whether the second round of elongation is affected. We prepared an 80S complex carrying a dipeptidyl-tRNA (MetPhe-tRNA^{Phe}) in the A site and a deacylated tRNA_i^{Met} in the P site (denoted as 80S 2C for dipeptide complex), added a TC with Val-tRNA^{Val} reading the GUU codon (TC-Val) and then monitored tripeptide formation (Fig 1A). In this case, the tripeptide MetPheVal was formed only when both eEF2 and eEF3 were added together with TC-Val (Fig 1C). The effect was less dramatic when Phe and Val codons were reverted, as some MetValPhe was also formed in the absence of eEF3, but the addition of eEF3 increased the rate of tripeptide formation by 10-fold, from 0.03/s to 0.3/s (Fig EV1C). Thus, eEF3 is required for the second—and presumably the following—rounds of translation elongation.

To form tripeptide, the ribosome has to move along the mRNA in a step referred to as translocation and then bind the next aminoacyl-tRNA (Fig 1A). In bacteria and higher eukaryotes, the factor that promotes translation, EF-G/eEF2, alone drives the reaction to completion. We then asked the question whether yeast eEF2 or eEF3 alone can promote translocation with longer incubation times. To test this, we incubated 80S 2C with eEF2 or eEF3 alone, or with both factors together, for 15 min and then added TC-Val (Fig 1D). The rate of tripeptide formation was very similar and high with eEF2, or eEF2 and eEF3, about 0.4/s, indicating that eEF2 alone can complete the translocation process given enough time, but to function within physiological timeframes, the reaction requires eEF3. This also indicates that eEF3 is not required for the decoding of the Val codon or peptide bond formation *per se*. Interestingly, eEF3 alone facilitated translocation, albeit only on a fraction of ribosomes, as seen by the endpoint defect (Fig 1D). We speculate that eEF3 on its own promoted tRNA translocation, albeit not to the full extent.

We next specifically studied the role of eEF3 in translocation. Translocation is a dynamic process that entails several steps. Analogous to the well-studied bacterial translocation process (Zhou *et al*, 2014; Belardinelli *et al*, 2016), translocation in yeast likely encompasses the following major steps. (1) Prior to eEF2 binding, the tRNAs move into hybrid states upon peptidyl transfer, with concomitant rotation of the ribosomal subunits. (2) eEF2 binds and

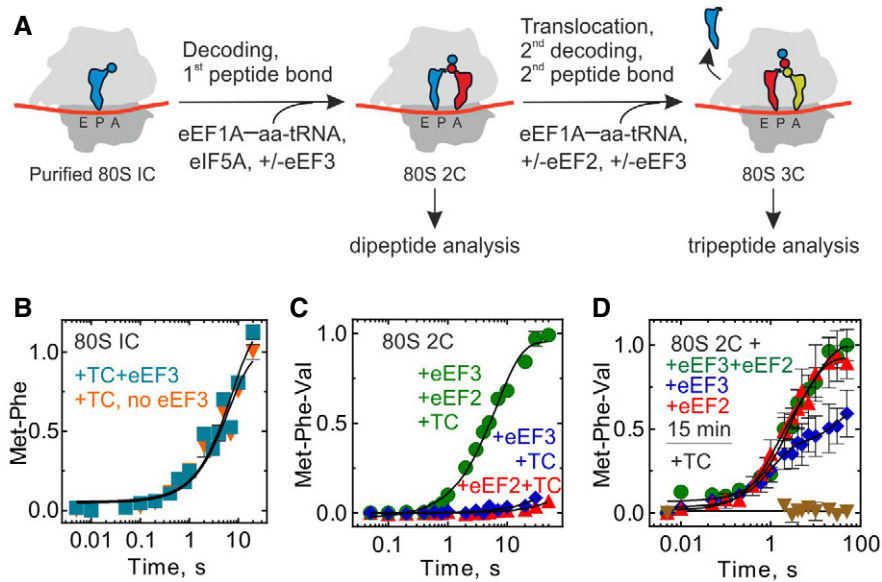


Figure 1. eEF3 is essential for tri- and polypeptide formation.

- A Schematic of the translation elongation cycle as studied here.
- B Met-Phe formation monitored upon rapidly mixing initiation complexes (80S IC) with ternary complexes eEF1A-GTP-[¹⁴C]Phe-tRNA^{Phe} in the absence (orange, 0.13 ± 0.02/s) or presence (cyan, 0.15 ± 0.02/s) of eEF3 (2 μM) in a quench-flow apparatus, and the extent of peptide formation was analyzed by HPLC and radioactivity counting. Data are normalized to Met-Phe formation in the absence of eEF3 with the maximum value in the dataset set to 1. Data are presented as mean ± SEM of n = 3 biological replicates.
- C Met-Phe-Val formation monitored upon rapidly mixing 80S complexes carrying MetPhe-tRNA^{Phe} (80S 2C) with ternary complexes eEF1A-GTP-[¹⁴C]Val-tRNA^{Val} in the presence of eEF2 and eEF3 (green, 0.15 ± 0.01/s), eEF2 (red), or eEF3 (blue). Data presented as mean ± SEM of n = 3 biological replicates.
- D Met-Phe-Val formation monitored with 80S 2C incubated with eEF2 and eEF3 (green, 0.4 ± 0.14/s), eEF2 (red, 1.0 ± 0.5/s), or eEF3 (blue), or in the absence of eEF2 and eEF3 (brown) for 15 min before adding with ternary complexes eEF1A-GTP-[¹⁴C]Val-tRNA^{Val} and monitoring the kinetics of Val incorporation. Data presented as mean ± SEM of n = 3.

Data information: Datasets in (C) and (D) are normalized to Met-Phe-Val formation in presence of eEF2 and eEF3 with the maximum value set to 1. Source data are available online for this figure.

catalyzes movement of tRNAs into the so-called chimeric states, with displacement of the mRNA together with tRNA anticodons on the small subunit and accommodation of the CCA-3' end of the peptidyl-tRNA in the P site (Fig 2A). (3) mRNA and the two tRNAs move to the E and P sites of the small subunit, the small subunit rotates backward relative to the large subunit, and eEF2 and the E-site tRNA dissociate from the ribosome (Fig 2A). One diagnostic test for the completion of step (2) is the reaction of peptidyl-tRNA with the antibiotic puromycin (Pmn). In the absence of translocation (the 80S 2C complex), peptidyl-tRNA does not react with Pmn, even with very long incubation times (Fig 2B, brown triangles). Upon addition of eEF2 and eEF3, or eEF2 alone, peptidyl-tRNA reacts with Pmn. The rate of reaction with puromycin is indistinguishable from that observed for the post-translocation complex prepared by prolonged pre-incubation with the factors (Fig EV1D-F), indicating that eEF2 alone is sufficient to facilitate the early stages of translocation through step (2). We note that in the presence of eEF3 and eEF2, the reaction with Pmn was faster than with eEF2 alone, and the endpoint of the reaction was somewhat lower, suggesting that binding of eEF3 to the ribosome stabilizes a ribosome conformation that influences the efficiency of Pmn reaction, possibly by affecting Pmn binding or by stabilizing peptidyl-tRNA in the exit tunnel (see cryo-EM data below). Also, consistent with the results of the tripeptide synthesis (Fig 1D), eEF3 alone appears to catalyze translocation,

but not to the same extent as in the presence of eEF2 (Fig 2B), which is not increased further with the pre-incubation time (not shown).

E-site tRNA release by eEF3 does not require ternary complex binding

The final step (3) of translocation involves dissociation of deacylated tRNA from the E site (Fig 2A) (Belardinelli et al, 2016). To monitor this step in real time, we used a rapid kinetics assay that follows a fluorescence change of tRNA^{fMet} labeled by fluorescein, tRNA^{fMet}(Flu), upon dissociation from the ribosome (Belardinelli et al, 2016). The tRNA is functionally active in the yeast translation system to the same extent as a non-modified tRNA_i^{fMet}, as validated by the tripeptide formation assay (Fig EV1G). When we initiate translation by rapidly mixing 80S 2C containing tRNA^{fMet}(Flu) and MetPhe-tRNA^{Phe} in the P and A sites, respectively, with eEF2, eEF3, and TC-Val in the stopped-flow apparatus, fluorescence decreases (Fig 2C, green trace). In the process of reaction, addition of eEF2 and eEF3 together with TC-Val leads to a first translocation, Val-tRNA^{Val} binding, next peptide bond formation, followed by a second translocation and the dissociation of tRNA^{fMet} from the E site. At the starting point of the experiment, tRNA^{fMet}(Flu) resides in the P/P or P/E state. The fluorescence change over the time course with eEF2,

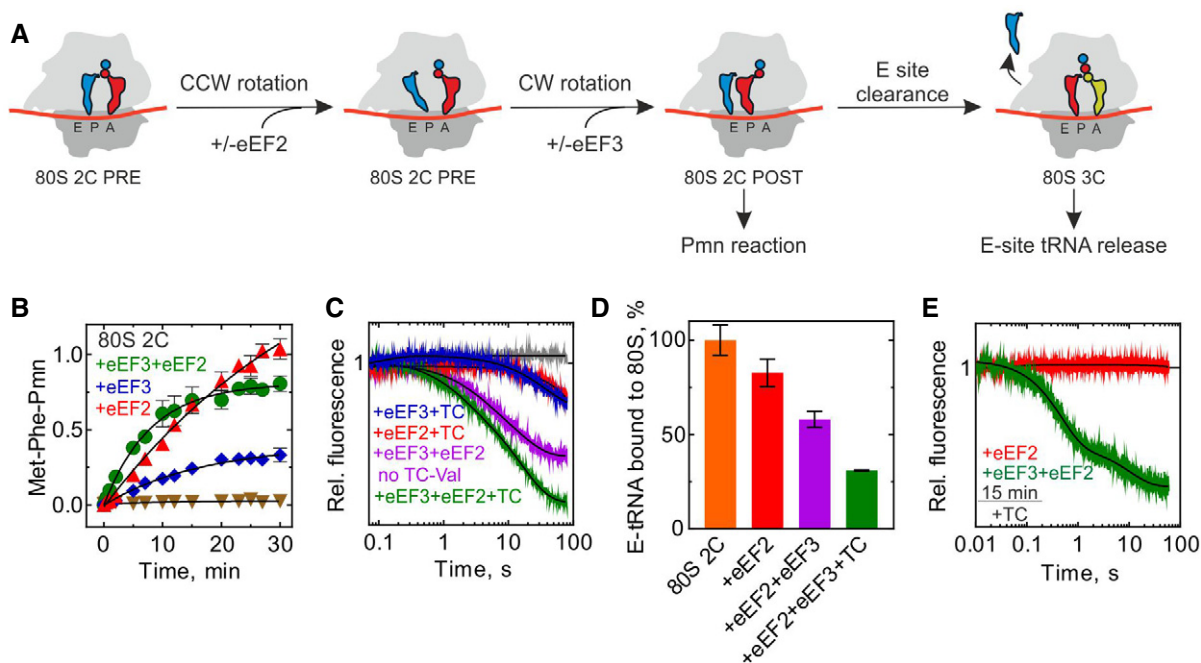


Figure 2. eEF3 in tRNA movement during translocation and E-site clearance.

A Schematic of tRNA translocation.

B mRNA-tRNA translocation monitored in a time-resolved Pmn assay upon mixing 80S 2C with Pmn in the absence (brown triangles) or presence of eEF2 and eEF3 (green, $0.13 \pm 0.01/\text{min}$), eEF2 (red, $0.030 \pm 0.005/\text{min}$), or eEF3 (blue, $0.10 \pm 0.01/\text{min}$). Data are normalized to Met-Phe-Pmn formation in presence of eEF2 with the maximum value set to 1. Data presented as mean \pm SEM of $n = 3$.

C Dissociation of deacylated tRNA from the E site by the fluorescence change of tRNA^{Met}(Flu) upon rapidly mixing of 80S 2C with buffer (gray), or with ternary complexes eEF1A-GTP-[¹⁴C]Val-tRNA^{Val} in the presence of eEF2 and eEF3 (green), eEF2 (red), eEF3 (blue), or eEF2 and eEF3 without the ternary complex (magenta) in a stopped-flow apparatus. Each trace is an average of 5–7 individual time courses and normalized at 1 for the fluorescence at the start of the reaction.

D tRNA^{Met}(Flu) co-eluting with 80S 2C incubated without factors (orange), with eEF2 (red), with eEF2 and eEF3 (magenta), or with eEF2, eEF3, and TC-Val (green) for 15 min before loading on a BioSuite 450 size-exclusion column to separate ribosome-bound and ribosome-unbound tRNA. Data are normalized to tRNA^{Met}(Flu) bound to 80S 2C in the absence of eEF2/eEF3 with the maximum value set to 100%. Data presented as mean \pm SEM of $n = 3$.

E Dissociation of tRNA^{Met}(Flu) from 80S 2C deacylated tRNA incubated with eEF2 and eEF3 (green) or eEF2 (red) for 15 min before adding with ternary complexes. Each trace is an average of 5–7 individual time courses and normalized at 1 for the fluorescence at the start of the reaction.

Source data are available online for this figure.

eEF3, and TC-Val gives the maximum signal difference anticipated upon E-site tRNA dissociation (Fig 2C, green trace). When a similar experiment is carried out in the absence of TC-Val, only the first translocation can occur; we observe that in this case, the fluorescence of tRNA^{Met} decreases considerably, but not to the same extent as when TC-Val is included (Fig 2C, magenta trace). This can reflect some movement of tRNA^{Met}(Flu) to the E site, where it has a somewhat lower fluorescence than in the P site, or a movement to the E site followed by partial dissociation of the tRNA from the ribosome. Addition of eEF3 or eEF2 alone resulted in only a very small fluorescence change (Fig 2C, blue and red traces). These results suggest that eEF2 and eEF3 together facilitate the movement of the E-site tRNA and its ultimate dissociation from the E site. By contrast, eEF2 alone can catalyze partial tRNA displacement (that promotes Pmn reactivity, Fig 2B), but is incapable of promoting dissociation of the E-site tRNA during the short (physiologically relevant) time window.

We further tested whether eEF2 is capable of releasing deacylated tRNA over a long incubation time, as in the tripeptide formation experiment. We incubated 80S 2C (with tRNA^{Met}(Flu)) and

MetPhe-tRNA^{Phe}) with eEF2 and eEF3 or with eEF2 alone for an extended period (15 min) and monitored how much tRNA^{Met}(Flu) is retained by the ribosome by following the fluorescence co-eluting with the ribosomes during gel filtration (Fig 2D). Upon 15-min incubation with eEF2 alone, very little tRNA is released (Fig 2D, orange and red bars). Upon incubation with eEF2 and eEF3, a significant fraction of tRNA^{Met}(Flu) is released during gel filtration, suggesting labile binding of the E-site tRNA (magenta). Addition of eEF2, eEF3, and TC-Val, which results in two rounds of translocation and should remove the E-site tRNA from all active ribosomes, results in about 70% tRNA^{Met}(Flu) dissociation (Fig 2D, green bar). To further test the E-site dissociation in a time-resolved way, we also monitored tRNA^{Met}(Flu) dissociation in a stopped-flow experiment (Fig 2E). No fluorescence change is observed when TC-Val is added to 80S 2C incubated with eEF2 alone (Fig 2E, red trace), although from the kinetics of tripeptide formation we observe that under these conditions, eEF2 alone promotes partial tRNA translocation (Fig 1D, red triangles). These experiments clearly establish that binding of the cognate TC into the A site following eEF-2 catalyzed translocation is not sufficient to promote dissociation of the E-site tRNA, in contrast

to previous suggestions (Triana-Alonso *et al*, 1995). Thus, eEF2 promotes partial translocation by facilitating movement of peptidyl-tRNA from the A to P site, which also implies that the deacylated tRNA has to move toward the E site, but does not allow the release of the deacylated tRNA from the ribosome. The role of eEF3 is to facilitate the late stages of translocation by promoting the dissociation of the deacylated tRNA from the E site, but has little effect on A-site binding (Figs 1D and 2D).

Ribosome profiling of eEF3-depleted yeast cells

Having shown *in vitro* that eEF3 is essential for late steps of translocation, we corroborated our findings *in vivo* using polysome and ribosome profiling. Because eEF3 is an essential gene in budding yeast, to observe its function *in vivo* we developed a system to conditionally deplete eEF3 using transcriptional shutoff and an auxin degron tag (maID) as described previously (Nishimura *et al*, 2009; Schuller *et al*, 2017). In the eEF3 depletion strain (dubbed eEF3d), expression of eEF3 is controlled by a *GAL1* promoter that is turned off in the presence of glucose. Following a switch to glucose in the media and the addition of auxin, eEF3 was not detectable by immunoblotting after 8 h (Fig EV2A). As anticipated based on its essential nature, depletion of eEF3 reduces cell growth compared to wild-type (WT) cells (Fig EV2B). Furthermore, we performed polysome run-off experiments (i.e., without elongation inhibitors included during lysis) and observed slightly increased polysome-to-monomosome ratios, indicative of defective translation elongation in the absence of eEF3 (Fig EV2C).

We next prepared libraries of ribosome footprints from WT and eEF3d strains after 8 h of conditional growth. Our recent study showed that using combinations of elongation inhibitors for library preparations allows us to distinguish three distinct ribosome functional states—pre-accommodation (PreAcc), pre-peptide bond formation (PrePT), and pre-translocation (PreTrans)—from different sized ribosome-protected footprints (RPFs) (Wu *et al*, 2019b) (Fig 3A). In a first set of experiments, we prepared libraries with a combination of cycloheximide (CHX) and tigecycline (TIG) added to cellular lysates to prevent interconversion between ribosome elongation states; CHX blocks translocation whereas TIG blocks aa-tRNA accommodation in the A site as indicated (Schneider-Poetsch *et al*, 2010; Jenner *et al*, 2013) (Fig 3A). In these libraries, 21 nt RPFs correspond solely to ribosomes with an empty A site on the small subunit, e.g., in a PreAcc state, whereas 28 nt RPFs predominantly correspond to ribosomes trapped in a PreTrans state (Fig 3A). In WT cells, we observe a distribution of 21 and 28 nt RPFs genome-wide, suggesting that no single step of translation elongation is rate-limiting under normal circumstances, but that instead ribosomes are found in a relatively even distribution of functional states (Fig 3B, black line). By contrast, in eEF3d cells, we observed a drastic reduction in 21 nt RPFs (and a concomitant increase in 28 nt RPFs) when compared to WT cells (Fig 3B), indicating an accumulation of ribosomes in either a PrePT or PreTrans state. This observation establishes a role for eEF3 in translation elongation, as its depletion causes a genome-wide change in the distribution of ribosome functional states. More specifically, the reduction in 21 nt RPFs in eEF3d cells is indicative of an increase in ribosomes with A sites occupied by aa-tRNAs. These data suggest that either peptide bond formation or translocation becomes rate-limiting *in vivo* in the absence of eEF3.

To determine the *in vivo* rate-limiting step (i.e., peptide bond formation or translocation) in the absence of eEF3, we next prepared libraries using a combination of CHX and anisomycin (ANS). Because ANS blocks peptidyl transfer (Grollman, 1967), 28 nt RPFs in these libraries report solely on ribosomes in a PreTrans state, whereas 21 nt RPFs correspond to ribosomes either in a PreAcc or PrePT state due to dissociation of the unreacted aa-tRNA from the A site (Fig 3C). As anticipated, libraries prepared from WT cells revealed a distribution of 21 and 28 nt RPFs, but with a slightly greater number of 21 nt RPFs than libraries prepared with CHX + TIG (Wu *et al*, 2019b). We further found that the footprints from eEF3d cells are almost devoid of 21 nt RPFs when compared to the WT samples prepared with CHX + ANS (Fig 3D). These data indicate that neither tRNA selection nor peptide bond formation is rate limiting in the absence of eEF3 but rather a step specific to translocation. In addition, we found that the modest association between eEF1A or eEF2 and the elongating ribosomes was not influenced by eEF3 depletion as monitored by polysome profiles and immunoblotting (Fig EV2D). Taken together, our experiments argue that eEF3 promotes the translocation step of elongation, consistent with our *in vitro* data (Fig 2B).

Codon level analysis of ribosome functional states in the eEF3d strain

In addition to global changes in the distribution of ribosome functional states, we asked whether ribosomes are disproportionately stalled at specific sites. By calculating A-site ribosome occupancies (i.e., pause scores) of 21 nt RPFs (from samples prepared with CHX + TIG) at all 61 sense codons, we observed a distribution of pause scores in WT cells, and a drastic reduction in this distribution in eEF3d cells; as a result, we see a nearly horizontal line comparing these different distributions with a slope of 0.18 (Fig 3E). Different ribosome occupancies on codons, i.e., “codon optimality”, is thought to be determined by several factors including codon usage, cellular tRNA concentrations, and the efficiency of wobble pairing (Percudani *et al*, 1997; dos Reis *et al*, 2004). For example, pause scores at rare codons (such as CGA) are substantially higher than those at common codons (such as AGG) in WT cell (Fig 3E and F), as shown in earlier studies (Weinberg *et al*, 2016; Wu *et al*, 2019b); these differences are however substantially smaller in eEF3d cells (Fig 3F, quantified by variance). Importantly, because the calculation of ribosome occupancies (pause scores) at codons from ribosome profiling experiments relies on internal normalization (i.e., an increase in ribosome occupancy at one codon necessarily reduces those at other codon(s)), we do not interpret the absolute values of these numbers in any manner. Given that 21 nt RPFs from samples prepared with CHX + TIG represent ribosomes poised for decoding (Fig 3A), these observations suggest that in the absence of eEF3, a step preceding decoding has become rate limiting, thereby reducing the decoding rate in the A site in a global manner such that codon-specific differences are lost (Fig 3F, e.g., AGG versus CGA).

We similarly characterized 28 nt RPFs in libraries prepared with CHX + ANS (Fig 3D), focusing on whether there are any sequence motifs that tend to be enriched in the PreTrans state (Fig 3C); in these libraries, 28 nt RPFs represent ribosomes trapped in a

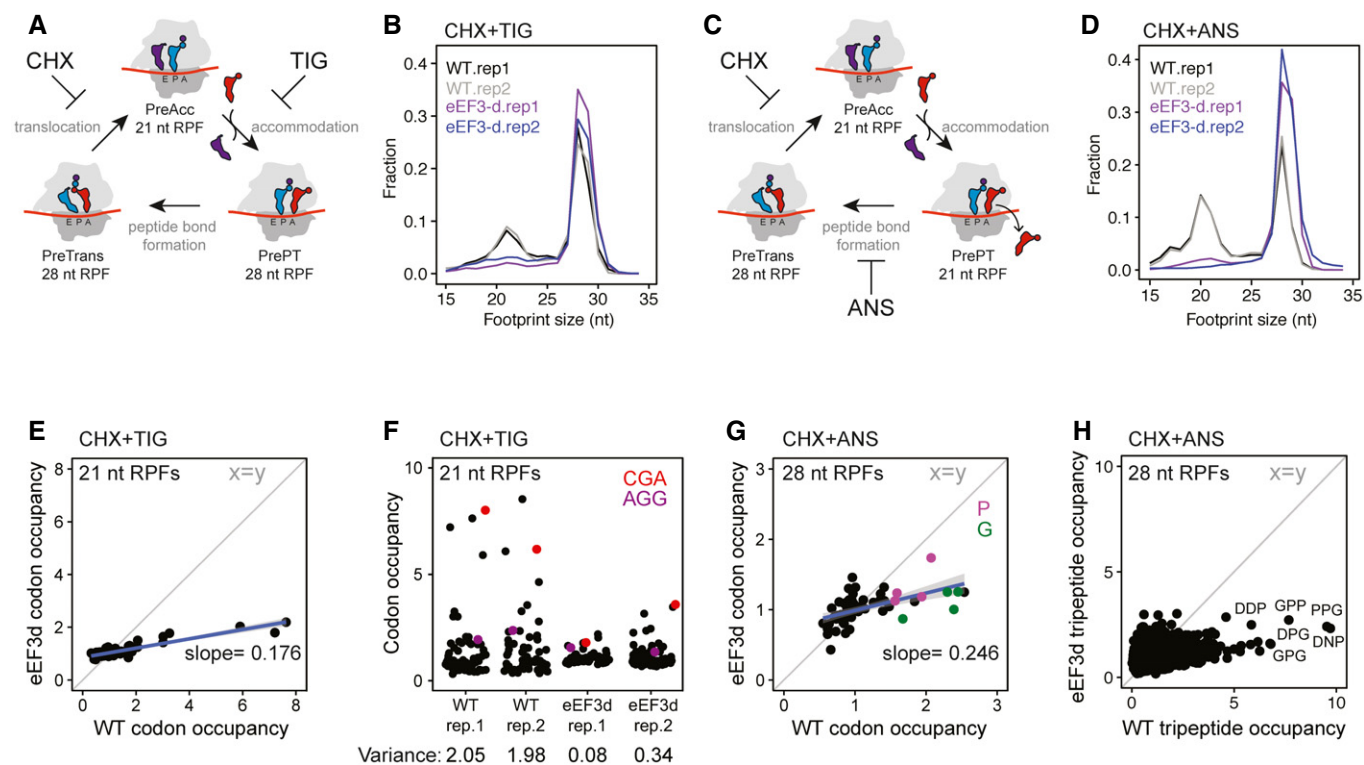


Figure 3. eEF3 depletion perturbs translation elongation transcriptome-wide.

- A Schematic representation of the eukaryotic elongation cycle with ribosome footprint sizes to illustrate the functional states isolated by CHX + TIG. PreAcc, pre-accommodation; PrePT, pre-peptide bond formation; PreTrans, pre-translocation.
- B Size distributions of ribosome footprints for WT (black and gray) and eEF3d (purple and blue) cells from libraries prepared with CHX + TIG. Two biological replicates are shown.
- C Similar to (A), with footprint sizes isolated by CHX + ANS.
- D Similar to (B), from libraries prepared with CHX + ANS.
- E Scatter plot of codon-specific ribosome occupancies for 21 nt RPFs comparing eEF3d to WT cells from libraries prepared with CHX + TIG. Trend line (blue) and its slope are shown. The diagonal line indicates the distribution expected for no change.
- F Codon-specific ribosome occupancies for 21 nt RPFs from WT and eEF3d cells (two biological replicates). CGA and AGG codons are shown in red and purple, respectively. Variance for each dataset is indicated.
- G Scatter plot of codon-specific occupancies for 28 nt RPFs comparing eEF3d to WT cells from libraries prepared with CHX + ANS. Trend line (blue) and its slope are shown. Codons that encode proline and glycine are colored in purple and green, respectively.
- H 28 nt RPF-ribosome occupancies of 5,771 tripeptide motifs are plotted for WT and eEF3d cells, for motifs more than 100 occurrences in yeast transcriptome. Motif sequences enriched upon eIF5A depletion are labeled.

PreTrans state. First, in the WT cells, we found a distribution of codon-specific occupancies that differ by as much as threefold; among the most enriched codons are those that correspond to those encoding proline (P, purple) and glycine (G, green) (Fig 3G). Second, as for our analysis of the 21 nt RPFs (Fig 3E), we observed a loss of codon-specific differences in ribosome occupancy when eEF3 is depleted, as evidenced by a flattening of the correlation plot (slope 0.25). Further analysis of peptide motifs revealed that among 8,000 tripeptides, the most enriched sequences were those encoding collections of P, G, and D amino acids (Figs 3H and EV2E). These observations are reminiscent of sequences that depend on eIF5A for peptide bond formation (Pelechano & Alepuz, 2017), (Schuller *et al.*, 2017), though here we are seeing that these same sequences are slowing the translocation step of protein synthesis. Consistent with the results of *in vitro* biochemistry, we conclude that eEF3 contributes to the translocation step of protein synthesis, and in its absence, an early step in the process becomes rate limiting.

A native structure of eEF3 on the yeast 80S ribosome

To investigate a physiologically relevant structure of eEF3 on the yeast 80S ribosome at different phases of the elongation cycle, we opted to obtain eEF3-80S complexes by employing a native pull-down approach using C-terminally TAP-tagged eEF3. The distant location of the C terminus with respect to the ribosome (Appendix Fig S2A and B), and the lack of effect of the C-terminal TAP-tag has on growth compared to the wild-type strain (Appendix Fig S2C–E), suggests that it has little if any effect on eEF3 function and therefore would be appropriate for obtaining native eEF3-80S complexes. Thus, to isolate native eEF3-80S complexes, a *S. cerevisiae* BY4741 strain expressing C-terminally TAP-tagged eEF3 was grown to log phase and eEF3-80S complexes were isolated using IgG-coupled magnetic beads (Fig 4A). The complex was eluted by TEV protease cleavage of the TAP-tag in the presence or absence of non-hydrolyzable ADPNP, and, in both cases SDS-PAGE

analysis indicated the presence of ribosomal proteins in addition to eEF3 (Appendix Fig S2F). By contrast, no ribosomal proteins were observed in a control purification performed using an untagged wild-type strain, suggesting that the ribosomal complexes observed in the TAP-tagged strains co-purified with the eEF3 (Appendix Fig S2F). The eluate containing the native eEF3-80S complexes, in the presence of ADPNP, was cross-linked with glutaraldehyde and directly applied to cryo-grids. It is important to note that in the absence of cross-linker, reconstructions yielded 80S ribosomes, but without additional density for eEF3, suggesting that eEF3 dissociated from the ribosomes during grid application. The native eEF3-80S complex was then analyzed using single-particle cryo-EM. After 2D classification, 211,727 ribosomal particles were initially sorted into eight classes, two of which had strong density for eEF3 (I: class 1 and 2), one had density for eEF2 and a weak density for eEF3 (II: class 3), two had weak density for eEF3 (III: class 4 and 5), and the remaining three classes (IV: class 6–8) were poorly defined and had low resolution (Appendix Fig S3). The two classes (I: class 1 and 2) with strong density for eEF3 were combined and a local mask was applied around eEF3 and a second round of focused sorting and refinement was undertaken, eventually yielding a cryo-EM reconstruction of the eEF3-80S complex (Fig 4B and Movie EV1) with an average resolution of 3.3 Å (Appendix Fig S4A). Local resolution calculations reveal that while the majority of the ribosome is well resolved (Appendix Fig S4B and C), the resolution of eEF3 varies, with ribosome-interacting regions being better resolved (3–4 Å) than the peripheral regions (4–6 Å) (Appendix Fig S4D). As observed in the previous eEF3-80S structure (Andersen *et al*, 2006), density for eEF3 spans between the head of the 40S subunit and the central protuberance of the 60S subunit (Fig 4B). We therefore also employed multi-body refinement (Appendix Fig S3), which led to slight improvements in the local resolution for the region of eEF3 that interacts with the head of the 40S subunit (Appendix Fig S4E–H). The resolution allowed an accurate domain-by-domain fit of the previous 2.4 Å X-ray structure of yeast eEF3 (Andersen *et al*, 2006) into the cryo-EM density map of the eEF3-80S complex (Appendix Fig S4A, S5A–C and Movie EV1). Electron density for many side chains could be observed, especially bulky and aromatic amino acids (Appendix Fig S5A–C), enabling us to generate an initial model for the N-terminal HEAT domain, as well as C-terminal ABC1/2 and CD. By contrast, the more peripheral 4HB domain was poorly resolved and was modeled only at the secondary structure level, and the final 68 residues of the C terminus including the TAP-tag had no density and were therefore not included in the model. We note that electron density consistent with ATP (or ADPNP) was observed in the active sites of the ABC1 and ABC2 nucleotide-binding domains (NBDs) (Appendix Fig S5D–K). This is consistent with the closed conformation we observed for ABC1 and ABC2 NBDs, which is similar to the closed conformations adopted in the 70S-bound ABCF protein VmlR from *B. subtilis* (Crowe-McAuliffe *et al*, 2018) and archaeal ABCE1-30S post-splitting complex (Nurenberg-Goloub *et al*, 2020), but distinct from the open conformation observed for the free state of ABCE1 (Barthelme *et al*, 2011) (Fig EV3A–D). Indeed, modeling of an open conformation of eEF3 on the ribosome suggests that it is incompatible with stable binding, leading to either a clash of the HEAT repeat region and the ABC2-CD with the 40S head and the central protuberance of the 60S subunit, respectively, or dissociation of the ABC1-HEAT-4HB domain from

the 40S subunit (Fig EV3E–J). These observations support the idea that eEF3 binds to the ribosome in the “closed” ATP-bound conformation and that ribosome-stimulated hydrolysis of ATP to ADP, with the associated conformational change into the open conformation, would destabilize eEF3 binding and promote dissociation (Chakraborty, 1999).

Interaction of eEF3 on the yeast 80S ribosome

The overall geometry of eEF3 on the 80S ribosome is similar to that reported previously for eEF3 (Andersen *et al*, 2006), as well as its homologue in yeast New1p (Kasari *et al*, 2019b), namely oriented such that the N-terminal HEAT interacts with the 40S subunit, whereas the C-terminal CD contacts exclusively the 60S subunit (Fig 4C–E). With the improved resolution compared to the previous eEF3-80S structure (Andersen *et al*, 2006), details of the interactions of eEF3 with the ribosomal components can now be more accurately described. As with New1p (Kasari *et al*, 2019b), the majority of the contacts with the 40S subunit are established by the HEAT domain of eEF3 with components of 40S head including the tip of ES39S of the 18S rRNA as well as r-proteins uS13 and uS19 (Figs 4D and E, and EV4A–D). The majority of the interactions involve positively charged residues located within the loops linking the HEAT repeat α -helices, such as Lys101 (loop α 3– α 4), Lys141 (loop α 5– α 6), and Lys182 (loop α 7– α 8) that are in close proximity to the nucleotides A1360 and U1361 of ES39S (Fig EV4C). Interactions are also observed between the HEAT domain loops (Gln143, Asp180, Glu184) with charged residues (Gln25, Arg130, Asp127, and Arg134) of eS19 (Fig EV4C). The distal end of the HEAT domain (conserved residues 302–307, Glu304, Arg306, Glu307) also establishes interactions with uS13 in the vicinity of His78 and Arg80 (Fig EV4D). The 4HB and ABC1 domains of eEF3 do not interact with any ribosomal components, whereas ABC2 bridges the inter-subunit space by forming protein–protein interactions with uS13 on the 40S involving Arg871 and Arg872 (Fig EV4D) and uL5 and uL18 on the 60S subunit (Fig EV4E and F). In addition, the loop between the β 2 and β 3 strands of the CD contains positively charged residues (Arg802, Arg803, Lys804, Lys806, and Asn807) that appear to interact with nucleotides U32-G41 of the 5S rRNA (Fig EV4F).

eEF3 facilitates E-site tRNA release by opening the L1 stalk

To address which functional states of the ribosome are stably bound by eEF3, we implemented additional rounds of 3D classification of the classes with strong density for eEF3 (group I: classes 1 and 2), but with a focus on the L1-stalk and tRNAs (Appendix Fig S3). This yielded four subclasses (Ia–Id) that all exhibited strong density for eEF3, but differed with respect to their functional state. Of these four classes, two pre-translocation (PRE) states were observed that could be refined to 3.5 and 4.0 Å, respectively (Fig 5A and B). PRE-1 contained classical A- and P-site tRNAs, whereas PRE-2 contained a classical A-site tRNA and a hybrid P/E-site tRNA. In both PRE-1 and PRE-2, density for the nascent polypeptide chain could be observed extending from the A-site tRNA and entering into the ribosomal exit tunnel (Fig 5A and B). Since eEF3 has been suggested to play a role in the dissociation of E-site tRNA from the ribosome, the observation of eEF3 bound to various PRE-state ribosomes was surprising and the implication of this with respect to dissociation of eEF3 from

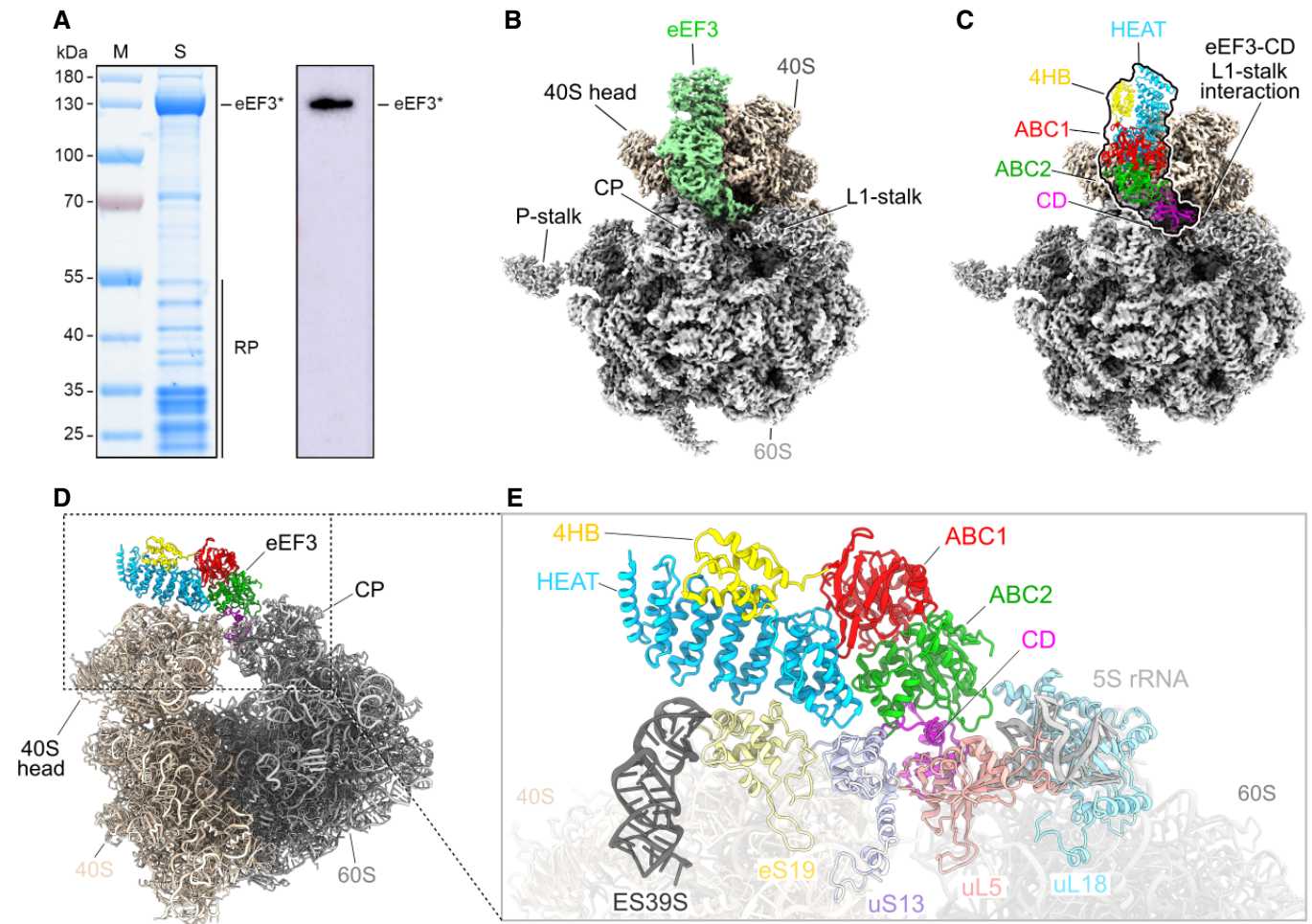


Figure 4. eEF3 in complex with the *Saccharomyces cerevisiae* 80S ribosome.

- A** SDS gel and Western blot of the native pull-out from *S. cerevisiae* TAP-tagged eEF3. eEF3* labels the TEV cleavage product of eEF3-TAP, which still carries the calmodulin binding peptide of the TAP-tag and which is recognized by the antibody. RP, ribosomal proteins.
- B** Cryo-EM reconstruction of the native eEF3-80S complex with segmented densities for the 60S (gray), the 40S (tan), and eEF3 (pastel green).
- C** Fitted eEF3 molecular model colored according to its domain architecture, HEAT (blue), 4HB (yellow), ABC1 (red), ABC2 (green), and CD (magenta).
- D, E** (D) Overview on the eEF3-80S molecular model and (E) zoom illustrating eEF3 and its ribosomal interaction partners. ES39S (dark gray), eS19 (pale yellow), uS13 (pastel violet), uL5 (coral), uL18 (light blue), 5S rRNA (light gray).

the ribosome will be discussed later where we focus on the identification of PRE-3, PRE-4, and POST-1 states that lack clear density for eEF3. In addition to the PRE-state complexes, two post-translocation (POST) state ribosomes were obtained, POST-2 and POST-3, which could be refined to 3.9 and 3.8 Å, respectively (Fig 5C and D). POST-2 contained classical P- and E-site tRNAs, whereas POST-3 contained a P-site tRNA, but lacked an E-site tRNA (Fig 5C and D). In both the POST-2 and POST-3 states, density for the nascent polypeptide chain could also be visualized attached to the P-site tRNA (Fig 5C and D). The presence and absence of E-site tRNA in the POST-2 and POST-3, respectively, suggested that these complexes could represent the states before and after eEF3-mediated E-site tRNA release, respectively. Consistent with this hypothesis, the L1 stalk is observed in a closed conformation in POST-2 that would prohibit release of the E-site tRNA from the ribosome. We term this closed conformation L1-“int” for intermediate since it is

not as closed as the L1-“in” conformation observed in the classical POST-1 state (Fig EV5A–D). By contrast, in POST-3 the L1 stalk has moved into an open or L1-“out” conformation that would enable E-site tRNA dissociation (Fig 5E and F). In POST-2, we observe no direct interaction between eEF3 and the E-site tRNA, but rather between the CD of eEF3 and the L1 stalk (Fig 5G and H). Specifically, the contact between eEF3 and the L1 stalk is from the tip of the CD with domain II of the uL1 protein (Fig 5H). Unfortunately, the L1 region is poorly ordered due to high flexibility, nevertheless, it appears that the interactions are dominated by charge complementarity between the conserved glutamates (Glu790, Glu819 and Glu826) in the CD that are in close proximity to a highly conserved lysine-rich region (Lys91–92, Lys95, Lys97–98, Lys101–102, Lys105–106) present in domain II of uL1 (Fig 5H). The large number of lysine residues in this region of uL1 is intriguing since CD are best known from chromatin remodeling proteins where they bind to

methylated lysines (me-K) present in histone tails (Nielsen *et al*, 2002; Taylor *et al*, 2007; Yap & Zhou, 2011). Methylation of few non-histone proteins has been reported, one of which is the uL1 protein that is methylated on a single lysine (me-K46) (Webb *et al*, 2011); however, K46 is located in domain I of uL1, far from the CD interaction site (Fig EV5E and F). Moreover, the hydrophobic pocket that is generally formed by three aromatic residues to interact with the me-K, does not appear to be present in eEF3 (Fig EV5G–I). Collectively, our findings imply that eEF3 is likely to facilitate E-site tRNA release (as we observe biochemically, Fig 2D) indirectly by promoting the transition of the L1 stalk from the “in” to the “out” conformation (Fig 5E and F), rather than from directly using the CD to dislodge the E-site tRNA from its binding site.

eEF3 binds stably to non-rotated ribosomal states

We noted that although eEF3 bound stably to a mixture of different PRE and POST states (Fig 5A–D), these ribosomal states nevertheless had a common feature in that they are all non-rotated, i.e., they have a non-rotated 40S with respect to the 60S subunit. This non-

rotated state is critical for eEF3 to establish simultaneous interactions with the ES39S, uS13 and eS19 on the head of the 40S as well as the 5S rRNA, uL5 and uL18 on the 60S subunit, as described for the high-resolution eEF3-80S complex (Figs 4D and E, and EV4), thereby providing an explanation for the strong density observed for eEF3 in the non-rotated PRE-1/-2 and POST-2/-3 state. To explore this idea further, we also analyzed the classes where the density for eEF3 was poorly resolved (Appendix Fig S3, group II and III). Refinement of group II (class 3) to an average resolution of 4.1 Å yielded an eEF2-bound ribosome with chimeric ap/P- and pe/E-tRNAs (POST-1) and poorly defined density for eEF3 (Fig 6A). In addition to intersubunit rotation by 8.5°, we also observed a counter-clockwise (toward the E site) head swivel of 20° (Fig 6B). As expected, the rotation and head swivel movements have a large impact on the eEF3-binding site, namely moving the 40S interaction partners, such as ES39S, eS19, and uS13, by 16 Å for the rRNA, 17 Å for eS19 up to 27 Å for uS13 relative to the 60S and their position in the non-rotated ribosome (e.g., POST-3) (Appendix Fig S6A and B). Closer inspection of the density for eEF3 in POST-1 indeed revealed that the majority of the density remains associated with the

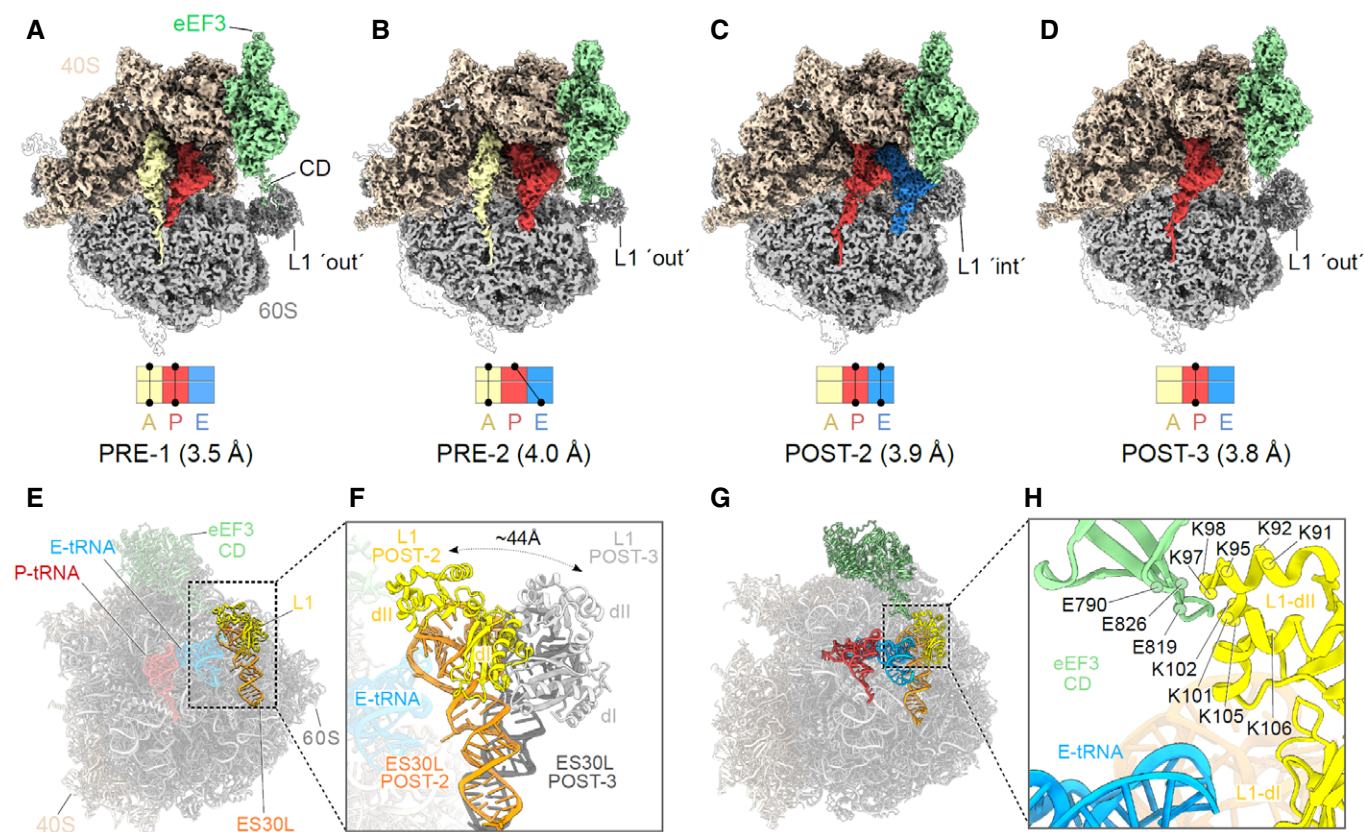


Figure 5. eEF3 bound to a non-rotated 80S ribosome.

A–D Cryo-EM maps of eEF3 bound to non-rotated ribosomal species with isolated densities for the 60S, 40S and eEF3 (colored as in Fig 1), as well as the A- (pale yellow), P- (red), and E-tRNA (blue). The eEF3 ligand is binding the ribosome in the pre-translocational (PRE) state termed as (A) PRE-1 (A/A-, P/P-tRNA) and (B) PRE-2 (A/A-, P/E-tRNA) as well as to the post-translocational (POST) version named (C) POST-2 (P/P-, E/E-tRNA) and (D) POST-3 (P/P-tRNA).
 E, F (E) Overview of the POST-2 eEF3-80S molecular model highlighting the L1 protein (yellow) and ES30L (orange) and its (F) zoom depicting the magnitude of the L1-stalk movement from the POST-2 state (L1-stalk' int') to the POST-3 state (L1-stalk' out'). L1-POST3 (light gray), ES30L-POST3 (dark gray).
 G Different view of the model shown in (E) highlighting eEF3, L1, ES30L as well as the P/P- and E/E-tRNA.
 H Zoom of (C) showing the contact of the eEF3-CD and the L1 protein as well as the distance of both to the E-tRNA. The residues are displayed as circles and labeled.

60S and that both rotation and swiveling causes a loss of connectivity between eEF3 and the head of the 40S (Appendix Fig S6C). Since there is defined density for eEF3 in the non-rotated POST-2 and POST-3, but eEF3 is disordered in the eEF2-bound rotated POST-1 state, this indicates that stable binding of eEF3 occurs during or subsequent to eEF2 dissociation from the ribosome when the 40S resets and the ribosome returns to a non-rotated and non-swiveled conformation. We suggest that eEF3 facilitates late stages of translocation by stabilizing the non-rotated state after eEF2 has promoted the movement of the tRNA–mRNA complex (Fig 1D).

Intersubunit rotation leads to unstable eEF3 binding on the ribosome

Further sorting and refinement of group III (Appendix Fig S3, classes 4 and 5) yielded two distinct PRE states, namely PRE-3 containing a classical A-site tRNA and a hybrid P/E-site tRNA, and PRE-4

containing hybrid A/P- and P/E-site tRNAs (Fig 6C and D), which could be refined to average resolutions of 4.2 and 3.3 Å, respectively. Analogous to PRE-1 and PRE-2, both PRE-3 and PRE-4 states also had density for the nascent polypeptide chain extending from the A-site tRNA into the ribosomal exit tunnel (Fig 6C and D). However, unlike PRE-1 and PRE-2, the 40S in PRE-3 and PRE-4 was rotated by 9.6° and 11° relative to the 60S subunit (Fig 6E and F). In the PRE-3 state, little to no density for eEF3 was observed (Fig 6C), suggesting that the factor had dissociated from the ribosome during sample and/or grid preparation. While significant density was observed for eEF3 in PRE-4, the density was poorly resolved (Fig 6D). Analogous to POST-1, the rotation observed in PRE-3 and PRE-4 appears to also disrupt the interactions with the 40S subunit such that the majority of the eEF3 density is connected to the 60S subunit (Appendix Fig S6D–I). Collectively, this supports the suggestion that stable binding of eEF3 to the ribosome requires a non-rotated state and that intersubunit rotation leads to

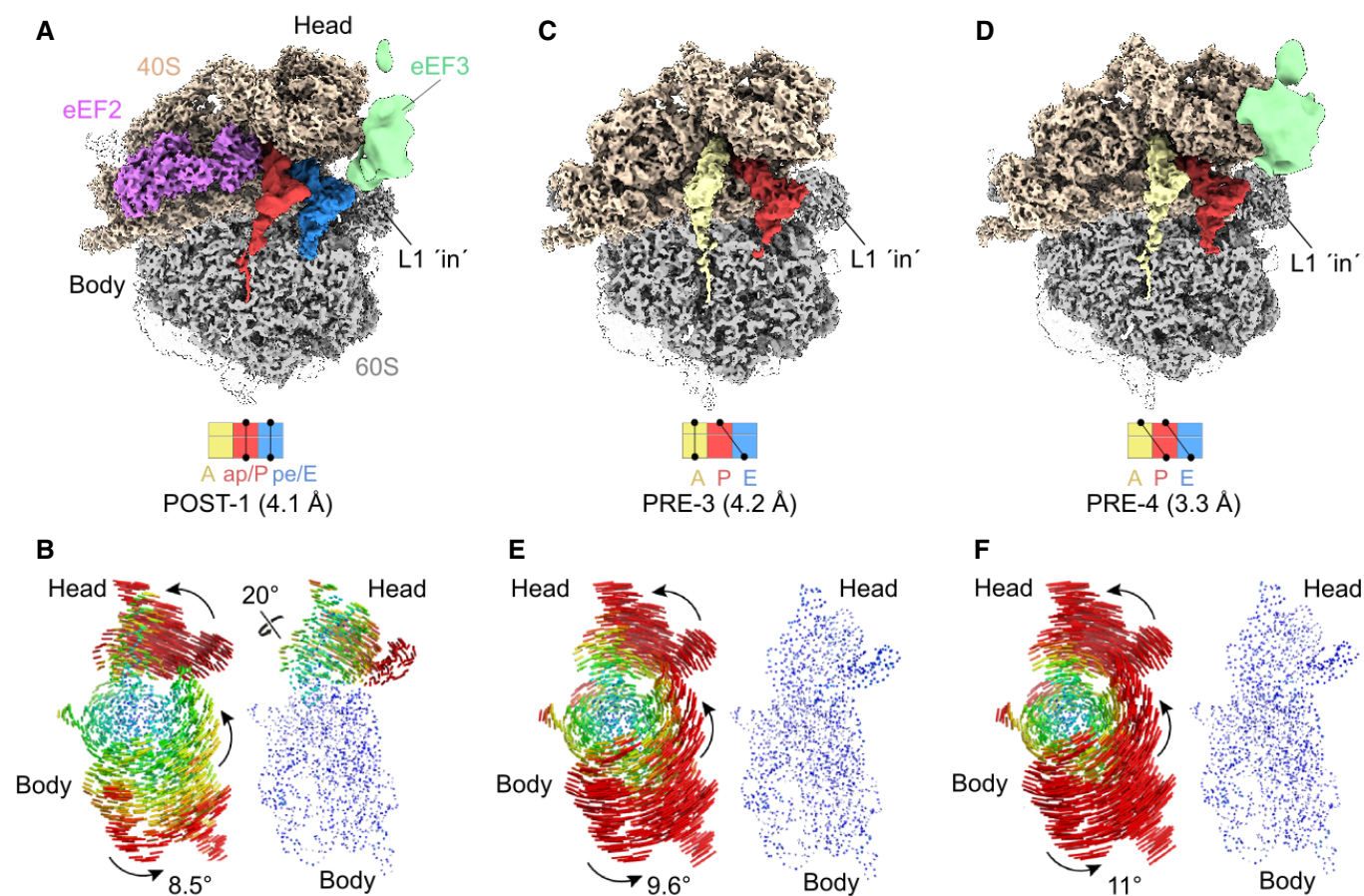


Figure 6. Rotated *Saccharomyces cerevisiae* ribosome partially bound by disordered eEF3 ligand.

- A Cryo-EM reconstruction of the eEF2 bound 80S ribosome adopting a rotated POST-1 state bearing chimeric ap/P- and pe/E-tRNA as well as a disordered eEF3.
- B Subunit rotation and head swivel observed in the *S. cerevisiae* eEF3-80S complex derived from the selected class from the 3D classification shown in (A). 18S rRNA structures illustrating the degree of rotation of the small subunit relative to the large subunit based alignments of the large subunit from a non-rotated structure reference (PDB ID: 6SNT) (Matsuo *et al*, 2020). The degree of head swiveling (right side) is illustrated based on alignments of the 18S rRNA body from a non-headed swivel reference structure (PDB ID: 6SNT) (Matsuo *et al*, 2020).
- C, D 80S ribosome in rotated (C) PRE-3 state containing an A/A- and P/E-tRNA and (D) PRE-4 state bearing the hybrid A/P- and P/E-tRNA and bound by the disordered eEF3 ligand.
- E, F Representation of the rotation of the subunit and the 40S-head swivel shown for volumes depicted in (C) and (D), respectively.

destabilization of eEF3 binding (Fig 6C and Appendix Fig S6F). eEF3 remains stably bound to the ribosome subsequent to E-site tRNA release and is still stably bound when the next aminoacyl-tRNA has accommodated into the A site and undergone peptide bond formation. Rather it appears that the critical step that leads to conformational rearrangements in eEF3 is the transition from non-rotated to rotated states. In this respect, it is interesting to note that PRE-3 has the same tRNA arrangement as PRE-2, namely both containing a classical A-site tRNA with nascent chain and a deacylated hybrid P/E-site tRNA, yet adopt completely different rotational states (Figs 5B and 6C). This is somewhat surprising since formation of hybrid states in higher eukaryotes is generally assumed to be concomitant with intersubunit rotation (Budkevich *et al*, 2011; Svidritskiy *et al*, 2014; Behrmann *et al*, 2015); however, we note that subunit rotation and tRNA movement is only loosely coupled on bacterial ribosomes (Fischer *et al*, 2010). Since rotation of PRE-2 would result in a state similar to PRE-3, we suggest that subunit rotation is what triggers the low affinity form of eEF3, effectively leading to unstable ribosome binding.

Discussion

Collectively, our findings suggest a model for the role of eEF3 during the translocation elongation cycle (Fig 7A–G and Movie EV2). The ability to capture four different PRE and three different POST states of the ribosome by co-immunoprecipitation of tagged eEF3 suggests that eEF3 is omnipresent during translation elongation in yeast, which is consistent with the similar copy number between eEF3 and ribosomes (Firczuk *et al*, 2013). Our biochemical data show that the main function of eEF3 is to accelerate the E-site tRNA release from the ribosome during late stages of mRNA-tRNA translocation (Figs 1 and 2). These *in vitro* findings are in strong agreement with the *in vivo* ribosome profiling experiments. Similar to previous studies where eEF3 was depleted in the cell (Kasari *et al*, 2019a), we observe general defects in translation elongation. However, our application of high-resolution ribosome profiling, using combinations of elongation inhibitors for library preparation, allowed us to follow ribosomes trapped in distinct functional states and thereby identify the specific elongation defect (Fig 3). In particular, we find that eEF3 depletion enriched ribosomes trapped in a pre-translocation state (28 nt RPFs), fully consistent with the observation that eEF3 promotes a late step in translocation that depends on E-site tRNA release. A strong prediction of the biochemical and ribosome profiling results is that the ribosomes that accumulate in cells on eEF3 depletion would contain three separate tRNAs.

Cryo-EM structures suggest two mechanisms by which eEF3 can facilitate translocation, namely by favoring the transition toward the non-rotated conformation of the ribosome and by influencing the conformation of the L1 stalk. As in all kingdoms of life, yeast eEF2 stabilizes the rotated state of the ribosome and accelerates the movement of the peptidyl-tRNA from the A to the P site (Fig 7D and E). In bacteria, the eEF2 homolog EF-G promotes the small subunit head swiveling, which allows the mRNA-tRNAs to move relative to the large subunit (Zhou *et al*, 2014; Belardinelli *et al*, 2016; Wasserman *et al*, 2016). Resetting the swiveled conformation triggers the release of EF-G and the E-site tRNA, which occurs rapidly on a

millisecond time scale (Belardinelli *et al*, 2016), and does not require auxiliary factors. The present structures suggest which features of the mechanism are conserved in yeast. Similar to EF-G, eEF2 catalyzes head swiveling and mRNA-tRNA translocation (Fig 7E), whereas dissociation of the factor and back-swivel occur in a later step (Fig 7E and F). The cryo-EM observation of discrete POST-1 and POST-2 states suggests that this transition is relatively slow in yeast cells, even in the presence of eEF3. Stabilization by eEF3 of the non-rotated state may accelerate the reaction and contribute to the directionality of translocation. Since we do not observe any difference in the association of eEF2 with ribosomes upon eEF3 depletion (Fig EV2D), we do not think that eEF3 plays an important role for eEF2 dissociation. Similarly, small differences in the rates of peptide bond formation (Figs 1D and 2B) can be attributed to the effect of eEF3 on the ribosome dynamics, but do not have a major effect *in vivo* (Fig 3D, G and H). By contrast, we observe dramatic differences in the rates of E-site tRNA release in the presence and absence of eEF3 (Fig 2C–E).

In contrast to bacterial ribosomes, which release the E-site tRNA quickly (Uemura *et al*, 2010; Belardinelli *et al*, 2016), dissociation of deacylated tRNA from yeast ribosome in the absence of eEF3 is very slow, occurring in the seconds range (this paper and (Garreau de Loubresse *et al*, 2014)). Even in the presence of eEF3, E-site tRNA release is observed as a separate step from POST-2 to POST-3 state (Fig 7F and G). In our POST-2 state, the CD of eEF3 is seen to directly contact the L1 stalk, but not the E-site tRNA, suggesting that dissociation of the E-site tRNA by eEF3 is facilitated by shifting the L1 stalk from an “int” to an “out” conformation (Fig 7F and G), as was hypothesized previously (Triana-Alonso *et al*, 1995; Andersen *et al*, 2006). We note, however, that we do not observe release of the E-site tRNA to be dependent on binding of the ternary complex to the A site (Fig 2C), as proposed previously (Triana-Alonso *et al*, 1995). We also do not observe the presence of eEF1A in any of our cryo-EM states, and depletion of eEF3 does not lead to accumulation of eEF1A (or eEF2) on the ribosome (Fig EV2D). Rather, our *in vivo* eEF3-depletion studies suggest that the ribosomes become blocked with all three tRNA binding sites being occupied (Fig 7H). As biochemical experiments show that peptidyl transfer can occur in the absence of eEF3 (Fig 1D), we envisage that ribosomes are trapped in the POST-2 state with deacylated tRNAs in the E and P sites and a peptidyl-tRNA in the A site. Importantly, the subsequent translocation step would not be possible, probably because the presence of deacylated tRNA at the E site inhibits the ribosome rotation and tRNA movement. Such a state with three tRNAs on the ribosome would be consistent with the loss of 21 nt RPFs in the ribosome profiling experiments observed when eEF3 is depleted from the cells (Figs 3B and D). While it has been shown by smFRET that bacterial ribosomes with three tRNAs assume a partially rotated state due to slow kinetics of E-site tRNA release which hinders translocation (Choi & Puglisi, 2017), it is tempting to speculate that fungi may have evolved to utilize eEF3 to overcome this kinetic hurdle, promoting rapid translation.

eEF3 has a marked binding preference for the non-rotated states of the ribosome, e.g., PRE-1 and PRE-2, as well as POST-2 and POST-3 states, and becomes destabilized in the rotated PRE-3 and PRE-4 that arise when the A- and/or P-site tRNAs move into hybrid sites (Fig 7C and D). Similarly, eEF3 does not stably interact with the eEF2-bound POST-1 state bearing chimeric ap/P- and p/E-

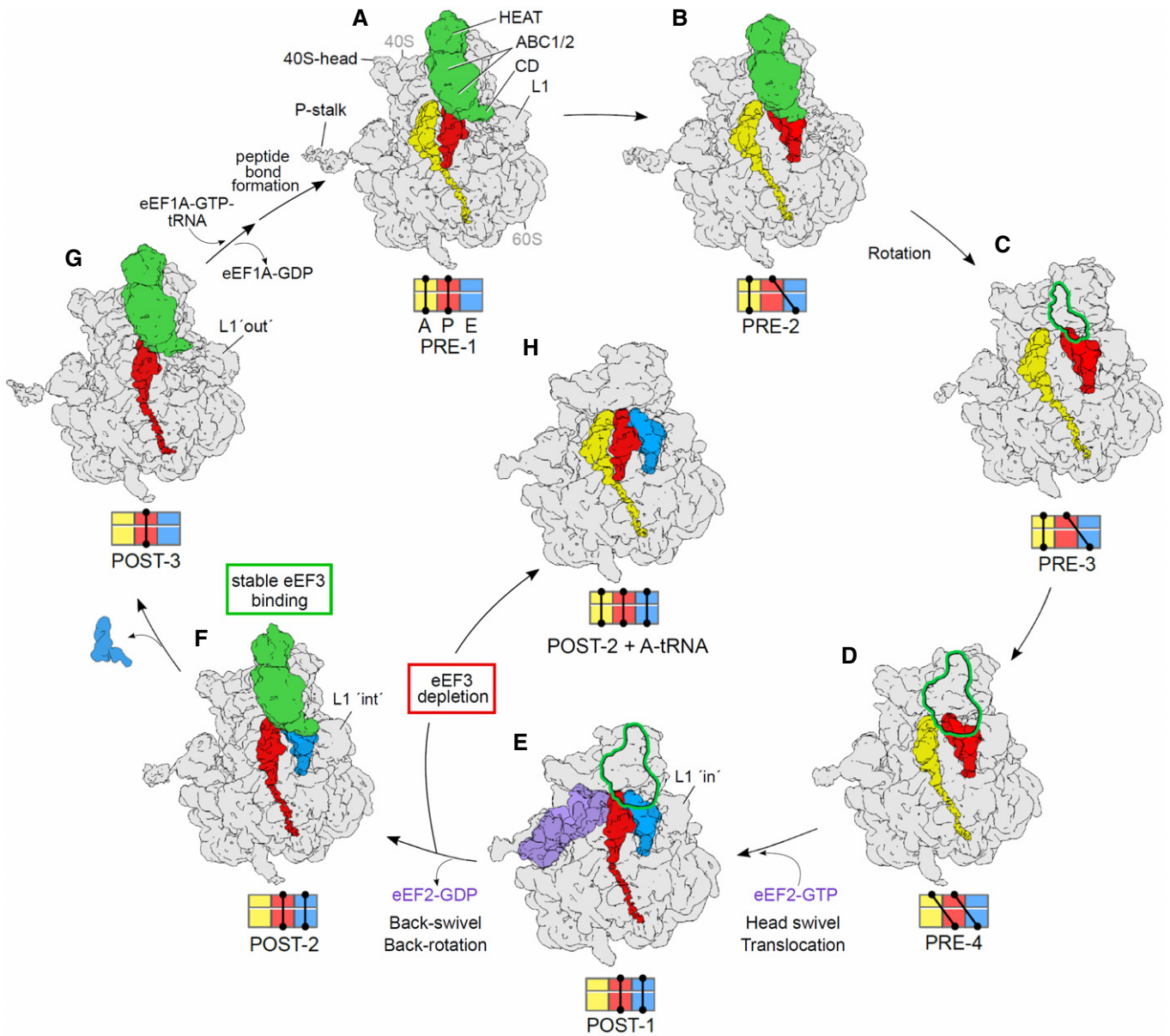


Figure 7. Functional role of eEF3 in the framework of the elongation cycle.

- A, B eEF3 binds to (A) non-rotated 80S in a pre-translocation (PRE) state bearing classical A/A- and P/P-tRNA (PRE-1) as well as to (B) non-rotated state occupied by A/ A- and a hybrid P/E-tRNA (PRE-2).
- C, D (C) Rotation of the ribosomal subunits leads to unstable binding of eEF3 to a ribosome with A/A- and P/E-tRNA (PRE-3) as well as to (D) a fully rotated ribosomal species bearing hybrid A/P- and P/E-tRNAs (PRE-4).
- E Binding of eEF2-GTP facilitates 40S-head swiveling and translocation of the hybrid A/P- and P/E-tRNA into the chimeric ap/P and pe/E-tRNA positions (POST-1). After dissociation of eEF2-GDP and the resulting back-swivel and back-rotation of the ribosome, eEF3 binds stably to the non-rotated ribosome with a classical P/ P- and E/E-tRNA (POST-2) with L1-stalk in the "int" position.
- G The eEF3-CD directly interacts with L1 stabilizing an "out" conformation that facilitates release of the E-site tRNA. eEF3 remains bound to the non-rotated ribosome bearing a P/P-tRNA (POST-3). Transition from states E to F and F to G are accelerated by eEF3. Binding of eEF1a-ATP-tRNA ternary complex and subsequent peptide bond formation results in formation of PRE-1, as seen in (A).
- H In the absence of eEF3, we suggest that POST-2 ribosomes formed after eEF2 dissociation can bind an A-tRNA, but cannot translocate further because of the presence of three tRNAs on the ribosome.

Data information: Volumes (A–G) are representing the cryo-EM reconstructions from the eEF3-TAP pull-out, whereas volume (H) shows a potential scenario based on the results of the eEF3-depletion studies. All maps are filtered to 6 Å. The outline shown in (C–E) assigns the disordered eEF3 ligand present in these volumes.

tRNAs (Fig 7E, Appendix Fig S6C). Comparison of rotated and non-rotated ribosome conformations reveals that subunit rotation disturbs the interactions between eEF3 and the 40S subunit,

providing a rationale for the destabilization (Appendix Fig S6). By contrast, the back-rotation and back-swivel of the head that accompanies eEF2 dissociation yields a classical non-rotated POST-2 state

with P- and E-site tRNAs that is an optimal substrate for stable binding of eEF3 (Fig 7F). In this state, we observe that eEF3 adopts a closed conformation, presumably with two molecules of ATP (or ADPNP) bound within the ABC1 and ABC2 NBDs (Appendix Fig S5D–K). The presence of ADPNP prevents eEF3-mediated E-site tRNA release, suggesting that ATP hydrolysis in at least one of the NBD of eEF3 is necessary for this process (Triana-Alonso *et al*, 1995). Although eEF3 appears to adopt a closed conformation in the POST-3 state following E-site tRNA release (Fig 7G), we cannot rule out that in the cell eEF3 adopts a partially open hybrid ATP/ADP state and that during the last purification step performed in the presence of ADPNP, the ADP is displaced by ADPNP, thereby reverting eEF3 from the partially closed into a fully closed conformation. If this were the case, one could speculate that hydrolysis of one ATP to ADP occurs concomitant with E-tRNA release when transitioning from POST-2 to POST-3 (Fig 7F and G) and hydrolysis of the second ATP to ADP may be stimulated by subunit rotation, explaining the destabilizing of eEF3 on the ribosome (Fig 7B and C). In the latter case, even if the ADPs are replaced with ADPNP leading to a closed conformation, the rotated state precludes stable binding of eEF3, although we cannot rule out that PRE-3, PRE-4, and POST-1 (Fig 7C–E) is stably bound by eEF3 in a partially closed state. Finally, the presence of eEF3 on the ribosome during decoding, e.g., at the transition from POST-3 to PRE-1 state may affect the relative rates of decoding reactions, which may explain the effect of eEF3 on translation fidelity (Uritani & Miyazaki, 1988) and account for the observed genetic interactions between eEF1A and eEF3 (Anand *et al*, 2003; Anand *et al*, 2006).

In addition to providing insight into the function of eEF3, our study fills the gap for various missing structures of the yeast translation elongation cycle (Fig 7 and Movie EV2). While yeast PRE-1 (Fig 7A) and PRE-4 (Fig 7D) states have been reported recently in yeast (Ikeuchi *et al*, 2019; Buschauer *et al*, 2020; Matsuo *et al*, 2020), those structures did not contain eEF3. We also observe the novel non-rotated PRE-2 (Fig 7B) as well as canonical rotated PRE-3 states (Fig 7C). PRE-1, PRE-3, and PRE-4 are similar to classical and rotated states observed in mammalian systems (Budkevich *et al*, 2011; Behrmann *et al*, 2015). While there have been multiple structures of yeast eEF2 on the ribosome (Gomez-Lorenzo *et al*, 2000; Spahn *et al*, 2004; Taylor *et al*, 2007; Sengupta *et al*, 2008; Pellegrino *et al*, 2018), none contained the physiological configuration of two tRNAs being translocated by eEF2, as observed in our POST-1 state (Fig 7E). We note however that similar functional states to POST-1 have been observed in rabbit and human systems (Behrmann *et al*, 2015; Flis *et al*, 2018). Finally, although an *in vitro* reconstituted POST-3 state with eEF3 (Fig 7G) has been reported at 9.9 Å resolution (Andersen *et al*, 2006), here we present a native POST-3 at 3.8 Å as well as additionally capturing POST-2 state with eEF3 and E-site tRNA (Fig 7F).

Collectively, our biochemical, genetic, and structural analysis sheds light into the critical function of eEF3 during translation in yeast. Ultimately, rapid translation in yeast requires fast movement of the tRNAs through the ribosome and their release from the E site. Here, we show that eEF3 fulfills both roles by facilitating late steps in tRNA translocation and by inducing the L1 stalk to adopt an out conformation allowing E-site tRNA release. Some questions for the future are to understand the role of ATP hydrolysis in eEF3 function and whether it is linked to E-site tRNA release and/or the stability

of eEF3 binding, as well as why a factor such as eEF3 that is essential for translation yeast does not appear to have a homolog in higher eukaryotes, such as humans.

Materials and Methods

E. coli-competent cells and growth conditions

eIF1 was cloned into a pET22b plasmid without affinity tag. eIF1A, eIF5, eIF5A, and eIF5B-397C (lacking 396 amino acids from the C-termini) were cloned into a pGEX-6P1 plasmid with a GST tag. Recombinant proteins were expressed in *E. coli* BL21(DE3) cells from IPTG-inducible plasmids at 37°C for eIF1, eIF5A, and eIF5B-397C. eIF1A and eIF5 were expressed from IPTG-inducible plasmids at 16°C.

Saccharomyces cerevisiae strain and growth conditions

The *S. cerevisiae* cells for ribosomal subunits, eIF2, eEF1A, eEF2, and eEF3, were grown in a 250 l bioreactor in 1xYPD (20 g/l peptone, 10 g/l yeast extract, 20 g/l glucose) at 30°C. The *S. cerevisiae* cells for eIF3 were grown in a 250 l bioreactor in CSM-LEU-URA media at 30°C. The *S. cerevisiae* eEF3-TAP strain (GE Healthcare/Dharmacon, Strain: BY4741, GeneID: 850951) was grown to OD₆₀₀ = 0.8 in an InnovaX large-capacity incubator shaker in 1xYPD at 30°C.

For ribosome profiling, WT (BY4741) and yCW35 (*MATA his3Δ1 leu2Δ0 met15Δ0 ura3Δ0 hef3::KanMX HO::adh1p-osTIR1-Ura3 SkHIS3-GAL1p-yef3-3mAID::NatMX*) strains were grown in YPGR (20 g/l peptone, 10 g/l yeast extract, 20 g/l galactose + 20 g/l raffinose) overnight at 30°C, collected by centrifugation, washed, and resuspended in YPD at OD 0.003 and 0.02, respectively. After 8 h, cells were harvested at OD 0.55 and 0.45, respectively. Cells were harvested by fast filtration and flash frozen in liquid nitrogen.

Buffers

The following buffers were used for purification of translation components:

- Buffer 1. 20 mM HEPES/KOH pH 7.5, 100 mM KOAc, 2.5 mM Mg(OAc)₂, 1 mg/ml heparin sodium salt, 2 mM DTT.
- Buffer 2. 20 mM HEPES/KOH pH 7.5, 100 mM KOAc, 400 mM KCl, 2.5 mM Mg(OAc)₂, 1 M sucrose, 2 mM DTT.
- Buffer 3. 20 mM HEPES/KOH pH 7.5, 100 mM KOAc, 400 mM KCl, 2.5 mM Mg(OAc)₂, 1 mg/ml heparin sodium salt, 2 mM DTT.
- Buffer 4. 50 mM HEPES-KOH pH 7.5, 500 mM KCl, 2 mM MgCl₂, 2 mM DTT.
- Buffer 5. 50 mM HEPES-KOH pH 7.5, 500 mM KCl, 5 mM MgCl₂, 2 mM DTT, 0.1 mM EDTA, 5% sucrose.
- Buffer 6. 50 mM HEPES-KOH pH 7.5, 500 mM KCl, 5 mM MgCl₂, 2 mM DTT, 0.1 mM EDTA, 30% sucrose.
- Buffer 7. 50 mM HEPES-KOH, 100 mM KCl, 250 mM sucrose, 2.5 mM MgCl₂, 2 mM DTT.
- Buffer 8. 20 mM HEPES-NaOH pH 7.5, 150 mM NaCl, 5% glycerol, 4 mM β-mercaptoethanol (β-me).

- Buffer 9. Same as buffer 8 with 1 M NaCl.
- Buffer 10. Same as buffer 8 without NaCl and glycerol.
- Buffer 11. 20 mM HEPES-KOH pH 7.5, 200 mM KCl, 2 mM DTT.
- Buffer 12. 20 mM HEPES-NaOH pH 7.5, 500 mM NaCl, 5% glycerol, 4 mM β -me.
- Buffer 13. 50 mM HEPES-NaOH pH 7.5, 400 mM NaCl, 5% glycerol, 4 mM β -me.
- Buffer 14. 20 mM HEPES-KOH pH 7.5, 500 mM KCl, 10% glycerol, 3 mM β -me.
- Buffer 15. 20 mM 3-(N-morpholino)propane sulfonic acid (MOPS)-KOH pH 6.7, 500 mM KCl, 10% glycerol, 3 mM β -me.
- Buffer 16. 20 mM HEPES-NaOH pH 7.5, 500 mM NaCl, 30 mM L-glutathione reduced, 5% glycerol, 4 mM β -me.
- Buffer 17. 20 mM HEPES-KOH pH 7.5, 100 mM KCl, 2 mM DTT.
- Buffer 18. 20 mM HEPES-KOH pH 7.5, 200 mM KCl, 2 mM DTT.
- Buffer 19. 20 mM HEPES-KOH pH 7.5, 100 mM KCl, 5% glycerol, 2 mM DTT.
- Buffer 20. 20 mM HEPES-KOH pH 7.5, 100 mM KCl, 5% glycerol, 2 mM DTT.
- Buffer 21. 20 mM HEPES-NaOH pH 7.5, 1 M NaCl, 5% glycerol, 4 mM β -me.
- Buffer 22. 50 mM Tris-HCl pH 7.5, 5 mM MgCl₂, 50 mM NH₄Cl, 0.2 mM PMSF, 10% glycerol, 0.1 mM EDTA pH 8.0, 1 mM DTT.
- Buffer 23. 20 mM Tris-HCl pH 7.5, 50 mM KCl, 0.1 mM EDTA pH 8.0, 0.2 mM PMSF, 25% glycerol, 1 mM DTT.
- Buffer 24. 20 mM Tris-HCl pH 7.5, 500 mM KCl, 0.1 mM EDTA pH 8.0, 0.2 mM PMSF, 25% glycerol, 1 mM DTT.
- Buffer 25. 20 mM Tris-HCl pH 7.5, 0.1 mM EDTA pH 8.0, 200 mM KCl, 25% glycerol, 1 mM DTT.
- Buffer 26. 20 mM HEPES-KOH pH 7.5, 500 mM KCl, 20 mM imidazole, 10% glycerol, 2 mM β -me.
- Buffer 27. 20 mM HEPES-KOH pH 7.5, 100 mM KCl, 250 mM imidazole, 10% glycerol, 2 mM β -me.
- Buffer 28. 20 mM HEPES-KOH pH 7.5, 100 mM KCl, 10% glycerol, 2 mM DTT.
- Buffer 29. 40 mM Tris-HCl pH 7.5, 15 mM MgCl₂, 2 mM spermidine, 10 mM NaCl.
- Buffer 30. 20 mM HEPES-KOH (pH 7.4). 100 mM KOAc, 10 mM Mg(OAc)₂, 1 mM DTT.

Preparation of ribosomal subunits, initiation, and elongation factors

80S ribosomal subunits, eIF2, eIF3, eEF2, and eEF3, were prepared from *S. cerevisiae* as described previously (Pavitt *et al.*, 1998; Phan *et al.*, 2001; Algire *et al.*, 2002; Jorgensen *et al.*, 2002; Acker *et al.*, 2007; Sasikumar & Kinzy, 2014).

For 80S ribosomal subunits purification, cells were harvested in mid-log phase and resuspended in 1 ml/g of cells in lysis buffer 1. Cell pellets frozen in liquid nitrogen were ground using an ultra-centrifugal mill according to the CryoMill protocol (Retsch®). The lysate was thawed at 4°C, 100 μ l DNase, and one EDTA-free protease inhibitor tablet was added and incubated at 4°C for 30 min. The thawed lysate was clarified by centrifugation at 13,000 rpm at 4°C for 30 min. The salt concentration of the supernatant was increased to 500 mM KCl and was then filtered using 1 μ m glass fiber filters. Ribosomes in the supernatant were collected in buffer 2 at 45,000 rpm at 4°C for 2 h in a Ti45 rotor.

Ribosomal pellets were resuspended in resuspension buffer 3 and were incubated on ice for 15 min. Ribosomes were collected once more through buffer 2 at 100,000 rpm at 4°C for 30 min in a MLA 130 rotor. The pellets were resuspended in buffer 4, incubated on ice for 15 min with 1 mM puromycin and then 10 min at 37°C. The sample was loaded on a 5–30% sucrose gradient (buffer 5 & 6) and centrifuged at 25,000 rpm at 4°C for 16 h in a Ti32 rotor. The 40S and 60S subunits were collected from gradient fractionation, were exchanged separately into buffer 7, concentrated, and stored at –80°C after being flash frozen in liquid nitrogen.

eIF1 cell pellets were resuspended in buffer 8, lysed in the presence of DNase and protease inhibitor tablet, and purified by HiTrap SP cation exchange chromatography with a linear gradient from 0 to 100% buffer 9 over 60 ml after equilibrating the column and loading eIF1 with buffer 8. The fractions containing eIF1 were pooled and diluted to decrease the salt concentration to 150 mM with buffer 10. Next, eIF1 was purified by HiTrap Heparin chromatography with a linear gradient from 0 to 100% buffer 9 over 60 ml after equilibrating the column and loading eIF1 with buffer 8. The fractions containing eIF1 were pooled and concentrated and further purification was attained by size-exclusion chromatography on a HiLoad 26/600 Superdex 75 pg column with buffer 11. The purified eIF1 protein was concentrated and stored in buffer 5 at –80°C.

eIF1A, eIF5, eIF5A, and eIF5B-397C cell pellets were resuspended in buffer 12, 13, 14, and 15, respectively, and lysed in the presence of DNase and protease inhibitor tablet. All GST-tagged proteins were purified by GSTrap column with 100% buffer 16. After cleavage of the fusion protein with PreScission protease (1 μ M final), further purification was attained by size-exclusion chromatography on a HiLoad 26/600 Superdex 75 pg (eIF1A with buffer 17, eIF5 with buffer 18, eIF5A with buffer 19) and HiLoad 26/600 Superdex 200 pg (eIF5B-397C with buffer 20) column. For eIF1A, before size-exclusion chromatography, an additional step of a Resource Q anion exchange chromatography was included after protease cleavage and protein was eluted with 0–100% buffer 21 over 60 ml. The purified proteins were concentrated and stored at –80°C.

eEF1A was purified from *S. cerevisiae*. eEF1A cell pellets were resuspended in buffer 22, lysed using an ultra-centrifugal mill, and the lysate was loaded on a tandem HiTrap Q anion exchange and HiTrap SP cation exchange column pre-equilibrated in buffer 23. eEF1A was eluted from HiTrap SP with 0–100% buffer 24 over 30 ml. Further purification was attained by size-exclusion chromatography on a HiLoad 26/600 Superdex 200 pg with buffer 25. The purified eEF1A protein was concentrated and stored at –80°C.

In vitro hypusination of eIF5A

eIF5A hypusination enzymes deoxyhypusine synthase (Dys1) and deoxyhypusine hydroxylase (Lia1) were co-expressed in *Escherichia coli* BL21(DE3) cells from IPTG-inducible pQLinkH plasmid with a His6 tag at 37°C. Cell pellet was resuspended in buffer 26, lysed in the presence of DNase and protease inhibitor tablet. The protein was purified by Protino Ni-IDA 2000 affinity chromatography with buffer 27, after equilibrating the column and loading the protein with buffer 26. The eluted protein was dialyzed in buffer 28, concentrated, and stored at –80°C. The *in vitro* hypusination of

eIF5A was performed as described previously (Park *et al*, 2011; Wolff *et al*, 2011).

Preparation of tRNAs and mRNAs

Initiator tRNA (tRNA_i^{Met}) was prepared by *in vitro* transcription using T7 polymerase from a plasmid containing a 92 nucleotides-long DNA with the T7 promoter (underlined) and the initiator tRNA sequence purchased from Eurofins.

5'TAATACGACTCACTATAAGCGCCGTGGCGCAGTGGAAAGCGCGCAGGGCTCATAACCCTGATGTCTCGGATCGAAACCGAGCGGCGCTACCA3'

The DNA was amplified using forward and reverse primers, and the amplified product was *in vitro* transcribed in buffer 29 with 10 mM DTT, 3 mM NTP mix, 0.005 U/μl inorganic Pyrophosphate (PPase), 0.1 U/μl RNase inhibitor, and 0.05 U/μl T7 RNA-polymerase for 4 h at 37°C. Aminoacylation and purification of [³H]Met-tRNA_i^{Met} and [³H]Met-tRNA_i^{Met} (Flu) were performed as described previously (Rodnina *et al*, 1994; Milon *et al*, 2007).

The elongator tRNAs [¹⁴C]Val-tRNA^{Val}, [¹⁴C]Phe-tRNA^{Phe}, and Phe-tRNA^{Phe} were prepared as described in (Rodnina *et al*, 1994). The unstructured 5' UTR mRNA Met-Phe-Val and mRNA Met-Val-Phe were purchased from IBA (mRNA Met-Phe-Val: 5'GGUCUCUCUCUCUCUCUAUGUUUUUUUCUCUCUCUCUC3' and mRNA Met-Val-Phe: 5'GGUCUCUCUCUCUCUCUCUAUGUUUUUUUCUCUCUCUCUC3').

Preparation of initiation and ternary complexes

80S initiation complexes were prepared by incubating 8 μM of eIF2 with 1 mM GTP and 4 μM [³H]Met-tRNA_i^{Met} or [³H]Met-tRNA_i^{Met} (Flu) in YT buffer (30 mM HEPES-KOH pH 7.5, 100 mM KOAc, 3 mM MgCl₂) at 26°C for 15 min to form the ternary complex. 2 μM 40S, 10 μM mRNA (uncapped mRNA with unstructured 5' UTR that alleviates the requirement of eIF4 (Acker *et al*, 2007)), 10 μM eIF-mix (mixture of initiation factors eIF1, eIF1A, eIF3, eIF5), 2 mM DTT, 0.25 mM spermidine, and 1 mM GTP were incubated for 5 min at 26°C before adding 3 μM 60S subunits and 6 μM eIF5B. After incubation, ternary complex was added to the ribosome mixture and the MgCl₂ was adjusted to a final concentration of 9 mM before layering on sucrose cushion. ICs were purified by ultracentrifugation through a 1.1 M sucrose cushion in YT9 buffer (30 mM Hepes-KOH pH 7.5, 100 mM KoAc, 9 mM MgCl₂), and pellets were dissolved in YT9 buffer.

Ternary complexes eEF1A-GTP-[¹⁴C]Phe-tRNA^{Phe} and eEF1A-GTP-[¹⁴C]Val-tRNA^{Val} were prepared by incubating 1 μM eEF1A, 0.1 μM eEF1Bα, 3 mM PEP, 1% PK, 1 mM DTT, 0.5 mM GTP in YT buffer for 15 min at 26°C. 0.2 μM [¹⁴C]Phe-tRNA^{Phe} or [¹⁴C]Val-tRNA^{Val} (5 eEF1A:1 aa-tRNA) was added and incubated for additional 5 min at 26°C, followed by addition of 2 μM modified eIF5A.

Rapid kinetics

Peptide bond formation assay was performed by rapidly mixing initiation complexes (1 μM, 0.25 μM active in tripeptide formation) with the respective ternary complexes as indicated (0.2 μM), eIF5A (2 μM) and eEF3 (4 μM) mixed with 40 μM ATP in a quench-flow apparatus at 26°C. After the desired incubation times, the reactions were quenched by adding KOH to a final concentration of 0.5 M.

Peptides were released by alkaline hydrolysis for 45 min at 37°C. After neutralization with acetic acid, the products were analyzed by HPLC (LiChrospher 100 RP-8 HPLC column, Merck). To form tripeptides, MetPhe-tRNA^{Phe} pre-translocation complexes (0.35 μM) were rapidly mixed with the respective ternary complex (0.7 μM) containing eEF2 (1 μM) and eEF3 (4 μM) with ATP (40 μM).

The amount of deacylated tRNA^{Met}(Flu) bound to 80S after translocation was monitored on a BioSuite 450 (Waters) size-exclusion chromatography. 80S 2C (0.35 μM) was incubated without eEF2/ eEF3, or with eEF2 (1 μM) alone, eEF2 (1 μM), and eEF3 (4 μM) together or with eEF2, eEF3, and TC-Val (0.7 μM) for 15 min before applying on a BioSuite 450 gel filtration column. Ribosome complexes and tRNA were eluted using YT buffer (30 mM HEPES-KOH pH 7.5, 100 mM KOAc, 3 mM MgCl₂). Fluorescence of tRNA^{Met}(Flu) co-eluting with 80S was monitored using a flow-through fluorescence detector after excitation at 463 nm and emission at 500 nm. Deacylated tRNA release from the E site were performed by rapidly mixing initiation complexes prepared using [³H]Met-tRNA^{Met} (Flu) with the respective ternary complexes as indicated (0.2 μM) and eEF1A (1 μM) in a stopped-flow apparatus (Applied Photophysics) at 26°C. Fluorescein fluorophore was excited at 463 nm, and emission was measured after passing through KV500 long-pass filters (Schott). Experiments were performed by rapidly mixing equal volumes of reactants and monitoring the time courses of fluorescence changes. Time courses depicted in the figures were obtained by averaging 5–7 individual traces.

Time-resolved Pmn assay

The time-resolved Pmn assay to monitor translocation for the MetPhe-tRNA^{Phe} PRE complex was performed as described previously (Ranjan & Rodnina, 2017). Briefly, PRE complex (0.35 μM) was rapidly mixed with Pmn (2 mM), and/or eEF2 (0.8 μM) and/or eEF3 (2 μM) with ATP (20 μM) in YT buffer at 26°C. Control experiments were carried out with POST complexes prepared by incubating PRE complexes with eEF2 (0.8 μM) and/or eEF3 (2 μM) with ATP (20 μM). POST complexes with MetPhe-tRNA^{Phe} (0.35 μM) in the P site were rapidly mixed with Pmn (2 mM) in a quench-flow apparatus. The reaction was quenched with KOH (0.5 M) and the peptides were released by alkaline hydrolysis for 45 min at 37°C, analyzed by reversed-phase HPLC (LiChrospher 100 RP-8, Merck), and quantified by double-label [³H]Met-[¹⁴C]Phe radioactivity counting (Wohlgemuth *et al*, 2008).

Preparation of libraries for yeast ribosome footprints

Preparation of libraries for yeast ribosome footprints was performed as described previously (Wu *et al*, 2019a). Cell pellets were ground with 1 ml yeast footprint lysis buffer [20 mM Tris-Cl (pH 8.0), 140 mM KCl, 1.5 mM MgCl₂, 1% Triton X-100 with specified elongation inhibitors] in a Spex 6870 freezer mill. Elongation inhibitors (CHX, ANS, and TIG) were used at 0.1 g/l. Lysed cell pellets were diluted to ~23 ml in yeast footprint lysis buffer containing specified antibiotics and clarified by centrifugation. The resultant supernatant was layered on a sucrose cushion [20 mM Tris-Cl (pH 8.0), 150 mM KCl, 5 mM MgCl₂, 0.5 mM DTT, 1M sucrose] to pellet polysomes in a Type 70Ti rotor (Beckman Coulter) (60,000 rpm for 106 min). Ribosome pellets were gently resuspended in 1 ml footprint lysis buffer (without elongation inhibitors). 400 μg of isolated

polysomes in 350 μ l of footprint lysis buffer (without elongation inhibitors) were treated with 500 units of RNaseI (Ambion) for 1 h at 25°C. Monosomes were isolated by sucrose gradients (10–50%). The extracted RNA was size-selected from 15% denaturing PAGE gels, cutting between 15 and 34 nt. An oligonucleotide adapter was ligated to the 3' end of isolated fragments. After ribosomal RNA depletion using RiboZero (Illumina), reverse transcription using SuperScript III reverse transcriptase (Thermo Fisher Scientific), circularization using CircLigase I (Lugicen), and PCR amplification. Libraries were sequenced on a HiSeq2500 machine at facilities at the Johns Hopkins Institute of Genetic Medicine.

Polysome profiles

One litre of yeast cultures of indicated strains were harvested by fast filtration and ground with 1 ml footprint lysis buffer [20 mM Tris-Cl (pH 8.0), 140 mM KCl, 1.5 mM MgCl₂, 1% Triton X-100, 0.1 mg/ml CHX] in a Spex 6870 freezer mill. CHX was omitted for run-off polysome profiles. Cellular lysates were first clarified by centrifugation (at 15,000 rpm for 10 min). Lysates containing 200 μ g of total RNA was spun through 10–50% sucrose gradients using a Beckman Coulter SW41 rotor at 40,000 rpm at 4°C for 2 h. Gradients were fractionated on a Biocomp piston gradient fractionator and the absorbance at 254 nm was recorded. Fractions were methanol precipitated and analyzed by immunoblotting using antibodies against eEF1 (Kerafast, ED7001), eEF2 (Kerafast, ED7002), and RPL4 (ProteinTech, 11302-1-AP).

Tandem affinity purification of the eEF3-80S complex

The eEF3 *in vivo* pull-out was performed using DynabeadsR[®]M-270 Epoxy (Invitrogen) with yeast strain expressing a C-terminally TAP-tagged eEF3 (Strain: BY4741, Genotype: MATa *his3 Δ 1 leu2 Δ 0 met15 Δ 0 ura3 Δ 0*) obtained from Horizon Discovery. The purification was essentially performed as described previously (Schmidt *et al*, 2016). Briefly, cultures were harvested at log phase, lysed by glass bead disruption, and incubated with IgG-coupled magnetic beads with slow tilt rotation for 1 h at 4°C in buffer 30 (20 mM HEPES (pH 7.4), 100 mM KOAc, 10 mM Mg(OAc)₂, 1 mM DTT). The beads were harvested and washed three times using detergent containing buffer 30 (+0.05% Triton X) followed by a fourth washing step using buffer 30. The elution of the complex was done by addition of AcTEV Protease (Invitrogen) for 3 h at 17°C in buffer 30 containing 1 mM ADPNP (Sigma) final concentration.

Sample and grid preparation

The final complex was cross-linked with 0.02% glutaraldehyde for 20 min on ice, and the reaction was subsequently quenched with 25 mM Tris-HCl pH 7.5. DDM (Sigma) was added to the sample to a final concentration of 0.01% (v/v). For grid preparation, 5 μ l (8 A₂₆₀/ml) of the freshly prepared cross-linked complex was applied to 2 nm precoated Quantifoil R3/3 holey carbon supported grids and vitrified using a Vitrobot Mark IV (FEI, Netherlands).

Cryo-electron microscopy and single-particle reconstruction

Data collection was performed on a FEI Titan Krios transmission electron microscope (TEM) (Thermo Fisher) equipped with a Falcon

II direct electron detector (FEI). Data were collected at 300 kV with a total dose of 25 e⁻/Å² fractionated over 10 frames with a pixel size of 1.084 Å/pixel and a target defocus range of -1.3 to -2.8 μ m using the EPU software (Thermo Fisher). The raw movie frames were summed and corrected for drift and beam-induced motion at the micrograph level using MotionCor2 (Zheng *et al*, 2017). The resolution range of each micrograph and the contrast transfer function (CTF) were estimated with Gctf (Zhang, 2016). A total of 22,856 micrographs were collected. After manual inspection, 18,016 micrographs were used for automated particle picking with Gautomatch (<http://www.mrc-lmb.cam.ac.uk/kzhang/>) resulting in 530,517 initial particles, of which 211,727 were selected for further processing upon 2D classification in RELION-2.1 (Kimanius *et al*, 2016). After initial alignment with a vacant 80S reference, the 211,727 particles (defined as 100%) were 3D classified into 8 classes (Appendix Fig S3). Classes 1 and 2 (joined to group I) contained 70,780 particles (~33%) and displayed density for the eEF3-80S complex but had mixed tRNAs with varying occupancy as well as a dynamic L1-stalk. Class 3 (group II) showed a density for eEF2, whereas classes 4 and 5 (group III) revealed rotated ribosomal species with hybrid tRNAs. Both groups (group I and II) showed weak density for eEF3. Classes 6, 7 and 8 (group IV) (~31%) had low-resolution ribosomal species with biased orientation; however, all of them showed an extra density for eEF3 (not shown). To increase the resolution of the eEF3 ligand and separate it from low-resolution eEF3 species, group I was subjected to focused sorting using a mask encompassing the eEF3 ligand (Appendix Fig S3). The resulting class 3 containing 45,032 particles (~21%) was 3D and CTF refined using RELION-3.0 (Zivanov *et al*, 2018). The final refined volume was furthermore subjected to multi-body (MB) refinement, for which three masks were used: the first one encompassed one portion of eEF3 (ABC1, ABC2, and CD; residue range 420–976, MB-1) and the 60S, the second mask covered the 40S body (MB-2), and the third mask included the remaining part of eEF3 (HEAT and 4HB; residue range 1–419, MB3-3) as well as the 40S head (Appendix Figs S3 and S4F). The final reconstructions were corrected for the modulation transfer function of the Falcon 2 detector and sharpened by applying a negative B-factor estimated by RELION-3.0 (Zivanov *et al*, 2018). For the sharpening, a mask for the whole eEF3-80S complex was applied resulting in a final reconstruction of 3.3 Å (Appendix Figs S3 and S4A). The same was done for each part of the multi-body refined volumes, which provided a resolution of 3.2 Å for the 60S-eEF3 (ABC1/2, CD), 3.3 Å for the 40S body, and 3.5 Å for the 40S head-eEF3 (HEAT, 4HB) (Appendix Fig S4E). To obtain a stoichiometric tRNA occupancy as well as defined position of the L1-stalk interacting with the EF3-CD, group I was also subjected to further sorting into four classes using a flat cylinder mask encompassing the relevant regions (tRNAs, L1-stalk, and the eEF3-CD) (Appendix Fig S3). Each class was subsequently subjected to 3D and CTF refinement and a final postprocessing step. All the resulting classes were in an unrotated state bearing an A/A-, P/P- (Ia, 3.7 Å), P/P- (Ib, 3.8 Å), A/A-, P/E- (Ic, 4.0 Å), and a P/P- and E/E-site (Id, 3.9 Å) tRNAs. Particles of group II were extracted and subjected to CTF and 3D refinement resulting in a final cryo-EM reconstruction at 4.1 Å. For distinct tRNA occupancy of each 80S ribosome, group III (66,551 particles) was further 3D classified into two classes and each class was subsequently 3D and CTF refined. Both resulted in a ribosomal species with a disordered

eEF3 (IIIa, IIIb), which was visible after low pass filtering of the map. IIIa showed a rotated-1 state containing A/A- and P/E-site tRNAs with a final resolution of 4.2 Å. IIIb presented a classical fully rotated state (rotated-2) bearing a hybrid A/P- and P/E-site tRNA at 3.8 Å resolution. The resolutions for all volumes were estimated using the “gold standard” criterion (FSC = 0.143) (Scheres, 2012). Local resolution estimation and local filtering of the final volumes were done using Relion-3.0 (Appendix Fig S4B and C, F and G).

Molecular modeling

The eEF3 model was based on the crystal structure of eEF3 in complex with ADP (PDB: 2IW3) with a 2.4 Å resolution (Andersen *et al*, 2006). The existing ribosome-bound eEF3 model (PDB: 2IX3) was used as a help for the rough fitting of the separate eEF3 domains (HEAT, 4 HB, ABC1, ABC2, and CD) of the crystal structure into the density (Andersen *et al*, 2006). The single domains were fitted with UCSF Chimera 1.12.1 (Pettersen *et al*, 2004) via the command “fit in map” and manually adjusted with Coot version 0.8.9.2 (Emsley & Cowtan, 2004). For the manual adjustment, the multi-body refined maps were used for the corresponding parts of the eEF3 model (MB-1 for ABC1, ABC2 and the CD; MB-3 for HEAT and 4HB). The model of the *S. cerevisiae* 80S ribosome was derived from PDB ID 6S47 (Kasari *et al*, 2019b) and the model for the L1 protein from the PDB ID 2NOQ (Schuler *et al*, 2006). The proteins of the 40S and 60S were fitted separately into locally filtered electron density maps using UCSF Chimera (Pettersen *et al*, 2004). The rRNA was fitted domain-wise in Coot (Emsley & Cowtan, 2004). Afterward, manual adjustments were applied to all fitted molecular models using Coot. The combined molecular model (proteins + rRNA) was refined using the phenix.real_space_refine command of phenix version 1.14 with restraints that were obtained via the phenix.secondary_structure_restraints command (Adams *et al*, 2010). Statistics for the model were obtained using MolProbity (Chen *et al*, 2010) and are represented in Appendix Table S1.

Calculation of rotation angles and vectors

Rotation angles were calculated using UCSF Chimera with the command “match show matrix”. The global rotation of the 18S rRNA was calculated relatively to the 23S rRNA by aligning all the models to the 23S rRNA of a non-rotated reference structure (PDB 6SNT) (Matsuo *et al*, 2020). The head swivel rotation degree was calculated relatively to the 18S rRNA body/platform by aligning all the model relative to the body of 18S rRNA from the reference structure (PDB 6SNT) (Matsuo *et al*, 2020). Vector calculation representing a shift between the phosphate atoms of the rRNA from the model compared with the reference structure was performed using PyMol Molecular Graphics System as previously described in (Beckert *et al*, 2018).

Figure preparation

Figures showing biochemical experiments are fitted and plotted with GraphPad Prism 8.0.

Figures showing ribosome profiling data are created using R 3.3.1.

Figures showing atomic models and electron densities were generated using either UCSF Chimera (Pettersen *et al*, 2004) or Chimera X (Goddard *et al*, 2018) and assembled with Inkscape.

Analysis of ribosome profiling data

Analysis of ribosome profiling data was performed as described previously (Wu *et al*, 2019a). The R64-1-1 S288C reference genome assembly (SacCer3) from the *Saccharomyces* Genome Database Project was used for yeast genome alignment. Ce10 reference genome assembly from UCSC was used for *C. elegans* genome alignment. Hg19 reference genome assembly from UCSC was used for human genome alignment. A human transcriptome file was generated to include canonical transcripts of known genes from UCSC genome browser. WT replicate 1 (CHX + TIG) and both WT replicates (CHX + ANS) are identical to that published previously (Wu *et al*, 2019b). Libraries were trimmed to remove ligated 3' adapter (NNNNNNCACTCGGGACCAAGGA), and 4 random nucleotides included in RT primer (RNNNAGATCGGAAGAGCGTCGTGTAGG GAAAGAGTGTAGATCTCGGT. GGTCGC/iSP18/TTCAGACGTGTGCT CTTCCGATCTGTCCCTTGGTGCCCGAGTG) were removed from the 5' end of reads. Trimmed reads longer than 15 nt were aligned to yeast ribosomal and non-coding RNA sequences using STAR (Dobin *et al*, 2013) with “--outFilterMismatchNoverLmax 0.3”. Unmapped reads were then mapped to genome using the following options “--outFilterIntronMotifs RemoveNoncanonicalUnannotated --outFilterMultimapNmax 1 --outFilterMismatchNoverLmax 0.1”. All other analyses were performed using software custom written in Python 2.7 and R 3.3.1.

For each dataset, the offset of the A site from the 5' end of reads was calibrated using start codons of CDS (Schuller *et al*, 2017). Relative ribosome occupancies (pause scores) for codons or peptide motifs (Fig 3E–H) were computed by taking the ratio of the ribosome density in a 3-nt window at the codon or motif of interest over the overall density in the coding sequence (excluding the first and the last 15 nt to remove start and stop codons). Peptide motif logos (Appendix Fig S3E) were generated with WebLogo (Crooks *et al*, 2004) by using motifs with a pause score greater than 4.

Cryo-EM data analysis

Bayesian selection using RELION software package was used to choose the cryo-EM data package (Scheres, 2012). Resolutions were calculated according to gold standard, and the estimation of variation within each group of data was performed using Bayesian calculation within RELION (Scheres, 2012).

Data availability

Cryo-EM maps generated during this study have been deposited in the Electron Microscopy Data Bank (EMDB; <https://wwwdev.ebi.ac.uk/pdbe/emdb>) with accession codes EMD-12081 (eEF3-80S complex), EMD-12059 (PRE-1), EMD-12061 (PRE-2), EMD-12075 (PRE-3) and EMD-12065 (PRE-4), EMD-12074 (POST-1) and EMD-12062 (POST-2), EMD-12064 (POST-3). The eRF3-80S complex model generated during this study has been deposited in the Protein Data Bank (PDB; <http://www.wwpdb.org>) with accession code

7B7D. Raw data for ribosome profiling have been deposited to the Gene Expression Omnibus (<https://www.ncbi.nlm.nih.gov/geo>) with the accession number GSE160206.

Expanded View for this article is available online.

Acknowledgements

We thank Prof. Ralf Ficner for providing the strains for eIF1 and eIF1A purification. We thank Theresia Steiger, Tessa Hübner, Olaf Geintzer, Susanne Rieder for expert technical assistance, Paul Huter for help with data processing, and Otto Berninghausen and Roland Beckmann (Gene Center, LMU, Munich) for data collection. This work has been supported by iNEXT (project number 2643 to D.N.W.), the Horizon 2020 program of the European Union (CEITEC MU), NIH (R37GM059425 to R.G.), HHMI (R.G and C.C.W.), and grants of the Deutsche Forschungsgemeinschaft (DFG) W13285/8-1 to D.N.W., RA 3194/1-1 to N.R., and Leibniz Prize to M.V.R.. This article reflects only the author's view and the European Commission is not responsible for any use that may be made of the information it contains. CIISB research infrastructure project LM2015043 funded by MEYS CR is gratefully acknowledged for the financial support of the measurements at the CF Cryo-electron Microscopy and Tomography CEITEC MU. Open Access funding enabled and organized by ProjektDEAL.

Author contributions

Biochemical and kinetic experiments: NR, SB; Ribosome profiling experiments and analysis: CCW; Cryo-EM analysis: AAP, BB; Manuscript writing: NR, SB, AAP, CC-CW, RG, MVR, DNW.

Conflict of interest

The authors declare that they have no conflict of interest.

References

- Acker MG, Kolitz SE, Mitchell SF, Nanda JS, Lorsch JR (2007) Reconstitution of yeast translation initiation. *Methods Enzymol* 430: 111–145
- Adams PD, Afonine PV, Bunkoczi G, Chen VB, Davis IW, Echols N, Headd JJ, Hung LW, Kapral GJ, Grosse-Kunstleve RW *et al* (2010) PHENIX: a comprehensive Python-based system for macromolecular structure solution. *Acta Crystallogr D Biol Crystallogr* 66: 213–221
- Algire MA, Maag D, Savio P, Acker MG, Tarun Jr SZ, Sachs AB, Asano K, Nielsen KH, Olsen DS, Phan L *et al* (2002) Development and characterization of a reconstituted yeast translation initiation system. *RNA* 8: 382–397
- Anand M, Balar B, Ulloque R, Gross SR, Kinzy TG (2006) Domain and nucleotide dependence of the interaction between *Saccharomyces cerevisiae* translation elongation factors 3 and 1A. *J Biol Chem* 281: 32318–32326
- Anand M, Chakraborty K, Marton MJ, Hinnebusch AG, Kinzy TG (2003) Functional interactions between yeast translation eukaryotic elongation factor (eEF) 1A and eEF3. *J Biol Chem* 278: 6985–6991
- Andersen CB, Becker T, Blau M, Anand M, Halic M, Balar B, Mielke T, Boesen T, Pedersen JS, Spahn CM *et al* (2006) Structure of eEF3 and the mechanism of transfer RNA release from the E-site. *Nature* 443: 663–668
- Balagopal V, Parker R (2011) Stm1 modulates translation after 80S formation in *Saccharomyces cerevisiae*. *RNA* 17: 835–842
- Barthelme D, Dinkelaker S, Albers SV, Londei P, Ermiler U, Tampe R (2011) Ribosome recycling depends on a mechanistic link between the FeS cluster domain and a conformational switch of the twin-ATPase ABCe1. *Proc Natl Acad Sci* 108: 3228–3233
- Beckert B, Turk M, Czech A, Berninghausen O, Beckmann R, Ignatova Z, Plitzko JM, Wilson DN (2018) Structure of a hibernating 100S ribosome reveals an inactive conformation of the ribosomal protein S1. *Nat Microbiol* 3: 1115–1121
- Behrmann E, Loerke J, Budkevich TV, Yamamoto K, Schmidt A, Penczek PA, Vos MR, Burger J, Mielke T, Scheerer P *et al* (2015) Structural snapshots of actively translating human ribosomes. *Cell* 161: 845–857
- Belardinelli R, Sharma H, Caliskan N, Cunha CE, Peske F, Wintermeyer W, Rodnina MV (2016) Choreography of molecular movements during ribosome progression along mRNA. *Nat Struct Mol Biol* 23: 342–348
- Ben-Shem A, Garreau de Loubresse N, Melnikov S, Jenner L, Yusupova G, Yusupov M (2011) The structure of the eukaryotic ribosome at 3.0 Å resolution. *Science* 334: 1524–1529
- Budkevich T, Giesebrecht J, Altman RB, Munro JB, Mielke T, Nierhaus KH, Blanchard SC, Spahn CM (2011) Structure and dynamics of the mammalian ribosomal pretranslocation complex. *Mol Cell* 44: 214–224
- Buschauer R, Matsuo Y, Sugiyama T, Chen YH, Alhusaini N, Sweet T, Ikeuchi K, Cheng J, Matsuki Y, Nobuta R *et al* (2020) The Ccr4-Not complex monitors the translating ribosome for codon optimality. *Science* 368
- Chakraborty K (1999) Functional interaction of yeast elongation factor 3 with yeast ribosomes. *Int J Biochem Cell Biol* 31: 163–173
- Chen VB, Arendall III WB, Headd JJ, Keedy DA, Immormino RM, Kapral GJ, Murray LW, Richardson JS, Richardson DC (2010) MolProbity: all-atom structure validation for macromolecular crystallography. *Acta Crystallogr D Biol Crystallogr* 66: 12–21
- Cherry JM, Hong EL, Amundsen C, Balakrishnan R, Binkley G, Chan ET, Christie KR, Costanzo MC, Dwight SS, Engel SR *et al* (2012) *Saccharomyces* Genome Database: the genomics resource of budding yeast. *Nucleic Acids Res* 40: D700–705
- Choi J, Puglisi JD (2017) Three tRNAs on the ribosome slow translation elongation. *Proc Natl Acad Sci USA* 114: 13691–13696
- Colthurst DR, Belfield GP, Tuite MF (1991) Analysis of a novel elongation factor: EF-3. *Biochem Soc Trans* 19: 279S
- Crooks GE, Hon G, Chandonia JM, Brenner SE (2004) WebLogo: a sequence logo generator. *Genome Res* 14: 1188–1190
- Crowe-McAuliffe C, Graf M, Huter P, Takada H, Abdelshahid M, Novacek J, Murina V, Atkinson GC, Hauryliuk V, Wilson DN (2018) Structural basis for antibiotic resistance mediated by the *Bacillus subtilis* ABCF ATPase VmlR. *Proc Natl Acad Sci USA* 115: 8978–8983
- Dever TE, Green R (2012) The elongation, termination, and recycling phases of translation in eukaryotes. *Cold Spring Harb Perspect Biol* 4: a013706
- Dobin A, Davis CA, Schlesinger F, Drenkow J, Zaleski C, Jha S, Batut P, Chaisson M, Gingeras TR (2013) STAR: ultrafast universal RNA-seq aligner. *Bioinformatics* 29: 15–21
- Emsley P, Cowtan K (2004) Coot: model-building tools for molecular graphics. *Acta Crystallogr D Biol Crystallogr* 60: 2126–2132
- Firczuk H, Kannambath S, Pahle J, Claydon A, Beynon R, Duncan J, Westerhoff H, Mendes P, McCarthy JE (2013) An *in vivo* control map for the eukaryotic mRNA translation machinery. *Mol Syst Biol* 9: 635
- Fischer N, Konevega AL, Wintermeyer W, Rodnina MV, Stark H (2010) Ribosome dynamics and tRNA movement by time-resolved electron cryomicroscopy. *Nature* 466: 329–333
- Flis J, Holm M, Rundlet EJ, Loerke J, Hilal T, Dabrowski M, Burger J, Mielke T, Blanchard SC, Spahn CMT *et al* (2018) tRNA Translocation by the eukaryotic 80S ribosome and the impact of GTP hydrolysis. *Cell Rep* 25: 2676–2688.e7

- Garreau de Loubresse N, Prokhorova I, Holtkamp W, Rodnina MV, Yusupova G, Yusupov M (2014) Structural basis for the inhibition of the eukaryotic ribosome. *Nature* 513: 517–522
- Goddard TD, Huang CC, Meng EC, Pettersen EF, Couch GS, Morris JH, Ferrin TE (2018) UCSF ChimeraX: meeting modern challenges in visualization and analysis. *Protein Sci* 27: 14–25
- Gomez-Lorenzo MG, Spahn CM, Agrawal RK, Grassucci RA, Penczek P, Chakraborty K, Ballesta JP, Lavandera JL, Garcia-Bustos JF, Frank J (2000) Three-dimensional cryo-electron microscopy localization of EF2 in the *Saccharomyces cerevisiae* 80S ribosome at 17.5 Å resolution. *EMBO J* 19: 2710–2718
- Grollman AP (1967) Inhibitors of protein biosynthesis. II. Mode of action of anisomycin. *J Biol Chem* 242: 3226–3233
- Grousl T, Ivanov P, Malcova I, Pompach P, Frydlova I, Slaba R, Senohrabkova L, Novakova L, Hasek J (2013) Heat shock-induced accumulation of translation elongation and termination factors precedes assembly of stress granules in *S. cerevisiae*. *PLoS One* 8: e57083
- Heym RG, Niessing D (2012) Principles of mRNA transport in yeast. *Cell Mol Life Sci* 69: 1843–1853
- Ikeuchi K, Tesina P, Matsuo Y, Sugiyama T, Cheng J, Saeki Y, Tanaka K, Becker T, Beckmann R, Inada T (2019) Collided ribosomes form a unique structural interface to induce Hel2-driven quality control pathways. *EMBO J* 38: e100276
- Jenner L, Starosta AL, Terry DS, Mikolajka A, Filonava L, Yusupov M, Blanchard SC, Wilson DN, Yusupova G (2013) Structural basis for potent inhibitory activity of the antibiotic tigecycline during protein synthesis. *Proc Natl Acad Sci USA* 110: 3812–3816
- Jorgensen R, Carr-Schmid A, Ortiz PA, Kinzy TG, Andersen GR (2002) Purification and crystallization of the yeast elongation factor eEF2. *Acta Crystallogr D Biol Crystallogr* 58: 712–715
- Kamath A, Chakraborty K (1989) Role of yeast elongation factor 3 in the elongation cycle. *J Biol Chem* 264: 15423–15428
- Kambampati R, Pellegrino C, Paiva A, Huang L, Mende-Mueller L, Chakraborty K (2000) Limited proteolysis of yeast elongation factor 3. Sequence and location of the subdomains. *J Biol Chem* 275: 16963–16968
- Kasari V, Margus T, Atkinson GC, Johansson MJO, Hauryliuk V (2019a) Ribosome profiling analysis of eEF3-depleted *Saccharomyces cerevisiae*. *Sci Rep* 9: 3037
- Kasari V, Pochopien AA, Margus T, Murina V, Turnbull K, Zhou Y, Nissan T, Graf M, Novacek J, Atkinson GC et al (2019b) A role for the *Saccharomyces cerevisiae* ABCF protein New1 in translation termination/recycling. *Nucleic Acids Res* 47: 8807–8820
- Kimanius D, Forsberg BO, Scheres SH, Lindahl E (2016) Accelerated cryo-EM structure determination with parallelisation using GPUs in RELION-2. *Elife* 5: e18722
- Kubitschek-Barreira PH, Curty N, Neves GW, Gil C, Lopes-Bezerra LM (2013) Differential proteomic analysis of *Aspergillus fumigatus* morphotypes reveals putative drug targets. *J Proteomics* 78: 522–534
- Kurata S, Shen B, Liu JO, Takeuchi N, Kaji A, Kaji H (2013) Possible steps of complete disassembly of post-termination complex by yeast eEF3 deduced from inhibition by translocation inhibitors. *Nucleic Acids Res* 41: 264–276
- Mateyak MK, Pupek JK, Garino AE, Knapp MC, Colmer SF, Kinzy TG, Dunaway S (2018) Demonstration of translation elongation factor 3 activity from a non-fungal species, *Phytophthora infestans*. *PLoS One* 13: e0190524
- Matsuo Y, Tesina P, Nakajima S, Mizuno M, Endo A, Buschauer R, Cheng J, Shounai O, Ikeuchi K, Saeki Y et al (2020) RQT complex dissociates ribosomes collided on endogenous RQC substrate SDD1. *Nat Struct Mol Biol* 27: 323–332
- Milon P, Konevega AL, Peske F, Fabbretti A, Gualerzi CO, Rodnina MV (2007) Transient kinetics, fluorescence, and FRET in studies of initiation of translation in bacteria. *Methods Enzymol* 430: 1–30
- Murina V, Kasari M, Takada H, Hinnu M, Saha CK, Grimshaw JW, Seki T, Reith M, Putrins M, Tenson T et al (2018) ABCF ATPases involved in protein synthesis, ribosome assembly and antibiotic resistance: structural and functional diversification across the tree of life. *J Mol Biol* 43: 3568–3590
- Nielsen PR, Nietlispach D, Mott HR, Callaghan J, Bannister A, Kouzarides T, Murzin AG, Murzina NV, Laue ED (2002) Structure of the HP1 chromodomain bound to histone H3 methylated at lysine 9. *Nature* 416: 103–107
- Nishimura K, Fukagawa T, Takisawa H, Kakimoto T, Kanemaki M (2009) An auxin-based degron system for the rapid depletion of proteins in nonplant cells. *Nat Methods* 6: 917–922
- Nurenberg-Goloub E, Kratzat H, Heinemann H, Heuer A, Kotter P, Berninghausen O, Becker T, Tampe R, Beckmann R (2020) Molecular analysis of the ribosome recycling factor ABCE1 bound to the 30S post-splitting complex. *EMBO J* 39: e103788
- Park JH, Wolff EC, Park MH (2011) Assay of deoxyhypusine hydroxylase activity. *Methods Mol Biol* 720: 207–216
- Pavitt GD, Ramaiah KV, Kimball SR, Hinnebusch AG (1998) eIF2 independently binds two distinct eIF2B subcomplexes that catalyze and regulate guanine-nucleotide exchange. *Genes Dev* 12: 514–526
- Pelechano V, Alepuz P (2017) eIF5A facilitates translation termination globally and promotes the elongation of many non polyproline-specific tripeptide sequences. *Nucleic Acids Res* 45: 7326–7338
- Pellegrino S, Demeshkina N, Mancera-Martinez E, Melnikov S, Simonetti A, Myasnikov A, Yusupov M, Yusupova G, Hashem Y (2018) Structural insights into the role of diphthamide on elongation factor 2 in mRNA reading-frame maintenance. *J Mol Biol* 430: 2677–2687
- Percudani R, Pavesi A, Ottonello S (1997) Transfer RNA gene redundancy and translational selection in *Saccharomyces cerevisiae*. *J Mol Biol* 268: 322–330
- Pettersen EF, Goddard TD, Huang CC, Couch GS, Greenblatt DM, Meng EC, Ferrin TE (2004) UCSF Chimera—a visualization system for exploratory research and analysis. *J Comput Chem* 25: 1605–1612
- Phan L, Schoenfeld LW, Valasek L, Nielsen KH, Hinnebusch AG (2001) A subcomplex of three eIF3 subunits binds eIF1 and eIF5 and stimulates ribosome binding of mRNA and tRNA(i)Met. *EMBO J* 20: 2954–2965
- Ranjan N, Rodnina MV (2017) Thio-Modification of tRNA at the wobble position as regulator of the kinetics of decoding and translocation on the ribosome. *J Am Chem Soc* 139: 5857–5864
- dos Reis M, Savva R, Wernisch L (2004) Solving the riddle of codon usage preferences: a test for translational selection. *Nucleic Acids Res* 32: 5036–5044
- Rodnina MV (2018) Translation in prokaryotes. *Cold Spring Harb Perspect Biol* 10: a032664
- Rodnina MV, Semenov YP, Wintermeyer W (1994) Purification of fMet-tRNA (fMet) by fast protein liquid chromatography. *Anal Biochem* 219: 380–381
- Sasikumar AN, Kinzy TG (2014) Mutations in the chromodomain-like insertion of translation elongation factor 3 compromise protein synthesis through reduced ATPase activity. *J Biol Chem* 289: 4853–4860
- Sattlegger E, Hinnebusch AG (2005) Polyribosome binding by GCN1 is required for full activation of eukaryotic translation initiation factor 2 {alpha} kinase GCN2 during amino acid starvation. *J Biol Chem* 280: 16514–16521
- Scheres SH (2012) RELION: implementation of a Bayesian approach to cryo-EM structure determination. *J Struct Biol* 180: 519–530

- Schmidt C, Kowalinski E, Shanmuganathan V, Defenouillere Q, Braunger K, Heuer A, Pech M, Namane A, Berninghausen O, Fromont-Racine M et al (2016) The cryo-EM structure of a ribosome-Ski2-Ski3-Ski8 helicase complex. *Science* 354: 1431–1433
- Schneider-Poetsch T, Ju J, Eylar DE, Dang Y, Bhat S, Merrick WC, Green R, Shen B, Liu JO (2010) Inhibition of eukaryotic translation elongation by cycloheximide and lactimidomycin. *Nat Chem Biol* 6: 209–217
- Schuler M, Connell SR, Lescoute A, Giesebrecht J, Dabrowski M, Schroerer B, Mielke T, Penczek PA, Westhof E, Spahn CM (2006) Structure of the ribosome-bound cricket paralysis virus IRES RNA. *Nat Struct Mol Biol* 13: 1092–1096
- Schuller AP, Wu CC, Dever TE, Buskirk AR, Green R (2017) eIF5A functions globally in translation elongation and termination. *Mol Cell* 66: 194–205.e5
- Sengupta J, Nilsson J, Gursky R, Kjeldgaard M, Nissen P, Frank J (2008) Visualization of the eEF2-80S ribosome transition-state complex by cryo-electron microscopy. *J Mol Biol* 382: 179–187
- Skogerson L, Wakatama E (1976) A ribosome-dependent GTPase from yeast distinct from elongation factor 2. *Proc Natl Acad Sci USA* 73: 73–76
- Spahn CM, Gomez-Lorenzo MG, Grassucci RA, Jorgensen R, Andersen GR, Beckmann R, Penczek PA, Ballesta JP, Frank J (2004) Domain movements of elongation factor eEF2 and the eukaryotic 80S ribosome facilitate tRNA translocation. *EMBO J* 23: 1008–1019
- Svidritskiy E, Brilot AF, Koh CS, Grigorieff N, Korostelev AA (2014) Structures of yeast 80S ribosome-tRNA complexes in the rotated and nonrotated conformations. *Structure* 22: 1210–1218
- Szklarczyk D, Gable AL, Lyon D, Junge A, Wyder S, Huerta-Cepas J, Simonovic M, Doncheva NT, Morris JH, Bork P et al (2019) STRING v11: protein-protein association networks with increased coverage, supporting functional discovery in genome-wide experimental datasets. *Nucleic Acids Res* 47: D607–D613
- Taylor DJ, Nilsson J, Merrill AR, Andersen GR, Nissen P, Frank J (2007) Structures of modified eEF2 80S ribosome complexes reveal the role of GTP hydrolysis in translocation. *EMBO J* 26: 2421–2431
- Triana-Alonso FJ, Chakraborty K, Nierhaus KH (1995) The elongation factor 3 unique in higher fungi and essential for protein biosynthesis is an E site factor. *J Biol Chem* 270: 20473–20478
- Uemura S, Aitken CE, Korlach J, Flusberg BA, Turner SW, Puglisi JD (2010) Real-time tRNA transit on single translating ribosomes at codon resolution. *Nature* 464: 1012–1017
- Uritani M, Miyazaki M (1988) Role of yeast peptide elongation factor 3 (EF-3) at the AA-tRNA binding step. *J Biochem* 104: 118–126
- Van Dyke N, Pickering BF, Van Dyke MW (2009) Stm1p alters the ribosome association of eukaryotic elongation factor 3 and affects translation elongation. *Nucleic Acids Res* 37: 6116–6125
- Wasserman MR, Alejo JL, Altman RB, Blanchard SC (2016) Multiperspective smFRET reveals rate-determining late intermediates of ribosomal translocation. *Nat Struct Mol Biol* 23: 333–341
- Webb KJ, Al-Hadid Q, Zurita-Lopez CI, Young BD, Lipson RS, Clarke SG (2011) The ribosomal I1 protuberance in yeast is methylated on a lysine residue catalyzed by a seven-beta-strand methyltransferase. *J Biol Chem* 286: 18405–18413
- Weinberg DE, Shah P, Eichhorn SW, Hussmann JA, Plotkin JB, Bartel DP (2016) Improved ribosome-footprint and mRNA measurements provide insights into dynamics and regulation of yeast translation. *Cell Rep* 14: 1787–1799
- Wohlgemuth I, Brenner S, Beringer M, Rodnina MV (2008) Modulation of the rate of peptidyl transfer on the ribosome by the nature of substrates. *J Biol Chem* 283: 32229–32235
- Wolff EC, Lee SB, Park MH (2011) Assay of deoxyhypusine synthase activity. *Methods Mol Biol* 720: 195–205
- Wu CC, Zinshteyn B, Wehner KA, Green R (2019a) High-resolution ribosome profiling defines discrete ribosome elongation states and translational regulation during cellular stress. *Mol Cell* 73: 959–970.e5
- Yap KL, Zhou MM (2011) Structure and mechanisms of lysine methylation recognition by the chromodomain in gene transcription. *Biochemistry* 50: 1966–1980
- Zhang K (2016) Gctf: Real-time CTF determination and correction. *J Struct Biol* 193: 1–12
- Zheng SQ, Palovcak E, Armache JP, Verba KA, Cheng Y, Agard DA (2017) MotionCor2: anisotropic correction of beam-induced motion for improved cryo-electron microscopy. *Nat Methods* 14: 331–332
- Zhou J, Lancaster L, Donohue JP, Noller HF (2014) How the ribosome hands the A-site tRNA to the P site during EF-G-catalyzed translocation. *Science* 345: 1188–1191
- Zivanov J, Nakane T, Forsberg BO, Kimanius D, Hagen WJ, Lindahl E, Scheres SH (2018) New tools for automated high-resolution cryo-EM structure determination in RELION-3. *Elife* 7: e42166



License: This is an open access article under the terms of the Creative Commons Attribution License, which permits use, distribution and reproduction in any medium, provided the original work is properly cited.

Expanded View Figures

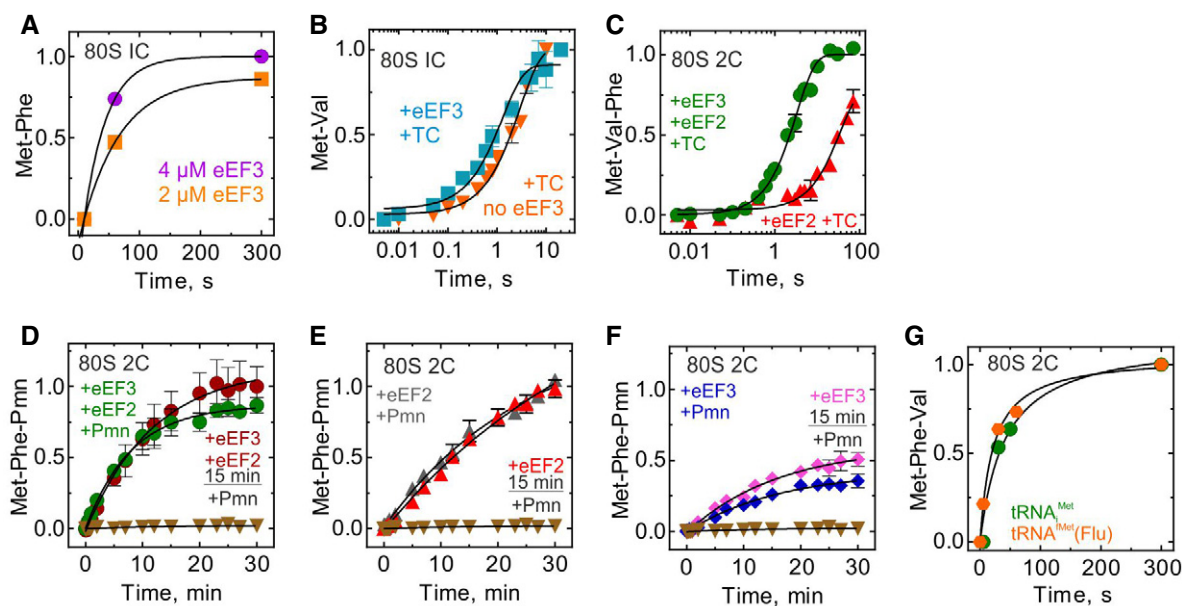


Figure EV1. Di- and tripeptide formation.

- A Time courses of MetPhe formation at different eEF3 concentrations. Data are normalized to Met-Phe formation in the presence of 4 μM eEF3 with the maximum value in the dataset set to 1.
- B Met-Val formation monitored upon rapidly mixing initiation complexes (80S IC; 1 μM) with ternary complexes eEF1A-GTP-[^{14}C]Val-tRNA^{Val} (0.2 μM) in the presence (cyan, $0.78 \pm 0.1/\text{s}$) or absence (orange, $0.34 \pm 0.03/\text{s}$) of eEF3 in a quench-flow apparatus, and the extent of peptide formation was analyzed by HPLC and radioactivity counting. Data are normalized to Met-Val formation in the presence of eEF3 with the maximum value in the dataset set to 1. Data presented as mean \pm SEM of $n = 3$ biological replicates.
- C Met-Val-Phe formation upon rapid mixing of 80S complexes carrying MetVal-tRNA^{Val} (80S 2C) with ternary complexes eEF1A-GTP-[^{14}C]Phe-tRNA^{Phe} in the presence of eEF2 and eEF3 (green, $0.3 \pm 0.02/\text{s}$), eEF2 (red, $0.03 \pm 0.006/\text{s}$). Data are normalized to Met-Val-Phe formation in the presence of eEF2 and eEF3 with the maximum value in the dataset set to 1. Data presented as mean \pm SEM of $n = 3$ biological replicates.
- D-F Comparison of time courses of 80S 2C reaction with Pmn. 80S 2C complexes with MetPhe-tRNA^{Phe} in the presence of eEF2 and eEF3 (D), eEF2 (E) or eEF3 (F), or in the absence of eEF2 and eEF3 (brown triangles), with Pmn in a quench-flow apparatus. As indicated, the reaction was started either by mixing all components, or by addition of Pmn to a mixture of 80S 2C with the factors preincubated for 15 min. The extent of MetPhe-Pmn formation was analyzed by HPLC and radioactivity counting. Data are normalized to Met-Phe-Pmn formation in the presence of eEF2 and eEF3 (D), eEF2, (E) or eEF3 (F) with the maximum value in the dataset set to 1. Data presented as mean \pm SEM of $n = 3$. For comparison, data from Fig 2B are plotted.
- G Met-Phe-Val formation upon rapid mixing of 80S complexes carrying either [^3H]Met-tRNA^{Met} (green) or [^3H]Met-tRNA^{Met}(flu) (orange) MetPhe-tRNA^{Phe} (80S 2C) with ternary complexes eEF1A-GTP-[^{14}C]Val-tRNA^{Val} in the presence of eEF2 and eEF3. Data are normalized to Met-Phe-Val formation in the presence of non-labeled initiator tRNA (green) with the maximum value in the dataset set to 1.

Source data are available online for this figure.

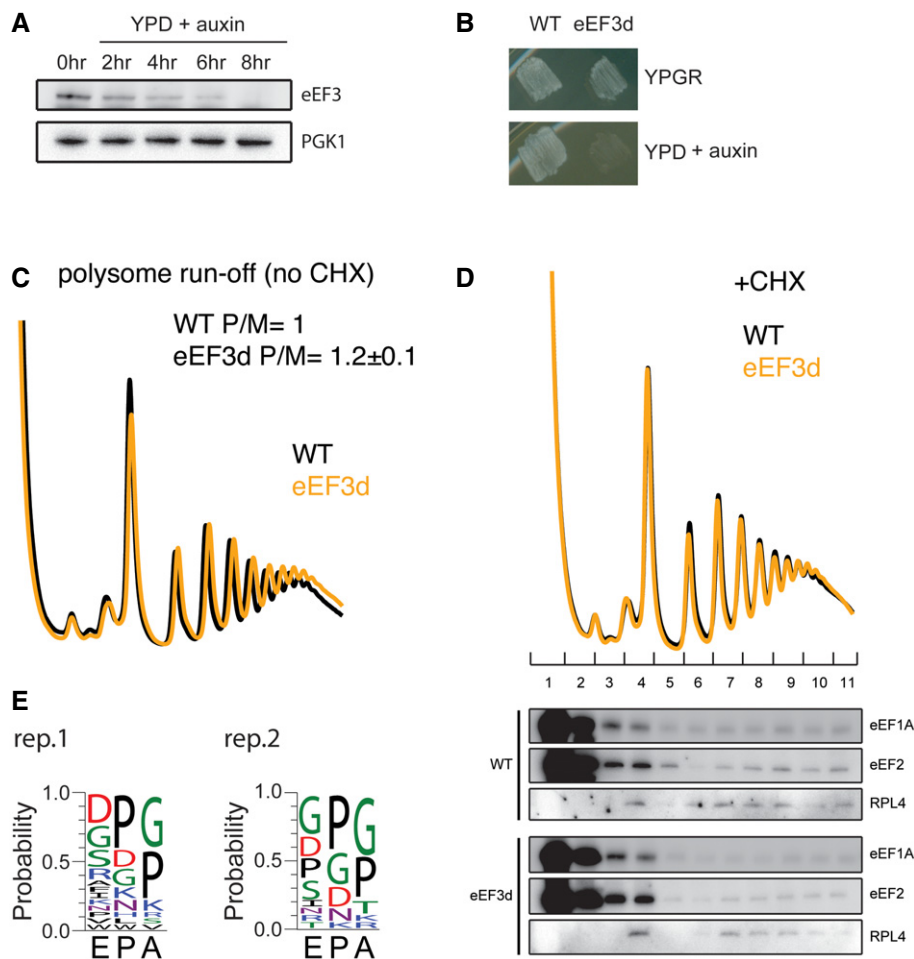


Figure EV2. Analysis of *in vivo* ribosome functional states by ribosome profiling.

- A Immunoblot of eEF3 depletion over time. Same amount of cells were harvested at indicated time points, lysed, and subjected to immunoblotting using antibodies against eEF3 or PGK1.
- B Growth of WT and eEF3d cells on YPGR and YPD + auxin plates. Plates were incubated at 30°C for 1 day.
- C Representative run-off polysome profiles for WT and eEF3d strains. Polysome-to-monomer ratios (P/M) are normalized to WT ratios. Data are presented as mean ± SD, *n* = 2.
- D Polysome profiles from WT or eEF3d cells with CHX added during cell lysis to stop translation (top). Fractions were analyzed by immunoblotting using antibodies against eEF1A, eEF2, or RPL4 (bottom).
- E De-enriched peptide motifs associated with ribosome pausing at the E, P, and A sites in the absence of eEF3. Peptide motif logos from two biological replicates are shown.

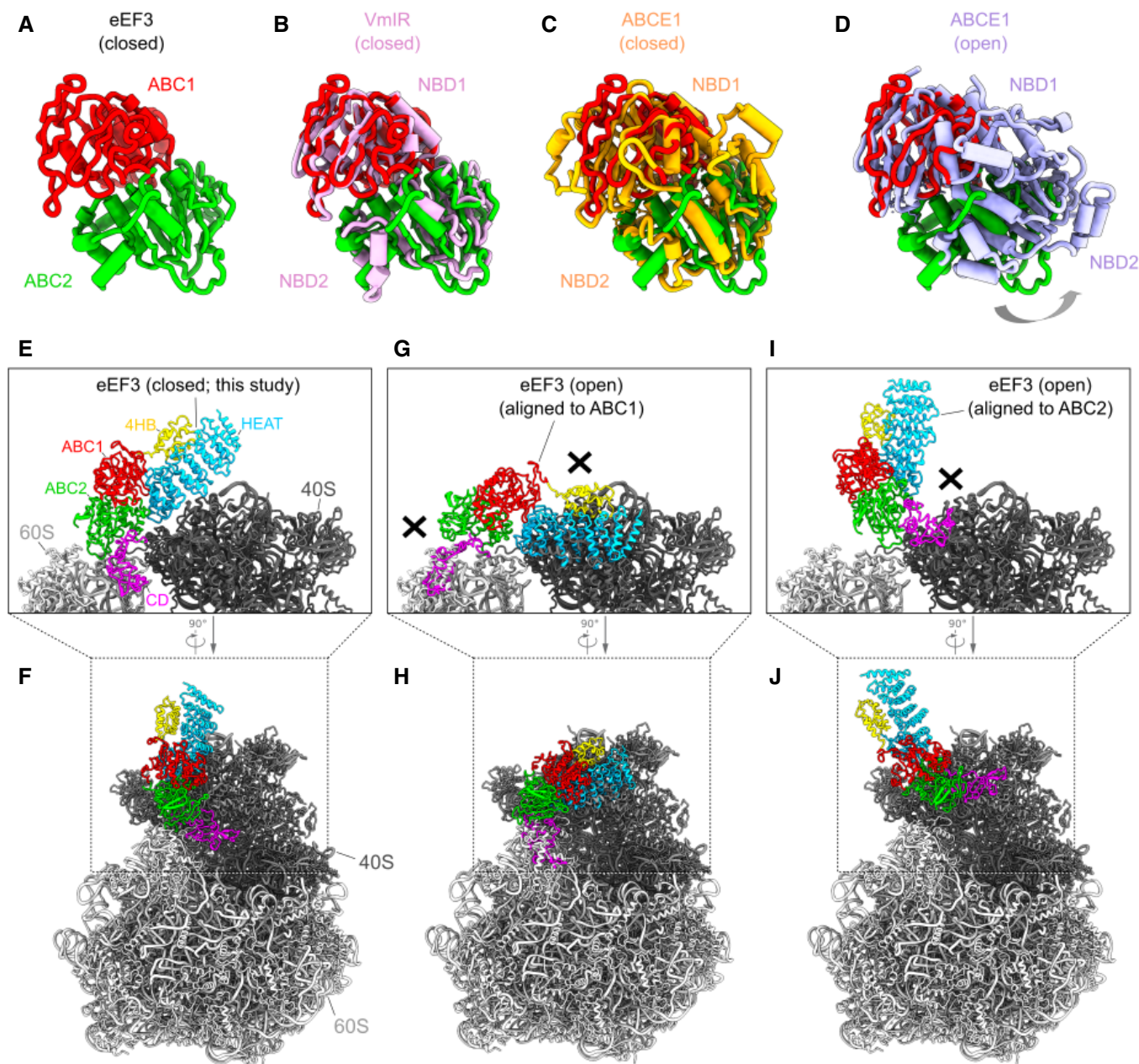


Figure EV3. The closed and open conformations of eEF3.

The closed and open conformations of eEF3

A The ABC1 (red) and ABC2 (green) domain of eEF3 in the eEF3-80S complex.

B–D Conformation of the eEF3 NBDs with respect to other ABC proteins. Alignment (based on ABC1) of the eEF3-ABCs with (B) the closed conformation of the NBDs of the *B. subtilis* ABCF ATPase VmIR (pink, PDB: 6HA8) (Crowe-McAuliffe et al, 2018), (C) the closed conformation of the archaeal ABCE1-30S post-splitting complex (orange, PDB: 6TMF) (Nureberg-Goloub et al, 2020), and (D) the *E. coli* ABCE1 protein observed in the open conformation (violet, PDB ID: 3OZX) (Barthelme et al, 2011).

E, F The eEF3 model in a closed conformation colored due to its different domain organization.

G–J Incompatibility of eEF3 to the 80S ribosome in a potential opened conformation. The eEF3 model was aligned to (G, H) ABC1 or (I, J) ABC2 of the ABCE1 protein in an opened conformation (PDB ID: 3OZX) (Barthelme et al, 2011).

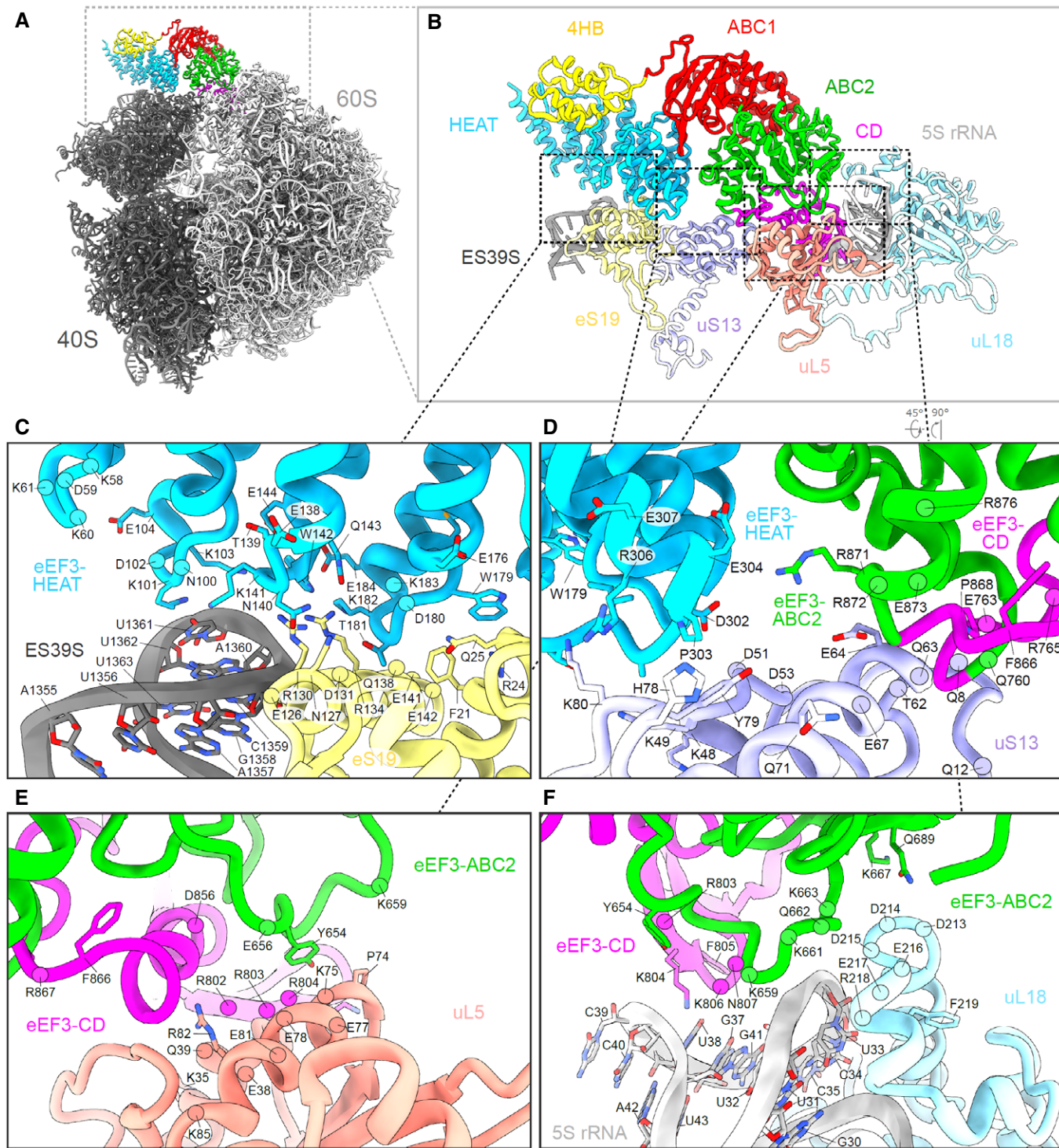


Figure EV4. Interactions of eEF3 with the 80S ribosome.

A, B (A) Overview of the eEF3-80S molecular model with (B) zoom on the eEF3 model (colored by domain) interacting with ribosomal components.
 C Interactions of the eEF3-HEAT (blue) with ES39S of the 18S rRNA (dark gray) and eS19 (pale yellow) of the SSU.
 D The 40S protein uS13 (violet) forms bridging contacts with the HEAT (blue), ABC2 (green), and CD (magenta) domains of eEF3.
 E, F The eEF3-CD and eEF3-ABC2 interact with (E) the LSU protein uL5 (coral) and (F) the 5S rRNA (light gray) and uL18 (pale blue).

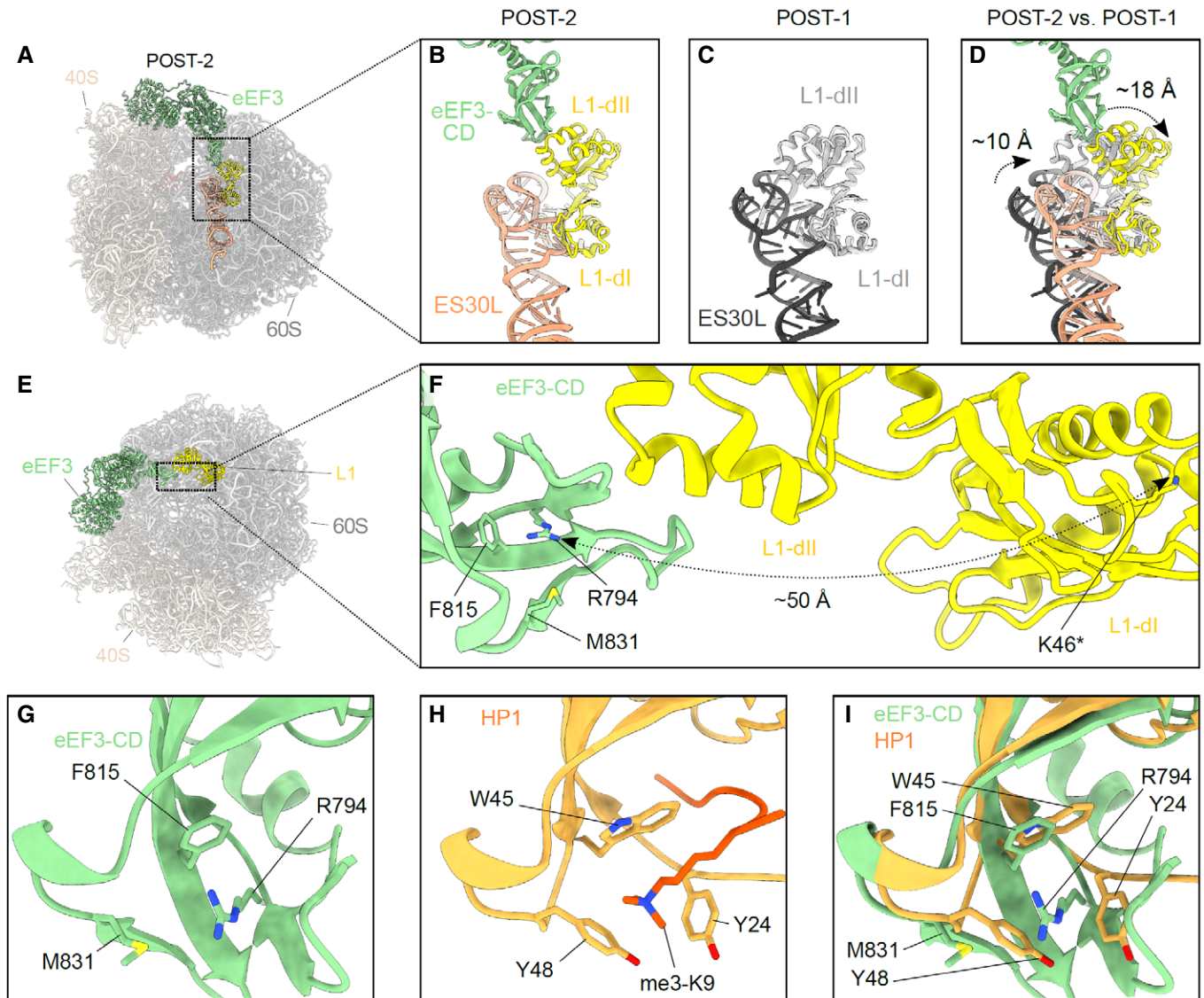


Figure EV5. The hydrophobic pocket of the eEF3 CD.

- A, B (A) Overview of the POST-2 eEF3-80S molecular model (B) highlighting the position of eEF3-CD (green) relative to L1 protein (yellow) and ES30L (orange).
- C, D (C) Same as (B) but for POST-1, and (D) comparison of (B) and (C) depicting the magnitude of the L1-stalk movement from the POST-2 state (L1-stalk'int') to the POST-1 state (L1-stalk'in'). L1-POST1 (light gray), ES30L-POST1 (dark gray).
- E, F (E) eEF3-80S molecular model highlighting eEF3 (pale green) and the L1 protein (yellow) and its (F) zoom showing the magnitude of the distance between the eEF3-CD hydrophobic pocket (based on the alignment with HP1 shown in (I)) and the K46 of the L1-dI. K46* labels the lysine, which is getting methylated by the Seven-β-strand methyltransferase (Webb et al, 2011).
- G, H (G) The eEF3-CD hydrophobic pocket based on the alignment with (H) the *D. melanogaster* HP1-CD.
- I Overlay of the eEF3 and HP1 CD based on their sequence.

SUPPLEMENTAL INFORMATION

FOR

eEF3 promotes late stages of tRNA translocation including E-tRNA release from the ribosome

Namit Ranjan^{1,#,*}, Agnieszka Pochopien^{2,3,#}, Colin Chih-Chien Wu^{4,#}, Bertrand Beckert³, Sandra Blanchet¹, Rachel Green^{4,5,*}, Marina V. Rodnina^{1,*}, Daniel N. Wilson^{2,3,*}

¹ Department of Physical Biochemistry, Max Planck Institute for Biophysical Chemistry, Am Fassberg 11, 37077 Göttingen, Germany.

² Gene Center, Department for Biochemistry and Center for integrated Protein Science Munich (CiPSM), University of Munich, Feodor-Lynenstr. 25, 81377 Munich, Germany

³ Institute for Biochemistry and Molecular Biology, University of Hamburg, Martin-Luther-King-Platz 6, 20146 Hamburg, Germany

⁴ Department of Molecular Biology and Genetics, Johns Hopkins University School of Medicine, MD21205 Baltimore, United States.

⁵ Howard Hughes Medical Institute, Johns Hopkins University School of Medicine, MD21205 Baltimore, United States.

These authors contributed equally

*Correspondence: daniel.wilson@chemie.uni-hamburg.de, rodnina@mpibpc.mpg.de,
ragreen@jhmi.edu, namit.ranjan@mpibpc.mpg.de

Table of contents

Appendix Figure S1 – page 2

Appendix Figure S2 – page 3

Appendix Figure S3 – page 4-5

Appendix Figure S4 – page 6

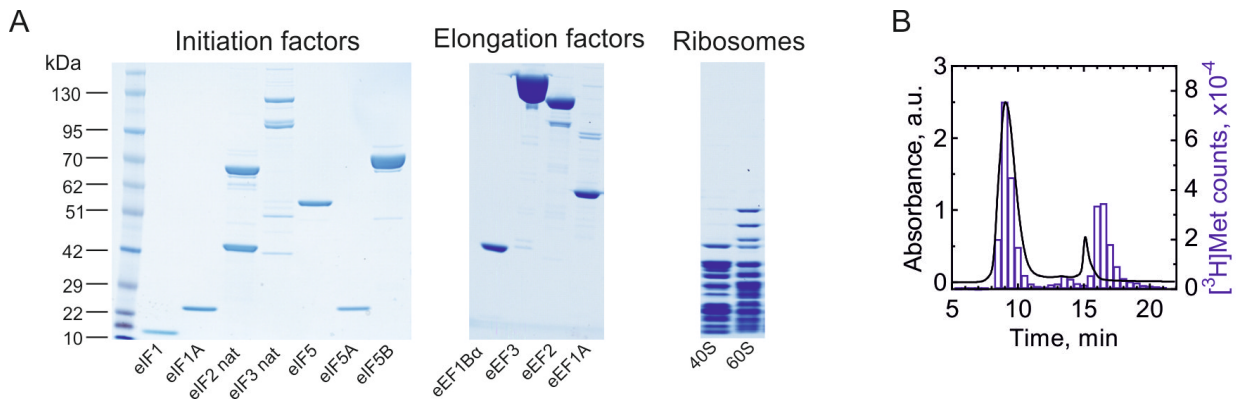
Appendix Figure S5 – page 7-8

Appendix Figure S6 – page 9

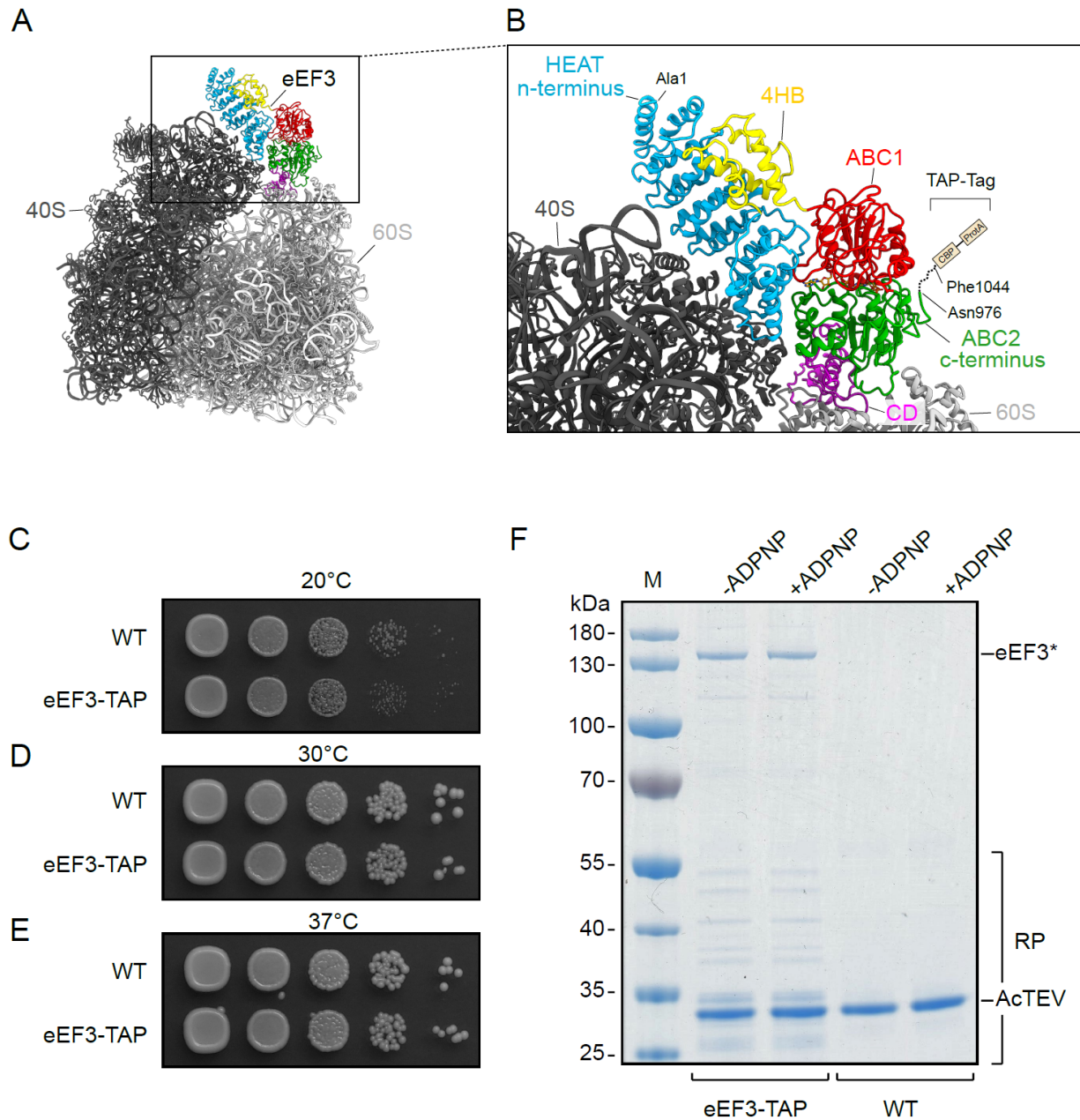
Appendix Table S1 – page 10

Supplemental References – page 11

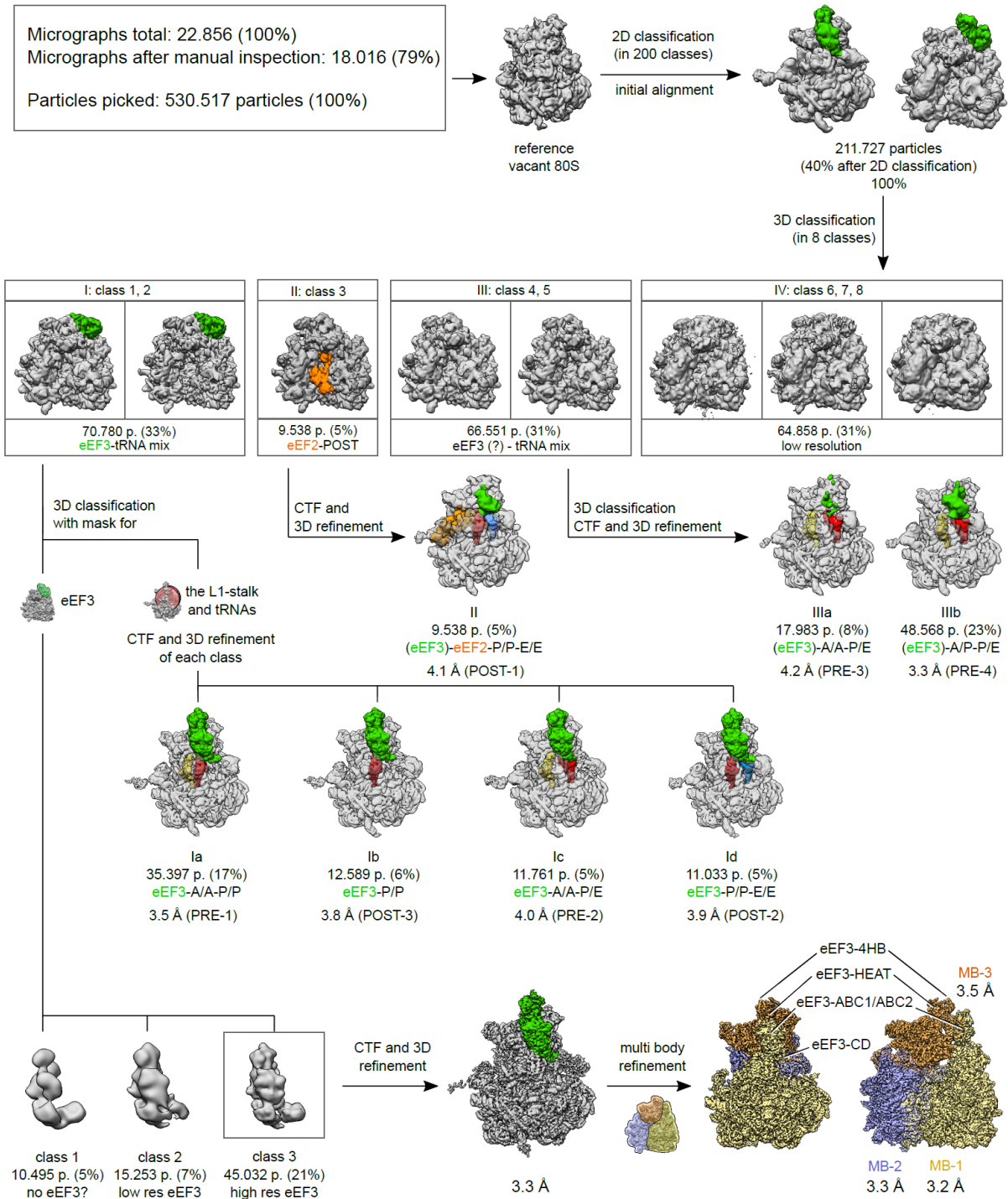
SUPPLEMENTAL FIGURES



Appendix Figure S1 Components of the reconstituted yeast translation system, related to Figure 1. (A) Quality control of the initiation and elongation factors and the ribosomes by PAGE. For each component, 50 to 100 pmol were loaded on a NuPAGE 4 to 12% gradient gel. “nat” denotes purification of native eIF2 and eIF3 from yeast. **(B)** Purification of the 80S IC by SEC on a Biosuite 450 using HPLC. The presence of 80S IC is identified as the overlap between the absorbance of the ribosomes at 260 nm (black) and the radioactivity from [³H]Met-tRNA_i^{Met} (blue).

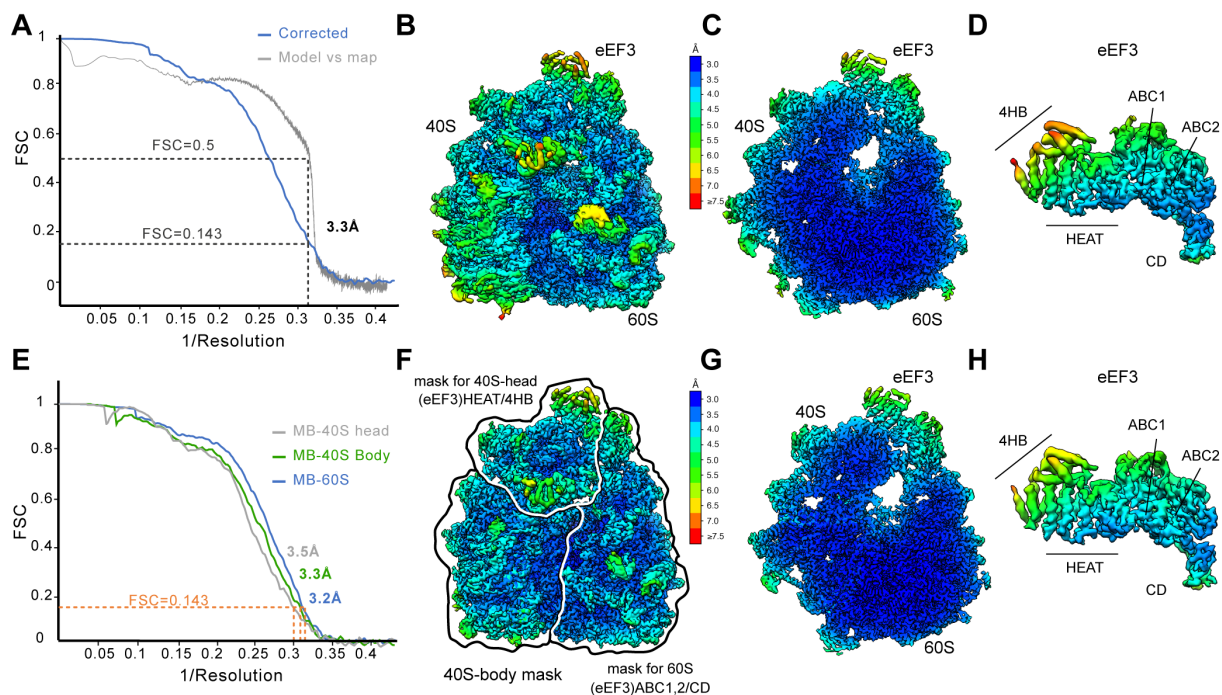


Appendix Figure S2. Analysis of eEF3-TAP tagged strains and purifications, related to Figure 4. (A) Overview and (B) Zoom of binding position of eEF3 on the 80S ribosome, highlighting in (B) the position of the C-terminal TAP-tag. (C-E) Growth of WT and eEF3-TAP tagged strain as a dilution series on agar plates incubated at (C) 20°C, (D) 30°C and (E) 37°C. (F) Coomassie stained SDS-PAGE of elution fractions of tandem affinity purification using eEF3-TAP and WT strains in the absence and presence of ADPNP. M, molecular weight marker (kDa); AcTEV indicates position of TEV protease, eEF3*, position of eEF3 and RP, ribosomal proteins

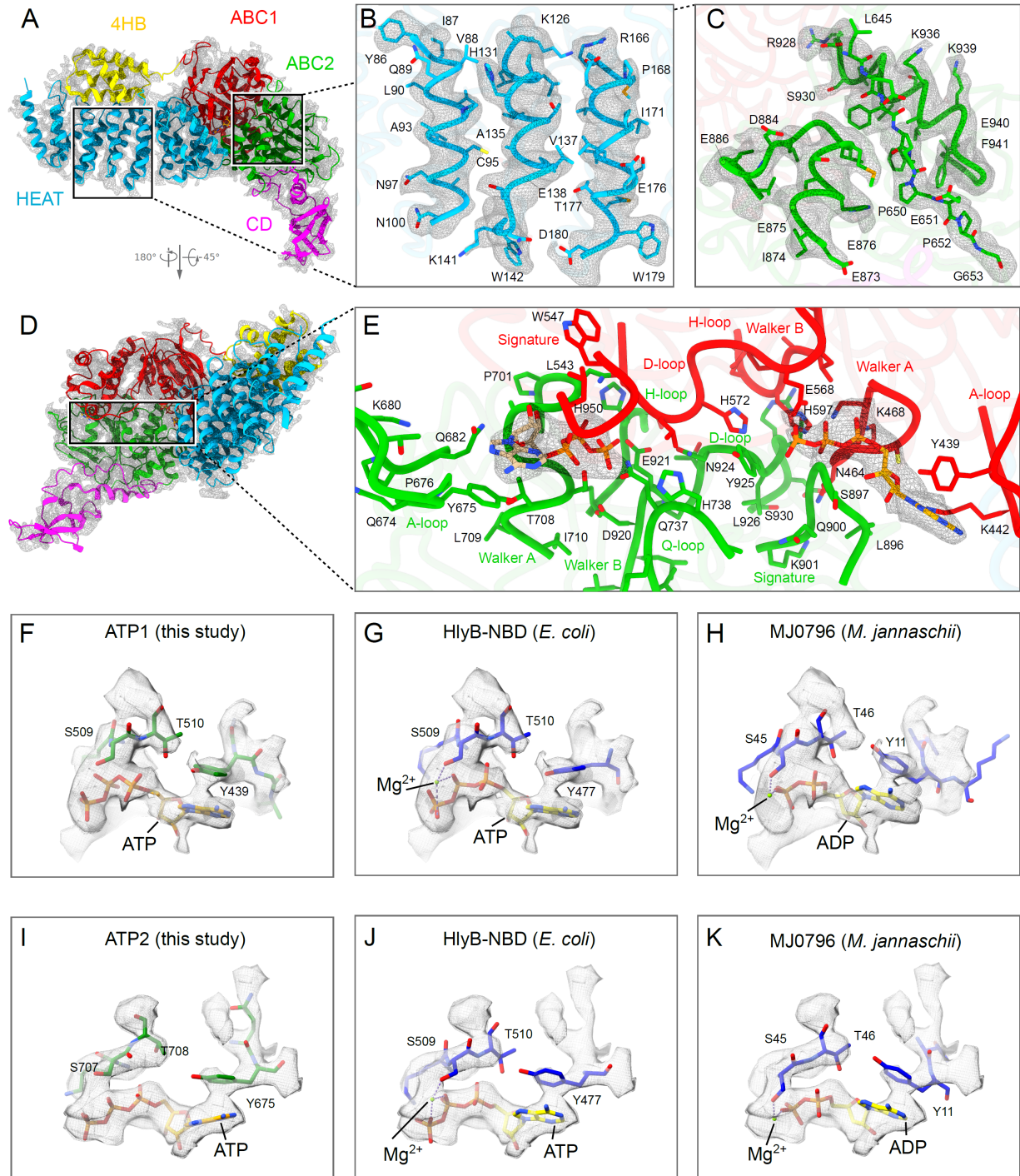


Appendix Figure S3. 3D classification of the *S. cerevisiae* eEF3-80S complex, related to Figure 4. Following 2D classification, 211,727 particles were initially aligned against a vacant *S. cerevisiae* 80S ribosome and subjected to 3D classification, sorting the particles into eight classes. The particles in class 1 and 2 bearing a stable eEF3-80S complex were joined in group I and subjected to two focused sortings using two different masks: the first encompassing the eEF3

ligand and the second covering the tRNAs, the L1-stalk and the eEF3-CD. The first classification allowed the sorting for a high resolution eEF3 bound volume (class 3, 21%, 45,032 particles), which was 3D and CTF refined resulting in a 3.3 Å final reconstitution. The final map was further multi body refined and provided a resolution of 3.2 Å for the LSU-eEF3 (ABC1/2, CD) (MB-1), 3.3 Å for the SSU body (MB-2) and 3.5 Å for the SSU head-eEF3 (HEAT, 4HB) (MB-3). The second sorting procedure enabled the classification of four EF3-bound non-rotated ribosomal classes with distinct tRNA occupancies (Ia-Id) with final resolutions denoted in the scheme. Class 3 (group II) showed a ribosomal species bearing eEF2, P/P- and E/E-tRNA and was finally refined to 4.1 Å. Class 4 and 5 (joined to group III) showed a rotated ribosome with mixed tRNA occupancy and after low pass filtering a disordered eEF3 ligand. This class was sorted further into two volumes (IIIa, IIIb) whereas each of them was 3D and CTF refined resulting in 4.2 Å and 3.8 Å resolution for the A/A- and P/E-tRNA occupied 80S (IIIa) and the A/P and P/E-tRNA bound ribosome (IIIb), respectively. Classes 6, 7, 8 (group IV) contained low resolution particles, which also showed a partial density for eEF3.

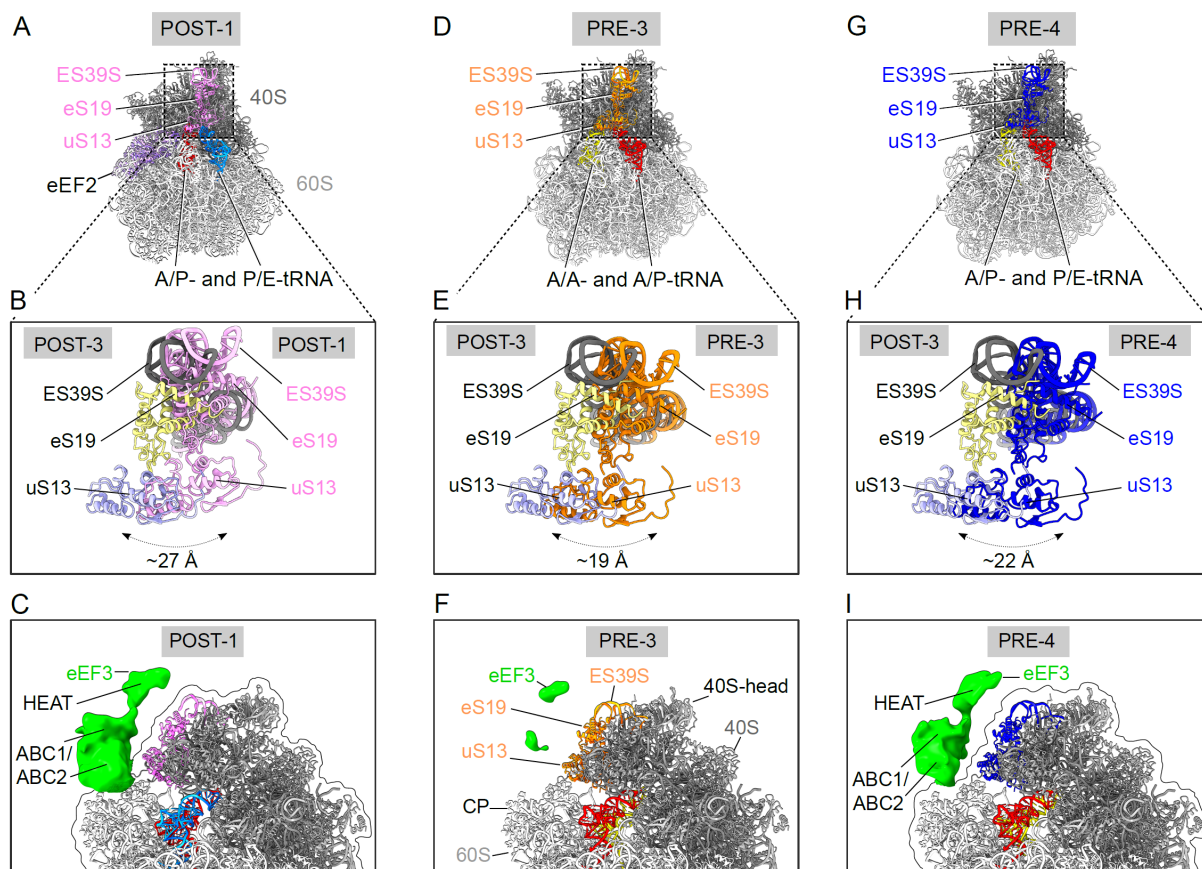


Appendix Figure S4. Overview of the final refined cryo-EM reconstruction of the eEF3-80S complex, related to Figure 4. (A) Fourier shell correlation (FSC) curve (blue curve) of the final refined cryo-EM map of the eEF3 ribosomal complex, indicating the average resolution of 3.3 Å, according to the gold-standard criterion (FSC=0.143). Overlay is the FSC curve calculated between the cryo-EM reconstruction and the final model (grey curve). (B) Cryo-EM map of the 3.3 Å EF3-80S complex filtered and colored according to local resolution and (C) its transverse section. (D) View of the isolated density for eEF3 from (B). (E) FSC curve of the three multibody (MB) refined cryo-EM map of the eEF3-80S complex, indicating the average resolution of 3.2 Å for MB-60S, 3.3 Å for MB-40S body and 3.5 Å for MB-40S head. (F) Cryo-EM map of the MB refined EF3-80S complex filtered and colored according to local resolution. The outlines are depicting the three masks, which were used for the MB refinement. (G) Transverse section of the volume shown in (F). (H) Isolated density for eEF3 from (F). The scale bar is valid for all showed resolution panels.



Appendix Figure S5. Model for *S. cerevisiae* eEF3 with bound ATP/ADPNP molecules, related to Figure 4. (A) Model of the 80S-bound eEF3 based on the multibody refined map (gray mesh) and colored by domain. HEAT (blue), 4HB (yellow), ABC1 (red), ABC2 (green) and CD (magenta). (B-C) Selected examples illustrating the quality of fit of the molecular model within (B) the HEAT repeat region and (C) the ABC2 domain to the unsegmented cryo-EM map (gray mesh). (D) eEF3-80S molecular model shown in (A), but in the orientation showing the

ATP-binding cassettes and **(E)** zoom of the two nucleotide-binding sites formed by ABC1 and ABC2. For the bound ATP/ADPNP molecules cryo-EM map densities of the multibody refined map (dark grey mesh) are illustrated. The residues, which show density are shown as sticks and labelled. **(F-K)** Isolated electron density (transparent grey) for nucleotide binding pocket of **(F-H)** ABC1 and **(I-K)** ABC2 modelled with **(F, I)** ATP in the eEF3 (green) structure, or rigid-body fitted with the crystal structures of **(G,J)** *E. coli* HlyB-NBD with ATP/Mg²⁺ (PDB ID: 1XEF) (Zaitseva, Jenewein, Jumpertz, Holland, & Schmitt, 2005) or **(H,K)** *M. jannaschii* MJ0796 ABC protein with ADP/Mg²⁺ (PDB ID: 1F3O) (Yuan et al., 2001).



Appendix Figure S6. The rotated 80S bound to disordered eEF3, related to Figure 6. (A) Rotated 80S molecular model corresponding to the POST-1 state (disordered density for eEF3 is not shown). The ribosomal residues ES39S, eS19 and uS13 responsible for eEF3-HEAT binding are depicted in pink. **(B)** Zoomed view of ES39S, eS19 and uS13 highlighted in **(A)** overlaid with corresponding residues from the non-rotated POST-3 state. The arrows are showing the magnitude of the movement of these residues from a non-rotated POST-3 to a rotated POST-1 state in **(A)**. **(C)** Segmented density for the disordered eEF3 from the POST-1 cryo-EM map highlighting the lack of association of the eEF3-HEAT repeat region with the moved ES39S, eS19 and uS13 resulting from the subunit rotation. **(D)** 80S model in rotated PRE-3 state depicting ES39S, eS19 and uS13 in orange and the **(E)** corresponding zoom of the displacement of the mentioned residues in the rotated ribosome. **(F)** Isolated density for the potential disordered ligand from the PRE-3 volume showing barely any density for eEF3. **(G)** PRE-4 ribosomal model with ES39S, eS19 and uS13 colored in blue as well as **(H)** the corresponding enlargement of these residues compared to the residues in the POST-3 state. **(I)** Segmented density of the eEF3 ligand from the rotated PRE-4 state. The isolated densities in **(C)**, **(F)** and **(I)** were low pass filtered to 8 Å.

Appendix Table S1 Cryo-EM data collection, refinement and validation statistics

eEF3-80S complex	
PDB ID	7B7D
EMDB ID	EMD-12081
Data collection and processing	
Microscope	Titan Krios
Magnification	129,151
Voltage (kV)	300
Electron exposure (e ⁻ /Å ²)	28
Defocus range (μm)	-0.8 to -2.5
Pixel size (Å)	1.084
Symmetry imposed	C1
Initial particle images (no.)	530,517
Final particle images (no.)	45,032
Map resolution (Å)	3.3
FSC threshold	0.143
Map resolution range (Å)	2.9-7.5
Detector	Falcon 2
Map sharpening <i>B</i> factor (Å ²)	-88,2563
Refinement	
Initial model used (PDB code)	6S47
CC _{Volume}	0.77
CC _{Mask}	0.78
CC _{Box}	0.75
Model composition	
Non-hydrogen atoms	211,145
Protein residues	12,111
RNA bases	5,430
R.m.s. deviations	
Bond lengths (Å)	0.010
Bond angles (°)	1.509
Validation	
MolProbity score	1.75
Clashscore	4.35
Poor rotamers (%)	0.99
Ramachandran plot	
Favored (%)	90.56
Allowed (%)	9.35
Disallowed (%)	0.08
Validation RNA	
Correct sugar pucker (%)	98.5
Good backbone conf. (%)	97.9

Supplemental References

- Barthelme, D., Dinkelaker, S., Albers, S. V., Londei, P., Ermler, U., & Tampe, R. (2011). Ribosome recycling depends on a mechanistic link between the FeS cluster domain and a conformational switch of the twin-ATPase ABCE1. *Proc Natl Acad Sci U S A*, *108*(8), 3228-3233. doi:10.1073/pnas.1015953108
- Crowe-McAuliffe, C., Graf, M., Huter, P., Takada, H., Abdelshahid, M., Novacek, J., . . . Wilson, D. N. (2018). Structural basis for antibiotic resistance mediated by the Bacillus subtilis ABCF ATPase VmlR. *Proc Natl Acad Sci U S A*, *115*(36), 8978-8983. doi:10.1073/pnas.1808535115
- Nurenberg-Goloub, E., Kratzat, H., Heinemann, H., Heuer, A., Kotter, P., Berninghausen, O., . . . Beckmann, R. (2020). Molecular analysis of the ribosome recycling factor ABCE1 bound to the 30S post-splitting complex. *EMBO J*, *39*(9), e103788. doi:10.15252/emboj.2019103788
- Webb, K. J., Al-Hadid, Q., Zurita-Lopez, C. I., Young, B. D., Lipson, R. S., & Clarke, S. G. (2011). The ribosomal I1 protuberance in yeast is methylated on a lysine residue catalyzed by a seven-beta-strand methyltransferase. *J Biol Chem*, *286*(21), 18405-18413. doi:10.1074/jbc.M110.200410
- Yuan, Y. R., Blecker, S., Martsinkevich, O., Millen, L., Thomas, P. J., & Hunt, J. F. (2001). The crystal structure of the MJ0796 ATP-binding cassette. Implications for the structural consequences of ATP hydrolysis in the active site of an ABC transporter. *J Biol Chem*, *276*(34), 32313-32321. doi:10.1074/jbc.M100758200
- Zaitseva, J., Jenewein, S., Jumpertz, T., Holland, I. B., & Schmitt, L. (2005). H662 is the linchpin of ATP hydrolysis in the nucleotide-binding domain of the ABC transporter HlyB. *EMBO J*, *24*(11), 1901-1910. doi:10.1038/sj.emboj.7600657



Structure of Gcn1 bound to stalled and colliding 80S ribosomes

Agnieszka A. Pochopien^{a,1}, Bertrand Beekert^{a,1}, Sergo Kasvandik^b, Otto Berninghausen^{c,d}, Roland Beckmann^{c,d}, Tanel Tenson^b, and Daniel N. Wilson^{a,2}

^aInstitute for Biochemistry and Molecular Biology, University of Hamburg, 20146 Hamburg, Germany; ^bInstitute of Technology, University of Tartu, 50411 Tartu, Estonia; ^cGene Center, University of Munich, 81377 Munich, Germany; and ^dDepartment of Biochemistry, University of Munich, 81377 Munich, Germany

Edited by Peter B. Moore, Yale University, New Haven, CT, and approved March 5, 2021 (received for review January 5, 2021)

The Gcn pathway is conserved in all eukaryotes, including mammals such as humans, where it is a crucial part of the integrated stress response (ISR). Gcn1 serves as an essential effector protein for the kinase Gcn2, which in turn is activated by stalled ribosomes, leading to phosphorylation of eIF2 and a subsequent global repression of translation. The fine-tuning of this adaptive response is performed by the Rbg2/Gir2 complex, a negative regulator of Gcn2. Despite the wealth of available biochemical data, information on structures of Gcn proteins on the ribosome has remained elusive. Here we present a cryo-electron microscopy structure of the yeast Gcn1 protein in complex with stalled and colliding 80S ribosomes. Gcn1 interacts with both 80S ribosomes within the disome, such that the Gcn1 HEAT repeats span from the P-stalk region on the colliding ribosome to the P-stalk and the A-site region of the lead ribosome. The lead ribosome is stalled in a nonrotated state with peptidyl-tRNA in the A-site, uncharged tRNA in the P-site, eIF5A in the E-site, and Rbg2/Gir2 in the A-site factor binding region. By contrast, the colliding ribosome adopts a rotated state with peptidyl-tRNA in a hybrid A/P-site, uncharged-tRNA in the P/E-site, and Mbf1 bound adjacent to the mRNA entry channel on the 40S subunit. Collectively, our findings reveal the interaction mode of the Gcn2-activating protein Gcn1 with colliding ribosomes and provide insight into the regulation of Gcn2 activation. The binding of Gcn1 to a disome has important implications not only for the Gcn2-activated ISR, but also for the general ribosome-associated quality control pathways.

disome | Gcn1 | ribosome | stress | translation

All living cells must adapt to a variety of different environmental stresses in a rapid and efficient way to survive. Critical to this adaptation is the integrated stress response (ISR), a central signaling network that enables cells to maintain cellular homeostasis or enter into apoptosis. In metazoans, the ISR comprises four different kinases that each phosphorylate serine 51 of the alpha subunit of eukaryotic initiation factor 2 (eIF2). In yeast and mammalian cells, the ancestral Gcn2 (general control nonderepressible 2) kinase modulates the response to nutrient deprivation (1, 2). In mammals, Gcn2 is important for long-term memory formation, feeding behavior, and immune system regulation and also has been implicated in various diseases, including neurologic disorders such as Alzheimer's, cancers, and viral infections (1, 2). Although phosphorylation of eIF2 causes a global repression of translation initiation, translations of specific mRNAs also become up-regulated, such as the transcriptional regulator Gcn4 (yeast) or ATF4 (mammals). This in turn induces expression of genes, such as those involved in amino acid biosynthesis, to counteract the amino acid deficiency.

The prevailing model for Gcn2 activation during nutrient deprivation is that Gcn2 recognizes and binds ribosomes that have become stalled during translation due to the accumulation of uncharged (deacylated) transfer RNAs (tRNAs) binding to the ribosomal A-site (1, 2). The activation of Gcn2 strictly requires its coactivator Gcn1 (3), a large protein (2,672 amino acids, or 297 kDa in yeast) conserved from yeast to humans (2). Based on secondary

structure predictions, Gcn1 is composed almost entirely of HEAT repeats (Fig. 1A). The N-terminal three-quarters (residues 1 to 2052) of Gcn1 are required for tight association with ribosomes in vivo (4) (Fig. 1A), and a reduction in ribosome binding of Gcn1 leads to a concomitant loss in Gcn2 activation (5). The central region of Gcn1 is highly homologous to the N-terminal HEAT repeat region of the eukaryotic elongation factor 3 (eEF3) (3) (Fig. 1A), and overexpression of eEF3 represses Gcn2 activity, suggesting that Gcn1 and eEF3 have overlapping binding sites on the ribosome (6).

The eEF3-like region of Gcn1 is also important for interaction with the N terminus of Gcn20 (7, 8) (Fig. 1A), a nonessential ATP-binding cassette (ABC) protein that enhances Gcn2 activity (8). Gcn20 itself does not interact with the ribosome or with Gcn2, suggesting that Gcn20 exerts its stimulatory effect on Gcn2 via interaction and stabilization of Gcn1 on the ribosome (8). By contrast, a region (residues 2052 to 2428) within the C terminus of Gcn1 mediates direct interaction with the N-terminal RWD domain of Gcn2 (Fig. 1A) (4, 9, 10). Moreover, mutations within these regions of either Gcn1 (F2291L or R2259A) or Gcn2 (Y74A) disrupt the Gcn1–Gcn2 interaction, resulting in loss of both eIF2 phosphorylation and derepression of Gcn4 translation (4, 10).

Like Gcn2, Gir2 (Genetically interacts with ribosomal genes 2) contains an N-terminal RWD domain and interacts with Gcn1 (11). Overexpression of Gir2 prevents Gcn2 activation by competing with

Significance

There is growing evidence that collisions between ribosomes represent a cellular signal for activating multiple stress pathways, such as ribosome-associated quality control (RQC), the ribotoxic stress response, and the integrated stress response (ISR). Here we illustrate how a single protein can monitor both ribosomes within a disome, by presenting a cryo-electron microscopy structure of a native complex of the ISR protein Gcn1 interacting with both the leading stalled ribosome and the following colliding ribosome. The structure provides insight into the regulation of Gcn2 activation in yeast and has implications for the interplay between the RQC and ISR pathways in eukaryotic cells.

Author contributions: D.N.W. designed research; A.A.P., B.B., S.K., and O.B. performed research; A.A.P., B.B., S.K., R.B., T.T., and D.N.W. analyzed data; and A.A.P., B.B., and D.N.W. wrote the paper.

The authors declare no competing interest.

This article is a PNAS Direct Submission.

This open access article is distributed under [Creative Commons Attribution License 4.0 \(CC BY\)](https://creativecommons.org/licenses/by/4.0/).

¹A.A.P. and B.B. contributed equally to this work.

²To whom correspondence may be addressed. Email: daniel.wilson@chemie.uni-hamburg.de.

This article contains supporting information online at <https://www.pnas.org/lookup/suppl/doi:10.1073/pnas.2022756118/-DCSupplemental>.

Published March 31, 2021.

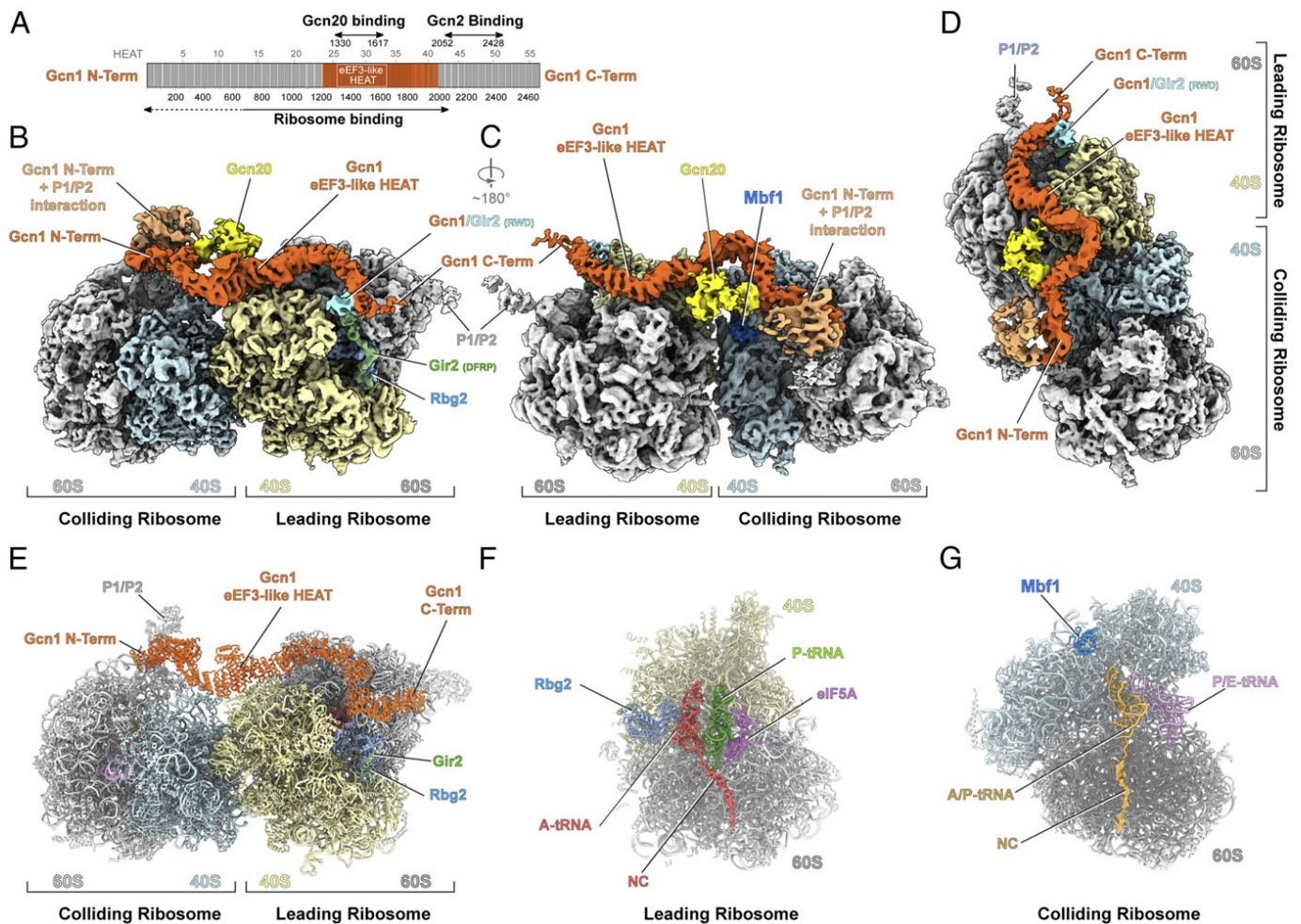


Fig. 1. The structure of the Gcn1-bound disome. **(A)** Schematic representation of the yeast Gcn1 protein with its predicted HEAT repeats (gray boxes). Areas of Gcn1 binding to the ribosome, Gcn20, and Gcn2 are indicated with arrows. **(B–D)** Cryo-EM reconstruction of the Gcn1-disome complex with segmented densities for Gcn1 (orange) and Gcn20 (yellow). On the leading ribosome, 40S (cyan), 60S (gray), Rbg2 (light blue), Gir2 (green), and Gir2-RWD (cyan); on the colliding ribosome, 40S (pale yellow), 60S (gray), Mbf1 (deep blue), and the Gcn1 interaction with P1/P2-stalk proteins (salmon). **(E–G)** Molecular models of the Gcn1-bound disome structure **(E)**; a cut-through view of the Gcn1-disome leading ribosome with Rbg2, peptidyl-tRNA (red) in the A-site, deacylated tRNA (green) in the P-site, and eIF5A (purple) in the E-site **(F)**; and the colliding ribosome with Mbf1 (dark blue), peptidyl-tRNA (gold) in the A/P-site, and deacylated tRNA (purple) in the P/E-site **(G)**.

Gcn2 for Gcn1 binding (11). Gir2 forms a complex with the ribosome binding GTPase 2 (Rbg2) (12, 13), which has been proposed to dampen the Gcn2 response (13). Despite the high conservation and importance of the Gcn pathway, as well as decades of research into the Gcn proteins (1, 2), a structural basis for their mechanism of action on the ribosome has been lacking.

Results

Cryo-Electron Microscopy Structure of a Native Gcn1-Disome Complex.

To investigate how Gcn proteins interact with the ribosome, we set out to determine a cryo-electron microscopy (EM) structure of a Gcn-ribosome complex. To obtain such a complex, we used affinity chromatography in combination with *Saccharomyces cerevisiae* cells expressing chromosomally TAP-tagged Gcn20. A C-terminal tag was favored since the N terminus of Gcn20 is required for Gcn1 interaction (7, 8), and C-terminally tagged Gcn20 was previously shown to be indistinguishable from wild-type in complementing Δ gcn20 deletion strains (8). Gcn1 is reported to interact with translating ribosomes in both the presence and absence of amino acid starvation (7); therefore, purification was performed with and without 3-amino-1,2,4-triazole (3-AT), which induces histidine starvation and leads to a loss of polysomes via

phosphorylation and inactivation of eIF2 (*SI Appendix, Fig. S1 A–D*). In both cases, copurification of Gcn1 and ribosomal proteins with Gcn20-TAP was observed (*SI Appendix, Fig. S1 B and C*) and validated by mass spectrometry (*Dataset S1*). The Gcn20-TAP eluate underwent a mild glutaraldehyde cross-linking treatment before being applied to cryo-grids and subjected to multiparticle cryo-EM. Despite repeated attempts, we were not able to visualize Gcn1 on the ribosomes from samples treated with 3-AT, whereas a low-resolution cryo-EM reconstruction of the untreated Gcn20-TAP sample revealed that a minor (5%) subpopulation of ribosomes contained an additional tube-like density, which we assigned to Gcn1 (*SI Appendix, Fig. S2*). Interestingly, this class also contained extra density located on the solvent side of the small 40S subunit, which after refinement (to 21 Å) using a larger box size, revealed that Gcn1 was associated with a disome (two 80S ribosomes) rather than a single 80S monosome (*SI Appendix, Fig. S2*). These findings suggest that if Gcn1 can interact with monosomes, the binding appears to be more labile than that to a disome.

To improve the resolution of the Gcn1-disome complex, we collected 16,823 micrographs on a Titan Krios transmission electron microscope with a Falcon II direct electron detector. Following

two-dimensional classification, the remaining 616,079 ribosomal particles were subjected to three-dimensional classification and divided into 15 different classes (*SI Appendix, Fig. S3*). A diverse range of ribosome functional states that did not contain Gcn1 were identified, most of which are likely to have copurified with the polysomes to which the Gcn1-Gcn20-disome was bound. Since many of the states have been previously reported, they will not be discussed further, with the exception of class 5, which contained a posttranslocational (P- and E-site tRNAs) state ribosome with eRF1 and eEF3 present (*SI Appendix, Fig. S3*). eEF3 has been previously reported to facilitate E-site tRNA release during elongation (14); however, our results suggest that eEF3 may also perform an analogous function during translation termination. Moreover, since the eEF3-binding site overlaps with Gcn1, and the previous eEF3-ribosome structure was at 9.9 Å (15), we refined the eRF1-eEF3-ribosome structure to an average resolution of 4.2 Å. Two of the 15 classes contained density that we attributed to Gcn1 (1, 2) (*SI Appendix, Fig. S3*) based on overlap with the eEF3-binding site on the ribosome as well as the tube-like density feature characteristic of linear solenoid HEAT repeat proteins (16).

Gcn1 Interacts with Both the Leading Stalled and Colliding Ribosomes.

Through further subsorting and local refinement (*SI Appendix, Fig. S3*), we could obtain a cryo-EM structure of the complete Gcn1-disome with an average resolution of 4.0 Å for the leading stalled ribosome; however, the colliding ribosome was poorly resolved (8.4 Å), indicating some flexibility with respect to the leading ribosome (*SI Appendix, Fig. S4 A–C*). Thus, we implemented focused refinement of the individual leading and colliding ribosomes, yielding average resolutions of 3.9 Å and 4.4 Å, respectively (*SI Appendix, Fig. S4 D–K and Table S1*). These maps were combined to generate a cryo-EM map of the complete disome, revealing how density for Gcn1 snakes its way along the disome and fuses at each end with density for the P-stalk proteins of both ribosomes (Fig. 1 *B–D* and *Movie S1*). We attributed the extra density contacting Gcn1 at the interface between the leading and colliding ribosomes to the N-terminal domain of Gcn20 (Fig. 1 *B–D*), since this region of Gcn1 is critical for interaction with the N terminus of Gcn20 (7, 8). However, the density is poorly resolved, and thus no model could be built for this region. In addition to Gcn1, we observed density for Rbg2/Gir2 in the A-site of the leading ribosome, as well as multiprotein bridging factor 1 (Mbf1) on the 40S subunit of the colliding ribosome (Fig. 1 *B–D* and *Movie S1*), the details and implications of which are discussed below.

To improve the density for Gcn1, an additional focused refinement was performed using a mask encompassing Gcn1 and the 40S head of the leading ribosome (*SI Appendix, Fig. S4 L–O*). The local resolution of Gcn1 was highest (4 to 7 Å) for the central eEF3-like region of Gcn1 and progressively decreased toward the N- and C-terminal ends (*SI Appendix, Fig. S4 L–O*). A molecular model for the central region of Gcn1 could be generated based on homology with eEF3 (*SI Appendix, Fig. S5 A–E*), and individual HEAT repeats could be fitted into the regions flanking the central region (Fig. 1*E* and *SI Appendix, Fig. S6 A and B*). Analogous to eEF3, the central eEF3-like region of Gcn1 contacts expansion segment 39 (ES39) and ribosomal proteins uS13 and eS19 in the head of the 40S subunit, as well as uL5 and uL18 in the central protuberance of the 60S subunit, of the leading ribosome (*SI Appendix, Fig. S6 C and D*). The flanking region N-terminal to the eEF3-like region of Gcn1 spans across the disome interface and establishes interactions with eS12 and eS31 within the beak of the 40S subunit of the colliding ribosome (*SI Appendix, Fig. S6 E and F*). Although we did not observe direct interactions between Gcn1 residues 1060 to 1777 and eS10, as suggested previously (17), we note that eS10 is adjacent to eS12 in the 40S head (*SI Appendix, Fig. S6 E and F*), and thus mutations or loss of eS10 could indirectly influence Gcn1 binding to the ribosome. While the central region of Gcn1 is relatively stable, the N- and C-terminal “arms” of Gcn1 are

highly flexible and wind their way across the disome toward the factor binding site and the P-stalk of the colliding and leading ribosomes (Fig. 1 *B–E*). The N-terminal arm of Gcn1 contacts ES43L, uL11, and P0 at the stalk base, whereas the remaining 600 N-terminal amino acids fuse with density from the other P-stalk proteins, precluding any molecular interpretation (*SI Appendix, Fig. S6 E and F*). Similarly, the C-terminal arm of Gcn1 also reaches toward the factor binding site, but on the leading ribosome, where the C terminus appears to extend and contact the P-stalk proteins, although this interaction is also poorly resolved (*SI Appendix, Fig. S6 G and H*). The interaction between Gcn1 and the P-stalk seen here provides a likely explanation for the observation that mutations or loss of the P-stalk proteins impairs Gcn2-dependent eIF2 phosphorylation (18). We note that the P-stalk proteins have been shown in vitro to activate Gcn2-dependent eIF2 phosphorylation in the absence of Gcn1 (19).

The conformation of the leading and colliding ribosomes within the Gcn1-bound disome are distinct from one another. The leading ribosome is in a nonrotated pretranslocational state with a peptidyl-tRNA in the A-site, a deacylated tRNA in the P-site, and the elongation factor eIF5A in the E-site (Fig. 1*F*). The presence of eIF5A in the Gcn1-disome suggests that translation by the leading ribosome may have slowed, or even stalled, due to the presence of problematic polypeptide motifs at the peptidyl-transferase center of the large subunit (20, 21). By contrast, the colliding ribosome adopts a rotated hybrid state with a peptidyl tRNA in the hybrid A/P-site and a deacylated tRNA in the P/E-site (Fig. 1*G*). In this case, peptide bond formation has ensued, but translocation of the mRNA and tRNAs on the small subunit has not occurred. The overall constellation of a nonrotated leading ribosome followed by a rotated colliding ribosome observed in our Gcn1-disome is reminiscent of that observed previously for other colliding disomes, namely disomes formed in the presence of an inactive eRF1^{AAAG} mutant (22) or stalled on CGA-CCG- and CGA-CGA-containing mRNAs (23, 24), but differs most greatly from the poly(A)-stalled disomes that also contained nonrotated colliding ribosomes (25) (*SI Appendix, Fig. S7*).

Visualization of Rbg2-Gir2 on the Leading Ribosome of the Gcn1-Disome.

In addition to the presence of eIF5A in the E-site, the leading ribosome of the Gcn1-disome contained additional density within the factor binding site, adjacent to the A-site, which resembled a GTPase but not one of the canonical translational GTPases (Fig. 2 *A–C*). A mass spectrometry analysis of the Gcn1-disome sample instead revealed the presence of the noncanonical ribosome-binding GTPase 2 (Rbg2), which had comparable intensities to ribosomal proteins as well as some ribosome-associated factors, such as eIF5A and Mbf1 (*Dataset S1*). Although there is no available structure for Rbg2, it was possible to generate a homology model based on the structure of the closely related (62% identity) Rbg1 (26), which could then be satisfactorily fitted to the cryo-EM density (*SI Appendix, Fig. S8 A–C*). Like Rbg1, Rbg2 comprises four domains: an N-terminal helix-turn-helix (HTH), a C-terminal TGS (ThrRS, GTPase, and SpoT), and a central GTPase domain (G-domain) that is interrupted by a ribosomal protein S5 domain 2-like (S5D2L) domain (Fig. 2*D*). While the binding site of Rbg2 overlaps that of other GTPases, such as eEF2 and Hbs1, the overall architecture is distinct (*SI Appendix, Fig. S8 D–F*).

In the Gcn1-disome, the TGS domain of Rbg2 interacts with the 40S subunit, contacting helix 5/15 (h5/15) of the 18S rRNA, whereas the G and HTH domains establish contacts with the 60S subunit, including the stalk base (H43/H44), sarcin-ricin loop (SRL; H95), and H89 (Fig. 2 *E and F*). By contrast, the S5D2L domain of Rbg2 makes contacts exclusively with the A-site tRNA, such that α -helix α 7 of Rbg2 approaches the minor groove of anticodon stem in the vicinity of nucleotides 27 to 29 of the A-site

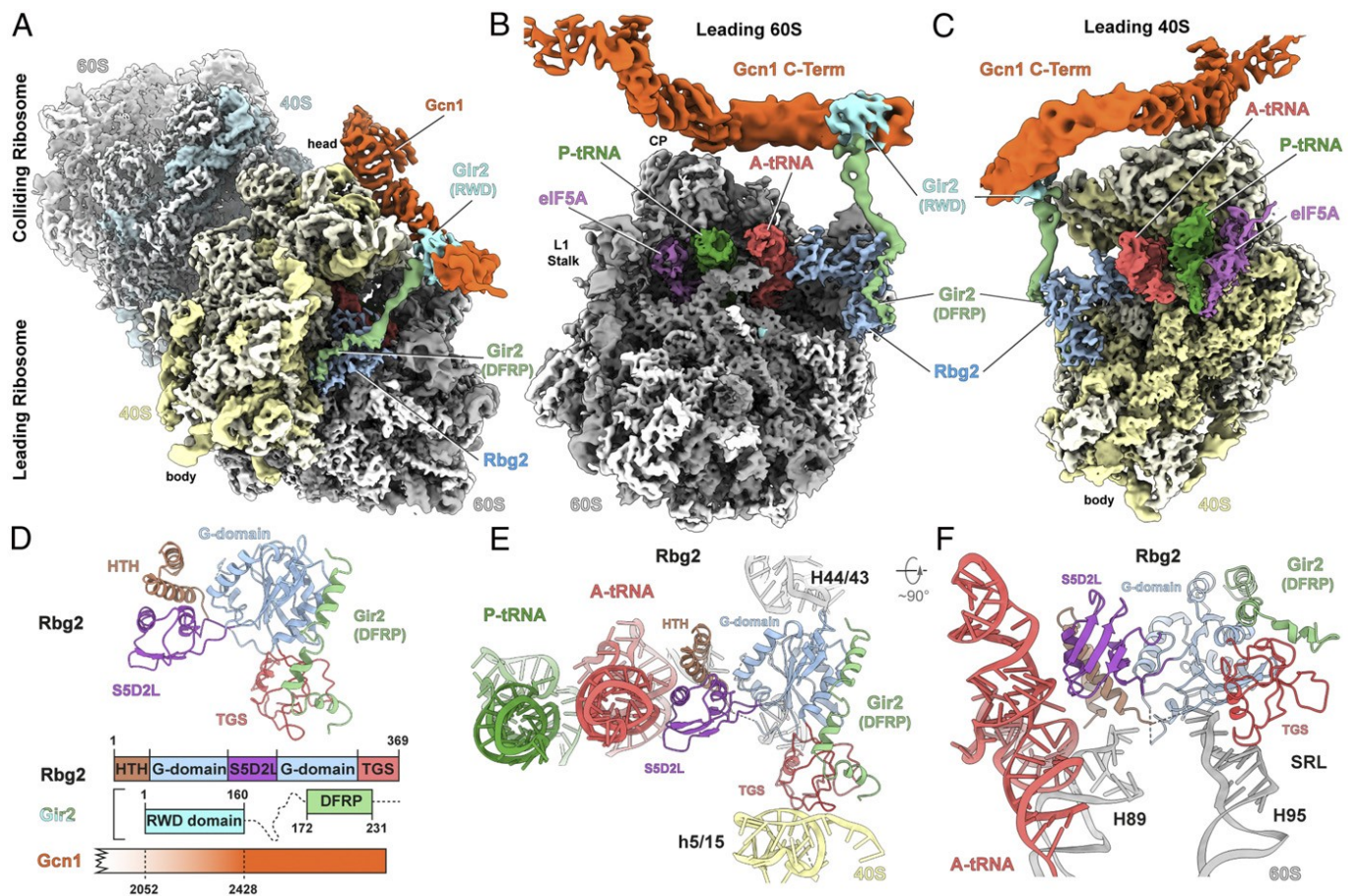


Fig. 2. Structure of Rbg2-Gir2 on the leading stalled ribosome. (A–C) Cryo-EM reconstruction of the Gcn1-disome complex (A) and interface views of the 60S subunit (B) and 40S subunit (C) of the leading stalled ribosome. Segmented densities for Gcn1 (orange), colliding ribosome (40S, cyan; 60S, gray), the leading ribosome (40S, pale yellow; 60S, gray), P-tRNA (green), A-tRNA (red), Rbg2 (light blue), Gir2-DFRP (green), Gir2-RWD (cyan), and eIF5A (purple). (D) Molecular model for Rbg2-Gir2-DFRP with schematic representation of the Rbg2-Gir2-Gcn1 interactions. Domains are colored as indicated. (E and F) Interactions of Rbg2 colored by domain as in D with 40S (pale yellow) and 60S (gray) components and A-site tRNA (red) and P-site tRNA (green).

tRNA (Fig. 2 E and F). This suggests that Rbg2 can stabilize the accommodated A-site tRNA and thus may work together with eIF5A to facilitate peptide bond formation at problematic peptide motifs. Rbg1 and Rbg2 homologs are encoded in the majority of eukaryotes, with the mammalian counterparts termed developmentally regulated GTP-binding proteins 1 (DRG1) and DRG2, respectively (27). The very high conservation (66% identity) between human (DRG1/2) and yeast (Rbg1/2) orthologs suggests that the interactions observed here for Rbg2 are likely identical for DRG2 on the human ribosome.

Under physiological conditions, Rbg2 is very labile but becomes stabilized through interactions with Gir2, whereas in contrast, Rbg1 forms a complex with Tma46 (13). Both Gir2 and Tma46 contain a C-terminal DRG family regulatory protein (DFRP) domain that is critical for interaction with Rbg2 and Rbg1, respectively (12, 13, 28). In the Rbg1-Tma46(DFRP) X-ray structure, four α -helices at the C terminus of the DFRP domain of Tma46 establish contact with the TGS and G domain of Rbg1 (26) (SI Appendix, Fig. S8G). Consistently, we observe an analogous interaction between the DFRP domain of Gir2 and the TGS and G domains of Rbg2 (Fig. 2D and SI Appendix, Fig. S8H); however, unlike Tma46, where the linker region wraps around the G domain of Rbg1, the linker region of Gir2 extends away from Rbg2 toward Gcn1 (Fig. 2 A–C and SI Appendix, Fig. S8 H and I). This suggests that in the absence of the ribosome, the intimate interaction between Tma46/Gir2 and Rbg1/Rbg2 stabilizes their respective complexes, whereas upon ribosome

binding, the N-terminal domains are freed to find new interaction partners. With respect to Rbg2-Gir2 in the Gcn1-disome structure, we observe that the density for the N-terminal region of Gir2 fuses with the C-terminal region (residues 2000 to 2200) of Gcn1 (Fig. 2 A–C).

Although the contact cannot be resolved in any detail owing to the high flexibility within this region, support for such an interaction is well documented. The N-terminal RWD domain of Gir2 is necessary and sufficient for interaction with Gcn1, and a construct containing only the C-terminal residues 2048 to 2382 of Gcn1 retains the ability to bind Gir2 (11). Moreover, the ribosome association of Gir2 also has been shown to be partially dependent on the presence of Gcn1 (11). Thus, taken together with the biochemical studies, our structural findings reveal that Gir2 indeed acts as a physical link between Rbg2 and Gcn1 and might prevent Gcn2 activation in situations where Rbg2 mediates successful restoration of translation of the leading ribosome by stimulating peptide bond formation. However, we note that a *GIR2* deletion did not alter the level of *GCN4* expression, suggesting that Gir2 likely does not have a general role in controlling Gcn2 activity (11).

Visualization of Mbfl on the Colliding Ribosome of the Gcn1-Disome.

Within the colliding ribosome of the Gcn1-disome, we observed additional density located between the head and body of the 40S subunit that we attributed to Mbfl (Fig. 3 A and B and SI Appendix, Fig. S9A), a conserved archaeal/eukaryotic protein that suppresses

+1 frameshifting at inhibitory CGA-CGA codon pairs in yeast (29). Recent findings indicate that the mammalian Mbf1 homolog, EDF1, stabilizes GIGYF2 at collisions to inhibit translation initiation in cis (30, 31); however, in our reconstruction, we did not observe any additional density for the yeast GIGYF2 homologs (Smy2/Syh1) or detect them in our mass spectrometry data (Dataset S1). The assignment of Mbf1 was based on the high intensity of Mbf1 peptides in the mass spectrometry analysis of the Gcn1-disome sample (Dataset S1) and the excellent agreement between the cryo-EM density and a homology model for Mbf1 generated from the NMR structure of the C-terminal HTH domain of Mbf1 from the fungus *Trichoderma reesei* (32) (SI Appendix, Fig. S9 B and C). Moreover, the binding site for Mbf1 observed here on the Gcn1-disome is consistent with that observed recently on stalled disomes/trisomes (31). The C-terminal HTH domain of Mbf1 connects h33 in the head with h16 and h18 within the body of the 40S subunit (Fig. 3C), thereby stabilizing a nonsweveled conformation of the head (SI Appendix, Fig. S9 D–F). Interaction with h33 is likely critical for Mbf1 function, since mutations (I85T, S86P, R89G, and R89K) within helix $\alpha 3$, which contacts h33, leads to loss of frameshift suppression (29). Binding of Mbf1 leads to a shift of h16 toward the body of the 40S subunit (Fig. 3D), which is stabilized by interactions of the C terminus and helix $\alpha 6$ of Mbf1 with the minor groove of h16 (Fig. 3D). In addition to the HTH domain, we were able to model the N-terminal residues 25 to 79 of Mbf1, including two short α -helices, $\alpha 1$ and $\alpha 2$, formed by residues 26 to 37 and 59 to 68 (Fig. 3B). Helix $\alpha 2$ of Mbf1 interacts directly with helices $\alpha 1$ and $\alpha 2$ of ribosomal protein uS3 (Fig. 3E). These interactions are

likely essential for Mbf1 function, since S104Y and G121D substitutions within these two helices of uS3 result in a loss of frameshift suppression, which can be partially restored by overexpression of Mbf1 (29). Mutations (R61T and K64E) located in the distal region of helix $\alpha 2$ of Mbf1 also abolish frameshift suppression (29). Arg61 comes into hydrogen-bonding distance with Asn111 of S3 (Fig. 3E), and Lys64 appears to interact with the backbone phosphate oxygens of h16. Asc1 (RACK1) is also critical for suppressing +1 frameshifting at CGA repeats (29, 33); however, our structure suggests that this is not due to direct interaction with Mbf1, but rather because Asc1 appears to be critical for disome formation by establishing multiple interface contacts between the leading and colliding ribosomes (SI Appendix, Fig. S7).

The N-terminal residues preceding helix $\alpha 2$ of Mbf1 wrap around the stem of h16, and consequently, the C terminus of eS30e becomes disordered (Fig. 3D and F and SI Appendix, Fig. S9 G–J). Helix $\alpha 1$ of Mbf1 is located within the major groove of h16 oriented toward the interface, suggesting that N-terminal 24 amino acids that are not observed in our structure may reach toward the leading ribosome (Fig. 3F and G). The shift of h16 induced by Mbf1 brings the minor groove of h16 into contact with the mRNA, which, together with the direct interaction observed between the mRNA and helix $\alpha 2$ of Mbf1, causes a re-direction in the path of the 3' end of the mRNA compared to the CGA-CGG stalled disome structure (Fig. 3F) (23, 24). Moreover, the mRNA appears to be kinked at the interface between the leading and colliding ribosomes, suggesting the adoption of a relaxed state instead of the more extended and potentially

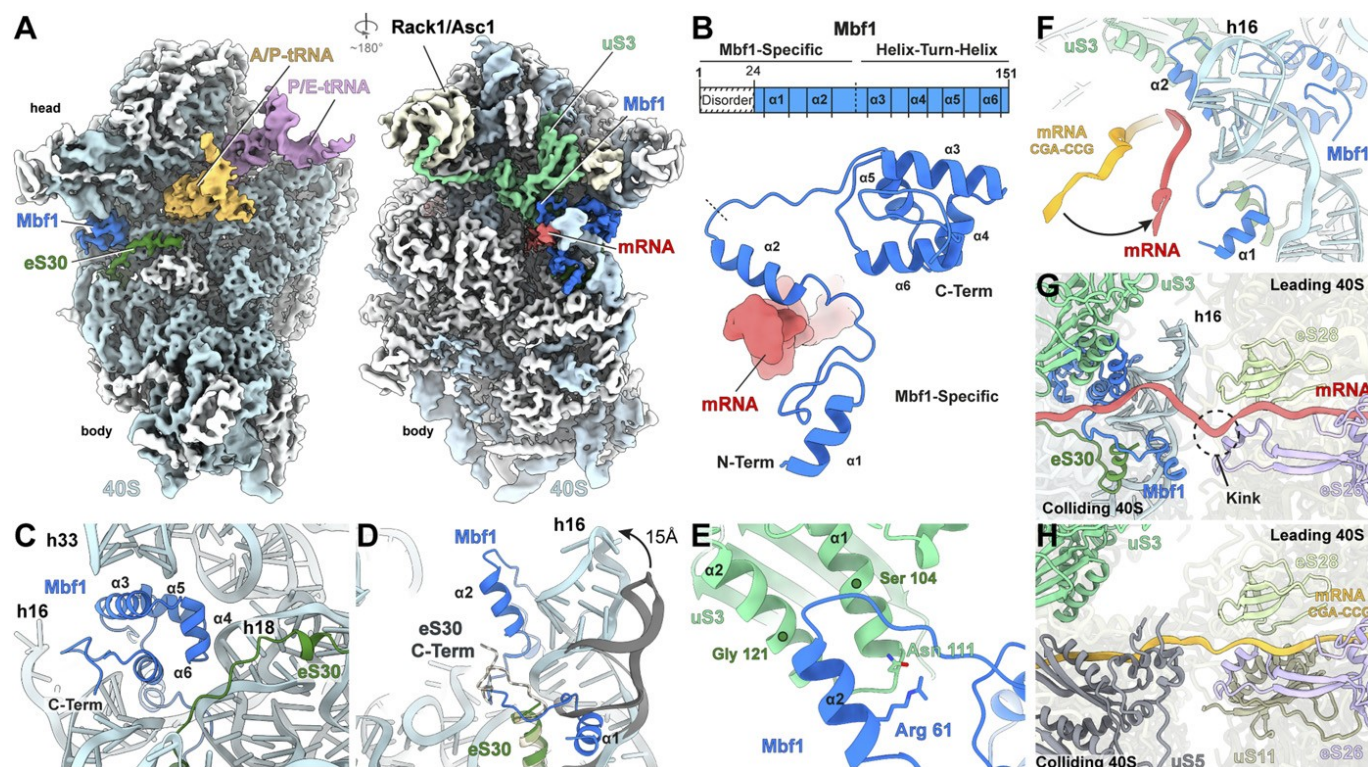


Fig. 3. Structure of Mbf1 on the colliding ribosome. (A) Cryo-EM map of the interface (Left) and solvent (Right) view of the 40S subunit from the colliding ribosome, with 40S proteins (white), 18S rRNA (cyan), A/P-tRNA (gold), P/E-tRNA (purple), eS30 (dark green), uS3 (light green), mRNA (red) and Mbf1 (deep blue). (B) Schematic and cartoon representation of the Mbf1 molecular model (deep blue). (C) Mbf1 helix-turn-helix motif bound to the 40S subunit. (D) Refolding of h16 and eS30 C terminus destabilization on Mbf1 binding. Comparison of h16 (cyan) and eS30 (dark green) in the Mbf1-bound colliding ribosome to h16 (gray) and eS30 (light green) in the colliding ribosome of an Mbf1-lacking disome (Protein Data Bank [PDB] ID 6SNT) (24). (E) Close-up view of uS3 and Mbf1 helix 2 interactions. (F) Comparison of the path of the mRNA (red) in the Mbf1-bound structure compared to the mRNA (orange) in a colliding ribosome of an Mbf1-lacking disome (PDB ID 6I7O) (23). (G and H) The mRNA path between the 40S of the colliding ribosome and the 40S of the leading ribosome within the Gcn1-disome (G) and the CGA-CCG stalled disome (PDB ID 6I7O) (H) (23). Components interacting with the mRNA at the 40S-40S interface are shown for each disome, respectively.

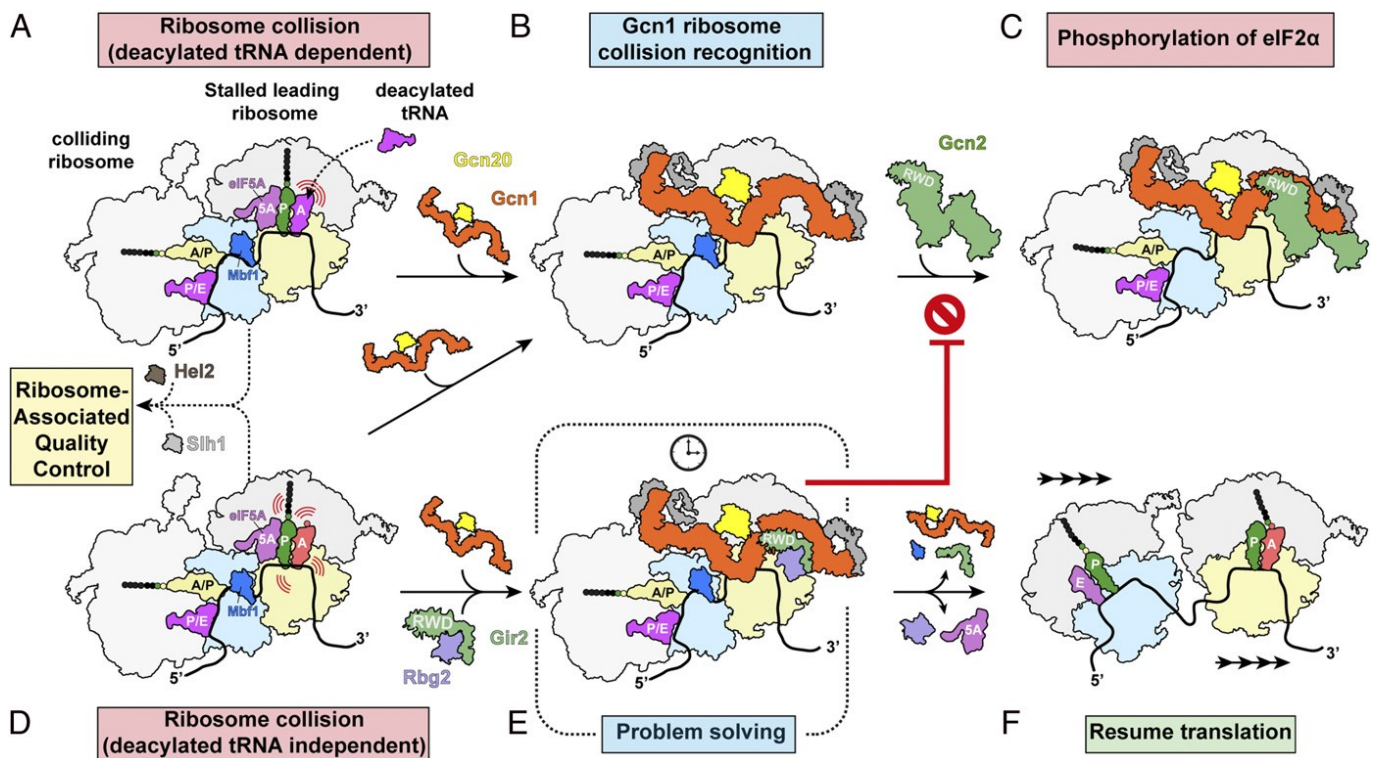


Fig. 4. Gcn1 as a checkpoint for disome collision. (A) Amino acid starvation leads to increased binding of uncharged tRNAs within the ribosomal A-site, leading to translation slowdown/stalling and collisions. (B) Colliding ribosomes (disomes) are recognized by Gcn1-Gcn20. (C) Gcn1 in turn recruits Gcn2 via direct interaction with the Gcn2 N-terminal RWD domain. Activation of Gcn2 results in the phosphorylation of eIF2 α and induction of the GAAC pathway. (D) Translating ribosomes may also encounter specific mRNA sequences/structures and/or nascent polypeptide motifs that induce a translational slow-down or pausing, also leading to collisions and disome formation, which are known as substrates for the ribosome quality control but are also recognized by Gcn1. (E) Concomitant recruitment of the Rbg2-Gir2 to the leading ribosome by Gcn1 allows Rbg2 to resolve the slowdown, while Gir2 prevents the recruitment and activation of Gcn2 and eventually allows translation to resume (F).

strained conformation seen in other disomes (Fig. 3G). Ribosome collisions have been shown to induce +1 frameshifting because the colliding ribosome exerts a pulling force on the mRNA during translocation that promotes slippage of the mRNA with respect to the tRNAs in the leading ribosome (34). Our findings suggest that Mbf1 suppresses +1 frameshifting on the leading ribosome by binding to the colliding ribosome and locking the 40S subunit in such a manner that mRNA movement is prevented. Specifically, Mbf1 prevents the head swiveling that is required for mRNA/tRNA translocation and stabilizes the mRNA via direct interactions, as well as indirectly by promoting additional interactions between the mRNA and the ribosome, especially h16. Finally, we note that the overall arrangement of the leading and colliding ribosomes in the Gcn1-disome is more compact than those observed for the CGA-CCG disome (23, 24) (Fig. 3G and H and *SI Appendix*, Fig. S10A–F). This results in a shorter path that the mRNA needs to traverse between the ribosomes, which may also contribute to maintaining a relaxed mRNA conformation on the leading ribosome. These findings imply that Gcn1 interaction with the 40S subunit of the colliding ribosome (*SI Appendix*, Fig. S6E and F), rather than Mbf1–40S interactions, are likely critical for promoting the novel compact architecture of the Gcn1-disome. Furthermore, because Mbf1 makes no contacts with Gcn1 or Rbg2, we have no reason to believe that the latter are instrumental in recruiting Mbf1 to a disome or in supporting the suppression of frameshifting at problematic codons by Mbf1.

Discussion

Together with the available literature, our findings lead us to present a model for how Gcn1 could sense stalled ribosomes and subsequently recruit Gcn2 to the stalled disome. Under

conditions of amino acid starvation, the binding of deacylated tRNA in the A-site of the ribosome causes translational stalling, which in turn increases the frequency of ribosome collisions and disome formation (35, 36) (Fig. 4A). We envisage that such disomes are recognized by the Gcn1-Gcn20 complex in an analogous manner to that observed here (Fig. 4B), and that Gcn1 can recruit and activate Gcn2 via direct interaction with its N-terminal RWD domain (Fig. 4C), analogous to the interaction established between Gcn1 and the RWD domain of Gir2. Moreover, there is growing evidence that Gcn2 activation also occurs in response to stimuli that promote collisions, but in a deacylated tRNA-independent manner (37–40) (Fig. 4D). This is consistent with our structural findings suggesting that Gcn1 recognizes the architecture of a disome, rather than directly monitoring the presence or absence of an A-site tRNA. Thus, an important prediction that we make from our study is that recognition of colliding ribosomes or disomes enables Gcn1 to facilitate Gcn2 activation in response to many diverse environmental stresses that act to inhibit translation.

Furthermore, the discovery of Rbg2-Gir2 bound to the leading ribosome of the Gcn1-disome provides support for the previously proposed concept that Gcn1 acts as a scaffold to interact with other accessory factors and thereby fine-tune the level of Gcn2 activation (2). One such example of this is the Rbg2-Gir2 complex, which is known to repress Gcn2 activation upon overexpression (11). Recent findings suggest that Rbg2 (and Rbg1) facilitate translation through problematic polybasic (Arg/Lys-rich) stretches in proteins (41). We observe Rbg2 interacting with the A-site tRNA on the leading ribosome of the Gcn1-disome, suggesting that it may stabilize the A-tRNA to promote peptide bond formation and restore the translational activity of the stalled ribosome (Fig. 4E and F). Moreover, we suggest that during this “problem-solving” phase,

Gcn2 recruitment and activation are prevented owing to the competing interaction of the RWD domain of Gnr2 with Gcn1 (11) (Fig. 4E). However, as noted above, deletion of *GIR2* did not alter the level of GCN4 expression, suggesting that Gnr2 likely does not play a general role in controlling Gcn2 activity (11). Wout et al. (11) suggested that Gnr2 may inhibit Gcn2 activation under certain conditions or within specific subcellular locations when or where Gcn2 activation is unfavorable for the cell.

Finally, our finding that colliding ribosomes are the substrate for Gcn1 recruitment provides a rationale for the emerging link between Gcn2 activation and the ribosome quality control (RQC) pathway. The RQC pathway targets stalled ribosomes for disassembly and promotes degradation of aberrant mRNAs and nascent polypeptide chains (42–44). A central player in the RQC pathway is Hel2/ZNF598, which recognizes colliding ribosomes and ubiquitylates specific 40S ribosomal proteins. This in turn recruits the helicase Slh1/ASCC to dissociate the leading ribosome from the mRNA, allowing the following ribosomes to continue translating (24, 45). Deletion of Hel2 in yeast has been recently reported to cause an increase in eIF2 phosphorylation (36), and activation of RQC by Hel2 has been shown to suppress that of Gcn2 (46). In light of our results, a likely explanation for this observation is that in the absence of Hel2, additional disome substrates become available for Gcn1 binding, leading to increased Gcn2 activation and eIF2 phosphorylation. Like Hel2, Slh1 is also nonessential in yeast, but loss of Slh1 is synthetic lethal when combined with a Rbg1/Tma46/Rbg2/Gnr2 quadruple knock-out (26). This implies that for survival, eukaryotic cells must remove the translational roadblock through either reactivation of the leading ribosome by, for example, Rbg2-Gnr2 (Fig. 4E and F), or disassembly of the stalled disome roadblock on the mRNA via the RQC pathway. While further work is needed to dissect out the mechanistic details and interplay between the factors and pathways, their conservation across all eukaryotes, including humans, implies a central and evolutionary importance.

Materials and Methods

The TAP-Tag in vivo pull-out was performed using the GCN20 TAP-tagged strain (SC0000; MATa; ura3-52; leu2-3,112; YFR009w::TAP-KIURA3) Euroscarf, essentially as described previously (47). Cells were harvested at the mid log

phase at an OD₆₀₀ of 2.5 and lysed via glass bead disruption. The cleared lysate was incubated with IgG-coated magnetic Dynabeads M-270 epoxy (Invitrogen) for 1 h at 4 °C with slow tilt rotation. The elution was performed by addition of ActEV Protease (Invitrogen) for 2 h at 17 °C in elution buffer containing 20 mM Hepes (pH 7.4), 100 mM KOAc, 10 mM Mg(OAc)₂, 1 mM DTT, and 1 mM ADPNP (Sigma-Aldrich). Since Gcn20 is an ABC ATPase, and ATP is known to stabilize binding and thus enhance Gcn2 activation (4, 5, 7, 8, 48), we included the nonhydrolyzable ATP analog ADPNP in the last step of the purification. The pull-out sample was analyzed by 4% to 12% sodium dodecyl sulfate polyacrylamide gel electrophoresis and immunoblot analysis, as well as by mass spectrometry. Here 0.02% glutaraldehyde was added to the freshly eluted TAP-Tag pull-out complex, followed by incubation for 20 min on ice. The cross-linking reaction was quenched by the addition of 25 mM Tris-HCl (pH 7.5), and n-dodecyl-D-maltoside (DDM) was added to a final concentration of 0.01% (vol/vol). Then 5 μL (8 A₂₆₀/mL) of the freshly purified and cross-linked complex was applied to 2-nm precoated Quantifoil R3/3 holey carbon supported grids and vitrified using a Vitrobot Mark IV (FEI). Low-resolution cryo-EM was performed on a 120-kV Tecnai G2 Spirit transmission electron microscope (FEI) equipped with a TemCam-F816 camera (TVIPS), whereas high-resolution cryo-EM was performed on an FEI Titan Krios transmission electron microscope operating at 300 kV equipped with a Falcon II direct electron detector. Automated particle picking was then performed using Gautomatch (<https://www.mrc-lmb.cam.ac.uk/kzhang/>) and processed using RELION-3.0 software package (49). Molecular models were generated using SWISS-MODEL (50), UCSF Chimera 1.13.1 (51), Coot (52), and ISOLDE (53), and refinement was performed using PHENIX (54). Figures showing atomic models and electron densities were generated using either UCSF Chimera (51) or ChimeraX (55) and assembled with Inkscape (<https://inkscape.org/>) and Adobe Illustrator.

Data Availability. The cryo-EM maps and associated molecular models for the leading stalled and colliding ribosomes have been deposited in the Electron Microscopy Data Bank (entries [EMD-12534](https://www.ebi.ac.uk/EMDB/entry/EMD-12534) and [EMD-12535](https://www.ebi.ac.uk/EMDB/entry/EMD-12535)) and the Protein Data Bank (PDB ID [7NRC](https://www.rcsb.org/entry/7NRC) and [7NRD](https://www.rcsb.org/entry/7NRD), respectively). Mass spectrometry data have been deposited in the ProteomeXchange database (dataset [PXD021365](https://www.ebi.ac.uk/PRIDE/entry/PXD021365)).

ACKNOWLEDGMENTS. We thank Charlotte Ungewickell for preparation of the cryo-grids and Alan Hinnebusch, Evelyn Sattlegger, Hani Zaher, Colin Wu, and Niladri Sinha for discussions and critical comments on the manuscript. This research was supported by grants from the Deutsche Forschungsgemeinschaft (WI3285/8-1 and SPP-1879, to D.N.W.), the European Union from the European Regional Development Fund through the Centre of Excellence in Molecular Cell Engineering (2014-2020.4.01.15-0013, to T.T.), and the Estonian Research Council (PRG335, to T.T.).

1. A. G. Hinnebusch, Translational regulation of GCN4 and the general amino acid control of yeast. *Annu. Rev. Microbiol.* **59**, 407–450 (2005).
2. B. A. Castilho et al., Keeping the eIF2 alpha kinase Gcn2 in check. *Biochim. Biophys. Acta* **1843**, 1948–1968 (2014).
3. M. J. Marton, D. Crouch, A. G. Hinnebusch, GCN1, a translational activator of GCN4 in *Saccharomyces cerevisiae*, is required for phosphorylation of eukaryotic translation initiation factor 2 by protein kinase GCN2. *Mol. Cell. Biol.* **13**, 3541–3556 (1993).
4. E. Sattlegger, A. G. Hinnebusch, Separate domains in GCN1 for binding protein kinase GCN2 and ribosomes are required for GCN2 activation in amino acid-starved cells. *EMBO J.* **19**, 6622–6633 (2000).
5. E. Sattlegger, A. G. Hinnebusch, Polyribosome binding by GCN1 is required for full activation of eukaryotic translation initiation factor 2alpha kinase GCN2 during amino acid starvation. *J. Biol. Chem.* **280**, 16514–16521 (2005).
6. J. Visweswaraiyah, S. J. Lee, A. G. Hinnebusch, E. Sattlegger, Overexpression of eukaryotic translation elongation factor 3 impairs Gcn2 protein activation. *J. Biol. Chem.* **287**, 37757–37768 (2012).
7. M. J. Marton, C. R. Vazquez de Aldana, H. Qiu, K. Chakraburty, A. G. Hinnebusch, Evidence that GCN1 and GCN20, translational regulators of GCN4, function on elongating ribosomes in activation of eIF2alpha kinase GCN2. *Mol. Cell. Biol.* **17**, 4474–4489 (1997).
8. C. R. Vazquez de Aldana, M. J. Marton, A. G. Hinnebusch, GCN20, a novel ATP-binding cassette protein, and GCN1 reside in a complex that mediates activation of the eIF-2 alpha kinase GCN2 in amino acid-starved cells. *EMBO J.* **14**, 3184–3199 (1995).
9. H. Kubota, Y. Sakaki, T. Ito, GI domain-mediated association of the eukaryotic initiation factor 2alpha kinase GCN2 with its activator GCN1 is required for general amino acid control in budding yeast. *J. Biol. Chem.* **275**, 20243–20246 (2000).
10. H. Kubota, K. Ota, Y. Sakaki, T. Ito, Budding yeast GCN1 binds the GI domain to activate the eIF2alpha kinase GCN2. *J. Biol. Chem.* **276**, 17591–17596 (2001).
11. P. K. Wout, E. Sattlegger, S. M. Sullivan, J. R. Maddock, *Saccharomyces cerevisiae* Rbg1 protein and its binding partner Gnr2 interact on polyribosomes with Gcn1. *Eukaryot. Cell* **8**, 1061–1071 (2009).
12. M. C. Daugeron, M. Prouteau, F. Lacroute, B. Séraphin, The highly conserved eukaryotic DRG factors are required for efficient translation in a manner redundant with the putative RNA helicase Slh1. *Nucleic Acids Res.* **39**, 2221–2233 (2011).
13. K. Ishikawa, K. Ito, J. Inoue, K. Semba, Cell growth control by stable Rbg2/Gnr2 complex formation under amino acid starvation. *Genes Cells* **18**, 859–872 (2013).
14. F. J. Triana-Alonso, K. Chakraburty, K. H. Nierhaus, The elongation factor 3 unique in higher fungi and essential for protein biosynthesis is an E site factor. *J. Biol. Chem.* **270**, 20473–20478 (1995).
15. C. B. Andersen et al., Structure of eEF3 and the mechanism of transfer RNA release from the E-site. *Nature* **443**, 663–668 (2006).
16. M. A. Andrade, C. Petosa, S. I. O'Donoghue, C. W. Müller, P. Bork, Comparison of ARM and HEAT protein repeats. *J. Mol. Biol.* **309**, 1–18 (2001).
17. S. J. Lee, M. J. Swanson, E. Sattlegger, Gcn1 contacts the small ribosomal protein Rps10, which is required for full activation of the protein kinase Gcn2. *Biochem. J.* **466**, 547–559 (2015).
18. H. P. Harding et al., The ribosomal P-stalk couples amino acid starvation to GCN2 activation in mammalian cells. *eLife* **8**, e50149 (2019).
19. A. J. Inglis et al., Activation of GCN2 by the ribosomal P-stalk. *Proc. Natl. Acad. Sci. U.S.A.* **116**, 4946–4954 (2019).
20. E. Gutierrez et al., eIF5A promotes translation of polyproline motifs. *Mol. Cell* **51**, 35–45 (2013).
21. A. P. Schuller, C. C. Wu, T. E. Dever, A. R. Buskirk, R. Green, eIF5A functions globally in translation elongation and termination. *Mol. Cell* **66**, 194–205.e5 (2017).
22. S. Juszkiewicz et al., ZNF598 is a quality control sensor of collided ribosomes. *Mol. Cell* **72**, 469–481.e7 (2018).
23. K. Ikeuchi et al., Collided ribosomes form a unique structural interface to induce Hel2-driven quality control pathways. *EMBO J.* **38**, e100276 (2019).
24. Y. Matsuo et al., RQT complex dissociates ribosomes collided on endogenous RQC substrate SDD1. *Nat. Struct. Mol. Biol.* **27**, 323–332 (2020).
25. P. Tesina et al., Molecular mechanism of translational stalling by inhibitory codon combinations and poly(A) tracts. *EMBO J.* **39**, e103365 (2020).

26. S. M. Francis, M. E. Gas, M. C. Daugeron, J. Bravo, B. Séraphin, Rbg1-Tma46 dimer structure reveals new functional domains and their role in polysome recruitment. *Nucleic Acids Res.* **40**, 11100–11114 (2012).
27. K. Ishikawa, S. Azuma, S. Ikawa, K. Semba, J. Inoue, Identification of DRG family regulatory proteins (DRFPs): Specific regulation of DRG1 and DRG2. *Genes Cells* **10**, 139–150 (2005).
28. K. Ishikawa, T. Akiyama, K. Ito, K. Semba, J. Inoue, Independent stabilizations of polysomal Drg1/Dfrp1 complex and non-polysomal Drg2/Dfrp2 complex in mammalian cells. *Biochem. Biophys. Res. Commun.* **390**, 552–556 (2009).
29. J. Wang, J. Zhou, Q. Yang, E. J. Grayhack, Multi-protein bridging factor 1(Mbf1), Rps3 and Asc1 prevent stalled ribosomes from frameshifting. *eLife* **7**, e39637 (2018).
30. S. Juszkievicz et al., Ribosome collisions trigger cis-acting feedback inhibition of translation initiation. *eLife* **9**, e60038 (2020).
31. N. K. Sinha et al., EDF1 coordinates cellular responses to ribosome collisions. *eLife* **9**, e58828 (2020).
32. R. K. Salinas et al., Solution structure of the C-terminal domain of multiprotein bridging factor 1 (MBF1) of *Trichoderma reesei*. *Proteins* **75**, 518–523 (2009).
33. A. S. Wolf, E. J. Grayhack, Asc1, homolog of human RACK1, prevents frameshifting in yeast by ribosomes stalled at CGA codon repeats. *RNA* **21**, 935–945 (2015).
34. C. L. Simms, L. L. Yan, J. K. Qiu, H. S. Zaher, Ribosome collisions result in +1 frameshifting in the absence of no-go decay. *Cell Rep.* **28**, 1679–1689.e4 (2019).
35. A. M. Darnell, A. R. Subramaniam, E. K. O'Shea, Translational control through differential ribosome pausing during amino acid limitation in mammalian cells. *Mol. Cell* **71**, 229–243.e11 (2018).
36. S. Meydan, N. R. Guydosh, Disome and trisome profiling reveal genome-wide targets of ribosome quality control. *Mol. Cell* **79**, 588–602.e6 (2020).
37. R. Ishimura, G. Nagy, I. Dotu, J. H. Chuang, S. L. Ackerman, Activation of GCN2 kinase by ribosome stalling links translation elongation with translation initiation. *eLife* **5**, e14295 (2016).
38. C. C. Wu, A. Peterson, B. Zinshteyn, S. Regot, R. Green, Ribosome collisions trigger general stress responses to regulate cell fate. *Cell* **182**, 404–416.e14 (2020).
39. S. Anda, R. Zach, B. Grallert, Activation of Gcn2 in response to different stresses. *PLoS One* **12**, e0182143 (2017).
40. J. Deng et al., Activation of GCN2 in UV-irradiated cells inhibits translation. *Curr. Biol.* **12**, 1279–1286 (2002).
41. F. Zeng, M. Pires-Alves, C. W. Hawk, X. Chen, H. Jin, Molecular functions of conserved developmentally-regulated GTP-binding protein Drg1 in translation. *bioRxiv* [Preprint] (2020).
42. O. Brandman, R. S. Hegde, Ribosome-associated protein quality control. *Nat. Struct. Mol. Biol.* **23**, 7–15 (2016).
43. C. A. P. Joazeiro, Mechanisms and functions of ribosome-associated protein quality control. *Nat. Rev. Mol. Cell Biol.* **20**, 368–383 (2019).
44. T. Inada, Quality controls induced by aberrant translation. *Nucleic Acids Res.* **48**, 1084–1096 (2020).
45. S. Juszkievicz, S. H. Speldewinde, L. Wan, J. Q. Svejstrup, R. S. Hegde, The ASC-1 complex disassembles collided ribosomes. *Mol. Cell* **79**, 603–614.e8 (2020).
46. L. L. Yan, H. S. Zaher, Ribosome quality control antagonizes the activation of the integrated stress response on colliding ribosomes. *Mol. Cell* **81**, 614–628.e4 (2021).
47. C. Schmidt et al., The cryo-EM structure of a ribosome-Ski2-Ski3-Ski8 helicase complex. *Science* **354**, 1431–1433 (2016).
48. M. Garcia-Barrio, J. Dong, S. Ufano, A. G. Hinnebusch, Association of GCN1-GCN20 regulatory complex with the N-terminus of eIF2alpha kinase GCN2 is required for GCN2 activation. *EMBO J.* **19**, 1887–1899 (2000).
49. J. Zivanov et al., New tools for automated high-resolution cryo-EM structure determination in RELION-3. *eLife* **7**, e42166 (2018).
50. S. Bienert et al., The SWISS-MODEL repository—New features and functionality. *Nucleic Acids Res.* **45**, D313–D319 (2017).
51. E. F. Pettersen et al., UCSF Chimera—A visualization system for exploratory research and analysis. *J. Comput. Chem.* **25**, 1605–1612 (2004).
52. P. Emsley, K. Cowtan, Coot: Model-building tools for molecular graphics. *Acta Crystallogr. Sect. D Biol. Crystallogr.* **60**, 2126–2132 (2004).
53. T. I. Croll, ISOLDE: A physically realistic environment for model building into low-resolution electron-density maps. *Acta Crystallogr. D Struct. Biol.* **74**, 519–530 (2018).
54. P. D. Adams et al., PHENIX: A comprehensive python-based system for macromolecular structure solution. *Acta Crystallogr. D Biol. Crystallogr.* **66**, 213–221 (2010).
55. T. D. Goddard et al., UCSF ChimeraX: Meeting modern challenges in visualization and analysis. *Protein Sci. Publ. Protein Soc.* **27**, 14–25 (2018).



Supplementary Information for
Structure of Gcn1 bound to stalled and colliding 80S ribosomes

Agnieszka A. Pochopien^{1,4}, Bertrand Beckert^{1,4}, Sergo Kasvandik², Otto Berninghausen³, Roland Beckmann³, Tanel Tenson² and Daniel N. Wilson^{1,*}

¹ Institute for Biochemistry and Molecular Biology, University of Hamburg, Martin-Luther-King-Pl. 6, 20146 Hamburg, Germany.

² University of Tartu, Institute of Technology, 50411 Tartu, Estonia

³ Gene Center and Department of Biochemistry, University of Munich, 81377 Munich, Germany

⁴ These authors contributed equally.

*Daniel N. Wilson.

Email: Daniel.Wilson@chemie.uni-hamburg.de

This PDF file includes:

Supplementary text
Figures S1 to S10
Tables S1
Legends for Movie S1
Legends for Dataset S1
SI References

Other supplementary materials for this manuscript include the following:

Movie S1
Datasets S1

Supplementary Information Text

Preparation of cell extracts and sucrose gradient analysis

Yeast whole-cell extracts of the TAP-tagged GCN20 strain (SC0000; MATa; *ura3-52*; *leu2-3,112*; YFR009w::TAP-KIURA3; Euroscarf) were prepared from cultures grown to OD₆₀₀ of 0.8-1.0 in either YPD or SC medium (plus supplements as required). Starvation conditions were induced by addition of 15 mM 3-amino-1,2,4-triazole (3-AT) (Sigma-Aldrich) to the SC culture 15 min before harvesting. Cells were harvested by centrifugation at 4,400 x g for 10 min at 4°C in a Sorvall SLC-6000 rotor (Marshall Scientific). The cell pellets were washed with ice cold water and lysis buffer (20 mM HEPES (pH 7.4), 100 mM KOAc, 10 mM Mg(OAc)₂, 1 mM DTT, Complete EDTA-free Protease Inhibitor cocktail (Roche)), transferred to a 50 ml falcon, resuspended in lysis buffer and disrupted using glass beads. Glass beads were removed by centrifugation for 5 min at 4,400 x g at 4°C in the Rotanta 460R falcon centrifuge (Hettich). The cell debris were further pelleted by centrifugation at 17,600 x g for 15 min at 4°C in a Sorvall RC 6 SS-34 rotor. The cleared lysate was layered onto 12 ml 10–60% sucrose gradient prepared in lysis buffer and centrifuged in an SW-41Ti rotor (Beckman Coulter) for 5 h at 99,000 x g at 4°C. The ribosomal fractions were analysed using a Gradient Station (Biocomp) with an Econo UV Monitor (Bio-Rad) (Fig. S1A).

Tandem affinity purification for cryo-EM analysis and Immunoblotting

The native TAP-Tag pull-out was performed using the GCN20 (and GCN1) TAP-tagged strain essentially as described before (1). Yeast whole-cell extracts of TAP-tagged GCN20 strain (SC0000; MATa; *ura3-52*; *leu2-3,112*; YFR009w::TAP-KIURA3; Euroscarf), were prepared from cultures grown in YPD or SC media (plus supplements as required). Cells grown in YPD media were harvested at the mid log phase at an OD₆₀₀ of 2.5. Cells cultured in the SC media were grown until OD₆₀₀ of 0.8 and starvation was induced for 15 min by addition of 15 mM 3-AT (Sigma-Aldrich) before harvesting. Both cell pellets were lysed via glass bead disruption and the cleared lysates were incubated with IgG-coated magnetic Dynabeads®M-270 Epoxy (Invitrogen) for 1 h at 4°C with slow tilt rotation. The elution was performed by addition of AcTEV Protease (Invitrogen) for 2 h at 17°C in elution buffer containing 20 mM HEPES (pH 7.4), 100 mM KOAc, 10 mM Mg(OAc)₂, 1 mM DTT and 1 mM ADPNP (Sigma-Aldrich). The pull-out samples were analyzed by 4-12% NuPAGE gel (ThermoFisher) and immunoblot analysis (Fig. S1B,C). For the latter one, the membrane with the transferred protein bands was shortly washed with phosphate-buffered saline (PBS) (pH 7.4) and blocked 3 x 15 min with 2% milk/PBS at RT. The blocked membrane was incubated for 1 h with the first TAP-tag polyclonal antibody (CAB1001, Rabbit/IgG, ThermoFisher #CAB1001), washed 3x15 min with PBS and incubated with the second anti-rabbit HRP antibody (Goat/IgG, ThermoFisher #31460) ON at 4°C. The next day, the membrane was shortly washed with PBS and protein bands were detected using Pierce™ ECL Western Blotting Substrate (ThermoFisher #32109) and the Amersham Imager600 (GE Healthcare). Control purifications were

also performed using an untagged wildtype strain, where no purification of ribosomal proteins was observed, as reported previously (2), suggesting that the ribosomal complexes observed in the TAP-tagged strains co-purified with the Gcn20. Moreover, purifications performed using eEF3-TAP strains did not enrich for Gcn1, Rbg2, Gir2 or Mbf1 (2), as we observed here for Gcn20-TAP, suggesting that the detection of these proteins is specific for the Gcn20 pull-out complex.

Detection of eIF2 phosphorylation

The yeast cell extract of the GCN20-TAP strain was prepared from culture grown to log-phase (OD_{600} of 0.8-1.0) in SC medium and starvation was induced by addition of 1, 5 or 15 mM 3-AT for 15 min before harvesting. 1 ml of cells with an OD_{600} of 1 was transferred into a 1.5 ml Eppendorf tube and centrifuged in a 5417R Microcentrifuge (Eppendorf) for 5 min at 20,000 x g at 4°C. The cell pellet was resuspended in 1 ml of ice-cold water and 150 μ L of NaOH/ β -Me buffer (2 M NaOH and 1.4 M β -Mercaptoethanol) was added to the sample and incubated on ice for 15 min with occasional vortexing. Subsequently, 150 μ L 72% (w/v) TCA was added to each sample and further incubated on ice for 15 min and then centrifuged at 4°C, 25,000 x g for 20 min. After removal of the supernatant, the dried pellets were resuspended in 50 μ L HU buffer (200 mM PBS (pH 7.4), 8 mM Urea, 5% (w/v) SDS, 1 mM EDTA, 100 mM freshly added DTT), denatured by heating 15 min at 65°C, separated on 10% SDS polyacrylamide gel and subjected to immunoblot analysis as described before. Phosphorylation level of eIF2 α was detected using eIF2 α antibody (Rabbit, Cell Signalling #3597) while PGK1, which was used as loading control, was detected using the commercially available PGK1 antibody (Mouse, Abcam #113687) (**Fig. S1D**).

Proteomics sample preparation and nano-LC/MS/MS analysis

Gcn20-pullout sample was loaded onto SDS-PAGE gels and run for a short time so that the samples entered into the gel and then the complete sample was excised from the gel as a single band. The gel band was then destained in 1:1 acetonitrile (ACN):100 mM ammonium bicarbonate (ABC) with vortexing, reduced with 10 mM dithiothreitol at 56°C and alkylated with 50 mM chloroacetamide in the dark. Protein digestion was carried out overnight with 10 ng/ μ l of dimethylated porcine trypsin (Sigma Aldrich) in 100 mM ABC at 37°C. Peptides were extracted from the gel matrix using bath sonication, followed by 30 min vortexing in 2 volumes of 1:2 5% formic acid (FA): ACN. The organic phase was evaporated in a vacuum-centrifuge, after which the peptides were desalted on in-house made C18 (3M) solid phase extraction tips. Purified peptides were reconstituted in 0.5% trifluoroacetic acid. Peptides were injected to an Ultimate 3000 RSLCnano system (Dionex) using a 0.3 \times 5 mm trap-column (5 μ m C18 particles, Dionex) and an in-house packed (3 μ m C18 particles, Dr Maisch) analytical 50 cm \times 75 μ m emitter-column (New Objective). Peptides were eluted at 200 nL/min with an 8-40% (30 min) A to B gradient (buffer A: 0.1% (v/v) FA; buffer B: 80% (v/v) ACN + 0.1% (v/v) FA) to a quadrupole-orbitrap Q Exactive Plus

(Thermo Fisher Scientific) MS/MS via a nano-electrospray source (positive mode, spray voltage of 2.5 kV). The MS was operated with a top-10 data-dependent acquisition strategy. Briefly, one 350-1,400 m/z MS scan at a resolution setting of $R = 70,000$ was followed by higher-energy collisional dissociation fragmentation (normalized collision energy of 26) of the 10 most intense ions (z : +2 to +6) at $R = 17,500$. MS and MS/MS ion target values were 3,000,000 and 50,000 ions with 50 and 100 ms injection times, respectively. Dynamic exclusion was limited to 15 s. MS raw files were processed with the MaxQuant software package (version 1.6.1.0) (3). Methionine oxidation, protein N-terminal acetylation were set as potential variable modifications, while cysteine carbamidomethylation was defined as a fixed modification. Identification was performed against the UniProt (www.uniprot.org) *Saccharomyces cerevisiae* (strain ATCC 204508 / S288c) reference proteome database using the tryptic digestion rule. Only identifications with at least 1 peptide ≥ 7 amino acids long (with up to 2 missed cleavages) were accepted. Intensity-based absolute quantification (iBAQ) (4) feature of MaxQuant was enabled. This normalizes protein intensities by the number of theoretically observable peptides and enables rough intra-sample estimation of protein abundance. Peptide-spectrum match, peptide and protein false discovery rate was kept below 1% using a target-decoy approach (5). All other parameters were default. Data are available via ProteomeXchange with identifier PXD021365.

Sample and grid preparation

0.02% glutaraldehyde were added to the freshly eluted TAP-Tag pull-out complex and incubated for 20 min on ice. The crosslinking reaction was quenched by addition of 25 mM Tris-HCl (pH 7.5) and n-dodecyl-D-maltoside (DDM) was added to a final concentration of 0.01% (v/v). 5 μ L (8 A_{260} /mL) of the freshly purified and crosslinked complex was applied to 2 nm precoated Quantifoil R3/3 holey carbon supported grids and vitrified using a Vitrobot Mark IV (FEI, Netherlands).

Low resolution data collection and image processing

The TAP-Tag *in vivo* Gcn20 pull-out sample was initially checked by generating a low resolution cryo-EM reconstruction with a dataset consisting of 264 micrographs collected on a 120 kV Tecnai G2 Spirit (FEI) transmission electron microscope (TEM) equipped with a TemCam-F816 camera (TVIPS) at a pixel size of 2.55 Å with a defocus range of -3.5 to -1.5 μ m. Particle picking was performed automatically using Gautomatch (<http://www.mrc-lmb.cam.ac.uk/kzhang/>) resulting in 40,012 particles (**Fig. S2**). An initial 3D reconstruction was obtained using a vacant *S. cerevisiae* 80S ribosome as a reference, followed by 3D classification into 5 classes. When compared to the vacant 80S ribosome, class 1 (5%; 2,033 particles) displayed additional density within the A-site factor binding site as well as a tube-like extra density spanning the head and central protuberance of the 80S ribosome. In addition, the class 1 ribosome displayed clear density for a neighbouring ribosome, suggesting the presence of a disome. Class 2 (14%; 5,589 particles) revealed a vacant

80S ribosome whereas class 3 (17%; 6,809 particles) had some density within the A-site region. Finally, class 4 and 5 were attributed to 'junk' classes. The particles from class 1 were selected and re-extracted with bigger box size (increased from 420 to 700) in order to encompass the full neighbouring ribosome and subsequently 3D refined at around 21 Å resolution, revealing the structure of disome with the extra 'worm-like' density for Gcn1 spanning both ribosomes within the disome (**Fig. S2**).

High resolution cryo-EM data collection and image processing

To obtain high resolution of the Gcn1-disome complex, a total of 16,823 micrographs with a total dose of 25 e-/Å² at a nominal pixel size of 1.084 Å and with a defocus ranging from -2.8 to -1.3 μm were collected using the EPU software (Thermo Fisher) on a FEI Titan Krios TEM (Thermo Fisher) operating at 300 kV equipped with a Falcon II direct electron detector. Each micrograph, consisting of a series of 10 frames, was summed and corrected for drift and beam-induced motion using MotionCor2 (6). The power spectra, defocus values, astigmatism and estimation of micrograph resolution were determined using Gctf (7). Automated particle picking was then performed using Gautomatch (<http://www.mrc-lmb.cam.ac.uk/kzhang/>), yielding initially 949,522 particles that were subjected to 2D classification using the RELION-3.0 software package (8) (**Fig. S3**). After 2D classification, 616,079 particles were selected and subsequently subjected to 3D refinement using a vacant *S. cerevisiae* 80S ribosome as initial reference. The initially refined particles were further 3D classified into 15 classes (**Fig. S3**). Class 1 (8.6%, 52,933 particles) was identified as the leading stalled ribosome containing densities for A- and P-site tRNAs, eIF5A, Gcn1, Rbg2 and Gir2, whereas class 2 (6.5%, 39,575 particles) was identified as the collided ribosome with densities for Gcn1, Mbf1, A/P- and P/E-site tRNAs. Class 3 (24.2%, 149,887 particles) and class 4 (24.4%, 151,167 particles) represent the major classes, both containing tRNAs. Class 3 had rotated ribosomes with hybrid A/P- and P/E-site tRNAs, analogous to that observed previously (9, 10), whereas class 4 was non-rotated with A- and P-site tRNAs. In addition, class 4 had additional density in the A-site that would be consistent with an open conformation of eEF1A that occurs after tRNA release and GTP hydrolysis (11). Class 5 (10.6%, 65,173 particles) contained non-rotated ribosomes with P- and E-site tRNAs and additional density for eRF1 in the A-site and eEF3 bound to the head and central protuberance of the 40S and 60S, respectively. Further sub-sorting of this class revealed subpopulations containing eEF3 and eRF1, eRF1 and eIF5A, as well as eRF1, substoichiometric eRF3 and eIF5A, however, these subpopulations could not be refined to high resolution due to the low particle number. Class 6 (7.7%, 47,171 particles) contained hibernating 80S ribosomes with the presence of eEF2 and Stm1, as reported previously (12, 13). Class 7 (1.3%, 8,169 particles) contained mature 60S particles, whereas the remaining classes (classes 8-15 totalling 16.7%, 102,004 particles) contained damaged and/or non-aligning particles and were considered as low resolution/junk.

In order to ensure that Gcn1-containing particles were not lost during the initial 3D classification, all classes (1-15) were pooled together and sub-sorted again but using a mask to focus sorting on Gcn1. This resulting in a major class with 88,453 particles. Sub-sorting of this class produced a high-resolution class (class 1 with 30,016 particles) as well as two low resolution or orientation biased classes (classes 2 and 3, totally 58,437 particles). The particles from class 1 were selected and re-extracted with bigger box size (increased from 420 to 700) in order to encompass the full neighbouring ribosome. Following 3D refinement, CTF refinement yielded a structure of the full disome (**Fig. S3**) with an average resolution of 4.0 Å for the leading stalled and 8.4 Å for the colliding ribosome (**Fig. S4A-C**). Local refinement of the of the individual ribosomes yielded average resolutions of 3.9 Å (**Fig. S4D-G**) and 4.4 Å, respectively (**Fig. S4H-K**). Local refinement of aligned particles was also performed on the 40S head/Gcn1 region of the leading stalled ribosome (**Fig. S3**), which improved the local resolution of Gcn1 (**Fig. S4L-O**). Finally sharpening of the final maps was performed by dividing the maps by the modulation transfer function of the detector and by applying an automatically determined negative B factor to the maps using Relion-3.0. For model building the final maps were locally filtered and the local resolution estimated using Relion-3.0. The final resolution of each volume was determined using the “gold standard” criterion (FSC = 0.143).

Molecular Modelling

A homology model of the Gcn1 eEF3-like HEAT repeat region (predicted residue 1330-1641) was created using the 80S-bound eEF3 model (this study) as a template for SWISS-MODELLER (14). Comparison of the two cryo-EM maps of the ribosome bound by eEF3 and Gcn1 revealed an identical overall conformation and ribosomal binding site of eEF3-HEATs and Gcn1 eEF3-like HEATs. Based on that similarity, the created Gcn1 model (8 HEAT repeats; residues 1324-1638) was fitted (cross-correlation (CC) of 0.75 between model and map) into the appropriate 7 Å low-pass filtered cryo-EM map using the command ‘fit in map’ in UCSF Chimera 1.13.1 (15) and manually adjusted with Coot version 0.8.9.2 (16). Beyond the Gcn1 EF3-like HEAT repeat region, three poly-alanine HEAT repeats were *de novo* modelled in the N-terminal direction (residues 1216-1323; (CC of 0.63 between model and map) and eight C-terminal HEAT repeats (residues 1639-1922; cross-correlation of 0.65 between model and map) using Coot version 0.8.9.2 (16). The peripheral N- and C-terminal regions could not be modelled due high flexibility of these regions in the cryo-EM map, however, the tube-like features of the density is consistent with secondary structure predictions of additional HEAT repeats, therefore, we tentatively fitted HEAT repeats from residues ~600-1100 (CC of 0.50 between model and map) and ~1950-2600 (CC of 0.57 between model and map). The very N- and C-terminal regions fuse with the stalk proteins and could not be modelled. Although Gcn20 was not well resolved, the location of the density and interaction region with Gcn1 would be consistent with the N-terminal region of Gcn20 based on available literature.

The extra density at the A-site entry factor of the stalled-leading ribosome was identified and modelled as Rbg2-Gir2. The crystal structure of the Rbg1 protein (PDB ID 4A9A) (17) was rigid body fitted into the isolated density using Chimera and the structure of Rgb2 was then generated by homology modelling within Coot (16) and Isolde (18) and subsequently refined in Phenix (19). Gir2-DFRP model was obtained using a homology model based on the Tma46 template from PDB ID 4A9A. However, due to the lack of side chain information, Gir2-DFRP has been modelled only as poly-Ala. Finally, to generate a full molecular model for the stalled leading Gcn1-Rbg2-Gir2-80S complex, existing models for the translating *S. cerevisiae* ribosome (PDB ID 6I7O), Phe-tRNA for A-tRNA and P-tRNA (PDB ID 1EVV), eIF5A (PDB ID 5GAK) (20) were used and combined with the Rbg2-Gir2 and Gcn1 model. The molecular model was then refined using Phenix (19).

The extra density located between the head and body of the colliding ribosome was identified and modelled as Mbf1 protein. The NMR structure of the C-terminal part of Mbf1 protein from the fungus *Trichoderma reesei* (PDB ID 2JVL) was rigid body fitted into the isolated density using Chimera and the *S. cerevisiae* structure of Mbf1 C-terminal region (residues 80-140) was then modelled by homology in Coot, while the N-terminal region (residues 24-79) was *de novo* modelled using Coot and Isolde. Helix 1 of Mbf1 was placed in the extra-density located in the major groove of h16, however, due to the lack of resolution, the model is only tentative and consists of a polyalanine trace. To generate a full molecular model for the colliding Gcn1-Mbf1-80S complex, existing models for the translating *S. cerevisiae* ribosome (PDB ID 6I7O), Phe-tRNA (PDB ID 1EVV) were used and combined with the Mbf1 and Gcn1 model. The molecular model was then refined using Phenix.

Figure preparation

Figures showing atomic models and electron densities were generated using either UCSF Chimera (15) or Chimera X (21) and assembled with Inkscape (<https://inkscape.org/>) and Adobe Illustrator.

Data Availability

The cryo-EM maps of the leading Gcn1(-Gcn20)-Rbg2-Gir2-80S) and the colliding ribosome (Gcn1-Mbf1-80S) have been deposited in the Electron Microscopy Data Bank with the accession codes EMD-12534 and EMD-12535. The associated molecular models of the leading (Gcn1-Rbg2-Gir2-80S) and the colliding (Mbf1-80S) ribosome are available in the Protein Data Bank with the accession PDB ID 7NRC and 7NRD, respectively.

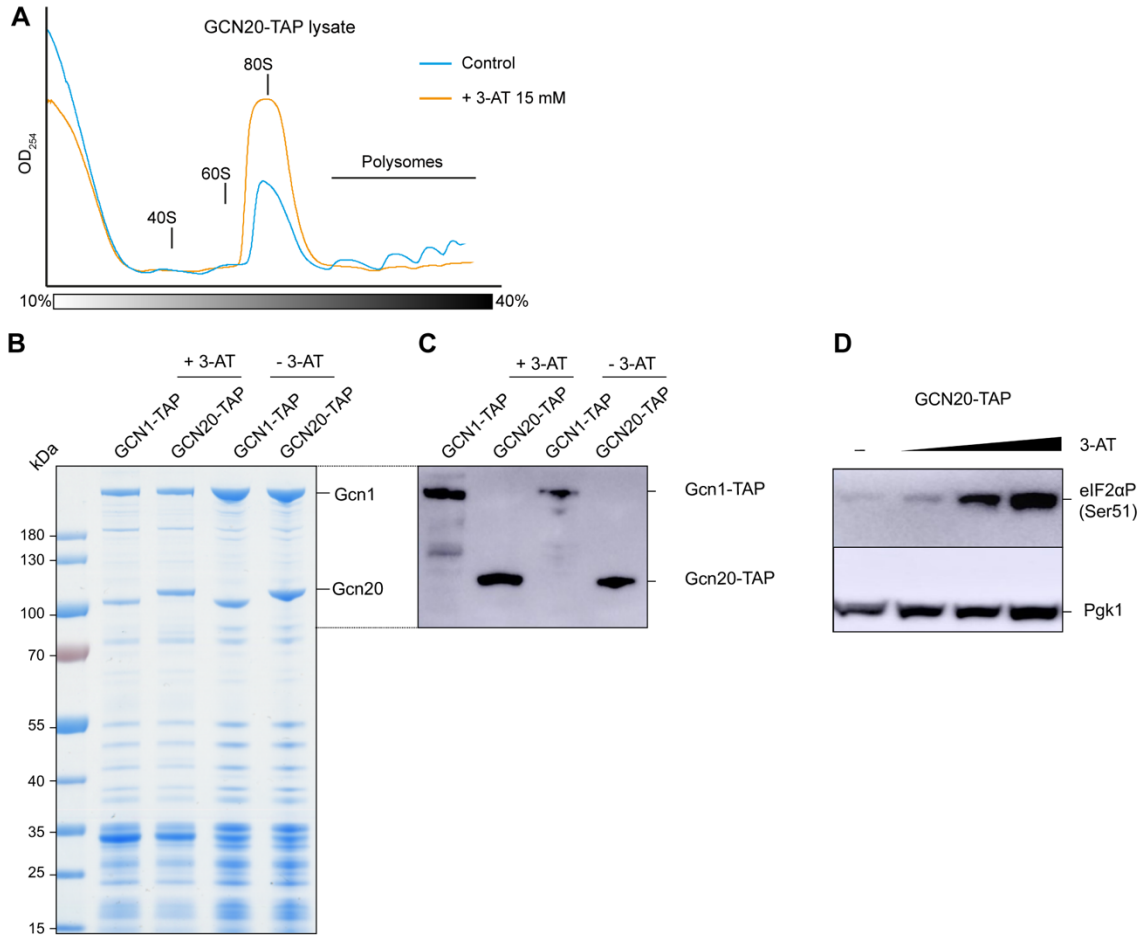


Fig. S1 Analysis of the pull-outs of the Gcn1- and Gcn20 C-terminally TAP-tagged samples. **(A)** GCN20-TAP whole cell extracts cultured with 15 mM (orange trace) or without (blue trace) 3-AT were subjected to sucrose density gradient centrifugation. Gradients were fractionated while scanning at 254 nm and the resulting absorbance profiles are shown. Positions of 40S, 60S, 80S and polysomes are indicated. **(B)** 4-12% NuPAGE gel of the Gcn1- and Gcn20-TAP-tag purified complexes from the cell cultures in presence or absence of 15 mM 3-AT. **(C)** as in **(B)**, but analyzed via SDS-PAGE and immunoblotting using a TAP-tag polyclonal antibody. **(D)** Phosphorylation level of eIF2 α analyzed by Western blotting. Whole cell extracts of the GCN20-TAP strain were prepared from exponential growing cell cultures treated with 1.5 and 15 mM 3-AT. The phosphorylation level of eIF2 α was then monitored by immunoblotting, while immunoblotting against PGK1 was used as loading control.

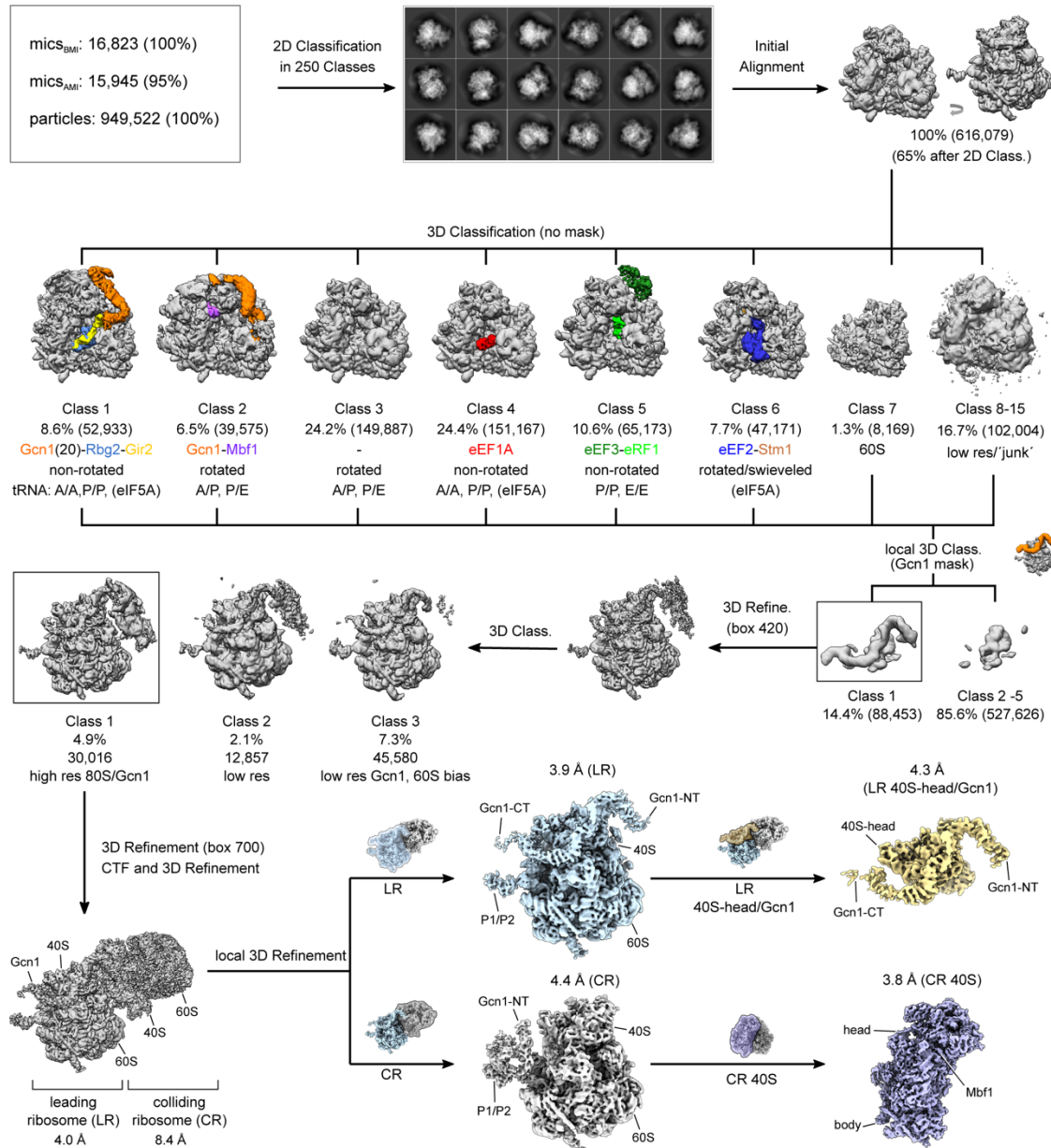


Fig. S3. Processing of the high resolution Gcn20-TAP dataset. After manual inspection (AMI; before manual inspection, BMI) of 16,823 micrographs, 15,945 were selected for the initial particle picking, resulting in 949,522 particles. Following 2D classification, 616,079 particles were initially aligned against a vacant *S. cerevisiae* 80S ribosome and subjected to 3D classification, sorting the particles into 15 initial classes as depicted. Subsequently, all classes (1-15) were re-combined and subjected to local sorting using a mask for Gcn1. Class 1 (14.3%, 88,453 particles) containing Gcn1 bound particles was subsequently refined and 3D classified into three classes. High resolution particles in Class1 (4.9%, 30,016 particles) were again 3D and CTF refined with an enlarged box size and resulted in a final disome reconstruction at 4.0 Å for the leading ribosome (LR) and 8.4 Å for the colliding ribosome (CR). The LR (blue) and CR (grey) were masked and individually local refined resulting to 3.9 Å and 4.4 Å, respectively. To increase the resolution of Gcn1 and Mbf1, the LR and CR were subjected to an further local refinement with an individual mask encompassing the important regions: the 40S head and Gcn1 (yellow mask) for the LR and 40S (purple mask) for the CR, which resulted in final reconstructions of the masked regions at a final resolution of 4.3 Å and 3.8 Å, respectively.

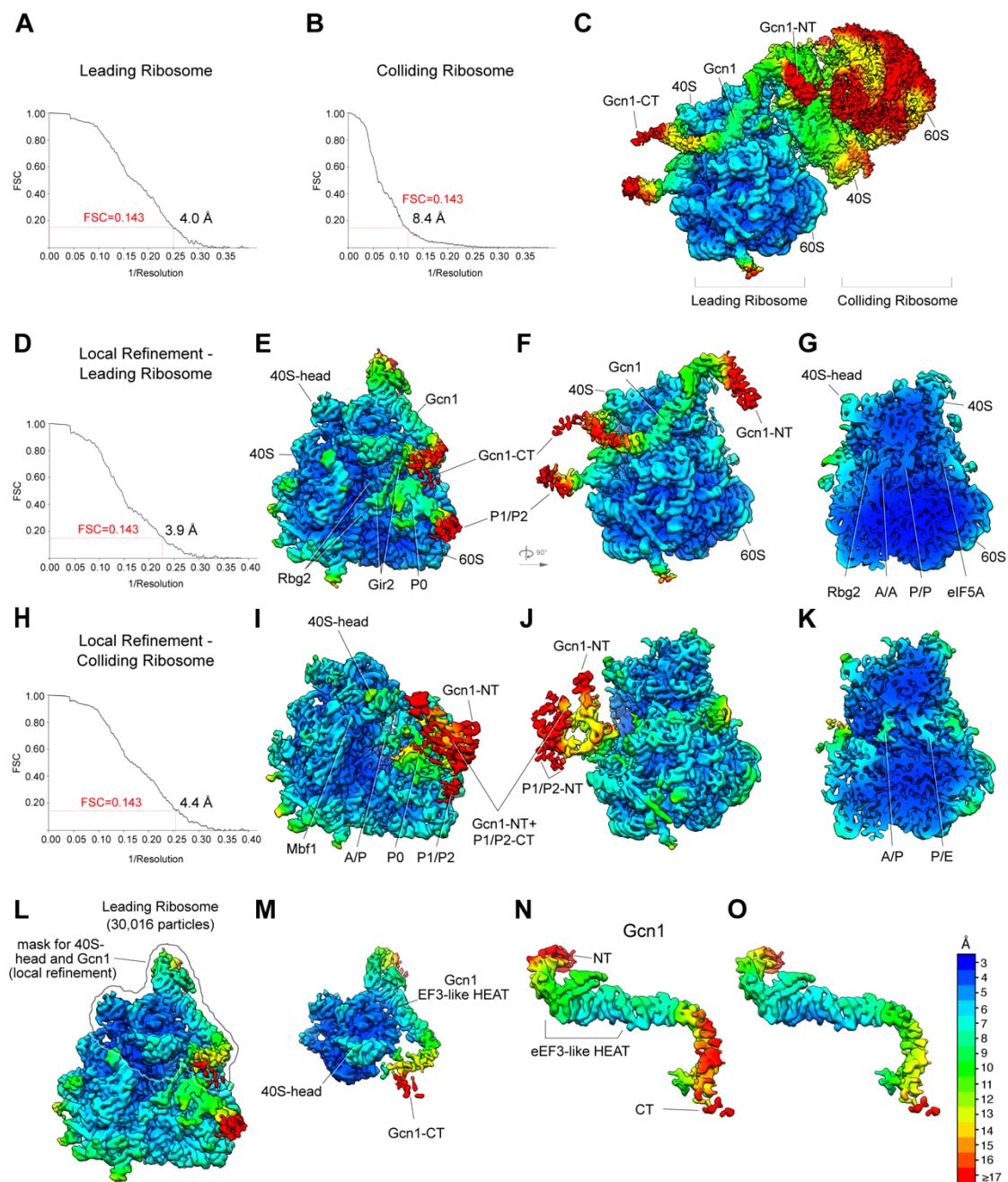


Fig. S4. Local resolution of cryo-EM reconstructions of the Gcn1-disome. (A-C) Cryo-EM reconstruction of the Gcn1-disome, with (A-B) Fourier shell correlation (FSC) curve of the final reconstructions indicating an average resolution of 4.0 Å for the leading and 8.4 Å for the colliding ribosome, according to the gold-standard criterion (FSC=0.143). (C) Cryo-EM map of the full disome filtered to 8 Å and colored according to local resolution. (D-G) Cryo-EM reconstruction of the leading ribosome, with (D) FSC curve of the final reconstruction indicating an average resolution of 3.9 Å (FSC=0.143). (E,F) Cryo-EM reconstruction of the leading ribosome filtered to 8 Å and colored according to the local resolution. (G) Transverse section of the volume shown in (F). (H-K) Cryo-EM reconstruction of the colliding ribosome, with (H) FSC curve of the final reconstruction indicating an average resolution of 4.4 Å (FSC=0.143). (I,J) Cryo-EM reconstruction of the leading ribosome filtered to 9 Å and colored according to the local resolution. (K) Transverse section of the

volume shown in **(J)**. **(L)** Cryo-EM reconstruction of the locally refined leading ribosome colored according to local resolution. The border represents the mask, which was used for the local refinement of Gcn1 including Gcn1 and the head of the 40S subunit of the leading ribosome. **(M)** Postprocessed volume shown in **(L)**. **(N-O)** Local resolution of Gcn1 **(N)** before and **(O)** after the local refinement.

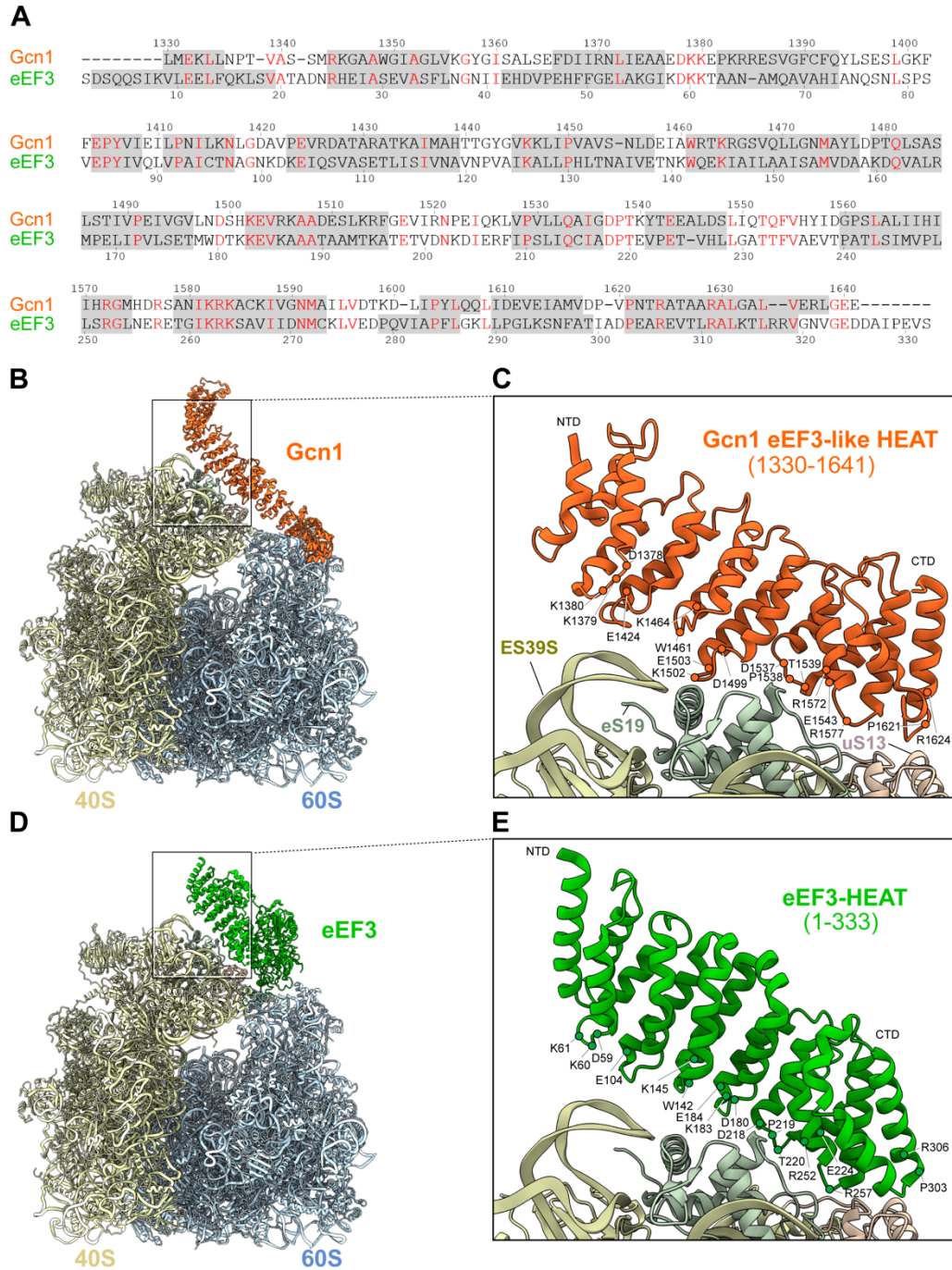


Fig. S5. Comparison between the Gcn1 eEF3-like HEAT region and eEF3 HEAT repeats. (A) Sequence alignment of the eEF3-like HEAT repeat region of Gcn1 with HEAT repeats in eEF3. Conserved residues are denoted in red and helices are marked as grey boxes. **(B)** Molecular model of the Gcn1-80S complex (Gcn1, orange; 40S, pale yellow; 60S, cyan) with **(C)** zoomed view showing the detailed amino acid composition of the Gcn1 region interacting with ES39S (pale yellow), eS19 (pale green), uS13 (pale coral) of the 40S on the leading ribosome. **(D)** The eEF3 ribosomal model (eEF3, green) with **(E)** enlarged view of the eEF3 interface contacting the ribosome.

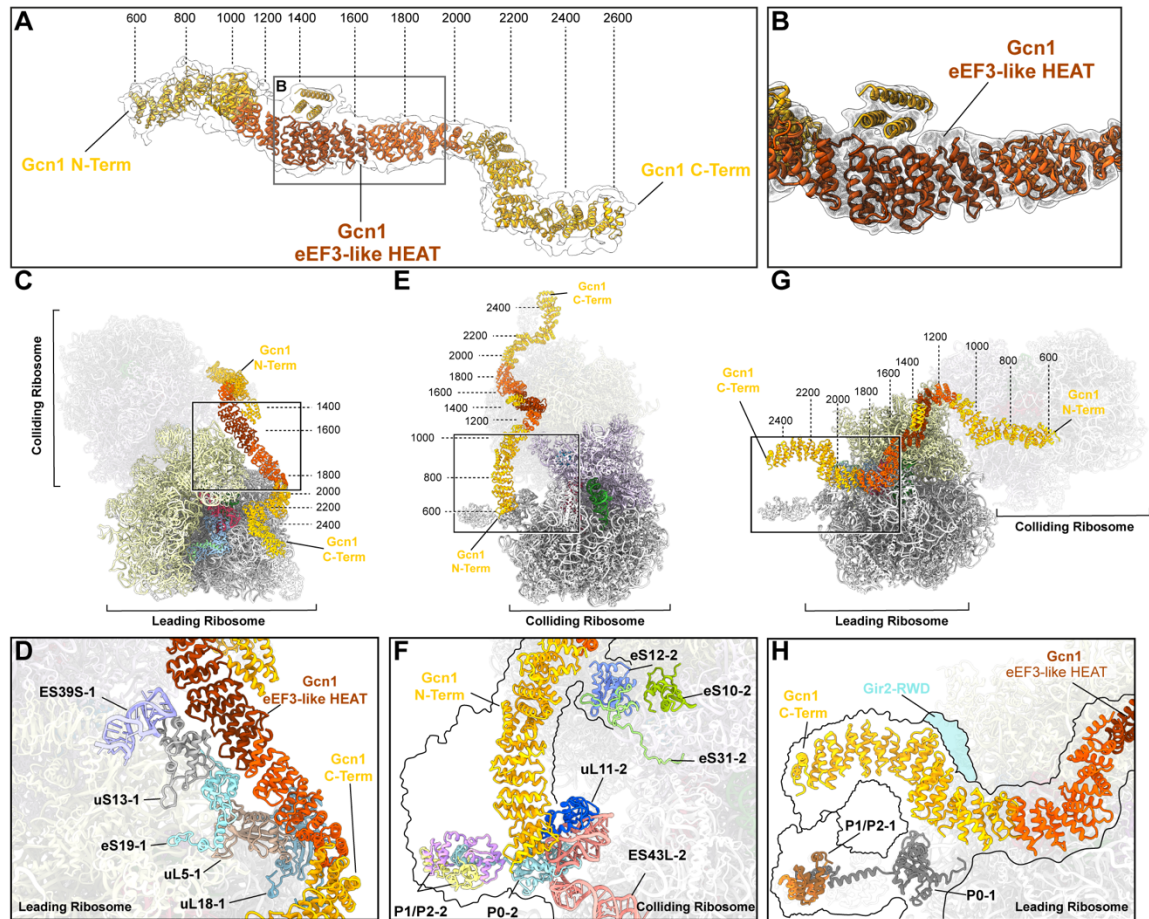


Fig. S6. Interactions of Gcn1 within the disome. (A) Molecular model of the Gcn1 within the cryo-EM density (gray transparent). The eEF3-like region (dark orange) is shown enlarged in (B). The bright orange HEAT repeats were fitted individually based on the features of the density for helices, whereas the yellow HEAT repeats are tentative placements fitted to the map to obtain an approximate estimation of the HEAT positions within Gcn1. (C-H) Interactions of Gcn1 within the disome, specifically focused on the (C-D) central region of Gcn1 interacting with ES39S, uS13 and eS19 of the 40S head and uL5 and uL18 of the central protuberance of the leading ribosome, (E-F) N-terminal region of Gcn1 interacting with uL11, ES43L and the P-stalk proteins P0, P1 and P2 of the colliding ribosome, and (G-H) the C-terminal region of Gcn1 interacting with the RWD domain of Gir2 (cyan) as well as the P-stalk proteins P0, P1 and P2 of the leading ribosome. The border shown in (F) and (H) reflects the density within the cryo-EM map.

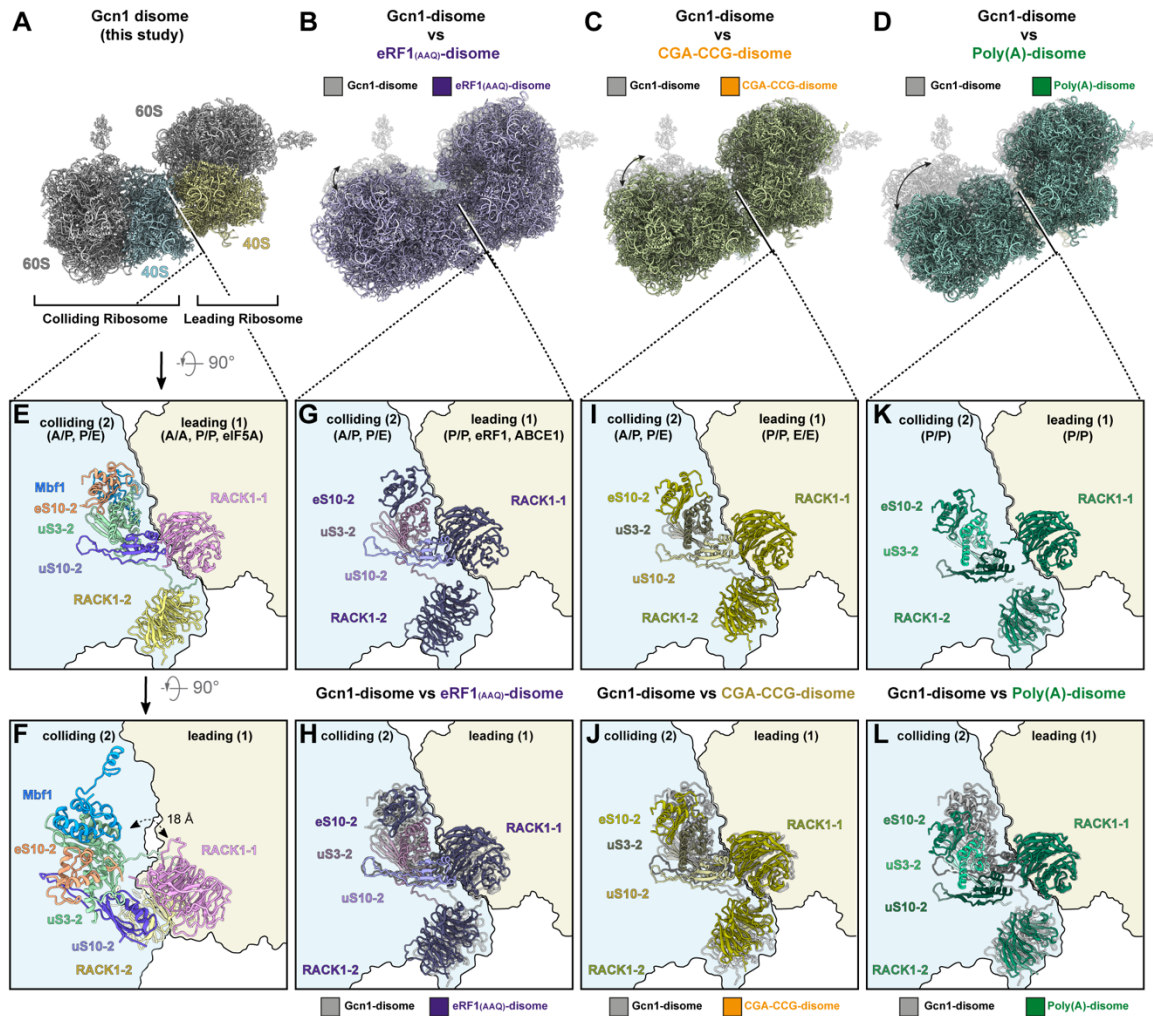


Fig. S7. 40S-40S interaction interface of the Gcn1-bound disome and its comparison to other disomes. (A) Overview of the Gcn1-disome molecular model. (B) Collided disome stalled by a catalytically nonactive eRF1 mutant (eRF1-AAQ) (PDB ID: 6hcm, 6hcq) (22) (purple) overlaid with the Gcn1-disome (grey) shown in (A). (C) Disome stalled on a CGA-CCG mRNA (PDB ID: 6i7o) (23) (orange) overlaid with the Gcn1-disome (grey) structure shown in (A). (D) Collided disome stalled on poly(A) mRNA (PDB ID: 6t83) (24) (dark green) overlaid with the Gcn1-disome (grey) structure shown in (A). (E, F) Close-up view on the Gcn1-disome interaction interface of the 40S subunits from the leading stalled ribosome (pale yellow) and the colliding ribosome (pale blue). (G) Close-up view on the interaction interface from the collided disome stalled by a eRF1-AAQ mutant. (H) Overlay of (E) and (G). (I) Close-up view on the interaction interface from the disome stalled on a CGA-CCG mRNA. (J) Overlay of (E) and (I). (K) Close-up view on the interaction interface from the collided disome stalled on poly(A) mRNA. (L) Overlay of (E) and (K).

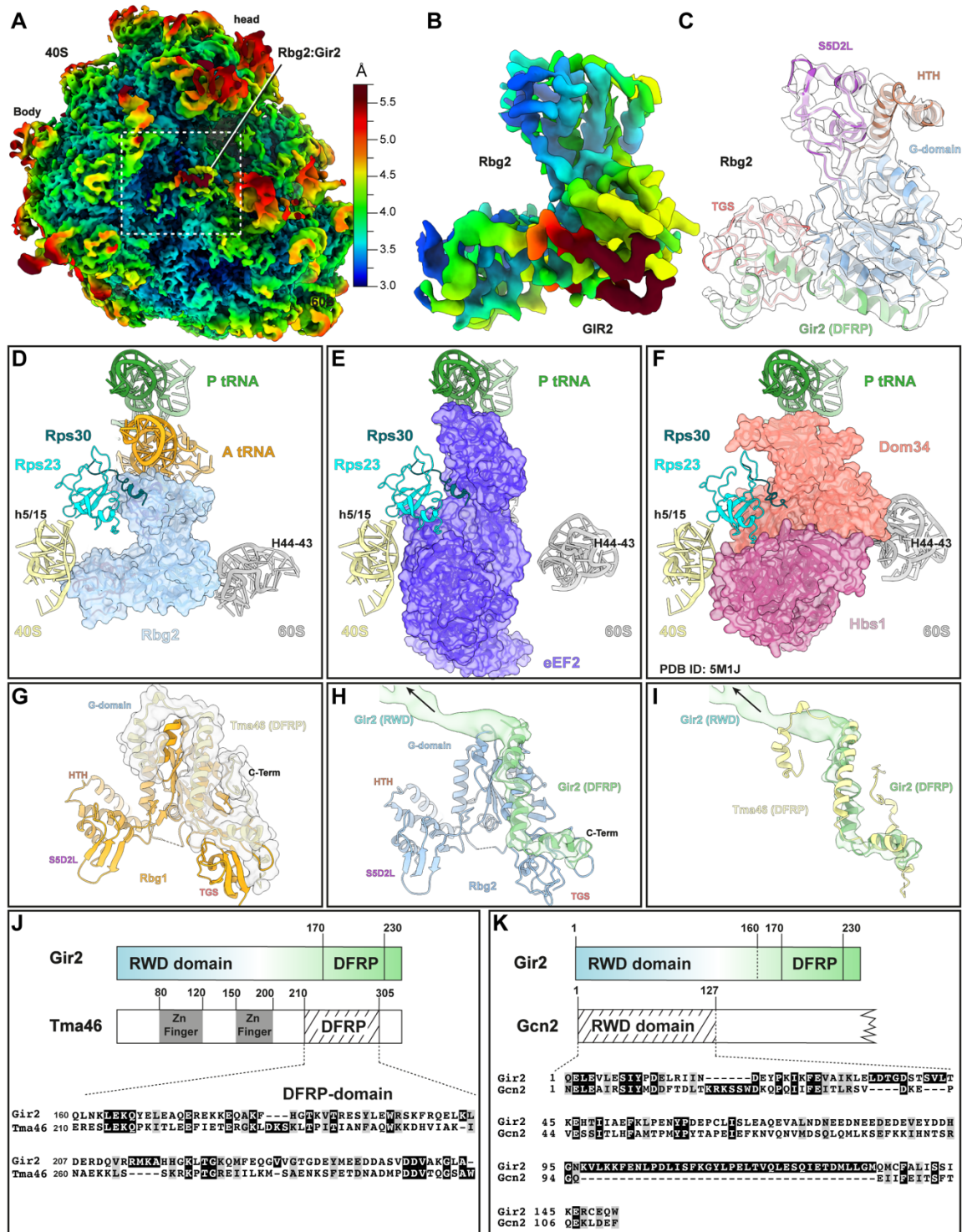


Fig. S8. Molecular model for Rbg2 and comparison of Gir2 with Tma46 and Gcn2. (A) Local resolution map of the leading ribosome with the binding site of Rbg2 indicated. (B) Isolated density of the Rbg2-Gir2 complex from the Gcn1-disome, coloured according to local resolution. (C) Molecular model for Rbg2 fitted into isolated cryo-EM density for Rbg2 (transparent grey) and colored by domain. (D-F) Comparison of (D) Rbg2 (cyan) and A-tRNA (orange) with (E) eEF2 (blue, PDB ID 6GQV) (25) and (F) Hbs1 (pink) and Dom34 (salmon, PDB ID 5M1J) (26). (G) Structure of Rbg1 (orange, PDB ID: 4A9A) (17) in complex with Tma46 (DFRP) domain (light yellow with transparent surface). (H) Conformation of Rbg2 (blue) and Gir2(DFRP) domain (green with transparent surface).

transparent surface) as found bound to a stalled leading ribosome in the Gcn1-disome. **(I)** comparison of cryo-EM density and model for Gir2 (green) with the model for Tma46 as obtained by aligning the Rbg1-Tma46 complex to Rbg2. **(J)** Schematic representation of the domain structure of Gir2 and Tma46 with zoom on a sequence alignment of their respective DFRP domains. **(K)** Schematic representation of the domain structure of Gir2 and Gcn2 with a zoom on a sequence alignment their respective RWD domains.

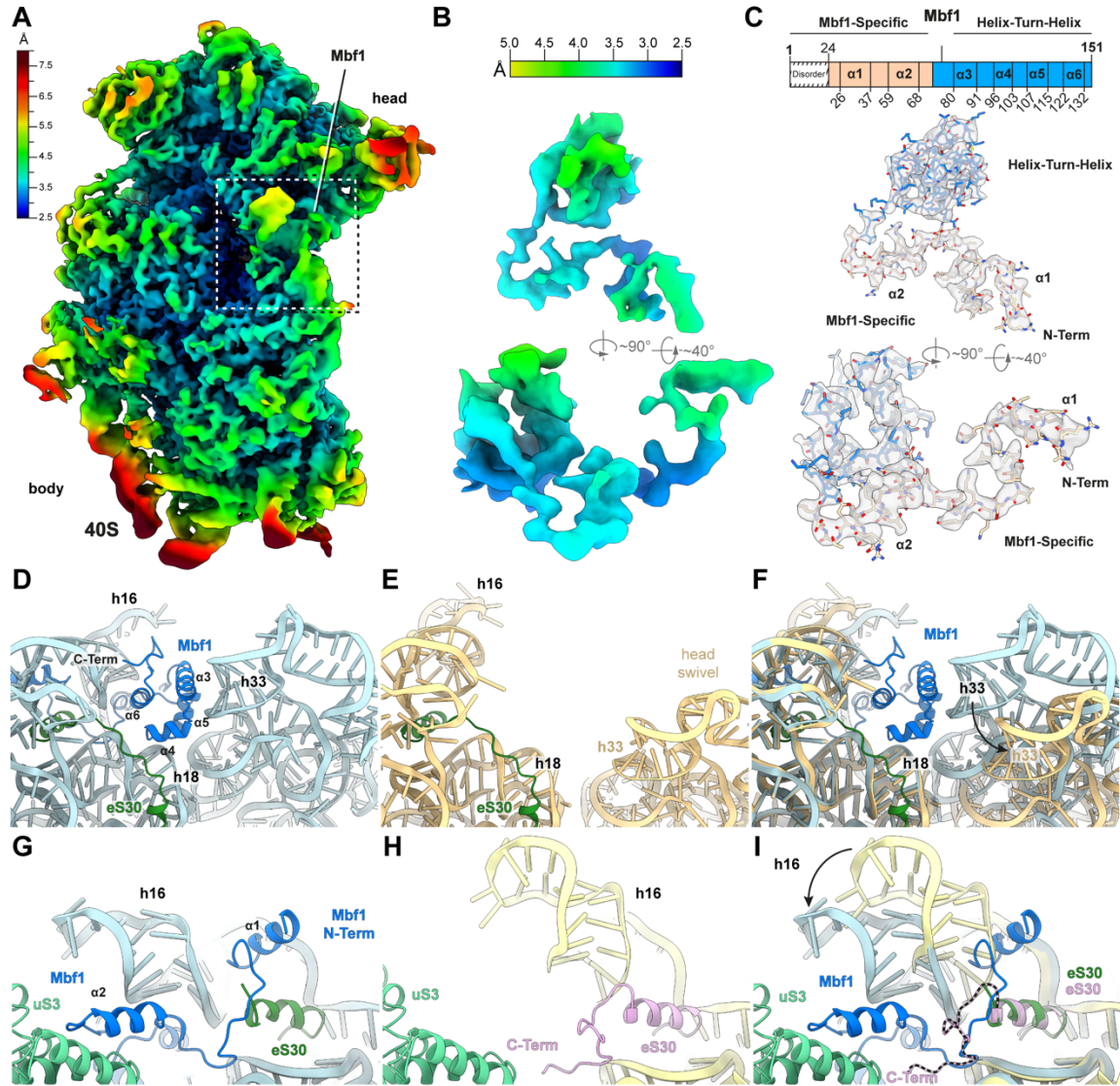


Fig. S9. Molecular model for Mbf1 on the Gcn1-disome. (A) Local resolution map of the 40S subunit of the colliding ribosome from the Gcn1-disome with the binding site of Mbf1 indicated. (B) Two views of the isolated density of the Mbf1 colored according to local resolution. (C) Schematic representation of Mbf1 showing the Mbf1-specific N-terminus (light brown, residues 44-79) and the C-terminal helix-turn-helix domain (blue). Isolated density (grey transparency) with fitted molecular model for Mbf1 (colored by domain as illustrated in the scheme). (D) Mbf1 C-terminal helix-turn-helix interacting with the 18S rRNA. (E) Head swivel 40S ribosome (yellow). (F) Similar view to (D and E) with an overlay of head swivel 40S ribosome (yellow). (G-I) Conformation change of eS30 C-terminal region and h16 in the Mbf1 bound structure compared to a reference structure (PDB ID 6SNT, pink for eS30 and yellow for h16).

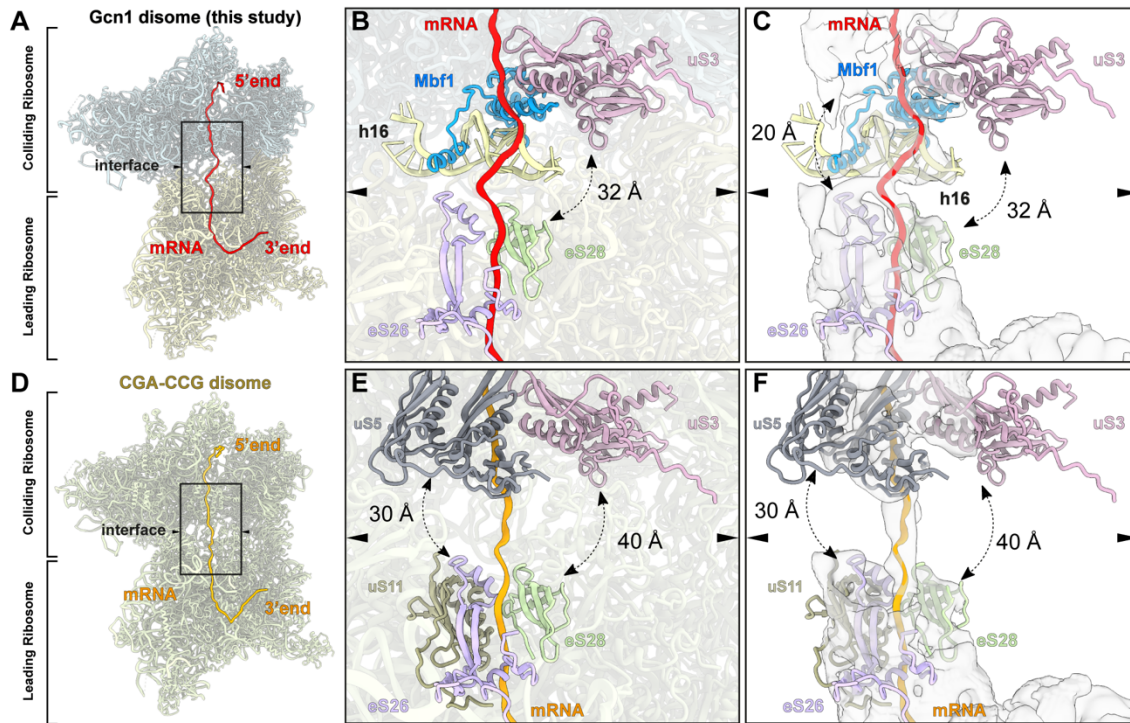


Fig. S10. Compaction of the Gcn1-disome. (a) 40S of the leading (pale yellow) and the colliding (cyan) ribosome of the Gcn1-stalled disome containing the mRNA (red). (b) Close-up view of the 40S-40S interface shown in (a). The ribosomal proteins and rRNA interacting with the mRNA are depicted and labelled. (c) View as in (b) including the locally isolated density for the mRNA and the surrounding ribosomal components. (d) 40S subunits (tan) of the disome stalled on CGA-CCG mRNA (PDB ID: 6I7O) (23) (mRNA in light orange) and its (e) enlarged view of the 40S-40S interface (f) including the locally isolated density for the mRNA and the surrounding ribosomal proteins.

Table S1 | Cryo-EM data collection, refinement and validation statistics.

	Leading stalled ribosome EMD ID 12534 PDB ID 7NRC	Colliding ribosome EMD ID 12535 PDB ID 7NRD
Data collection		
Microscope	FEI Titan Krios	FEI Titan Krios
Camera	Falcon II	Falcon II
Magnification	131,703	131,703
Voltage (kV)	300	300
Electron dose (e ⁻ /Å ²)	25	25
Defocus range (μm)	-1.3 to -2.8	-1.3 to -2.8
Pixel size (Å)	1.084	1.084
Initial particles (no.)	616,079	616,079
Final particles (no.)	30,016	30,016
Map resolution (Å)	3.85	4.36
Box size	700,700,700	700,700,700
Model composition		
Protein residues	11829	11163
RNA bases	5391	5430
Refinement		
Resolution range (Å)	3.0-15	3.3-15
Map CC (around atoms)	0.74	0.74
Map sharpening <i>B</i> factor (Å ²)	-84.4315	-120.184
R.m.s. deviations		
Bond lengths (Å) (#>4σ)	0.006	0.012
Bond angles (°) (#>4σ)	1.311	1.384
Validation		
MolProbity score	1.76	2.06
Clashscore	4.43	9.22
Poor rotamers (%)	0.27	1.21
Ramachandran plot		
Favored (%)	90.44	89.29
Allowed (%)	9.46	10.50
Disallowed (%)	0.09	0.16

Movie S1 (separate file). Overview of Gcn1 and interactions within colliding disome structure. Overview of the model of Gcn1 (orange), then zoom out to show electron density for disome and Gcn1 and Gcn20. Rotations to highlight factor in complex with leading ribosome including A-tRNA (red), P-tRNA (green), Rbg2 (blue) and Gir2 (green), as well as in colliding ribosome with Mbf1 (blue), A/P-tRNA (tan) and P/E-tRNA (pink).

Dataset S1 (separate file). Mass spectrometry analysis of Gcn20 affinity purification samples.

SI References

1. Schmidt C, *et al.* (2016) The cryo-EM structure of a ribosome-Ski2-Ski3-Ski8 helicase complex. *Science* 354(6318):1431-1433.
2. Ranjan N, *et al.* (2021) Yeast translation elongation factor eEF3 promotes late stages of tRNA translocation. *EMBO J*:e106449.
3. Tyanova S, Temu T, & Cox J (2016) The MaxQuant computational platform for mass spectrometry-based shotgun proteomics. *Nat Protoc* 11(12):2301-2319.
4. Schwanhaussner B, *et al.* (2011) Global quantification of mammalian gene expression control. *Nature* 473(7347):337-342.
5. Elias JE & Gygi SP (2007) Target-decoy search strategy for increased confidence in large-scale protein identifications by mass spectrometry. *Nature methods* 4(3):207-214.
6. Zheng SQ, *et al.* (2017) MotionCor2: anisotropic correction of beam-induced motion for improved cryo-electron microscopy. *Nature methods* 14(4):331-332.
7. Zhang K (2016) Gctf: Real-time CTF determination and correction. *Journal of structural biology* 193(1):1-12.
8. Zivanov J, *et al.* (2018) New tools for automated high-resolution cryo-EM structure determination in RELION-3. *eLife* 7.
9. Svidritskiy E, Brilot AF, Koh CS, Grigorieff N, & Korostelev AA (2014) Structures of yeast 80S ribosome-tRNA complexes in the rotated and nonrotated conformations. *Structure* 22(8):1210-1218.
10. Behrmann E, *et al.* (2015) Structural snapshots of actively translating human ribosomes. *Cell* 161(4):845-857.
11. Pittman YR, *et al.* (2006) Mg²⁺ and a key lysine modulate exchange activity of eukaryotic translation elongation factor 1B alpha. *The Journal of biological chemistry* 281(28):19457-19468.
12. Anger AM, *et al.* (2013) Structures of the human and Drosophila 80S ribosome. *Nature* 497(7447):80-85.
13. Brown A, Baird MR, Yip MC, Murray J, & Shao S (2018) Structures of translationally inactive mammalian ribosomes. *eLife* 7.
14. Bienert S, *et al.* (2017) The SWISS-MODEL Repository-new features and functionality. *Nucleic acids research* 45(D1):D313-D319.

15. Pettersen EF, *et al.* (2004) UCSF Chimera--a visualization system for exploratory research and analysis. *Journal of computational chemistry* 25(13):1605-1612.
16. Emsley P & Cowtan K (2004) Coot: model-building tools for molecular graphics. *Acta crystallographica. Section D, Biological crystallography* 60(Pt 12 Pt 1):2126-2132.
17. Francis SM, Gas ME, Daugeron MC, Bravo J, & Seraphin B (2012) Rbg1-Tma46 dimer structure reveals new functional domains and their role in polysome recruitment. *Nucleic acids research* 40(21):11100-11114.
18. Croll TI (2018) ISOLDE: a physically realistic environment for model building into low-resolution electron-density maps. *Acta Crystallogr D Struct Biol* 74(Pt 6):519-530.
19. Adams PD, *et al.* (2010) PHENIX: a comprehensive Python-based system for macromolecular structure solution. *Acta crystallographica. Section D, Biological crystallography* 66(Pt 2):213-221.
20. Schmidt C, *et al.* (2016) Structure of the hypusinylated eukaryotic translation factor eIF-5A bound to the ribosome. *Nucleic acids research* 44(4):1944-1951.
21. Goddard TD, *et al.* (2018) UCSF ChimeraX: Meeting modern challenges in visualization and analysis. *Protein science : a publication of the Protein Society* 27(1):14-25.
22. Juskiewicz S, *et al.* (2018) ZNF598 Is a Quality Control Sensor of Collided Ribosomes. *Molecular cell* 72(3):469-481 e467.
23. Ikeuchi K, *et al.* (2019) Collided ribosomes form a unique structural interface to induce Hel2-driven quality control pathways. *EMBO J* 38(5).
24. Tesina P, *et al.* (2020) Molecular mechanism of translational stalling by inhibitory codon combinations and poly(A) tracts. *EMBO J* 39(3):e103365.
25. Pellegrino S, *et al.* (2018) Structural Insights into the Role of Diphthamide on Elongation Factor 2 in mRNA Reading-Frame Maintenance. *J Mol Biol* 430(17):2677-2687.
26. Hilal T, *et al.* (2016) Structural insights into ribosomal rescue by Dom34 and Hbs1 at near-atomic resolution. *Nat Commun* 7:13521.